

Cover Page



Universiteit Leiden



The handle <http://hdl.handle.net/1887/138670> holds various files of this Leiden University dissertation.

**Author:** Gagestein, B.

**Title:** Chemical tools to study lipid signaling

**Issue Date:** 2020-12-16

# **Chemical Tools to Study Lipid Signaling**

PROEFSCHRIFT

ter verkrijging van  
de graad van Doctor aan de Universiteit Leiden,  
op gezag van Rector Magnificus prof.mr. C.J.J.M. Stolker,  
volgens besluit van het College voor Promoties  
te verdedigen op woensdag 16 december 2020  
klokke 11:15 uur

door

**Berend Gagestein**

geboren te Capelle aan den IJssel in 1992

# **Promotiecommissie**

Promotoren: Prof. dr. M. van der Stelt

Prof. dr. H.S. Overkleeft

Overige leden: Prof. dr. J.M.F.G. Aerts

Prof. dr. G.A. van der Marel

Prof. dr. R.E.M. Toes

Dr. A. Ioan-Facsinay

Prof. dr. M. Maccarrone

Dr. S.I. van Kasteren

Prof. dr. N.I. Martin

ISBN: 978-94-6416-241-7

Printed by: Ridderprint BV

Cover pattern: [www.freepik.com](http://www.freepik.com)





# Table of Contents

<b>Chapter 1</b> General introduction	<b>7</b>
<b>Chapter 2</b> Lipid photoaffinity probes	<b>17</b>
<b>Chapter 3</b> Bioorthogonal photoaffinity probes of omega-3 signaling lipids reveal PTGR1 as a metabolic hub in human macrophages	<b>37</b>
<b>Chapter 4</b> Exploring the neuroprotective role of DHEA in inflammation	<b>71</b>
<b>Chapter 5</b> An expeditious synthesis of DHA-alkyne	<b>97</b>
<b>Chapter 6</b> Profiling the targets of anandamide reuptake inhibitor WOBE437	<b>115</b>
<b>Chapter 7</b> Cyclopropene probes for live-cell imaging of signaling lipids	<b>143</b>
<b>Chapter 8</b> Summary and future prospects	<b>159</b>
<b>Nederlandse samenvatting</b>	<b>175</b>
<b>List of Publications</b>	<b>182</b>
<b>Curriculum Vitae</b>	<b>183</b>
<b>Dankwoord</b>	<b>184</b>



# Chapter 1

## General introduction

### Lipids and their diversity

Lipids are defined as hydrophobic biomolecules that dissolve in organic solvents, but not in water. They have a wide variety of functions inside the cell, such as structural building block of membranes, energy storage and cell signaling. The discovery that aspirin affects prostaglandin synthesis demonstrated that lipids can modulate the immune system and that enzymes involved in their metabolism constitute interesting drug targets.<sup>1</sup> Many different signaling activities have subsequently been discovered for multiple lipid classes, such as endocannabinoids, resolvins, steroid hormones and vitamins A and D.<sup>2–5</sup> However, many signaling lipids have a low abundance, high lipophilicity and are short-lived, and as a consequence the mode of action and protein interaction partners of many lipids have remained elusive.

In an effort to systematically classify the rapidly expanding collection of identified lipids, the Lipid Metabolites and Pathways Strategy (LIPID MAPS) consortium has come up with a more concise definition of a lipid. In this definition, a lipid comprises a small hydrophobic or amphipathic molecule that is formed at least partially by the condensation of ketoacyl thioesters and/or isoprene units.<sup>6</sup> Based on these two building blocks, eight major lipid classes are defined: fatty acyls, glycerolipids, prenol lipids, sphingolipids, glycerophospholipids, sterol lipids, saccharolipids and polyketides (Figure 1).<sup>7</sup>

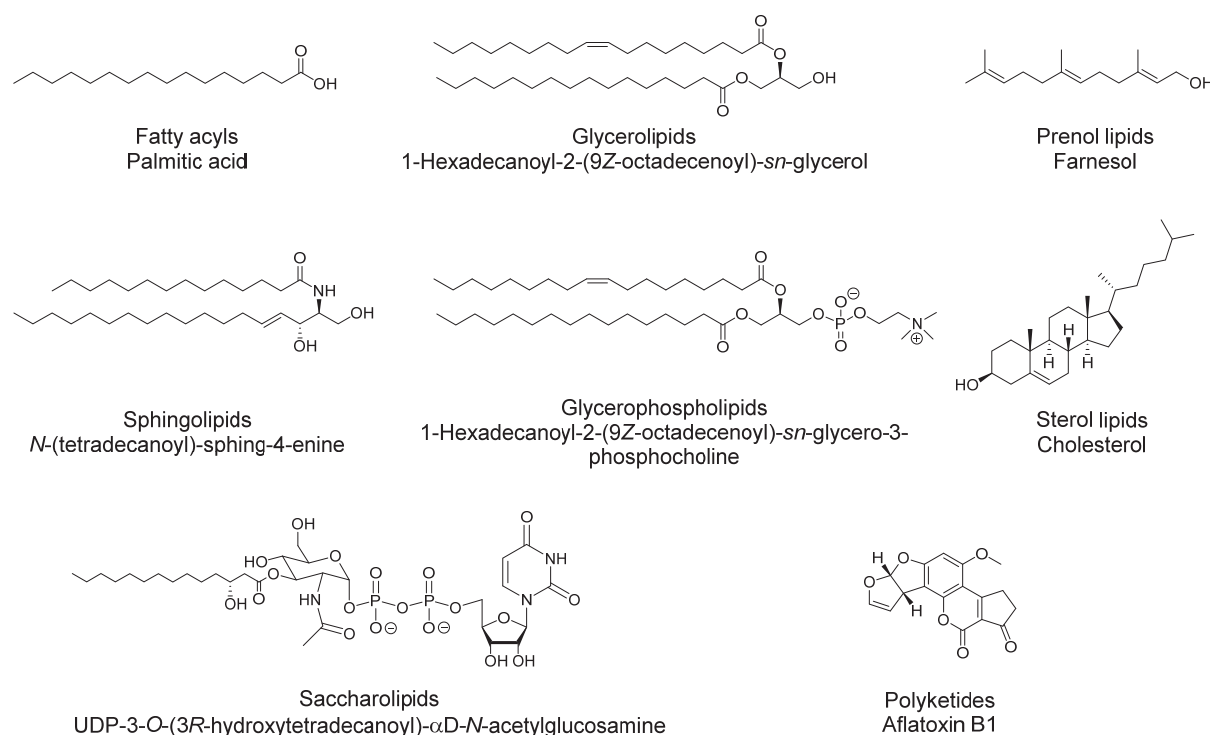


**Figure 1 | Representative structures of the eight lipid categories as defined by the LIPID MAPS consortium.<sup>6,7</sup>**

The variation in chemical characteristics between lipid families makes it a challenge to analyze multiple lipid species in one experiment. Different methods of sample preparation and analytical techniques are required to detect and quantify different classes of lipids.<sup>8</sup> Adding to the challenge is the wide range of metabolic modifications lipids can undergo, thereby yielding potential new bioactive lipid species. Since its inception, the field of lipidomics, which is defined as the analysis of lipids and their interacting partners within a biological system, has made great strides forward.<sup>9</sup> Standardization of protocols, increased availability of isotopically labelled lipids and the high mass accuracy and resolution of modern mass spectrometers have enabled the measurement of many different lipid species in complex biological samples.<sup>10</sup> However, bulk analysis of lipids after sample homogenization and lipid extraction discards the information on spatial distribution, therefore other methods are required to investigate lipid localization and protein interaction partners. Spatial information is important to study the role of lipids as signaling molecules, as signaling events occur through localized alterations in membrane lipid composition and activation of specific receptors such as peroxisome proliferator-activated receptors (PPARs)<sup>11</sup> and the G-protein coupled receptors GPR40<sup>12</sup> and GPR120.<sup>13</sup> In recent years, several technical advances in mass spectrometry and innovative chemical biology strategies have shed light on the lipid-protein interaction landscape and thereby facilitate studies of their biological function.

## Polyunsaturated fatty acids

Fatty acids are an important component of cell membranes and are integral to a wide variety of lipid classes. In vertebrates, fatty acid production is initiated in the cytosol by a system collectively referred to as fatty acid synthase.<sup>14</sup> When this system completes the biosynthesis of an acyl chain 16 carbon atoms in length, it releases the formed palmitate for further processing by enzymes located at the endoplasmic reticulum. One of these processes is the introduction of one or more cis double bonds, which is performed in eukaryotes by desaturases. This results in the formation of mono- or polyunsaturated fatty acids (PUFAs), where the double bonds in the latter are separated by methylene groups. When incorporated into membrane lipids, cis double bonds introduce disorder and increase fluidity, which has an impact on membrane protein function and on the assembly of lipid rafts.<sup>15</sup>

Fatty acids have common and systematic names, but are also referred to by a nomenclature that denotes the number of carbon atoms of the acyl chain, the number of double bonds, and the position of the first double bond relative to the terminal methyl, termed the omega ( $\omega$ , or  $n$ ) carbon. The major PUFAs found in mammals are omega-3 and omega-6 fatty acids. As mammals lack the enzymes required for certain biosynthetic steps, these fatty acids are conditionally essential nutrients. In principle, only  $\alpha$ -linolenic acid (ALA, 18:3 n-3) and linoleic acid (LA, 18:2 n-6) are essential for the biosynthesis of other PUFAs. However, the multiple chain elongation and desaturation steps to form higher order PUFAs like eicosapentaenoic acid (EPA, 20:5 n-3) and docosahexaenoic acid (DHA, 22:6 n-3) are highly inefficient, and the bulk of these fatty acids are derived from the diet (Figure 2).<sup>16</sup> Diets rich in omega-3 fatty acids, along with omega-3 supplements, are of great interest as they are linked to a number of health benefits, such as reduced risk for ischemic stroke,<sup>17</sup> neuroprotective and antidepressant effects,<sup>18,19</sup> and improvements in chronic inflammatory conditions.<sup>20-22</sup> Moreover, they are essential for neuronal development<sup>23</sup> and inadequate intake is associated with many neurological diseases, including depression,<sup>24</sup> anxiety disorders,<sup>25</sup> and neuroinflammation.<sup>26,27</sup> However, as often as these benefits are reported, they are also the subject of discussion. For example, omega-3 fatty acids are known to prevent a number of risk factors for cardiovascular disease, including high blood pressure,<sup>28</sup> reduced arterial compliance,<sup>29</sup> cardiac arrhythmias<sup>30</sup> and abnormal platelet reactivity and thrombosis.<sup>31</sup> However, this prevention of cardiovascular risk factors does not translate to benefit to human health. Recent meta-analyses<sup>32,33</sup> of clinical trials investigating omega-3 supplementation found no clinical benefit for fatal or nonfatal coronary heart disease or any major vascular events. This discrepancy highlights the limited knowledge on the molecular and cellular pathways by which omega-3 fatty acids confer their benefits. It has been suggested that many of the beneficial effects on human health derive from modulation of the immune system,<sup>21,34</sup> which has been supported by the discovery of anti-inflammatory oxidized metabolites.<sup>35</sup>

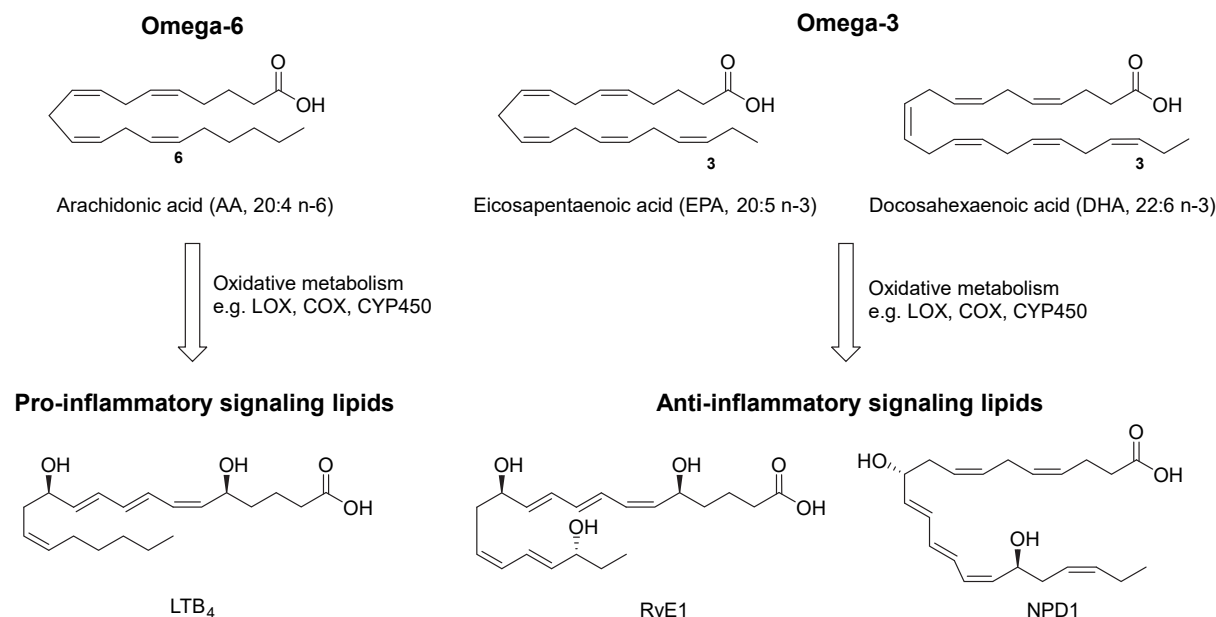


**Figure 2 | Omega-3 and omega-6 fatty acids and examples of their oxidative metabolites.** COX, cyclooxygenase; LOX, lipoxygenase; CYP450, cytochrome P450; NPD1, neuroprotectin D1; RvE1, resolvin E1; LTB<sub>4</sub>, leukotriene B4.

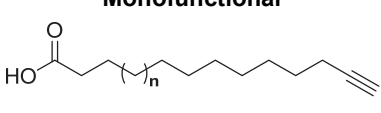
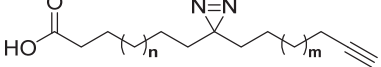
Oxidized derivatives of PUFA s have long been established as immunomodulatory signaling lipids. Arachidonic acid (AA, 20:4 n-6) can be oxidized by cyclooxygenases (COX) and lipoxygenases (LOX) into bioactive eicosanoids such as prostaglandins and leukotrienes, respectively (Figure 2). Most of these metabolites are pro-inflammatory and inhibition of their biosynthesis by non-steroidal anti-inflammatory drugs (NSAIDs) results in alleviation of pain, swelling and fever. In contrast, oxidized metabolites of omega-3 fatty acids act as anti-inflammatory lipids involved in the resolution of inflammation.<sup>3</sup> Although many of these metabolites and their anti-inflammatory effects have been reported, their mechanisms and biosynthetic pathways remain to be characterized. Consequently, the proteins involved in their biosynthesis, degradation and signaling are of interest for investigation as potential drug targets for inflammatory diseases.<sup>22</sup>

## Tools to study lipid signaling molecules

The field of chemical biology has developed two main approaches to study lipids: design and synthesis of chemically modified lipids to track their metabolism and localization, and chemical tools to identify the protein interaction partners involved in their signaling functions.

To track lipids in a biological system, they can be functionalized with a reporter tag. These tags traditionally consist of radioactive isotopes<sup>36</sup> and fluorophores.<sup>37,38</sup> However, radioactive isotopes require special equipment and procedures, while fluorophores are relatively large and rigid structures, affecting metabolism, distribution and trafficking.<sup>39,40</sup> A more versatile and less intrusive modification is the introduction of an alkyne (Table 1).<sup>41,42</sup> Using bioorthogonal ligation chemistry, such as ‘click’ chemistry, alkyne-functionalized lipids can be ligated to fluorescent groups for detection, or to affinity handles for isolation.<sup>43</sup> These functionalized lipids have been used for the visualization of lipids in membranes, their metabolism and modification of proteins by lipids, for example myristoylation<sup>44</sup> or prenylation<sup>45</sup> of proteins.<sup>46–49</sup> However, these tools will only reveal covalent lipid-protein interactions. To study noncovalent lipid-protein interactions, the chemical tool requires additional functionality.

**Table 1 | General structures and exemplary applications of fatty-acid based chemical tools.**

General structure	Functionality
<b>Monofunctional</b> 	Tracking metabolism <sup>49–51</sup> Incorporation as post-translational modification <sup>47</sup> Localization by Raman spectroscopy or fluorescence microscopy <sup>46,52</sup>
<b>Bifunctional</b> 	All of the above, as well as: Mapping protein-lipid interactions <sup>53,54</sup> Mapping protein-protein interactions <sup>55</sup>

To detect lipid-interacting proteins, a photoactivatable group, such as a diazirine, benzophenone or aryl azide, can be incorporated into an alkyne-tagged lipid, providing a bifunctionalized lipid. Irradiation with light results in the formation of a reactive intermediate that can form a stable, covalent bond with an interacting protein.<sup>56</sup> The bioorthogonal handle can subsequently be ligated to a fluorophore to visualize the interaction partner. Alternatively, ligation to an affinity handle such as biotin allows for enrichment and identification of the tagged protein by mass spectrometry. Bifunctional lipids have been successfully used to map lipid-protein interaction networks, lipid signaling functions, lipid metabolism, lipid localization and protein-protein interactions.<sup>53–55,57</sup> However, currently reported lipid probes do not cover all lipid classes. In part, this is due to the challenges of chemically synthesizing these functionalized lipids.

## Aim and outline

The overarching aim of the research presented in this thesis was to develop and apply chemical tools to study lipid metabolism, transport and signaling.

**Chapter 2** reviews lipid-based photoaffinity probes published in the last decade and their applications. Additionally, a list of promiscuous lipid binding proteins is presented and the challenges inherent to lipid probes are discussed. **Chapter 3** describes the synthesis of photoaffinity probes based on the omega-3 fatty acid DHA and an oxidized derivative, 17-hydroxy-DHA (17-HDHA), using a combination of chemical and chemoenzymatic transformations. The probes are used in comparative photoaffinity-based protein profiling, which reveals that PTGR1 is capable of converting 17-HDHA to 17-oxo-DHA in human macrophages. **Chapter 4** investigates the design and application of a photoaffinity probe based on the neuroprotective ethanolamide derivative of DHA, DHEA. This probe is used to study the molecular mechanism of action of this signaling lipid in a microglial cell line. **Chapter 5** reports on an improved method for the synthesis of DHA derivatives. Regioselective hydrobromination of DHA enables the synthesis of DHA-alkyne, which is used to study DHA metabolism and intracellular exchange by flow cytometry. **Chapter 6** describes the investigation of WOBE437, a reported inhibitor of anandamide uptake with no known protein target. The effects of WOBE437 on anandamide uptake and metabolism are investigated, and a photoaffinity probe is used to identify the protein targets of this inhibitor. **Chapter 7** demonstrates the use of cyclopropene lipids to perform live-cell fluorescence microscopy using quenched fluorophores. A cyclopropene-modified version of arachidonic acid is synthesized for the purpose of studying anandamide transport and localization in real-time. **Chapter 8** summarizes the work described in this thesis and provides future directions.

## References

- (1) Vane, J. R. Inhibition of Prostaglandin Synthesis as a Mechanism of Action for Aspirin-like Drugs. *Nature. New Biol.* **1971**, *231* (25), 232–235.
- (2) Pandey, R.; Mousawy, K.; Nagarkatti, M.; Nagarkatti, P. Endocannabinoids and Immune Regulation. *Pharmacol. Res.* **2009**, *60* (2), 85–92.
- (3) Serhan, C. N.; Petasis, N. A. Resolvins and Protectins in Inflammation Resolution. *Chem. Rev.* **2011**, *111* (10), 5922–5943.
- (4) Marshall-Gradisnik, S.; Green, R.; Brenu, E.; Weatherby, R. Anabolic Androgenic Steroids Effects on the Immune System: A Review. *Open Life Sci.* **2009**, *4* (1), 19–33.
- (5) Mora, J. R.; Iwata, M.; Andrian, U. H. V. Vitamin Effects on the Immune System. *Nat. Rev. Immunol.* **2008**, *8* (9), 685–698.
- (6) Fahy, E.; Cotter, D.; Sud, M.; Subramaniam, S. Lipid Classification, Structures and Tools. *Biochim. Biophys. Acta* **2011**, *1811* (11), 637–647.
- (7) Fahy, E.; Subramaniam, S.; Murphy, R. C.; Nishijima, M.; Raetz, C. R. H.; Shimizu, T.; Spener, F.; Meer, G. van; Wakelam, M. J. O.; Dennis, E. A. Update of the LIPID MAPS Comprehensive Classification System for Lipids. *J. Lipid Res.* **2009**, *50*, S9–S14.
- (8) Yang, K.; Han, X. Lipidomics: Techniques, Applications, and Outcomes Related to Biomedical Sciences. *Trends Biochem. Sci.* **2016**, *41* (11), 954–969.
- (9) Wenk, M. R. The Emerging Field of Lipidomics. *Nat. Rev. Drug Discov.* **2005**, *4* (7), 594–610.
- (10) Wenk, M. R. Lipidomics: New Tools and Applications. *Cell* **2010**, *143*, 888–895.
- (11) Berger, J.; Moller, D. E. The Mechanisms of Action of PPARs. *Annu. Rev. Med.* **2002**, *53* (1), 409–435.
- (12) Tan, J. K.; McKenzie, C.; Mariño, E.; Macia, L.; Mackay, C. R. Metabolite-Sensing G Protein-Coupled Receptors—Facilitators of Diet-Related Immune Regulation. *Annu. Rev. Immunol.* **2017**, *35* (1), 371–402.
- (13) Oh, D. Y.; Talukdar, S.; Bae, E. J.; Imamura, T.; Morinaga, H.; Fan, W.; Li, P.; Lu, W. J.; Watkins, S. M.; Olefsky, J. M. GPR120 Is an Omega-3 Fatty Acid Receptor Mediating Potent Anti-Inflammatory and Insulin-Sensitizing Effects. *Cell* **2010**, *142* (5), 687–698.
- (14) Nelson, D. L.; Lehninger, A. L.; Cox, M. M. *Lehninger Principles of Biochemistry*; Macmillan, 2008.
- (15) Calder, P. C. Docosahexaenoic Acid. *Ann. Nutr. Metab.* **2016**, *69* (Suppl. 1), 8–21.
- (16) Spector, A. A. Essentiality of Fatty Acids. *Lipids* **1999**, *34* (1), S1–S3.
- (17) Hengeveld, L. M.; Praagman, J.; Beulens, J. W. J.; Brouwer, I. A.; van der Schouw, Y. T.; Sluijs, I. Fish Consumption and Risk of Stroke, Coronary Heart Disease, and Cardiovascular Mortality in a Dutch Population with Low Fish Intake. *Eur. J. Clin. Nutr.* **2018**, *72* (7), 942–950.
- (18) Larrieu, T.; Layé, S. Food for Mood: Relevance of Nutritional Omega-3 Fatty Acids for Depression and Anxiety. *Front. Physiol.* **2018**, *9*, 1047.
- (19) Bazinet, R. P.; Layé, S. Polyunsaturated Fatty Acids and Their Metabolites in Brain Function and Disease. *Nat. Rev. Neurosci.* **2014**, *15* (12), 771–785.
- (20) Calder, P. C. Marine Omega-3 Fatty Acids and Inflammatory Processes: Effects, Mechanisms and Clinical Relevance. *Biochim. Biophys. Acta BBA - Mol. Cell Biol. Lipids* **2015**, *1851* (4), 469–484.
- (21) Calder, P. C. Omega-3 Fatty Acids and Inflammatory Processes: From Molecules to Man. *Biochem. Soc. Trans.* **2017**, *45* (5), 1105–1115.
- (22) Serhan, C. N.; Levy, B. D. Resolvins in Inflammation: Emergence of the pro-Resolving Superfamily of Mediators. *J. Clin. Invest.* **2018**, *128* (7), 2657–2669.
- (23) Salem, N.; Litman, B.; Kim, H.-Y.; Gawrisch, K. Mechanisms of Action of Docosahexaenoic Acid in the Nervous System. *Lipids* **2001**, *36* (9), 945–959.
- (24) Liu, J. J.; Green, P.; John Mann, J.; Rapoport, S. I.; Sublette, M. E. Pathways of Polyunsaturated Fatty Acid Utilization: Implications for Brain Function in Neuropsychiatric Health and Disease. *Brain Res.* **2015**, *1597*, 220–246.
- (25) Müller, C. P.; Reichel, M.; Mühle, C.; Rhein, C.; Gulbins, E.; Kornhuber, J. Brain Membrane Lipids in Major Depression and Anxiety Disorders. *Biochim. Biophys. Acta BBA - Mol. Cell Biol. Lipids* **2015**, *1851* (8), 1052–1065.
- (26) Kiecolt-Glaser, J. K.; Belury, M. A.; Porter, K.; Beversdorf, D. Q.; Lemeshow, S.; Glaser, R. Depressive Symptoms, Omega-6:Omega-3 Fatty Acids, and Inflammation in Older Adults. *Psychosom. Med.* **2007**, *69* (3), 217–224.
- (27) Calder, P. C. N-3 Polyunsaturated Fatty Acids, Inflammation, and Inflammatory Diseases. *Am. J. Clin. Nutr.* **2006**, *83* (6), 1505S–1519S.
- (28) Geleijnse, J. M.; Giltay, E. J.; Grobbee, D. E.; Donders, A. R. T.; Kok, F. J. Blood Pressure Response to Fish Oil Supplementation: Metaregression Analysis of Randomized Trials. *J. Hypertens.* **2002**, *20* (8), 1493–1499.
- (29) Nestel, P.; Shige, H.; Pomeroy, S.; Cehun, M.; Abbey, M.; Raederstorff, D. The N-3 Fatty Acids Eicosapentaenoic Acid and Docosahexaenoic Acid Increase Systemic Arterial Compliance in Humans. *Am. J. Clin. Nutr.* **2002**, *76* (2), 326–330.

## Chapter 1

- (30) von Schacky, C. Omega-3 Fatty Acids: Antiarrhythmic, Proarrhythmic or Both? *Curr. Opin. Clin. Nutr. Metab. Care* **2008**, *11* (2), 94–99.
- (31) Foundation, B. N. *Unsaturated Fatty Acids: Nutritional and Physiological Significance: The Report of the British Nutrition Foundation's Task Force*; Chapman & Hall, 1992.
- (32) Aung, T.; Halsey, J.; Kromhout, D.; Gerstein, H. C.; Marchioli, R.; Tavazzi, L.; Geleijnse, J. M.; Rauch, B.; Ness, A.; Galan, P.; Chew, E. Y.; Bosch, J.; Collins, R.; Lewington, S.; Armitage, J.; Clarke, R. Associations of Omega-3 Fatty Acid Supplement Use With Cardiovascular Disease Risks: Meta-Analysis of 10 Trials Involving 77 917 Individuals. *JAMA Cardiol.* **2018**, *3* (3), 225–233.
- (33) Abdelhamid, A. S.; Brown, T. J.; Brainard, J. S.; Biswas, P.; Thorpe, G. C.; Moore, H. J.; Deane, K. H.; AlAbdulghafoor, F. K.; Summerbell, C. D.; Worthington, H. V.; Song, F.; Hooper, L. Omega-3 Fatty Acids for the Primary and Secondary Prevention of Cardiovascular Disease. *Cochrane Database Syst. Rev.* **2018**, No. 11.
- (34) de Bus, I.; Witkamp, R.; Zuilhof, H.; Albada, B.; Balvers, M. The Role of N-3 PUFA-Derived Fatty Acid Derivatives and Their Oxygenated Metabolites in the Modulation of Inflammation. *Prostaglandins Other Lipid Mediat.* **2019**, *144*, 106351.
- (35) Bannenberg, G. L.; Chiang, N.; Ariel, A.; Arita, M.; Tjonahen, E.; Gotlinger, K. H.; Hong, S.; Serhan, C. N. Molecular Circuits of Resolution: Formation and Actions of Resolvins and Protectins. *J. Immunol.* **2005**, *174* (7), 4345–4355.
- (36) Brown, M. S.; Goldstein, J. L. Cholesterol Feedback: From Schoenheimer's Bottle to Scap's MELADL. *J. Lipid Res.* **2009**, *50* (Supplement), S15–S27.
- (37) Wüstner, D. Fluorescent Sterols as Tools in Membrane Biophysics and Cell Biology. *Chem. Phys. Lipids* **2007**, *146* (1), 1–25.
- (38) Gimpl, G.; Gehrig-Burger, K. Probes for Studying Cholesterol Binding and Cell Biology. *Steroids* **2011**, *76* (3), 216–231.
- (39) Laguerre, A.; Schultz, C. Novel Lipid Tools and Probes for Biological Investigations. *Curr. Opin. Cell Biol.* **2018**, *53*, 97–104.
- (40) Sezgin, E.; Can, F. B.; Schneider, F.; Clausen, M. P.; Galiani, S.; Stanly, T. A.; Waithe, D.; Colaco, A.; Honigmann, A.; Wüstner, D.; Platt, F.; Eggeling, C. A Comparative Study on Fluorescent Cholesterol Analogs as Versatile Cellular Reporters. *J. Lipid Res.* **2016**, *57* (2), 299–309.
- (41) Gaebler, A.; Milan, R.; Straub, L.; Hoelper, D.; Kuerschner, L.; Thiele, C. Alkyne Lipids as Substrates for Click Chemistry-Based in Vitro Enzymatic Assays. *J. Lipid Res.* **2013**, *54* (8), 2282–2290.
- (42) Robichaud, P. P.; Poirier, S. J.; Boudreau, L. H.; Doiron, J. A.; Barnett, D. A.; Boilard, E.; Surette, M. E. On the Cellular Metabolism of the Click Chemistry Probe 19-Alkyne Arachidonic Acid. *J. Lipid Res.* **2016**, *57* (10), 1821–1830.
- (43) Hein, J. E.; Fokin, V. V. Copper-Catalyzed Azide–Alkyne Cycloaddition (CuAAC) and beyond: New Reactivity of Copper(I) Acetylides. *Chem. Soc. Rev.* **2010**, *39* (4), 1302–1315.
- (44) Wright, M. H.; Paape, D.; Storck, E. M.; Serwa, R. A.; Smith, D. F.; Tate, E. W. Global Analysis of Protein N-Myristoylation and Exploration of N-Myristoyltransferase as a Drug Target in the Neglected Human Pathogen Leishmania Donovani. *Chem. Biol.* **2015**, *22* (3), 342–354.
- (45) Storck, E. M.; Morales-Sanfrutos, J.; Serwa, R. A.; Panyain, N.; Lanyon-Hogg, T.; Tolmachova, T.; Ventimiglia, L. N.; Martin-Serrano, J.; Seabra, M. C.; Wojciak-Stothard, B.; Tate, E. W. Dual Chemical Probes Enable Quantitative System-Wide Analysis of Protein Prenylation and Prenylation Dynamics. *Nat. Chem.* **2019**, *11* (6), 552–561.
- (46) Gaebler, A.; Penno, A.; Kuerschner, L.; Thiele, C. A Highly Sensitive Protocol for Microscopy of Alkyne Lipids and Fluorescently Tagged or Immunostained Proteins. *J. Lipid Res.* **2016**, *57* (10), 1934–1947.
- (47) Tate, E. W.; Kalesh, K. A.; Lanyon-Hogg, T.; Storck, E. M.; Thinon, E. Global Profiling of Protein Lipidation Using Chemical Proteomic Technologies. *Curr. Opin. Chem. Biol.* **2015**, *24*, 48–57.
- (48) Hofmann, K.; Thiele, C.; Schött, H.-F.; Gaebler, A.; Schoene, M.; Kiver, Y.; Friedrichs, S.; Lütjohann, D.; Kuerschner, L. A Novel Alkyne Cholesterol to Trace Cellular Cholesterol Metabolism and Localization. *J. Lipid Res.* **2014**, *55* (3), 583–591.
- (49) Thiele, C.; Papan, C.; Hoelper, D.; Kusserow, K.; Gaebler, A.; Schoene, M.; Piotrowitz, K.; Lohmann, D.; Spandl, J.; Stevanovic, A.; Shevchenko, A.; Kuerschner, L. Tracing Fatty Acid Metabolism by Click Chemistry. *ACS Chem. Biol.* **2012**, *7* (12), 2004–2011.
- (50) Gaebler, A.; Milan, R.; Straub, L.; Hoelper, D.; Kuerschner, L.; Thiele, C. Alkyne Lipids as Substrates for Click Chemistry-Based in Vitro Enzymatic Assays. *J. Lipid Res.* **2013**, *54* (8), 2282–2290.
- (51) Thiele, C.; Wunderling, K.; Leyendecker, P. Multiplexed and Single Cell Tracing of Lipid Metabolism. *Nat. Methods* **2019**, *16* (11), 1123–1130.
- (52) Jamieson, L. E.; Greaves, J.; McLellan, J. A.; Munro, K. R.; Tomkinson, N. C. O.; Chamberlain, L. H.; Faulds, K.; Graham, D. Tracking Intracellular Uptake and Localisation of Alkyne Tagged Fatty Acids Using Raman Spectroscopy. *Spectrochim. Acta. A. Mol. Biomol. Spectrosc.* **2018**, *197*, 30–36.
- (53) Niphakis, M. J.; Lum, K. M.; Cognetta III, A. B.; Correia, B. E.; Ichu, T.-A.; Olucha, J.; Brown, S. J.; Kundu, S.; Piscitelli, F.; Rosen, H.; Cravatt, B. F. A Global Map of Lipid-Binding Proteins and Their Ligandability in Cells. *Cell* **2015**, *161* (7), 1668–1680.

- (54) Haberkant, P.; Raijmakers, R.; Wildwater, M.; Sachsenheimer, T.; Brügger, B.; Maeda, K.; Houweling, M.; Gavin, A.-C.; Schultz, C.; van Meer, G.; Heck, A. J. R.; Holthuis, J. C. M. In Vivo Profiling and Visualization of Cellular Protein–Lipid Interactions Using Bifunctional Fatty Acids. *Angew. Chem. Int. Ed.* **2013**, *52* (14), 4033–4038.
- (55) Peng, T.; Hang, H. C. Bifunctional Fatty Acid Chemical Reporter for Analyzing S-Palmitoylated Membrane Protein–Protein Interactions in Mammalian Cells. *J. Am. Chem. Soc.* **2015**, *137* (2), 556–559.
- (56) Haberkant, P.; Holthuis, J. C. M. Fat & Fabulous: Bifunctional Lipids in the Spotlight. *Biochim. Biophys. Acta BBA - Mol. Cell Biol. Lipids* **2014**, *1841* (8), 1022–1030.
- (57) Haberkant, P.; Stein, F.; Höglunger, D.; Gerl, M. J.; Brügger, B.; Van Veldhoven, P. P.; Krijgsveld, J.; Gavin, A.-C.; Schultz, C. Bifunctional Sphingosine for Cell-Based Analysis of Protein-Sphingolipid Interactions. *ACS Chem. Biol.* **2016**, *11* (1), 222–230.



# Chapter 2

## Lipid photoaffinity probes<sup>1</sup>

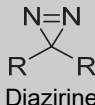
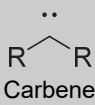
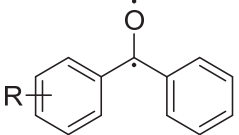
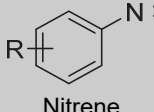
### Introduction

Photoactivatable lipids are synthetic analogues of natural lipids that are designed to retain the overall structure and interactions of the parent lipid, and contain a photoactivatable moiety that can form an irreversible covalent bond with its protein interacting partner upon irradiation. This covalent bond essentially ‘freezes’ the interaction and allows for investigation of lipid-protein interactions as they occur in their complex native environments.<sup>2</sup>

To generate a photoaffinity probe, a number of photoreactive moieties are available with differing synthetic accessibility, reactivity, efficiency and structural impact. Three photoreactive groups are routinely used: diazirines, benzophenones and aryl azides (Table 1). The reactivity of the highly energetic intermediates formed upon irradiation affects their labeling properties. The reactive carbene formed upon irradiation of a diazirine reacts for a significant portion with water or intramolecularly, reducing its labeling efficiency. However, its reactivity ensures a short half-life, allowing less time for the probe to diffuse and react nonspecifically (that is, with proteins other than its natural interaction partner).<sup>3</sup> Nonetheless, some of the excited diazirine isomerizes to the linear diazo form, which has a longer lifetime and is less reactive. Irradiation of a benzophenone results in the formation of a less reactive diradical, which has more time to diffuse and to react nonspecifically.<sup>4</sup> However, it favors the insertion into C-H bonds as reaction with water results in a reversible hydrate, thereby yielding higher labeling efficiencies.<sup>5</sup>

Irradiation of an aryl azide leads to the formation of a nitrene, which has a high reactivity, but like the diazirine, suffers from spontaneous rearrangement reactions resulting in other reactive species with a longer lifetime.<sup>6</sup> Another drawback of the aryl azide is that the wavelength required to activate an aryl azide is damaging to biological material.

**Table 1 | Structures and properties of most commonly used photoactivatable groups.<sup>5,7,8</sup>**

Structure	Most reactive intermediate	Absorption	Reactivity	Remarks
 Diazirine	 Carbene	Activated at 350-360 nm	High, lifetime 21 ns	Can isomerize to less reactive diazo form
 Benzophenone	 Diradical	Activated at 350-360 nm	Slow, lifetime 80-120 μs	Diradical can collapse to reform the benzophenone
 Aryl azide	 Nitrene	Activated at 254 nm	Medium to high	Can rearrange to form less reactive intermediates

The choice of photoactivatable group depends on a number of factors. Since their conception, lipid probes have seen a shift from benzophenones to diazirines. Contributing factors to this trend have been increased synthesis abilities, the desire for smaller modifications and the application in a relatively water-free inner membrane, where the reactivity of the diazirine is optimal. In this chapter, lipid photoaffinity probes for glycero(phospho)lipids, fatty acyls, sphingolipids and sterols reported in the last decade and their main discoveries are discussed.

## Lipid-based photoaffinity probes

### Glycero(phospho)lipids

One of the most well-studied lipid classes is the family of glycero(phospho)lipids. Their amphipathic nature is essential for the formation of lipid bilayers and they are universally present in cellular membranes. Glycerolipids are composed of a glycerol backbone that has been mono-, di- or trisubstituted with a fatty acyl group. In glycerophospholipids, the *sn*-3-position is esterified with a phosphate moiety, which in turn can be substituted with different head groups. The most common substituents are a choline, ethanolamine, glycerol, serine or inositol, thereby giving rise to various classes of glycerophospholipids, such as phosphatidylcholine (PC), phosphatidylethanolamine (PE), phosphatidylglycerol (PG), phosphatidylserine (PS) and phosphatidylinositol (PI), respectively. The length and degree of unsaturation of the fatty acyl groups at the *sn*-1 and *sn*-2 position determine the physical

properties of the glycerophospholipid and its substitution pattern on the phosphate group dictates its protein interactions partners on the membrane surface.<sup>9</sup>

The composition of the different types of lipids and their compartmentalization between cellular substructures does not only determine the physical properties of the biomembrane, but also regulates protein activity, localization and cellular signaling events via lipid-protein interactions. Such types of interactions can be discovered via application of lipid-based photoaffinity probes. Phosphatidylserine lipids, for example, are primarily found on intracellular membrane surfaces. When this asymmetry is disturbed during apoptosis, PS presentation is a trigger for phagocytosis. PS analogues **1-5** (Figure 1), containing a benzophenone and alkyne click handle were developed, and shown to label interacting proteins, such as prothrombin-1.<sup>10</sup>

Phosphatidylcholine-based probes were made to study membrane-associated proteins, which are traditionally underrepresented in proteomic experiments.<sup>11</sup> The goal was to detect proteins interacting with the phospholipid head groups of inner mitochondrial membranes. To this end, a photoreactive group was installed on the solvent-exposed head group of the lipid. Aryl azide probe **6** and benzophenone probe **7** (Figure 1) were used to isolate proteins from *Saccharomyces cerevisiae* mitochondria. The identified targets consisted of known membrane-interacting proteins, including Gut2p and Cox2p, but also new proteins not previously known to be membrane-associated, such as Ald4p and MRP7p. Of note, the authors concluded that aryl azide **6** is the preferred probe due to lower background labeling compared to benzophenone **7**.<sup>11</sup>

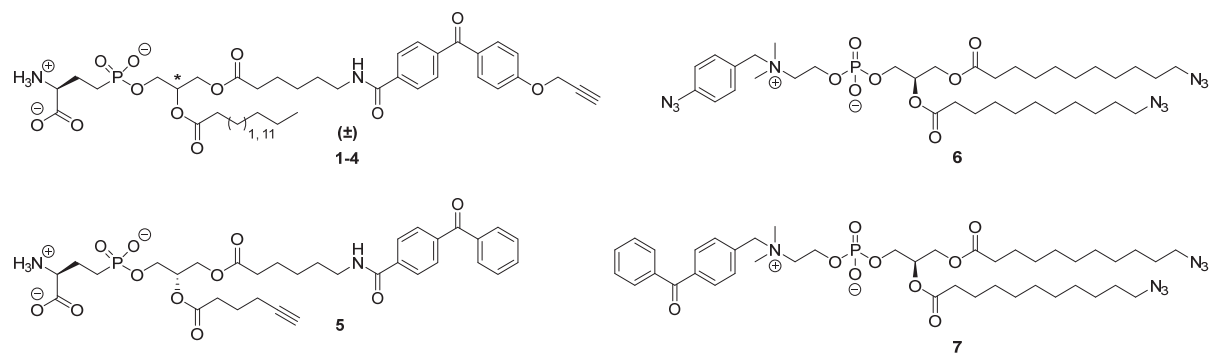


**Figure 1 |** Structures of photoaffinity probes based on phosphatidylserine **1-5** and phosphatidylcholine **6-7**.

Phosphatidylinositol polyphosphates are a family of signaling lipids that act as anchors for protein association to the membrane. To discover interacting proteins, two probes based on phosphatidylinositol 3,4,5-triphosphate were synthesized.<sup>12</sup> Probes **8** and **9** (Figure 2) were tested on the purified pleckstrin homology domain of protein kinase B, a known phosphatidylinositol phosphate binder. Probe **8** gave better signal, which was attributed to its shorter linker length, which positioned the benzophenone closer to the protein. Probe **8** was also applied to MDA-MB-435 cell extracts, which resulted in the identification of 265 phosphatidylinositol 3,4,5-triphosphate-binding proteins.<sup>12</sup> To study the membrane-binding domain of PON1, a high-density lipoprotein (HDL)-associated protein, phospholipid probe **10** was made (Figure 2). Covalent photocrosslinking of **10**, digestion and mass spectrometry analysis resulted in the identification of several closely localized residues on the surface of PON1, revealing the HDL-binding domain.<sup>13</sup>

To study the ability of cardiolipin to form a complex with the mitochondrial protein cytochrome *c*, photoaffinity probes **11-13** were synthesized (Figure 2).<sup>14</sup> These probes all induced similar or higher cytochrome *c* peroxidase activity compared to endogenous tetraoleoyl cardiolipin. This indicated that the central hydroxyl group is not necessary for activation. No follow-up study applying the labeling functionality has appeared yet.<sup>14</sup>

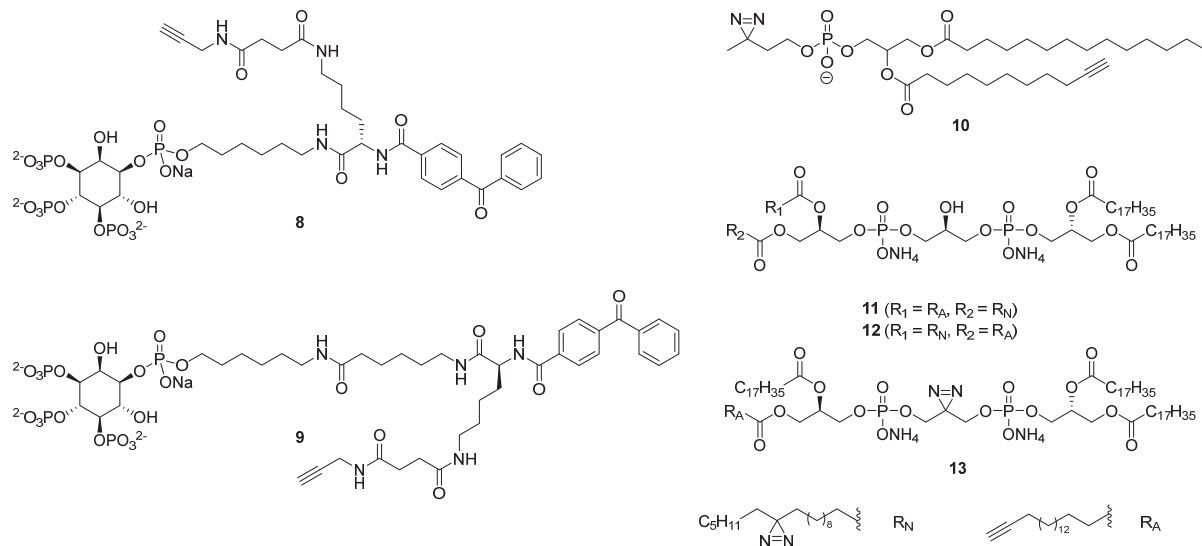


**Figure 2** | Structures of photoaffinity probes based on phosphatidylinositol 3,4,5-triphosphate **8-9**, phospholipid **10** and cardiolipin **11-13**.

Currently, several photoactivatable analogs of phosphatidylcholines are commercially available. It is argued, however, that lipids supplied to a cell are distributed differently than endogenously produced lipids, which are synthesized within the cell. This may distort the interaction profile reported by the probe.<sup>15</sup> Moreover, palmitoyl- and myristoyl-based probes can be incorporated in various glycerolipids or as post-translational modifications (PTMs), thereby further complicating the analysis of a photoaffinity experiment. To solve these issues, Yao and co-workers reported on alkyne-containing choline **14** and diazirine-containing fatty acid **15** (Figure 3).<sup>16</sup> When cells were incubated with these separate probe components, the subsequent photoaffinity experiment only captured the proteins that interact with the *in situ* synthesized phosphatidylcholine probe (**14+15**). This strategy yielded an interaction map of 211 high-confidence PC-interacting proteins, mostly present in the cytosol, endoplasmic reticulum (ER), mitochondria and nucleus. The authors concluded that the double incorporation strategy offered improvement for global mapping of genuine protein-lipid interactions and indicated that the strategy is expandable to different lipid classes, such as phosphatidylinositols.<sup>16</sup>

Monogalactosyldiacylglycerol (MGDG) is a type of anti-inflammatory signaling lipid.<sup>17</sup> Three photoactivatable probes (**16-18**) were synthesized to elucidate its mode of action (Figure 3). The linolenoyl groups were replaced with a similar photoaffinity-click fatty acid (pacFA) or a minimalist linker<sup>18</sup> was added to the sugar moiety. When tested in an inflammatory assay, **16** did not show any activity, while **17** and **18** had comparable activity to MGDG. This indicated that an unmodified galactosyl moiety is essential for MGDG activity. Moreover, when incubated, UV-exposed and washed, **17** lost all anti-inflammatory activity whereas **18** was still active. This implied that **18** was capable of both binding and labeling unidentified targets without disrupting its biological function. With structure **16** as negative control, TLR-4 was identified as a probe target in human chondrocytes. Subsequent orthogonal experiments demonstrated MGDG acted as TLR-4 antagonist.<sup>19</sup>

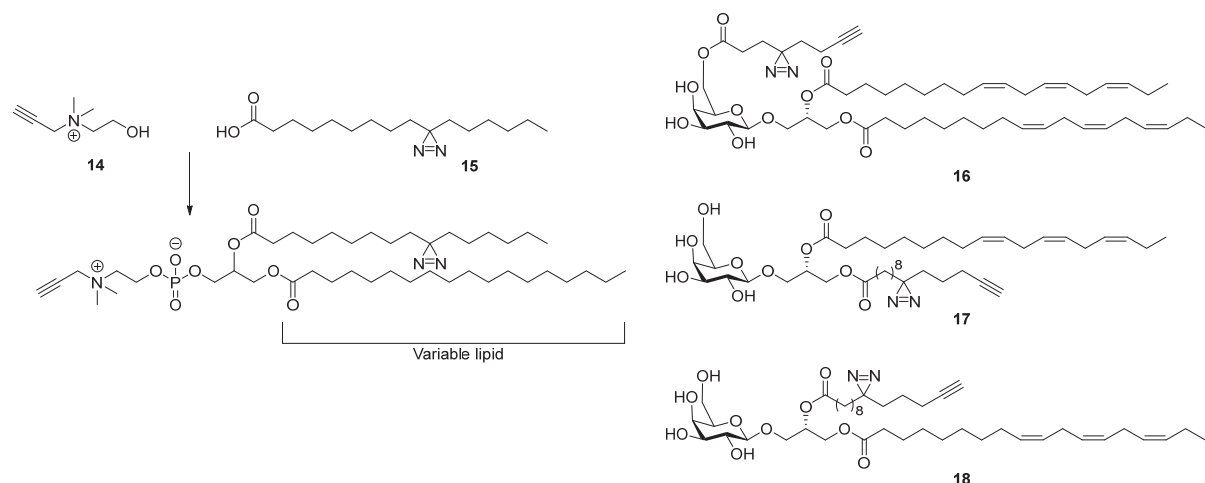


**Figure 3 |** Structures of photoaffinity probes based on phosphatidylcholine **14+15** and dilinolenoyl MGDG **16-18**.

Recently, caged photoaffinity probes based on diacylglycerol (**19**, Figure 4), saturated fatty acid (**20**, Figure 5), and sphingosine (**21**, Figure 6) were developed by Schultz and co-workers.<sup>20</sup> These probes were used to study biologically active signaling molecules with temporal, spatial, and subcellular resolution. The caging groups consists of a fluorescent coumarin group, which prevents recognition of the lipid by the cellular machinery. This caging group can then be released upon irradiation with a wavelength that does not activate the diazirine moiety. Microscopy experiments indicated that all probes were indiscriminately localized to internal membranes and the cytoplasm. Uncaging, photocrosslinking and ligation with a fluorophore showed that each probe localized to distinct cellular components. It also proved feasible to use the uncaging for controlled release of DAG. Elevated DAG levels are known to trigger translocation of C1-domain-containing proteins to the plasma membrane.<sup>21</sup> When **19** was uncaged in HeLa cells, immediate translocation of C1-linked green fluorescent protein (GFP) was observed.<sup>20</sup> Moreover, DAG turnover could be quantified on a population-wide and single-cell level. The authors suggested that standard biochemical experiments to measure DAG metabolism are inherently flawed, since they only measure combined lipid transport and metabolism. Moreover, striking differences were found between DAG turnover on a cell-to-cell level, indicating that heterogeneity might be an underrated complication of lipid signaling.<sup>20</sup> In addition, a pulldown experiment with probes **19-21** was performed using HeLa cell proteome affording 130 **19**-specifically binding proteins. As the probe contains arachidonic acid, the hits were compared to the targets of arachidonic acid-based probes **22** and **23** (Figure 5). Remarkably, only 17 of the proteins identified using DAG probe **19** were previously identified with probes **22** and **23**, showing that probe **19** has mostly genuine DAG-specific interactions. Overall, the two activatable functionalities within the probe allowed to investigate different aspects of the lipids such as the protein interaction partners, metabolism and signaling functions.<sup>20</sup>

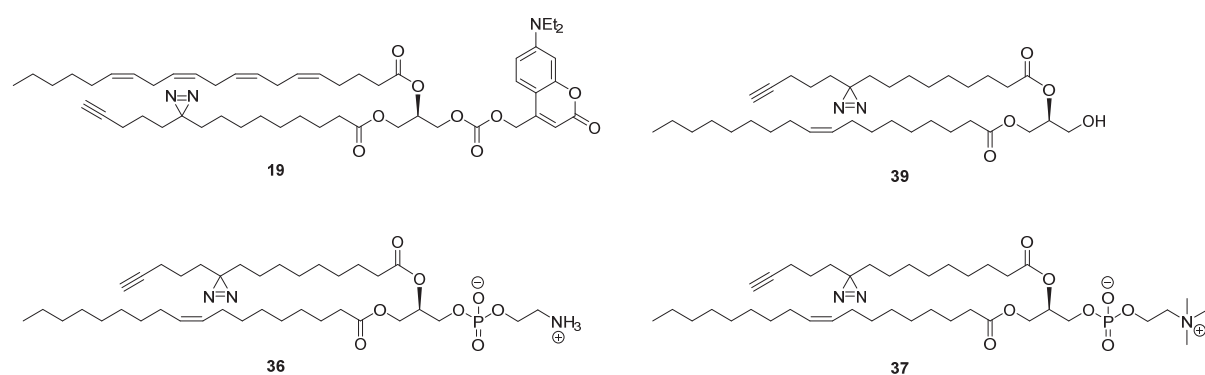


**Figure 4 |** Structures of photoaffinity probes based on diacylglycerol **19** and **39**, phosphatidylethanolamide **36** and phosphatidylcholine **37**.

## Fatty acids and their derivatives

Fatty acids are constituents of other lipid classes, such as glycerol(phospho)lipids, glycolipids and ceramides, but they also have their own signaling roles. In addition, they can be incorporated in proteins as post-translational modification (PTM), thereby anchoring the protein to the membrane. Furthermore, oxidative enzymes, such as lipoxygenases, cyclooxygenases and cytochrome P450s metabolize polyunsaturated fatty acids into bioactive signaling molecules. For example, endothelium-derived epoxyeicosatrienoic acids (EETs) are lipid signaling molecules with various biological activities.<sup>22</sup> In search of a high-affinity G protein-coupled EET receptor for 14,15-epoxyeicosatrienoic acid, epoxide-containing lipid **24** equipped with a photoactivatable aryl azide and radioactive iodide as reporter group was synthesized (Figure 5). The probe showed EET agonist activity and labeled a 47 kDa band which could be outcompeted with several EET agonists and antagonists.<sup>23</sup> However, with no bioorthogonal ligation handle present, the protein could not be identified.

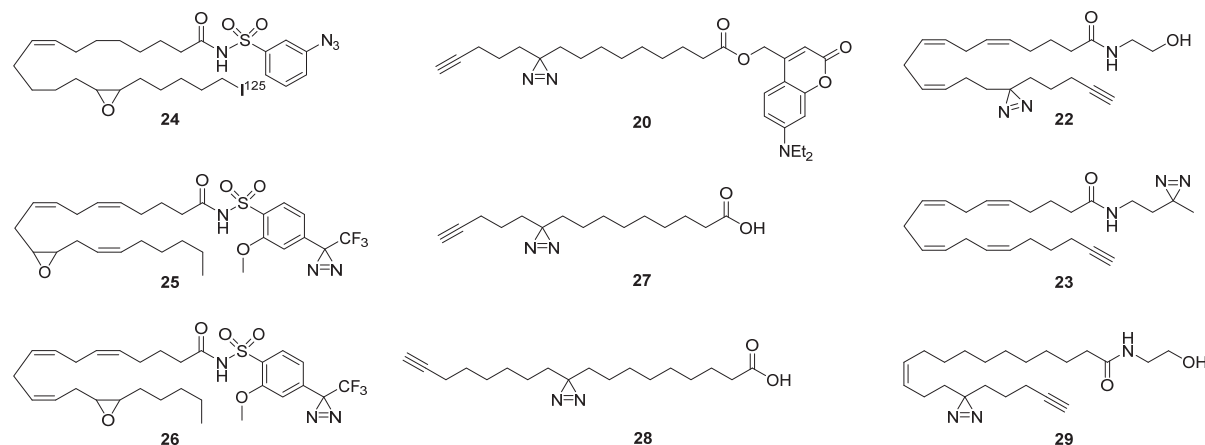


**Figure 5 |** Structures of photoaffinity probes based on 14,15-epoxyeicosatrienoic acid **24-26**, bifunctional lipid probes **27-28**, trifunctional lipid probe **20**, anandamide-based probes **22**, **23** and probe **29**.

The structurally related probes **25** and **26** (Figure 5) have been used to study the binding mode of EETs in the soluble epoxide hydrolase (sEH) enzyme.<sup>24</sup> Photoaffinity experiments combined with computational modeling indicated that the stereochemistry of the epoxide dictates the binding orientation of the substrate into the enzyme.

Bifunctional probe **27** (Figure 5) was synthesized to study *in vivo* protein-lipid interactions.<sup>2</sup> Fatty acids can be incorporated in different lipid classes and in proteins as PTM. Proteomic analysis using **27** resulted in the identification of a large number of lipid-interacting proteins in CHO and HeLa cells. Enrichment of proteins by UV irradiation indicated noncovalent interactions, while proteins that were enriched in the absence of UV irradiation were designated as putative palmitoylated proteins. This observation was supported by an increase in identified palmitoylated proteins when the incubation time was increased. The authors continued by demonstrating the usage of the probe to visualize lipid-interacting proteins in

nematode larvae using fluorescence microscopy. Overall, this report demonstrates the versatility of bifunctional probes in studying protein-lipid interactions.<sup>2</sup>

Other groups have also exploited metabolic incorporation of lipids as PTM. For example, probe **28** (Figure 5) was incorporated in S-palmitoylated membrane proteins.<sup>25</sup> The photoaffinity group allowed the capture of protein-protein interactions of interferon-induced transmembrane protein 3 (IFITM3), a protein with antiviral properties. This method was validated by studying VAPA—a known interaction partner of IFITM3—after which a pulldown experiment afforded 12 novel interaction partners of IFITM3.<sup>25</sup>

Anandamide is a signaling lipid involved in neurotransmission. To map anandamide-binding proteins, photoaffinity probes **22** and **23** were synthesized in the lab of Cravatt. More than a thousand interacting proteins were identified in Neuro-2a and HEK-293 cells, including NUCB1, NENF and VAT1. Probes **22** and **23** were subsequently employed to discover ligands for the lipid-binding pockets of said targets using competitive fluorescence polarization assays.<sup>26</sup> In addition, lipid probes **22**, **23** and oleoylethanolamide-based **29** (Figure 5) were utilized in another study to determine the selectivity profile of small molecules occupying lipid-binding pockets. This strategy was referred to as lipid-protein interaction profiling (LiPIP).<sup>27</sup>

## Sphingolipids

Sphingolipids are lipids that have sphingosine or a sphingosine derivative as a scaffold. Similar to glycerolipids, most of the sphingolipids exist in the form of a phosphate ester and have a fatty acyl attached through an amide bond. Sphingomyelin, one of the most common sphingolipids, serves mainly a structural purpose, but its derivatives are increasingly recognized as important signaling molecules.

The last decade has witnessed a continuous progression in the development of chemical probes to identify sphingolipid-binding proteins. For example, Haberkant *et al.* have synthesized tritium-functionalized probes **30** and **31** (Figure 6), which are rapidly incorporated into sphingolipids when applied to tissue cultures.<sup>28</sup> Caveolin-1 and nicastrin were identified as sphingolipid-interacting proteins. In 2010, photoactivatable sphingosine **32** (Figure 6) was made and co-incubated with radioactive [<sup>3</sup>H]choline in fibroblasts from healthy subjects or patients with Niemann-Pick A disease.<sup>29</sup> The sphingomyelin storage was found to be dysregulated in fibroblasts of the patients.

In 2015, Schultz and co-workers developed photoaffinity-click sphingosine (pacSph) **33** (Figure 6), which was used to identify 186 pacSph-interacting proteins.<sup>30</sup> As a control, fatty acid probe **27** was used. Although probes **27** and **33** are based on different lipids and are metabolized via different pathways, substantial overlap between the interacting proteins was found. Four potential issues were mentioned: (i) both lipid probes could be incorporated into

phosphatidyl choline lipids, (ii) proteins may have two or more lipid-binding sites, (iii) a single lipid-binding site may be able to recognize multiple lipids, and (iv) alterations made on the lipids may alter their physiochemical properties.<sup>30</sup> Nevertheless, pacSph probe **33** proved to be a more versatile tool to discover new sphingosine-binding proteins compared to **30** and **31**. The probe was further developed into trifunctional pacSph **21**, which was used in similar experiments to afford 64 pacSph-specific binding proteins after uncaging,<sup>20</sup> of which only 14 were also found using non-caged pacSph **33**.

Since pacSph **33** has become commercially available, other groups have also employed it in their research of sphingolipids. PacSph **33** was used to distinguish between sphingolipid-protein interactions resulting from ceramides synthesized through ceramide synthase 5 (CerS5) or CerS6. This resulted in the discovery that only CerS6-derived sphingolipids bind to the mitochondrial fission factor (Mff).<sup>31</sup> In another study, pacSph **33** was used to visualize the localization of pacSph by microscopy and its binding to the SPCA1 calcium pump in gel-based experiments.<sup>32</sup>

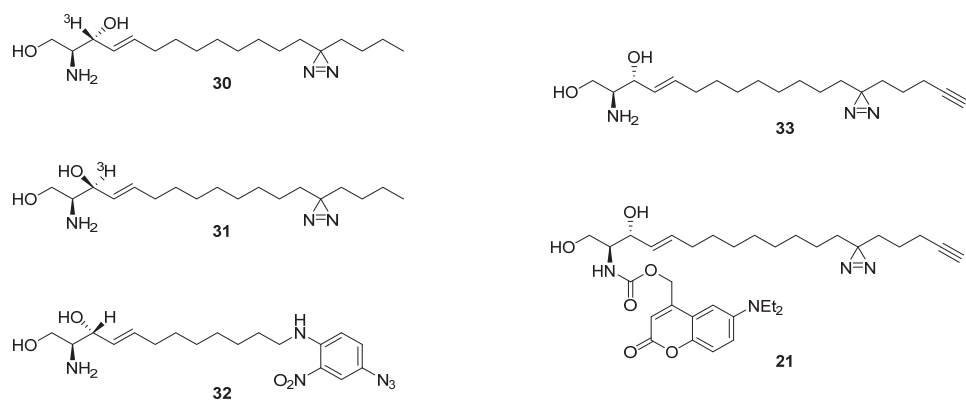


**Figure 6 |** Structures of photoaffinity probes based on sphingosine **30**, **31**, **32**, **33** and **21**.

Ceramide, a sphingosine containing a fatty acyl amide, is a signaling molecule with pro-apoptotic activity. In search of ceramide-binding proteins, photoaffinity probes **34-39** (Figures 4, 7) with pacFA **27** as basis were developed by Holthuis and co-workers.<sup>33</sup> The targets of ceramide probe (pacCer) **34** were compared to the interaction partners of glucosylceramide (pacGlcCer) **35** in cytosolic fractions of various cell lines. A protein with a STAR-related lipid-transfer domain, CERT, was chosen as model protein to study structure-activity relationships of the lipid-binding pocket. This was done using probes **34-39** to distinguish probe-specific interactions (Figures 4, 7).<sup>33</sup> This set of probes was used by the same group to study ceramide binding to VDAC2, which was found to be a direct effector of ceramide-mediated cell death.<sup>34</sup> Since it has become commercially available, other groups have used pacCer **34** to study its binding to tubulin<sup>35</sup> and downstream effect on VDAC1 closure in mitochondria.<sup>36</sup>

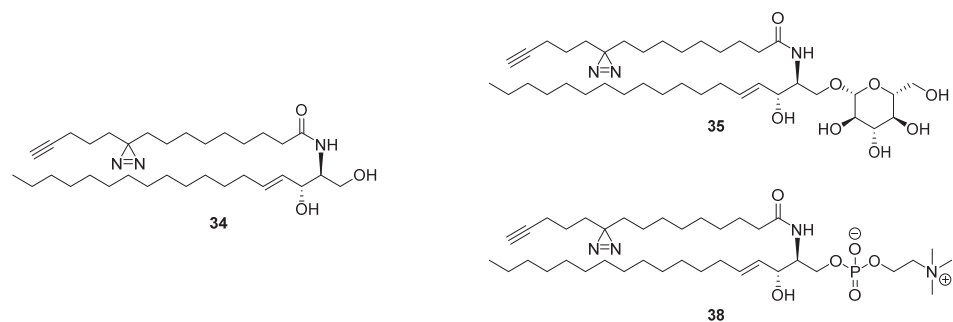


**Figure 7 |** Structures of photoaffinity probes based on ceramide **34**, glucosylceramide **35** and sphingomyelin **38**.

## Sterols

Sterols are lipids with rigid, fused rings with one or more hydroxyl groups, which gives them amphiphilic properties. Cholesterol is the most abundant sterol found in mammalian cells. Cholesterol alters the fluidity of the membrane and is a constituent of lipid rafts, which are liquid-ordered regions of the plasma membrane high in cholesterol and glycosphingolipids, sequestering specific proteins.<sup>37</sup> The lipid environment alters the biological properties of the embedded proteins. The noncovalent interaction of sterols to proteins, specifically in lipid rafts, has received a surge of interest in recent years.

Various types of cholesterol-based probes have been synthesized (Figure 8). Structures **40-42** are diastereomers which showed similar protein labeling patterns on gel with the most intense labeling by the trans-sterol structure **40**.<sup>38</sup> In a large-scale proteomics experiment in cells using probe **40**, about 850 proteins were found to be UV-enriched. Nearly 700 of these proteins showed preference over a palmitoylethanolamide-based probe and could be annotated as cholesterol-interacting proteins.

Compounds **43** and **44** were synthesized to map cholesterol binding sites in VDAC1 (Figure 8). Purified recombinantly expressed mouse VDAC1 was used in a top-down and bottom-up proteomics analysis to map the binding pocket. The binding site was found to include Thr83 and Glu73.<sup>39</sup> To study the transfer of cholesterol between NPC1 and NPC2, the linked cholesterol pair **45** has been synthesized to stabilize the protein transition state during the hand-off (Figure 8). Supported by previous studies, the probe was thought to stabilize protein dimer complexes, but no follow-up report has appeared yet.<sup>40</sup>

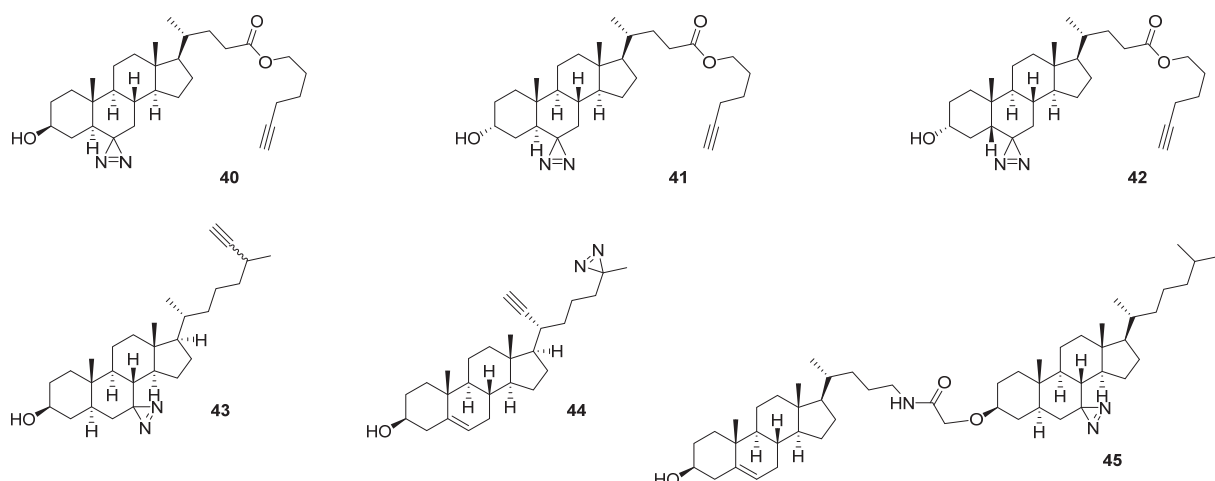


**Figure 8 |** Structures of photoaffinity probes based on cholesterol **40-45**.

Bile acids are sterols that aid in digestion of dietary lipids, but may also act as signaling molecules regulating lipid and glucose metabolism.<sup>41</sup> Three probes based on bile acids have been synthesized with the diazirine and alkyne located on different parts of the sterol.<sup>42</sup> Probes **46-48** (Figure 9) afforded 331 proteins that were labeled by all three structures and outcompeted with a twofold excess of competitor. Three known and three unknown bile acid binding proteins were validated by overexpression, labeling with or without a competitor and immunoblotting. Of note, 146 of these probe targets were shared by cholesterol probe **40**.<sup>38,42</sup>

The development of betulinic acid-based probes, including photoactivatable probes **49** and **50** (Figure 9), has been reported.<sup>43</sup> Probe **49** was armed with a 2-aryl-5-carboxytetrazole, a recently developed photoactivatable linker with high crosslinking efficiency.<sup>44</sup> A pulldown experiment performed with both probes afforded 150 probe targets, which were subsequently triaged using control experiments. This afforded 9 and 13 unique proteins identified by structure **49** and **50**, respectively. Surprisingly, there was no overlap in protein targets between the two probes, which was rationalized by the difference in location and reactivity of the photoactivatable groups.

To explore the molecular mechanisms of oleanolic acid, two probes based on this sterol have been synthesized.<sup>45</sup> To test functional similarity to the parent structure, they were tested in a RMGPa inhibition assay, where **51** showed a twofold and **52** (Figure 9) a fivefold reduction of potency compared to oleanolic acid. Probe **51** labeled two gel bands UV-dependently in soluble proteomes prepared from HepG2 cells which could be outcompeted with oleanolic acid, but the probe targets were not identified.<sup>45</sup>

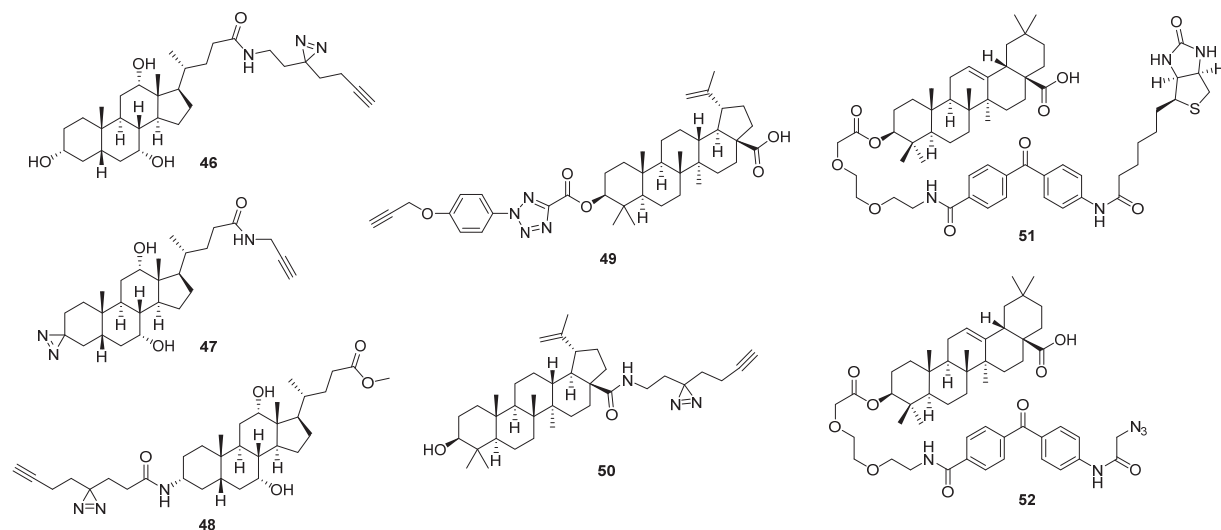


**Figure 9 |** Structures of photoaffinity probes based on bile acid **46-48**, betulinic acid **49-50** and on oleanolic acid **51-52**.

## Promiscuous lipid binding proteins

Chemical proteomic datasets contain a large amount of data with a significant amount of noise, making it challenging to distinguish the specific interaction partners of a probe in a pulldown experiment. This necessitates careful design of the experiment with appropriate controls. Due to a bias toward highly abundant proteins and potential co-purification of other proteins with probe targets, the negative controls of a proteomics experiment often do not cover the whole spectrum of background proteins. To combat this problem, twelve laboratories have combined the datasets of >300 negative control experiments to establish a database of common background proteins. This contaminant repository for affinity purification (CRAPome) is a useful database to identify common background proteins.<sup>46</sup> In case of affinity-based protein profiling, one also needs to keep in mind the specific background labeling proteins associated with each individual photoreactive group, which were mapped by Sieber and co-workers.<sup>47</sup> These datasets can be used to triage probe hits, but they are limited to background proteins based on the purification method<sup>46</sup> or photoreactive group.<sup>47</sup> When conducting chemical proteomics with lipid probes, one also has to account for the nonspecific interactions due to the inherent lipophilic character of these probes. A different set of background proteins could therefore be envisioned based on hydrophobic interactions with lipid probes.

To compile a database of promiscuous lipid-binding proteins, the reported enriched proteins from representative probes **8, 14, 15, 19, 21, 22, 23, 27, 29, 33, 40** and **47** were combined, compared and ranked. For each probe, the criteria of the authors for assigning probe targets were used. Where possible, the proteins identified in multiple cell lines were used. This resulted in a list of 1367 distinct proteins of which 176 targets were found in  $\geq 4$  experiments (from a total of 11 experiments) (Figure 10A). Of note, only 13 of these proteins were identified as background proteins by the CRAPome (using  $\geq 20\%$  of total entries as cut-off criteria).<sup>46</sup> An overview of the 176 promiscuous lipid-binding proteins can be found in the supplementary information (Table S1). It was found that photoaffinity probes **8, 19** and **21** were highly selective with the smallest number of common targets (Figure 10B). For probe **8**, this was likely due its dissimilarity to the other probes with a highly negative charge at physiological pH. On the other hand, the caging groups of probes **19** and **21** seem to be effective for the reduction of non-specific labeling. All other probes had significant overlap of protein targets, and without diligent controls caution would be advised before calling these targets specific interaction partners.

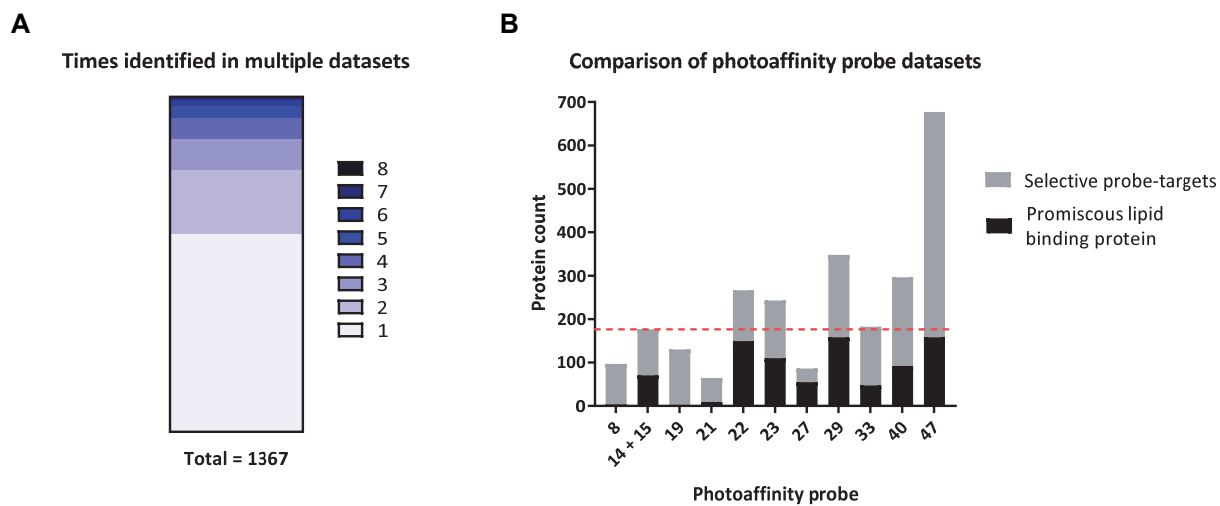


**Figure 10 | Promiscuous lipid binder analysis.** **(A)** Bar graph giving an overview of the amount of times proteins were identified in multiple datasets. In total 1367 proteins were identified of which 176 (13%) were found in at least 4 of the 11 datasets. A list is provided in Table S1. **(B)** Overview of the amount of probe-targets and promiscuous lipid binding proteins identified by each probe. The red line at 176 visualizes the maximum amount of promiscuous lipid binding proteins.

## Conclusion

In summary, the aim of this chapter was to review the lipid-based photoaffinity probes published in the last decade. These probes constituted mainly of glycerol(phospho)lipid-, fatty acid-, sphingolipid- or sterol-based structures. Since the early development of lipid probes, the reported compounds have gained functionality while more closely resembling the structure of their parent lipids. Early probes usually contained benzophenones as reactive handles and a fluorescent or radiolabeled detection tag, which limited their application. Usually, binding to a known protein interaction partner was investigated. Benzophenones and aryl azides have made way for the diazirine moiety, due to the higher reactivity and smaller structural impact of this photoreactive group. The various detection tags on lipid probes have been replaced by an alkyne, which is minimally intrusive while being able to react with a large range of azide reagents. With improved synthetic and commercial access to photoreactive tools, lipid probes are now being used to map global lipid-protein interactions. Increasingly complex biological questions are being addressed, including lipid uptake, metabolism and localization.

There are number of caveats, however, to take into account when using lipid-based photoaffinity probes. For example, non-specific binding proteins, such as membrane-associated and internal membrane-bound proteins, are overrepresented as probe targets. Specific interaction partners might, therefore, be hard to identify. To combat this problem, appropriate controls should be included in the design of the experiment. Conventional competition experiments with an excess of non-probe competitor may give confounding results due to high lipophilicity and membrane accumulation of the competitor lipids.<sup>48</sup> It is, therefore, recommended to include structurally similar, but biologically inactive, probes to obtain a list of specific targets, which should be compared to lists of commonly found targets.<sup>1,46,47</sup> Another challenge is the fast metabolism of exogenous lipids, making it difficult to identify the biologically active lipid species. The addition of a caging group has been a successful strategy to allow for indiscriminate distribution of the probe before activation.<sup>20,49</sup> Lipid metabolism can also be exploited by incorporating the photoreactive and bioorthogonal handle into different lipid species, which results in the formation of a probe molecule *in situ*.<sup>16</sup>

Overall, lipid-based photoaffinity probes are useful chemical tools to study multiple aspects of lipid biology, using different techniques and compatible click reagents. Further development of these tools and their applications will allow for a more complete understanding of the many roles lipids play.

## References

- (1) Koenders, S. T. A.; Gagestein, B.; van der Stelt, M. Opportunities for Lipid-Based Probes in the Field of Immunology. In *Activity-Based Protein Profiling*; Cravatt, B. F., Hsu, K.-L., Weerapana, E., Eds.; Current Topics in Microbiology and Immunology; Springer International Publishing: Cham, 2019; pp 283–319.
- (2) Haberkant, P.; Rajmakers, R.; Wildwater, M.; Sachsenheimer, T.; Brügger, B.; Maeda, K.; Houweling, M.; Gavin, A. C.; Schultz, C.; Van Meer, G.; Heck, A. J. R.; Holthuis, J. C. M. In Vivo Profiling and Visualization of Cellular Protein-Lipid Interactions Using Bifunctional Fatty Acids. *Angew. Chem. - Int. Ed.* **2013**, *52*(14), 4033–4038.
- (3) Bush, J. T.; Walport, L. J.; McGouran, J. F.; Leung, I. K. H.; Berridge, G.; van Berk, S. S.; Basak, A.; Kessler, B. M.; Schofield, C. J. The Ugi Four-Component Reaction Enables Expedient Synthesis and Comparison of Photoaffinity Probes. *Chem. Sci.* **2013**, *4*(11), 4115.
- (4) Sakurai, K.; Ozawa, S.; Yamada, R.; Yasui, T.; Mizuno, S. Comparison of the Reactivity of Carbohydrate Photoaffinity Probes with Different Photoreactive Groups. *ChemBioChem* **2014**, *15*(10), 1399–1403.
- (5) Dormán, G.; Prestwich, G. D. Benzophenone Photophores in Biochemistry. *Biochemistry* **1994**, *33*(19), 5661–5673.
- (6) Buchmueller, K. L.; Hill, B. T.; Platz, M. S.; Weeks, K. M. RNA-Tethered Phenyl Azide Photocrosslinking via a Short-Lived Indiscriminant Electrophile. *J. Am. Chem. Soc.* **2003**, *125*(36), 10850–10861.
- (7) Modarelli, D. A.; Morgan, S.; Platz, M. S. Carbene Formation, Hydrogen Migration, and Fluorescence in the Excited States of Dialkyldiazirines. *J. Am. Chem. Soc.* **1992**, *114*(18), 7034–7041.
- (8) Ford, F.; Yuzawa, T.; Platz, M. S.; Matzinger, S.; Fülscher, M. Rearrangement of Dimethylcarbene to Propene: Study by Laser Flash Photolysis and Ab Initio Molecular Orbital Theory. *J. Am. Chem. Soc.* **1998**, *120*(18), 4430–4438.
- (9) Yeagle, P. L. *The Membranes of Cells*; Academic Press, 2016.
- (10) Bandyopadhyay, S.; Bong, D. Synthesis of Trifunctional Phosphatidylserine Probes for Identification of Lipid-Binding Proteins. *Eur. J. Org. Chem.* **2011**, No. 4, 751–758.
- (11) Gubbens, J.; Ruijter, E.; de Fays, L. E. V.; Damen, J. M. A.; de Kruijff, B.; Slijper, M.; Rijkers, D. T. S.; Liskamp, R. M. J.; de Kroon, A. I. P. M. Photocrosslinking and Click Chemistry Enable the Specific Detection of Proteins Interacting with Phospholipids at the Membrane Interface. *Chem. Biol.* **2009**, *16*(1), 3–14.
- (12) Rowland, M. M.; Bostic, H. E.; Gong, D.; Speers, A. E.; Lucas, N.; Cho, W.; Cravatt, B. F.; Best, M. D. Phosphatidylinositol 3,4,5-Trisphosphate Activity Probes for the Labeling and Proteomic Characterization of Protein Binding Partners. *Biochemistry* **2011**, *50*(51), 11143–11161.
- (13) Gu, X.; Huang, Y.; Levison, B. S.; Gerstenecker, G.; DiDonato, A. J.; Hazen, L. B.; Lee, J.; Gogonea, V.; DiDonato, J. A.; Hazen, S. L. Identification of Critical Paraoxonase 1 Residues Involved in High Density Lipoprotein Interaction. *J. Biol. Chem.* **2016**, *291*(4), 1890–1904.
- (14) Abe, M.; Nakano, M.; Kosaka, A.; Miyoshi, H. Syntheses of Photoreactive Cardiolipins for a Photoaffinity Labeling Study. *Tetrahedron Lett.* **2015**, *56*(17), 2258–2261.
- (15) Peng, T.; Yuan, X.; Hang, H. C. Turning the Spotlight on Protein-Lipid Interactions in Cells. *Curr. Opin. Chem. Biol.* **2014**, *21*, 144–153.
- (16) Wang, D.; Du, S.; Cazenave-Gassiot, A.; Ge, J.; Lee, J. S.; Wenk, M. R.; Yao, S. Q. Global Mapping of Protein–Lipid Interactions by Using Modified Choline-Containing Phospholipids Metabolically Synthesized in Live Cells. *Angew. Chem. - Int. Ed.* **2017**, *56*(21), 5829–5833.
- (17) Ulivi, V.; Lenti, M.; Gentili, C.; Marcolongo, G.; Cancedda, R.; Descalzi Cancedda, F. Anti-Inflammatory Activity of Monogalactosyldiacylglycerol in Human Articular Cartilage in Vitro: Activation of an Anti-Inflammatory Cyclooxygenase-2 (COX-2) Pathway. *Arthritis Res. Ther.* **2011**, *13*(3), R92.
- (18) Li, Z.; Hao, P.; Li, L.; Tan, C. Y. J.; Cheng, X.; Chen, G. Y. J.; Sze, S. K.; Shen, H.-M.; Yao, S. Q. Design and Synthesis of Minimalist Terminal Alkyne-Containing Diazirine Photo-Crosslinkers and Their Incorporation into Kinase Inhibitors for Cell- and Tissue-Based Proteome Profiling. *Angew. Chem. Int. Ed.* **2013**, *52*(33), 8551–8556.
- (19) Liu, X.; Dong, T.; Zhou, Y.; Huang, N.; Lei, X. Exploring the Binding Proteins of Glycolipids with Bifunctional Chemical Probes. *Angew. Chem. - Int. Ed.* **2016**, *55*(46), 14330–14334.
- (20) Höglinder, D.; Nadler, A.; Haberkant, P.; Kirkpatrick, J.; Schifferer, M.; Stein, F.; Hauke, S.; Porter, F. D.; Schultz, C. Trifunctional Lipid Probes for Comprehensive Studies of Single Lipid Species in Living Cells. *Proc. Natl. Acad. Sci.* **2017**, *114*(7), 1566–1571.
- (21) Nadler, A.; Reither, G.; Feng, S.; Stein, F.; Reither, S.; Müller, R.; Schultz, C. The Fatty Acid Composition of Diacylglycerols Determines Local Signaling Patterns. *Angew. Chem. Int. Ed.* **2013**, *52*(24), 6330–6334.
- (22) Spector, A. A.; Fang, X.; Snyder, G. D.; Weintraub, N. L. Epoxyeicosatrienoic Acids (EETs): Metabolism and Biochemical Function. *Prog. Lipid Res.* **2004**, *43*(1), 55–90.
- (23) Chen, Y.; Falck, J. R.; Manthati, V. L.; Jat, J. L.; Campbell, W. B. 20-Iodo-14,15-Epoxyeicos-8(Z)-Enoyl-3-Azidophenylsulfonamide: Photoaffinity Labeling of a 14,15-Epoxyeicosatrienoic Acid Receptor. *Biochemistry* **2011**, *50*(18), 3840–3848.

- (24) Lee, K. S. S.; Henriksen, N. M.; Ng, C. J.; Yang, J.; Jia, W.; Morisseau, C.; Andaya, A.; Gilson, M. K.; Hammock, B. D. Probing the Orientation of Inhibitor and Epoxy-Eicosatrienoic Acid Binding in the Active Site of Soluble Epoxide Hydrolase. *Arch. Biochem. Biophys.* **2017**, *613*, 1–11.
- (25) Peng, T.; Hang, H. C. Bifunctional Fatty Acid Chemical Reporter for Analyzing S-Palmitoylated Membrane Protein-Protein Interactions in Mammalian Cells. *J. Am. Chem. Soc.* **2015**, *137*(2), 556–559.
- (26) Niphakis, M. J.; Lum, K. M.; Cognetta, A. B.; Correia, B. E.; Ichu, T. A.; Olucha, J.; Brown, S. J.; Kundu, S.; Piscitelli, F.; Rosen, H.; Cravatt, B. F. A Global Map of Lipid-Binding Proteins and Their Ligandability in Cells. *Cell* **2015**, *161* (7), 1668–1680.
- (27) Lum, K. M.; Sato, Y.; Beyer, B. A.; Plaisted, W. C.; Anglin, J. L.; Lairson, L. L.; Cravatt, B. F. Mapping Protein Targets of Bioactive Small Molecules Using Lipid-Based Chemical Proteomics. *ACS Chem. Biol.* **2017**, *12* (10), 2671–2681.
- (28) Haberkant, P.; Schmitt, O.; Contreras, F.-X.; Thiele, C.; Hanada, K.; Sprong, H.; Reinhard, C.; Wieland, F. T.; Brügger, B. Protein-Sphingolipid Interactions within Cellular Membranes. *J. Lipid Res.* **2008**, *49* (1), 251–262.
- (29) Aureli, M.; Prioni, S.; Mauri, L.; Loberto, N.; Casellato, R.; Ciampa, M. G.; Chigorno, V.; Prinetti, A.; Sonnino, S. Photoactivable Sphingosine as a Tool to Study Membrane Microenvironments in Cultured Cells. *J. Lipid Res.* **2010**, *51* (4), 798–808.
- (30) Haberkant, P.; Stein, F.; Höglinger, D.; Gerl, M. J.; Brügger, B.; Van Veldhoven, P. P.; Krijgsveld, J.; Gavin, A. C.; Schultz, C. Bifunctional Sphingosine for Cell-Based Analysis of Protein-Sphingolipid Interactions. *ACS Chem. Biol.* **2016**, *11* (1), 222–230.
- (31) Hammerschmidt, P.; Ostkotte, D.; Nolte, H.; Gerl, M. J.; Jais, A.; Brunner, H. L.; Sprenger, H.-G.; Awazawa, M.; Nicholls, H. T.; Turpin-Nolan, S. M.; Langer, T.; Krüger, M.; Brügger, B.; Brüning, J. C. CerS6-Derived Sphingolipids Interact with Mff and Promote Mitochondrial Fragmentation in Obesity. *Cell* **2019**, *177* (6), 1536–1552.e23.
- (32) Deng, Y.; Pakdel, M.; Blank, B.; Sundberg, E. L.; Burd, C. G.; von Blume, J. Activity of the SPCA1 Calcium Pump Couples Sphingomyelin Synthesis to Sorting of Secretory Proteins in the Trans-Golgi Network. *Dev. Cell* **2018**, *47*(4), 464–478.e8.
- (33) Bockelmann, S.; Mina, J. G. M.; Korneev, S.; Hassan, D. G.; Müller, D.; Hilderink, A.; Vlieg, H. C.; Raijmakers, R.; Heck, A. J. R.; Haberkant, P.; Holthuis, J. C. M. A Search for Ceramide Binding Proteins Using Bifunctional Lipid Analogs Yields CERT-Related Protein StarD7. *J. Lipid Res.* **2018**, *59* (3), 515–530.
- (34) Dadseha, S.; Bockelmann, S.; Mina, J. G. M.; Hassan, D. G.; Korneev, S.; Razzera, G.; Jahn, H.; Niekamp, P.; Müller, D.; Schneider, M.; Tafesse, F. G.; Marrink, S. J.; Melo, M. N.; Holthuis, J. C. M. Ceramides Bind VDAC2 to Trigger Mitochondrial Apoptosis. *Nat. Commun.* **2019**, *10* (1), 1–12.
- (35) Jiang, X.; Zhu, Z.; Qin, H.; Tripathi, P.; Zhong, L.; Elsherbini, A.; Karki, S.; Crivelli, S. M.; Zhi, W.; Wang, G.; Spassieva, S. D.; Bieberich, E. Visualization of Ceramide-Associated Proteins in Ceramide-Rich Platforms Using a Cross-Linkable Ceramide Analog and Proximity Ligation Assays With Anti-Ceramide Antibody. *Front. Cell Dev. Biol.* **2019**, *7*.
- (36) Kong, J.-N.; Zhu, Z.; Itokazu, Y.; Wang, G.; Dinkins, M. B.; Zhong, L.; Lin, H.-P.; Elsherbini, A.; Leanhart, S.; Jiang, X.; Qin, H.; Zhi, W.; Spassieva, S. D.; Bieberich, E. Novel Function of Ceramide for Regulation of Mitochondrial ATP Release in Astrocytes. *J. Lipid Res.* **2018**, *59* (3), 488–506.
- (37) Pike, L. J. Lipid Rafts. *J. Lipid Res.* **2003**, *44* (4), 655–667.
- (38) Hulce, J. J.; Cognetta, A. B.; Niphakis, M. J.; Tully, S. E.; Cravatt, B. F. Proteome-Wide Mapping of Cholesterol-Interacting Proteins in Mammalian Cells. *Nat. Methods* **2013**, *10* (3), 259–264.
- (39) Budelier, M. M.; Cheng, W. W. L.; Bergdoll, L.; Chen, Z. W.; Janetka, J. W.; Abramson, J.; Krishnan, K.; Mydock-McGrane, L.; Covey, D. F.; Whitelegge, J. P.; Evers, A. S. Photoaffinity Labeling with Cholesterol Analogues Precisely Maps a Cholesterol-Binding Site in Voltage-Dependent Anion Channel-1. *J. Biol. Chem.* **2017**, *292* (22), 9294–9304.
- (40) Byrd, K. M.; Arieno, M. D.; Kennelly, M. E.; Estiu, G.; Wiest, O.; Helquist, P. Design and Synthesis of a Crosslinker for Studying Intracellular Steroid Trafficking Pathways. *Bioorg. Med. Chem.* **2015**, *23* (13), 3843–3851.
- (41) Zhou, H.; Hylemon, P. B. Bile Acids Are Nutrient Signaling Hormones. *Steroids* **2014**, *86*, 62–68.
- (42) Zhuang, S.; Li, Q.; Cai, L.; Wang, C.; Lei, X. Chemoproteomic Profiling of Bile Acid Interacting Proteins. *ACS Cent. Sci.* **2017**, *3* (5), 501–509.
- (43) Guo, H.; Xu, J.; Hao, P.; Ding, K.; Li, Z. Competitive Affinity-Based Proteome Profiling and Imaging to Reveal Potential Cellular Targets of Betulinic Acid. *Chem. Commun.* **2017**, *53* (69), 9620–9623.
- (44) Herner, A.; Marjanovic, J.; Lewandowski, T. M.; Marin, V.; Patterson, M.; Miesbauer, L.; Ready, D.; Williams, J.; Vasudevan, A.; Lin, Q. 2-Aryl-5-Carboxytetrazole as a New Photoaffinity Label for Drug Target Identification. *J. Am. Chem. Soc.* **2016**, *138* (44), 14609–14615.
- (45) Zhang, L.; Zhang, Y.; Dong, J.; Liu, J.; Zhang, L.; Sun, H. Design and Synthesis of Novel Photoaffinity Probes for Study of the Target Proteins of Oleanolic Acid. *Bioorg. Med. Chem. Lett.* **2012**, *22* (2), 1036–1039.
- (46) Mellacheruvu, D.; Wright, Z.; Couzens, A. L.; Lambert, J. P.; St-Denis, N. A.; Li, T.; Miteva, Y. V.; Hauri, S.; Sardiu, M. E.; Low, T. Y.; Halim, V. A.; Bagshaw, R. D.; Hubner, N. C.; Al-Hakim, A.; Bouchard, A.; Faubert, D.; Fermin, D.; Dunham, W. H.; Goudreault, M.; Lin, Z. Y.; Badillo, B. G.; Pawson, T.; Durocher, D.;

- Coulombe, B.; Aebersold, R.; Superti-Furga, G.; Colinge, J.; Heck, A. J. R.; Choi, H.; Gstaiger, M.; Mohammed, S.; Cristea, I. M.; Bennett, K. L.; Washburn, M. P.; Raught, B.; Ewing, R. M.; Gingras, A. C.; Nesvizhskii, A. I. The CRAPome: A Contaminant Repository for Affinity Purification-Mass Spectrometry Data. *Nat. Methods* **2013**, *10*(8), 730–736.
- (47) Kleiner, P.; Heydenreuter, W.; Stahl, M.; Korotkov, V. S.; Sieber, S. A. A Whole Proteome Inventory of Background Photocrosslinker Binding. *Angew. Chem. - Int. Ed.* **2017**, *56*(5), 1396–1401.
- (48) Mbarik, M.; Biam, R. S.; Robichaud, P.-P.; Surette, M. E. The Impact of PUFA on Cell Responses: Caution Should Be Exercised When Selecting PUFA Concentrations in Cell Culture. *Prostaglandins Leukot. Essent. Fatty Acids* **2020**, 102083.
- (49) Laguerre, A.; Hauke, S.; Qiu, J.; Kelly, M. J.; Schultz, C. Photorelease of 2-Arachidonoylglycerol in Live Cells. *J. Am. Chem. Soc.* **2019**, *141*(42), 16544–16547.

## Supplementary data

**Table S1 | List of proteins identified as promiscuous lipid binding proteins.** Proteins are listed with their accession number, gene name and the number of datasets in which they were identified as a probe target. Proteins colored red are the proteins flagged by the CRAPome database.

Accession number	Gene name	Count	Accession number	Gene name	Count	Accession number	Gene name	Count	Accession number	Gene name	Count
Q9NRG9	AAAS	4	A0FGR8	ESYT2	4	Q9Y5Y5	PEX16	5	P43307	SSR1	8
P28288	ABCD3	5	Q9NRV5	FAM114A2	7	O00264	PGRMC1	7	P51571	SSR4	6
O95870	ABHD16A	4	Q96A26	FAM162A	4	O15173	PGRMC2	6	Q9NQZ5	STARD7	4
Q8WTS1	ABHD5	4	Q8WVX9	FAR1	4	P35232	PHB	6	Q9UJZ1	STOML2	4
Q9BV23	ABHD6	7	P37268	FDFT1	4	<b>Q99623</b>	<b>PHB2</b>	<b>7</b>	P46977	STT3A	4
O95573	ACSL3	4	P22830	FECH	4	Q92643	PIGK	5	Q8TCJ2	STT3B	4
Q9BRR6	ADPGK	5	O00461	GOLIM4	5	Q96S52	PIGS	5	Q9UH99	SUN2	4
<b>O95831</b>	<b>AIFM1</b>	<b>5</b>	Q9P035	HACD3	4	Q9H490	PIGU	4	O15260	SURF4	5
P51648	ALDH3A2	7	P40939	HADHA	6	Q10713	PMPCA	4	Q9Y4P3	TBL2	6
P53365	ARFIP2	6	Q9NRV9	HEBP1	4	P50897	PPT1	5	Q9NZ01	TECR	4
Q8NHH9	ATL2	4	Q8TCT9	HM13	6	Q9BZL6	PRKD2	4	P0DO92	T-ENOL	4
Q6DD88	ATL3	4	P30519	HMOX2	6	Q9H7Z7	PTGES2	4	Q8WUY1	THEM6	4
Q9HD20	ATP13A1	6	Q53GQ0	HSD17B12	6	P18031	PTPN1	4	O60830	TIMM17B	4
<b>P16615</b>	<b>ATP2A2</b>	<b>6</b>	Q3SX5	HSDL1	5	P61026	RAB10	5	O14925	TIMM23	5
<b>P25705</b>	<b>ATP5A1</b>	<b>4</b>	<b>P14625</b>	<b>HSP90B1</b>	<b>4</b>	P62491	RAB11A	4	O43615	TIMM44	5
<b>P06576</b>	<b>ATP5B</b>	<b>4</b>	P11021	HSPA5	4	P62820	RAB1A	4	<b>Q3ZCQ8</b>	<b>TIMM50</b>	<b>5</b>
P24539	ATP5F1	5	O60725	ICMT	4	Q9H0U4	RAB1B	4	Q13445	TMED1	4
Q93050	ATP6V0A1	4	Q8TCB0	IFI44	4	Q8TC12	RDH11	4	P49755	TMED10	5
Q9UHQ4	BCAP29	4	Q70UQ0	IKBIP	4	<b>P04843</b>	<b>RPN1</b>	<b>6</b>	Q15363	TMED2	5
P51572	BCAP31	7	Q16891	IMMT	4	P04844	RPN2	5	Q9Y3B3	TMED7	4
Q8WY22	BRI3BP	5	Q8N5M9	JAGN1	4	O95197	RTN3	5	Q9NX00	TMEM160	5
P35613	BSG	4	P24390	KDELR1	4	Q9NQC3	RTN4	5	Q9HC07	TMEM165	4
<b>P27824</b>	<b>CANX</b>	<b>6</b>	Q06136	KDSR	5	Q9NTJ5	SACM1L	4	Q6NUQ4	TMEM214	5
Q96A33	CCDC47	8	Q86SY8	KTN1-AS1	5	Q9Y512	SAMM50	7	Q4ZIN3	TMEM259	4
Q96G23	CERS2	6	Q14739	LBR	4	Q9NR31	SAR1A	4	P57088	TMEM33	5
Q9NZ45	CISD1	6	O95202	LETM1	5	Q9Y6B6	SAR1B	4	Q9BTV4	TMEM43	5
Q07065	CKAP4	6	<b>P20700</b>	<b>LMNB1</b>	<b>4</b>	Q8WTV0	SCARB1	4	<b>P42166</b>	<b>TMPO</b>	<b>6</b>
Q9UBD9	CLCF1	4	Q6P1A2	LPCAT3	4	Q14108	SCARB2	4	Q9H3N1	TMX1	5
O96005	CLPTM1	6	Q96AG4	LRRC59	7	Q8NBX0	SCCPDH	5	Q9Y320	TMX2	5
P23786	CPT2	5	Q9NZJ7	MTC1H	5	O43819	SCO2	4	Q9NS69	TOMM22	5
P07339	CTSD	5	Q9Y6C9	MTCH2	6	P67812	SEC11A	4	O96008	TOMM40	4
Q6UW02	CYP20A1	4	Q86UE4	MTDH	7	Q9UGP8	SEC63	4	O14656	TOR1A	5
Q16850	CYP51A1	7	Q969V3	NCLN	5	Q9UBV2	SEL1L	7	Q9H4I3	TRABD	4
Q8WVC6	DCAKD	5	Q9Y6Q9	NCOA3	6	Q8IWL2	SFTPA1	5	O95292	VAPB	4
O15121	DEGS1	4	Q9BTX1	NDC1	4	O95470	SGPL1	5	P21796	VDAC1	6
Q9BUN8	DERL1	5	Q9Y639	NPTN	4	P53007	SLC25A1	4	P45880	VDAC2	5
Q15392	DHCR24	6	Q15738	NSDHL	5	Q9UBX3	SLC25A10	5	<b>P08670</b>	<b>VIM</b>	<b>4</b>
Q96LJ7	DHRS1	5	Q02818	NUCB1	5	Q02978	SLC25A11	4	Q8N0U8	VKORC1L1	6
Q9Y394	DHRS7	5	P80303	NUCB2	4	O75746	SLC25A12	5	Q96GC9	VMP1	4
Q96KC8	DNAJC1	4	Q8TEM1	NUP210	4	O43772	SLC25A20	4	Q5BJH7	YIF1B	4
Q8N766	EMC1	4	Q8NFH5	NUP35	4	Q9H2D1	SLC25A32	4	O75844	ZMPSTE24	7
P50402	EMD	7	Q9NX40	OCIAD1	6	<b>P05141</b>	<b>SLC25A5</b>	<b>4</b>			
P07099	EPHX1	5	O60313	OPA1	4	Q8TAD4	SLC30A5	4			
Q75477	ERLIN1	5	<b>P07237</b>	<b>P4HB</b>	<b>4</b>	Q15005	SPCS2	4			
Q9BSJ8	ESYT1	4	Q9UHG3	PCYOX1	6	Q14534	SQLE	4			





# Chapter 3

## Bioorthogonal photoaffinity probes of omega-3 signaling lipids reveal PTGR1 as a metabolic hub in human macrophages\*

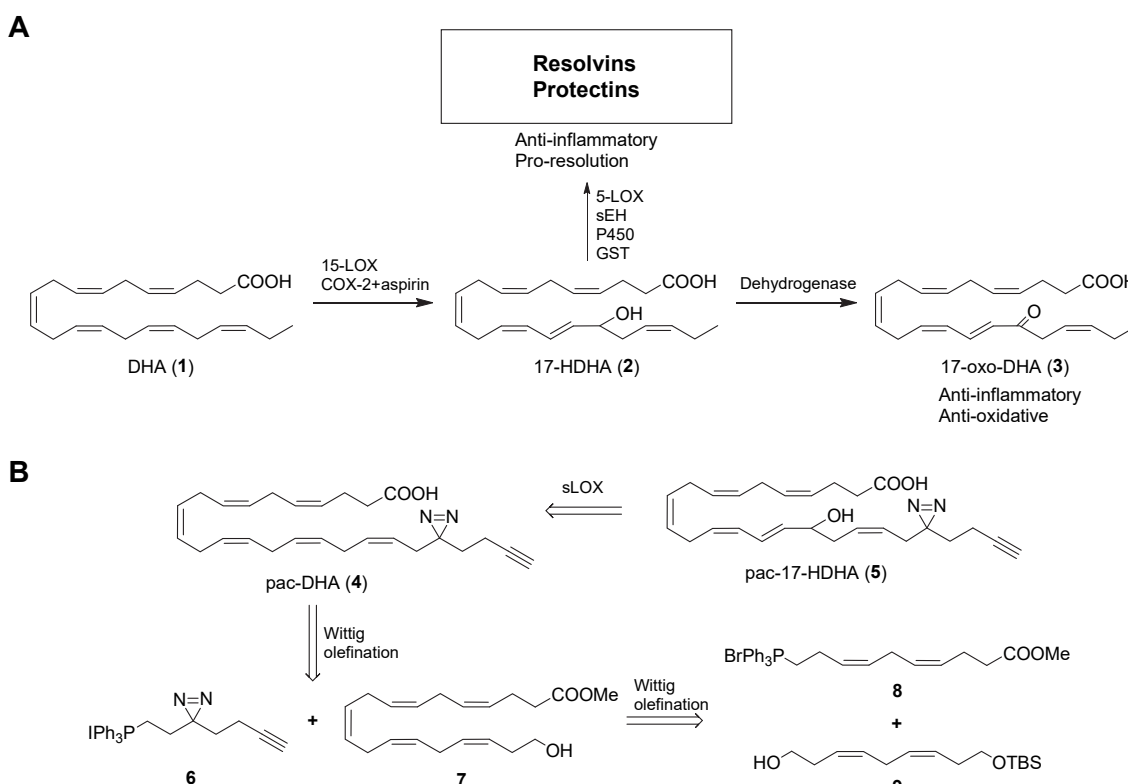
### Introduction

Dietary omega-3 polyunsaturated fatty acids (PUFAs) are generally considered to be beneficial for human health.<sup>1–3</sup> For example, the fish oil constituent docosahexaenoic acid (DHA, 22:6 n-3, **1**) is important for brain development, neuronal protection and the immune system (Scheme 1A).<sup>2–7</sup> Mechanistic studies indicate that many of the favorable effects of omega-3 fatty acids are due to their interaction with immunological processes,<sup>1,2</sup> which has been reiterated by the discovery of their oxidized metabolites involved in the resolution of inflammation.<sup>8,9</sup> Malfunction of this resolution phase of inflammation is hypothesized to contribute to many chronic inflammatory diseases, such as rheumatoid arthritis and asthma.<sup>10,11</sup> A better molecular understanding of the biological role of these lipids in the resolution phase of inflammation is required to develop therapeutics for these diseases.

---

\*The data presented in this chapter was gathered in collaboration with Joost von Hegedus, Joanneke C. Kwekkeboom, Marieke Heijink, Bogdan I. Florea, Hans van den Elst, Kim Wals, Herman S. Overkleef, Martin Giera, René E. M. Toes, Andreea Ioan-Facsinay, Mario van der Stelt.

The resolution of inflammation requires the intricate orchestration of cells of the innate immune system via soluble mediators. Among these, oxidative metabolites of DHA play a central role.<sup>7,12</sup> Biochemical studies have shown that DHA is oxidized into a central precursor, 17-hydroxy-docosahexaenoic acid (17-HDHA, **2**) via multiple pathways, including 15-lipoxygenase and cyclooxygenase acetylated by aspirin (Scheme 1A).<sup>13</sup> Oxidation by 15-lipoxygenase results in the formation of 17(S)-HDHA, while acetylated COX generates 17(R)-HDHA.<sup>14</sup> Importantly, 17-HDHA has protective effects in various animal models of colitis, arthritis and renal reperfusion.<sup>15–18</sup> *In vitro*, human macrophages produce less TNFα and more IL-10 following exposure to 17-HDHA.<sup>19,20</sup> Treatment with 17-HDHA also reduces LTB4 production in both isolated murine and human neutrophils.<sup>20,21</sup> Moreover, 17-HDHA can be further metabolized to specialized proresolving lipid mediators (SPMs), such as D-series resolvins and protectins (Scheme 1A), a process involving several enzymes. Resolvins and protectins are bioactive lipids with potent pro-resolving activities, including halting the infiltration of neutrophils and enhancing the non-phlogistic clearance of apoptotic cells, cellular debris and microbes by macrophages, thereby stimulating the resolution of inflammation, while promoting tissue regeneration.<sup>8,22</sup> On the other hand, 17-HDHA can be metabolized to 17-oxo-docosahexaenoic acid (17-oxo-DHA, **3**), which may limit the formation of SPMs. Insight into its protein interaction partners in human immune cells would be of great benefit in obtaining a better molecular understanding of the biological role and metabolism of 17-HDHA.



**Scheme 1 | Oxidative metabolism of DHA (**1**) and synthetic strategy of photoaffinity probes **4** and **5**.** **(A)** Metabolic pathway of DHA to 17-oxo-DHA, resolvins and protectins. **(B)** Structures of photoaffinity-click (pac-)probes based on DHA (**1**) and 17-HDHA (**2**). The synthetic strategy included the use of soybean lipoxygenase (sLOX) to introduce the hydroxyl and the use of Wittig reactions to join building blocks **6**, **8** and **9**.

Lipid photoaffinity probes have been successfully used to map protein-lipid interactions on a global scale in their native environment.<sup>23</sup> Bioorthogonal photoaffinity lipid probes consist of a lipid modified with a photoreactive group and bioorthogonal ligation handle.<sup>24</sup> The photoreactive group is activated by irradiation with light, generating a reactive species that may form a covalent and irreversible bond with the interacting protein. The ligation handle is used to attach a reporter group via bioorthogonal chemistry, which allows for visualization or isolation of the probe-bound protein in a complex biological sample. This affinity-based protein profiling (AfBPP) approach has been reported for multiple lipid classes including phospholipids,<sup>25,26</sup> fatty acids,<sup>23,27</sup> sphingolipids<sup>28,29</sup> and sterols,<sup>24,30</sup> but has not been applied to omega-3 PUFAs, arguably due to the synthetic challenges associated with their preparation.<sup>31</sup>

An important drawback of photoreactive lipid-based probes is their inherent high lipophilicity and nonspecific binding to proteins. Significant overlap between protein targets of lipid probes has been documented, making it difficult to assign specific interaction partners to a given probe and to study their biological role.<sup>32,33</sup> Competition experiments with non-labeled lipids have been applied to identify specific binding partners, but were not always successful, possibly due to accumulation of both probe and competitor lipids in the cellular membrane.<sup>34,35</sup>

Here, the design, synthesis and application of a pair of complementary photoaffinity probes is described (**4** and **5**) based on the structure of DHA and 17-HDHA, respectively (Scheme 1B). The aim was to map the specific binding partners of 17-HDHA in primary human macrophages by comparative AfBPP, an approach capable of uncovering genuine, specific probe targets (Figure 1). Probe **5** retained the anti-inflammatory properties of the parent lipid in human M2 macrophages. Using chemical proteomics, specific protein binding partners of the probes were mapped. Prostaglandin reductase 1 (PTGR1) was identified and validated as a probe **5**-specific target. Subsequent biochemical studies revealed that PTGR1 oxidizes 17-HDHA into the anti-inflammatory 17-oxo-DHA in human macrophages. 17-oxo-DHA reduced the biosynthesis of the proinflammatory lipids in primary human neutrophils. These results demonstrate the potential of comparative photoaffinity protein profiling for the discovery of metabolic enzymes of bioactive lipids and highlight the power of chemical proteomics to uncover new biological insights.

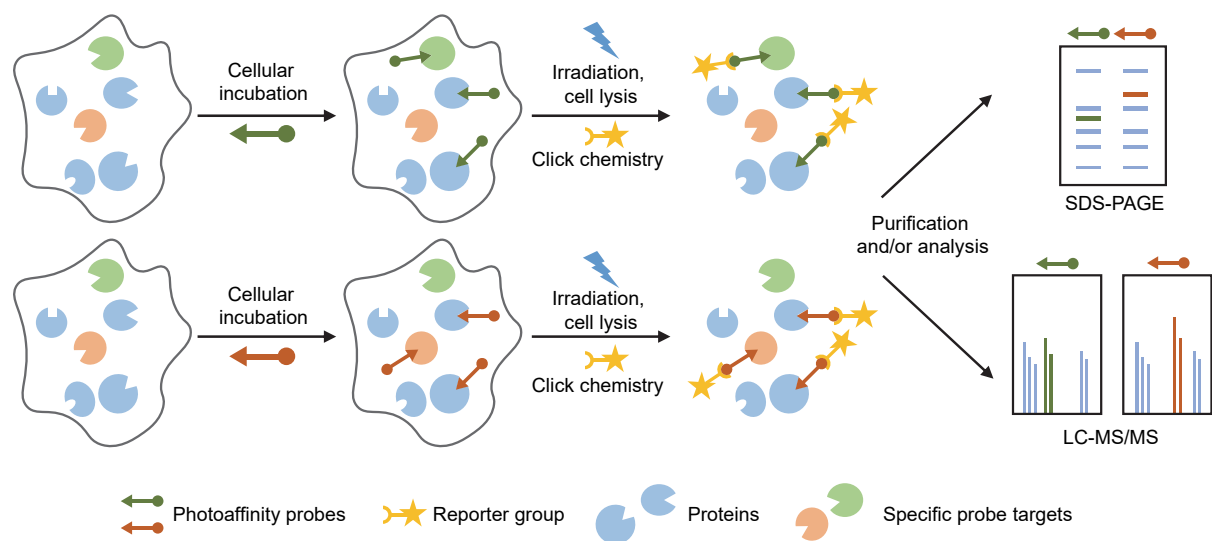


**Figure 1 | Schematic overview of comparative AfBPP experiment.** Two probes are used to identify all probe-interacting proteins. Then, probe-specific targets (green and red) can be identified after eliminating common (blue) probe targets.

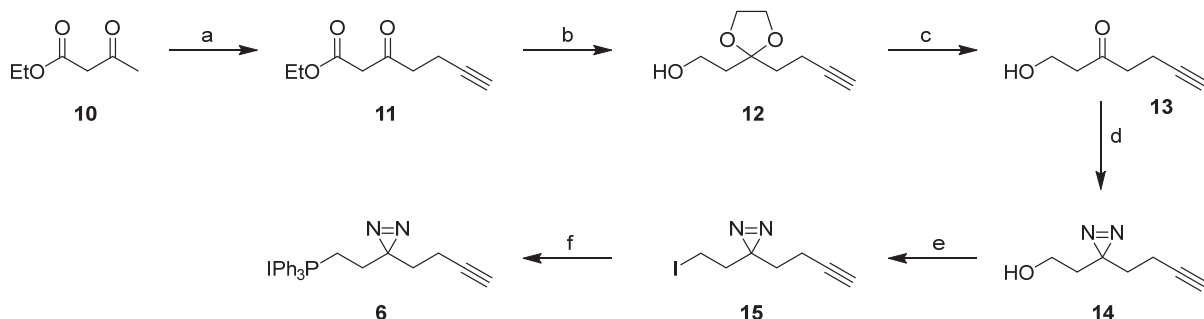
## Results

### Design and synthesis of photoaffinity probes **4** and **5**

In the design of photoaffinity probes **4** and **5** (Scheme 1B) and to ensure they closely resemble the signaling lipids DHA and 17-HDHA, respectively, the polyunsaturated fatty acid scaffold was kept intact and the omega carbon was substituted with a diazirine- and alkyne-containing minimalistic bifunctional group.<sup>36</sup> Diazirines are small photoreactive groups with short reactive half-lives upon activation, thereby minimizing the interference and reducing non-specific labeling. The alkyne is the smallest bioorthogonal tag available and has similar physio-chemical properties to the alkyl chain of fatty acids.<sup>37,38</sup>

To synthesize the probes in an efficient manner, a chemoenzymatic approach was used. Probe **5** was produced by soybean lipoxygenase using probe **4** as substrate (Scheme 1B). Probe **4** was synthesized by combining two strategic building blocks, the minimalistic bifunctional photoreactive linker **6** and the polyunsaturated fatty acid scaffold (**7**), using a Wittig reaction. Building block **7** was generated by combining the two dienes **8** and **9**, also via a Wittig reaction. This synthetic strategy avoids the reduction of six skipped (non-conjugated) alkynes at the same time, which would lead to a complex mixture of partially hydrogenated products.<sup>39</sup> Moreover, this strategy did not require the assembly of large, skipped polyalkyne structures, which are inherently unstable.<sup>40,41</sup>

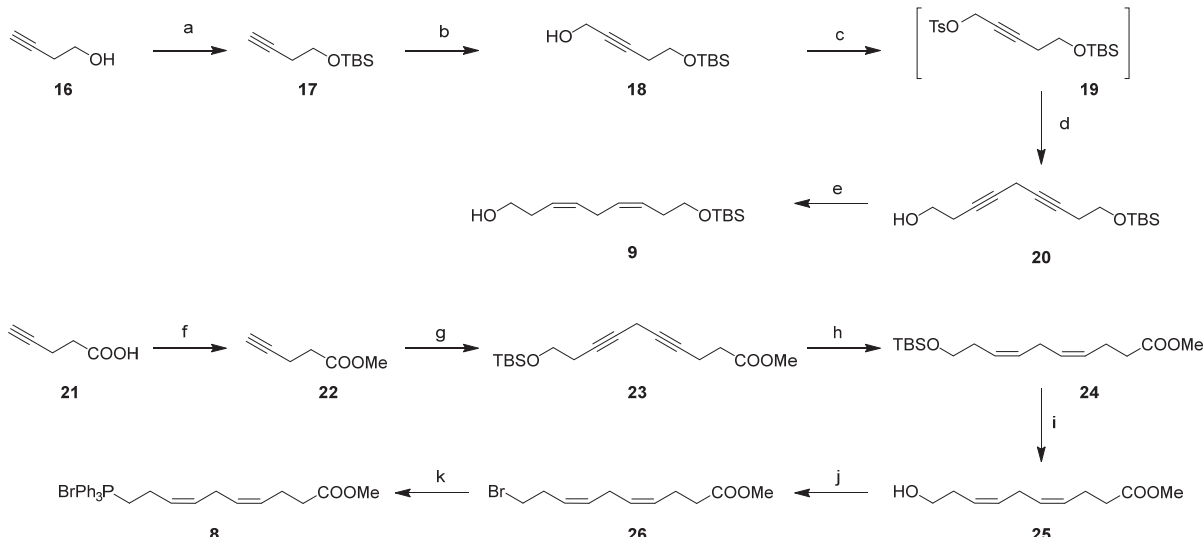
The synthesis of building block **6** started with reacting commercially available ethyl 3-oxobutanoate (**10**) with propargyl bromide using a protocol adapted from literature (Scheme 2).<sup>36</sup> Alkyne **11** was purified by fractional vacuum distillation and subsequently protected as a ketal by using ethylene glycol, followed by reduction of the ester with LiAlH<sub>4</sub>. The resulting alcohol **12** was hydrolyzed under acidic conditions to form ketone **9**. This ketone was transformed into a diazirine in a three-step sequence. First, an imine was formed with saturated ammonia in methanol, after which reaction with hydroxylamine-*o*-sulfonic acid generated the diaziridine, which was oxidized with elemental iodine in methanol to form diazirine **14** in a yield of 37%. Alcohol **14** was halogenated using iodine in an Appel reaction to obtain compound **15**, after which the iodide was substituted with triphenylphosphine at 70 °C to form **6** in 73% yield over two steps.



**Scheme 2 | Synthesis of diazirine- and alkyne-containing building block 6.** Reagents and conditions: (a) diisopropylamine, *n*-BuLi, THF, -78 °C to -40 °C, then **6**, propargyl bromide, -40 °C to 0 °C, 45%; (b) ethylene glycol, *p*-TsOH, triethyl orthoformate, 80 °C; then LiAlH<sub>4</sub>, THF, 0 °C to rt, 94% over 2 steps; (c) acetone, H<sub>2</sub>O, *p*-TsOH, 50 °C, 93%; (d) NH<sub>3</sub>, hydroxylamine-*α*-sulfonic acid, MeOH, 0 °C to rt, then I<sub>2</sub>, Et<sub>3</sub>N, MeOH, 0 °C, 37%; (e) imidazole, I<sub>2</sub>, PPh<sub>3</sub>, DCM, 0 °C to rt, 73%; (f) PPh<sub>3</sub>, ACN, 70 °C, quant.

The double bond system in building block **7** was assembled by joining fragments **8** and **9** (Scheme 3). To this end, butynol (**16**) was protected with a TBS group to afford alkyne **17** in 98% yield. This compound was deprotonated using *n*-butyllithium and reacted with paraformaldehyde to afford alcohol **18**, which was tosylated to obtain **19**. This intermediate was used without further purification for a copper(I)-mediated coupling to butynol to afford skipped alkyne **20** in 71% yield over three steps. The skipped alkyne was partially hydrogenated using a nickel boride catalyst to furnish alcohol **9** in 64% yield.

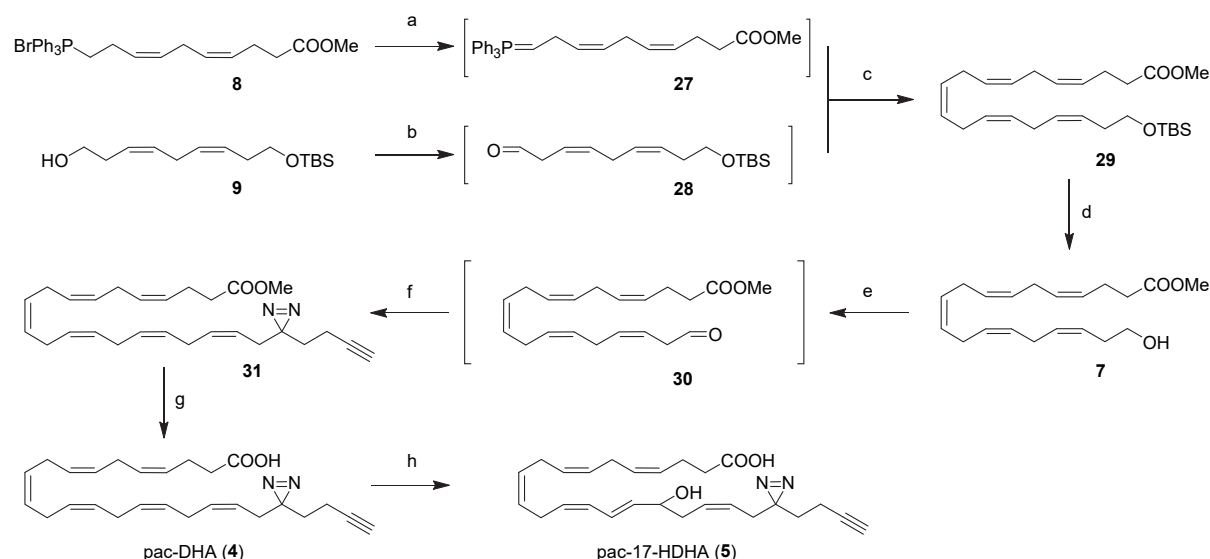
For fragment **8**, pentynoic acid (**21**) was protected by esterification in methanol to obtain **22**, which was reacted with sulfonate ester **19** in a second copper(I)-mediated coupling to afford skipped alkyne **23** (Scheme 2). Skipped alkyne **23** was partially hydrogenated to afford silylated **24**. The TBS group was removed using TBAF to afford alcohol **25**, which was halogenated to form **26**. This was then substituted with triphenylphosphine to afford phosphonium salt **8** in 43% yield from pentynoic acid.



**Scheme 3 | Synthesis of diene fragments 8 and 9.** Reagents and conditions: (a) imidazole, TBSCl, DMF, 0 °C, 98%; (b) *n*-BuLi, paraformaldehyde, THF, -40 °C, 82%; (c) TsCl, KOH, Et<sub>2</sub>O, 0 °C to rt; (d) CuI, NaI, Cs<sub>2</sub>CO<sub>3</sub>, but-3-yn-1-ol, DMF, 86%; (e) Ni(OAc)<sub>2</sub>·4H<sub>2</sub>O, NaBH<sub>4</sub>, ethylenediamine, EtOH, 64%; (f) SOCl<sub>2</sub>, MeOH, 0 °C to rt, 92%; (g) **19**, CuI, NaI, Cs<sub>2</sub>CO<sub>3</sub>, DMF, 74%; (h) Ni(OAc)<sub>2</sub>·4H<sub>2</sub>O, NaBH<sub>4</sub>, ethylenediamine, EtOH, 89%; (i) TBAF, THF, 0 °C to rt, 71%; (j) CBr<sub>4</sub>, PPh<sub>3</sub>, DCM, -30 °C to 0 °C, quant.; (k) PPh<sub>3</sub>, ACN, 92 °C, quant.

To join intermediates **8** and **9**, a Wittig reaction was performed by deprotonation of **8** to form ylid **27** using LiHMDS at reduced temperature, and addition of freshly prepared aldehyde **28** at -100 °C (Scheme 4). Alcohol **9** was oxidized using DMP to generate aldehyde **28** directly before use due to the instability of  $\beta,\gamma$ -unsaturated aldehydes.<sup>42,43</sup> This resulted in isolation of **29** with the newly generated alkene in *Z*-configuration in 57% yield, which was deprotected using TBAF to obtain alcohol **7** in 87% yield.

Building block **6** was installed in probe **4** by generating the final double bond using another Wittig reaction, for which alcohol **7** was oxidized with DMP, while phosphonium salt **6** was deprotonated with KO*t*Bu at reduced temperature. Higher temperatures or stronger bases resulted in loss of the diazirine. The freshly generated aldehyde **30** was added to the ylid at -105 °C which afforded methyl ester **31** in 38% yield after purification. The configuration of the last double bond was confirmed with NMR. Saponification of the ester yielded photoaffinity probe **4** in 83% yield.



**Scheme 4 | Formation of probes **4** and **5** by assembly of building blocks **6**, **8** and **9**.** Reagents and conditions: (a) LiHMDS, THF, HMPA, -60 °C; (b) DMP, DCM, 0 °C to rt; (c) THF, HMPA, -100 °C to 0 °C, 57%; (d) TBAF, THF, 0 °C to rt, 87%; (e) DMP, DCM, 0 °C to rt; (f) **6**, *t*-BuOK, THF, -70 °C to -50 °C, then **30**, -105 °C to -30 °C, 38%; (g) LiOH, H<sub>2</sub>O, THF, 0 °C to rt, 83%; (h) sLOX, borate buffer pH 12.0, 0 °C, then NaBH<sub>4</sub>, then AcOH, 5%.

To generate photoaffinity-click (pac)-17-HDHA (**5**), commercially available soybean lipoxygenase (sLOX) was used, which catalyzes the oxidation of DHA (**1**) to 17-hydroperoxy-DHA, which can be reduced to 17-HDHA (**2**).<sup>44,45</sup> While DHA (**1**) was fully converted into 17-HDHA by sLOX using previously reported conditions,<sup>46</sup> this resulted in the complete loss of the diazirine when using probe **4** as substrate. To this end, the reaction conditions with probe **4** were optimized for enzyme loading, temperature and incubation time. This resulted in the formation of probe **5**, which could be obtained after high-performance liquid chromatography (HPLC) purification in sufficient quantities for cellular experiments, but not to determine the absolute configuration.

## Mapping protein interaction partners of probe **4** and **5**

Probe **5** was tested in a cellular assay using primary human M2 macrophages to confirm it was biologically equivalent to 17-HDHA. M2 macrophages were differentiated from monocytes of healthy donors in the presence of macrophage colony-stimulating factor (M-CSF). Upon stimulation with  $\text{Ca}^{2+}$  ionophore, M2 macrophages rapidly synthesize the proinflammatory lipid 5-HETE from arachidonic acid (AA) by 5-lipoxygenase (Figure 2A). A liquid chromatography-mass spectrometry (LC-MS) method was developed to quantify 5-HETE and its precursor AA in these human macrophages. Upon pre-incubation with 17-HDHA lipid or probe **5**, conversion of AA into 5-HETE was reduced to the same extent by both molecules. Moreover, in primary human neutrophils also no loss in anti-inflammatory signaling was observed (Figure S1). These results indicate that the probe retains the anti-inflammatory signaling capacity of 17-HDHA and can be used to investigate the binding partners of its parent lipid.

Next, the protein interaction landscape of probe **5** in human M2 macrophages was investigated using two-step AfBPP. To identify specific targets of 17-HDHA, probe **4** was also used to map general, promiscuous lipid binding proteins. To this end, cells were incubated with probe **4** or **5** in serum-free medium for 30 min. Crosslinking was effected by UV-irradiation ( $\lambda = 350 \text{ nm}$ , 10 min) using a CaproBox,<sup>47</sup> which irradiated the cells with simultaneous cooling at 4 °C to counteract the heat induced by the irradiation. Next, the cells were harvested, lysed and subjected to copper(I)-catalyzed azide-alkyne cycloaddition (CuAAC, “click”-reaction)<sup>48</sup> conditions utilizing Cy5-N<sub>3</sub> to enable the visualization of the probe-bound proteins by sodium dodecyl sulfate polyacrylamide gel electrophoresis (SDS-PAGE) analysis and in-gel fluorescence scanning (Figure 2B). This resulted in the visualization of many fluorescent bands for both probes, which were absent in the non-irradiated samples, demonstrating that the probes do not covalently interact with proteins without UV-irradiation. Although a large overlap in fluorescent bands was revealed after labeling by either probe **4** or **5**, there were also several probe-specific bands observed (Figure 2B).

To identify the probe-interacting proteins, the cell lysates were ligated to biotin-N<sub>3</sub> and a chemical proteomics experiment was performed. Briefly, the probe-labeled proteins were enriched using avidin-coated agarose beads, digested using trypsin and the resulting tryptic peptides analyzed by LC-MS. This resulted in the identification of 179 proteins after deselection based on identified unique peptides and appearance in the CRAPome.<sup>49</sup> Of these, 34 were significantly UV-enriched by probe **5** (Figure 2C/D, Table S1). To identify probe **5**-specific interacting proteins, the UV enrichment profiles of both probes were compared (Figure 2D, Table 1). Proteins which were previously identified as promiscuous lipid probe binders<sup>33</sup> are indicated in red. All promiscuous lipid probe binders, with the singular exception of voltage-dependent anion channel 2 (VDAC2), were equally enriched by both probes. This demonstrated that comparative AfBPP is capable of discovering genuine probe-specific interactions. Eight and ten proteins were specifically labeled by probe **4** and **5**, respectively.

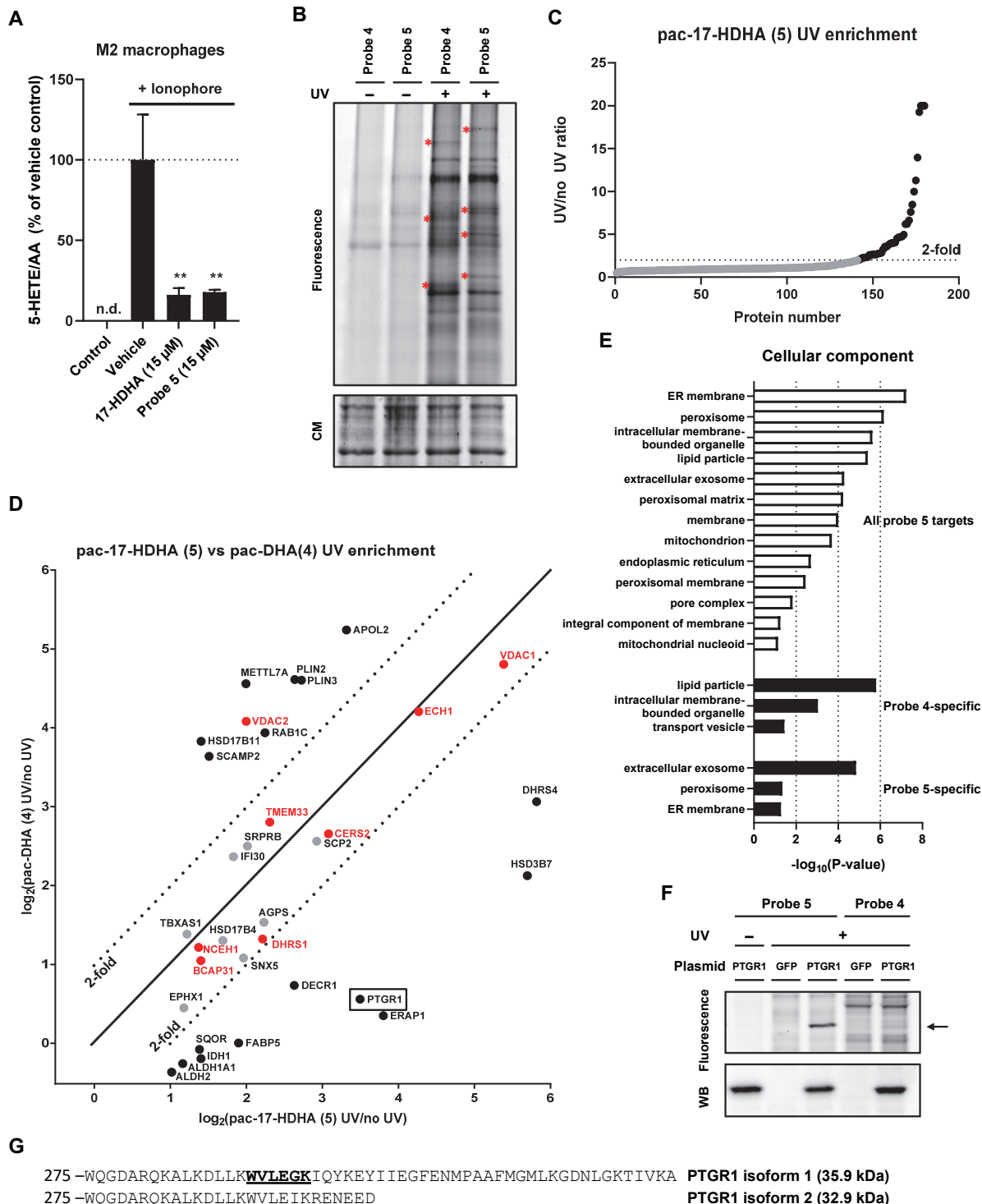


**Figure 2 | Comparative ABPP in human M2 macrophages using pac-17-HDHA and pac-DHA.** **(A)** 5-HETE/AA ratio (LC-MS/MS) produced by ionophore-stimulated M2 macrophages. Data represent means  $\pm$  SD of representative donor ( $n = 3$ ). \*\*  $p < 0.01$  in comparison to ionophore-treated control using a one-way ANOVA with Dunnett's multiple comparisons correction. n.d.; not detected. **(B)** Probe targets of pac-17-HDHA (**5**) and pac-DHA (**4**) conjugated to Cy5-N<sub>3</sub> analyzed by SDS-PAGE and in-gel fluorescent scanning show UV-dependent and probe-specific labeling. Coomassie (CM) served as a protein loading control. Asterisks indicate probe-specific labeling. **(C)** Waterfall plot of proteins identified using probe **5** in M2 macrophages. **(D)** UV enrichment by probe **4** and probe **5** is shown and a 2-fold cutoff indicates probe-specific targets, promiscuous lipid probe binders<sup>33</sup> are indicated in red. **(E)** Cellular component analysis of probe **5**-interacting proteins by gene ontology (GO). **(F)** Gel-based AfBPP of GFP- or PTGR1-overexpressing HEK-293-T using probes **4** and **5**. Expression of PTGR1 was shown by anti-FLAG western blot. **(G)** PTGR1 amino acid sequence starting at W275. One of the identified tryptic peptides is indicated.

Gene ontology (GO) enrichment analysis revealed that the proteins significantly UV-enriched by probe **5** are mainly found in organelles in lipid metabolism, such as the endoplasmic reticulum and mitochondria. However, when the targets are narrowed down to probe-**5**-specific targets, the proteins are significantly associated with the extracellular exosomes gene ontology term (Figure 2E).<sup>50</sup> The probe **5**-specific targets are also predominantly involved in lipid metabolism (ALDH2/1A1, DECR1, DHRS4, HSD3B7, PTGR1) or transport (FABP5).

**Table 1 | List of probe-specifically enriched targets of probe 5.**

Uniprot accession	Gene name	Unique peptides	Description	Specific
Q9H2F3	HSD3B7	3	3 beta-hydroxysteroid dehydrogenase type 7	Probe 5
Q9NZ08	ERAP1	20	Endoplasmic reticulum aminopeptidase 1	
<b>Q14914</b>	<b>PTGR1</b>	<b>11</b>	<b>Prostaglandin reductase 1</b>	
Q9BTZ2	DHRS4	10	Dehydrogenase/reductase SDR family member 4	
Q16698	DECR1	4	2,4-dienoyl-CoA reductase, mitochondrial	
Q01469	FABP5	2	Fatty acid-binding protein, epidermal	
O75874	IDH1	8	Isocitrate dehydrogenase [NADP], cytoplasmic	
Q9Y6N5	SQOR	6	Sulfide:quinone oxidoreductase, mitochondrial	
P00352	ALDH1A1	17	Retinal dehydrogenase 1	
P05091	ALDH2	16	Aldehyde dehydrogenase, mitochondrial	
Q92928	RAB1C	2	Putative Ras-related protein Rab-1C	
Q99541	PLIN2	11	Perilipin-2	
Q9BQE5	APOL2	4	Apolipoprotein L2	
O60664	PLIN3	2	Perilipin-3	Probe 4
P45880	VDAC2	7	Voltage-dependent anion-selective channel protein 2	
O15127	SCAMP2	2	Secretory carrier-associated membrane protein 2	
Q8NBQ5	HSD17B11	2	Estradiol 17-beta-dehydrogenase 11	
Q9H8H3	METTL7A	2	Methyltransferase-like protein 7A	

Prostaglandin reductase 1 (PTGR1) is known for its role in inflammatory lipid metabolism and was therefore selected for further investigation.<sup>51</sup> PTGR1 (isoform 1, Figure 2G) expression is, for example, increased during inflammation and is involved in the resolution of inflammation through modulation of the HMGB1-miR522-3P-PTGR1 axis.<sup>52</sup> PTGR1 functions as 15-oxo-prostaglandin 13-reductase and acts on 15-oxo-PGE1 and 15-oxo-PGE2.<sup>51,52</sup> Furthermore, it catalyzes the conversion of the proinflammatory leukotriene B4 (LTB4) into its biologically less active metabolite, 12-oxo-LTB4, which is an initial and key step of metabolic inactivation of LTB4.<sup>53</sup> To validate PTGR1 as a specific target of probe **5**, a recombinant PTGR1-FLAG-tag fusion construct in a pcDNA3.1 plasmid was transfected in HEK-293-T cells. These cells and GFP-transfected control cells were subsequently subjected to gel-based AfBPP analysis with probe **4** and **5** (Figure 2F). Western blotting confirmed successful expression of PTGR1. In line with previous experiments, PTGR1 was labeled in a UV-dependent manner by probe **5**, but not by probe **4**, thereby confirming that PTGR1 is a specific target of probe **5**.

## Biological role of PTGR1 in 17-HDHA metabolism

Since PTGR1 is capable of oxidizing the proinflammatory lipid LTB4, thereby converting the 12-hydroxyl group to form 12-oxo-LTB4,<sup>51,54</sup> it was hypothesized that by analogy PTGR1 may oxidize 17-HDHA into 17-oxo-DHA in human M2 macrophages. To this end, a targeted lipidomics method was developed to quantify 17-oxo-DHA in human cells. Upon incubation of M2 macrophages with 17-HDHA, the formation of 17-oxo-DHA could be detected in a concentration-dependent manner (Figure 3A). To investigate the role of PTGR1 in 17-HDHA metabolism, M2 macrophages were pre-incubated with two compounds with PTGR1 inhibitory activity. Indomethacin, better known as a COX-2 inhibitor, has a weak ( $IC_{50}$  8.7 – 97.9  $\mu$ M)<sup>51,55</sup> activity on PTGR1 (Figure 3E), whereas the anticancer compound licochalcone A is a potent, covalent inhibitor by covalently binding to C239.<sup>56,57</sup> Preincubation with indomethacin resulted in a relatively small reduction in the cellular levels of 17-oxo-DHA, whereas licochalcone A abolished 17-oxo-DHA formation (Figure 3B). Furthermore, 17-HDHA levels remained high upon addition of licochalcone A, which indicated a direct substrate-product relationship (Figure 3C). Of note, stimulation of M2 macrophages using calcium ionophore resulted in detection of formation of endogenous 17-HDHA and 17-oxo-DHA (Figure S2). Finally, it was investigated whether 17-oxo-DHA is instrumental in the 17-HDHA-induced inhibition of 5-HETE production. Therefore, the effect of 17-oxo-DHA on the activation of human macrophages and neutrophils was investigated. When primary immune cells were incubated with 17-oxo-DHA, a dose-dependent inhibition in the inflammatory response of M2 macrophages and neutrophils was observed as measured by the production of 5-HETE and LTB4. (Figure 3D, F and G).

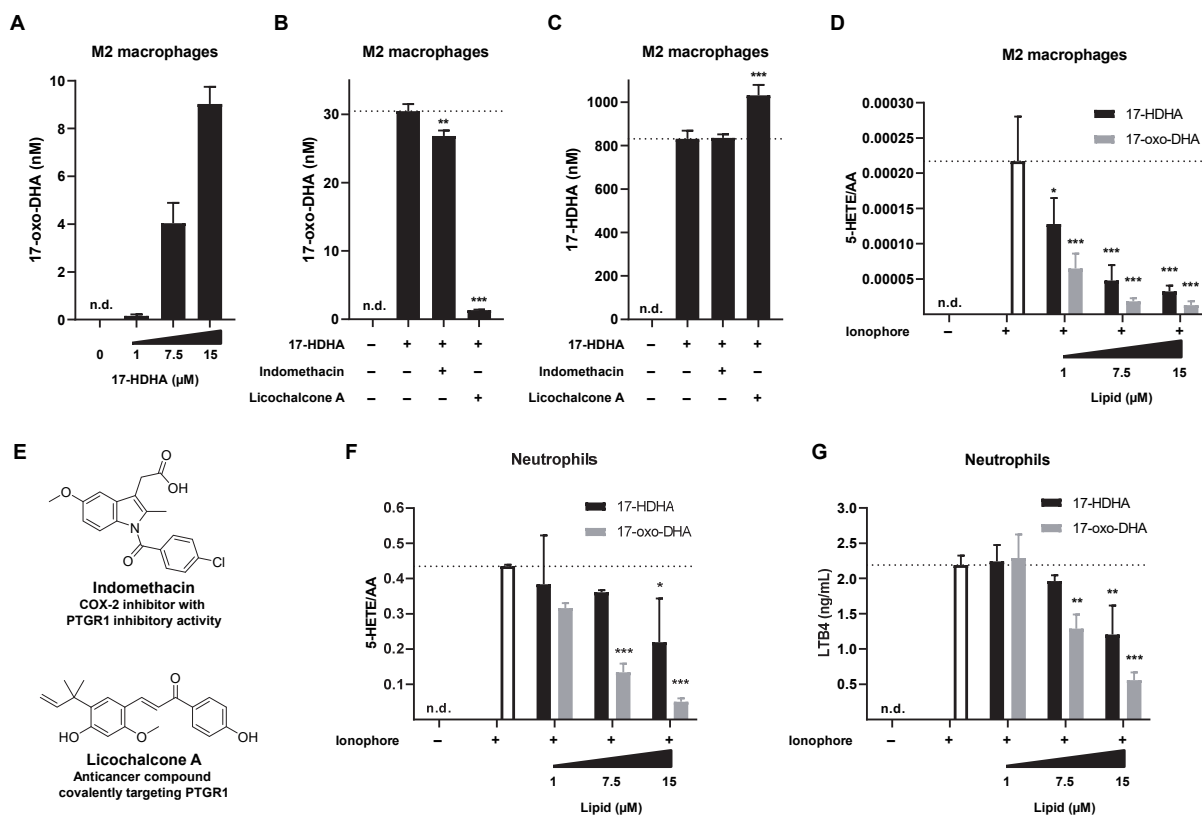


**Figure 3 | Immune cells convert 17-HDHA into 17-oxo-DHA, which is reduced by inhibiting PTGR1.**

(A) 17-oxo-DHA produced by M2 macrophages. Cells were either pretreated for 2 h with 17-HDHA or vehicle control. (B) 17-oxo-DHA and (C) 17-HDHA measured in M2 macrophages show that inhibition of PTGR1 by indomethacin and licochalcone A reduces conversion of 17-HDHA to 17-oxo-DHA. Cells were pretreated for 30 min with 10 μM indomethacin, licochalcone A or vehicle before treatment with 17-HDHA (15 μM) or vehicle for 2 h. (D) 5-HETE/AA ratio (LC-MS/MS) produced by ionophore-stimulated M2 macrophages. Cells were either pretreated for 15 min with 17-HDHA, 17-oxo-DHA or vehicle control. (E) Structures of indomethacin and licochalcone A. (F) 5-HETE/AA ratio and (G) LTB4 levels (LC-MS/MS) produced by ionophore-stimulated neutrophils. Cells were either pretreated for 10 min with 17-HDHA, 17-oxo-DHA or vehicle control. Data represent means ± SD of representative donor ( $n = 2-3$ ). \* $p < 0.05$ , \*\* $p < 0.01$ , \*\*\* $p < 0.001$  in comparison to vehicle control (dotted line) using a one-way ANOVA with Dunnett's multiple comparisons correction. n.d.; not detected.

## Discussion & Conclusion

Omega-3 fatty acids have well-established anti-inflammatory effects. Mechanistic studies indicate that the anti-inflammatory properties of omega-3 fatty acids are linked to their oxidative metabolism, but the molecular mode of action of the oxidative metabolites in human immune cells remains poorly understood.<sup>1,2</sup> In this chapter, a comparative chemical proteomic approach was developed using two complementary bifunctional photoreactive probes **4** and **5**, which were based on the scaffold of the polyunsaturated fatty acid DHA and its oxidative metabolite 17-HDHA. This allowed the identification of PTGR1 as an enzyme catalyzing the conversion of 17-HDHA into 17-oxo-DHA in human M2 macrophages. This finding is important, as it demonstrates that like lipoxygenase enzymes, PTGR1 is simultaneously metabolizing pro- and anti-inflammatory lipids. Macrophages are important players in both the initiation and resolution phase of inflammation and the metabolic network of immunomodulatory lipids needs to be uncovered to understand how this process is dysregulated in chronic inflammatory disease.

Previously, it was reported that 17-oxo-DHA is formed via COX-2-mediated oxidation of DHA, followed by a dehydrogenation step by an undetermined dehydrogenase enzyme.<sup>58</sup> 17-oxo-DHA acts as an anti-inflammatory lipid in leukocytes of COPD patients by inhibiting the NLRP3 inflammasome<sup>59</sup> and as a PPAR $\alpha/\gamma$  dual agonist.<sup>60</sup> Moreover, it was shown to induce an anti-oxidant response through Nrf2 in mice<sup>61</sup> and by inhibiting ROS generation.<sup>62</sup> Here, it was discovered that 17-HDHA formed by 15-LOX metabolism is also used as a substrate for the formation of 17-oxo-DHA in human macrophages, which can be inhibited by two distinct inhibitors of PTGR1. It was also found that 17-oxo-DHA reduces the formation of the proinflammatory lipids 5-HETE and LTB4 in macrophages and neutrophils, thereby exerting anti-inflammatory effect. This suggests that 17-oxo-DHA could act as an inhibitor of 5-lipoxygenase, which is responsible for the production of 5-HETE and LTB4. Alternatively, it is conceivable that 17-oxo-DHA may indirectly modulate the activity of 5-lipoxygenase, for example, by reducing its expression or binding to 5-lipoxygenase activating protein (FLAP).<sup>63</sup>

Altogether, this study extends previous reports suggesting that PTGR1 serves as a metabolic hub that inactivates proinflammatory LTB4 and produces anti-inflammatory DHA derivatives, thereby modulating the cellular levels of these important signaling lipids that act in concert to affect the human macrophage-neutrophil axis. Finally, these results highlight the use of complementary bifunctional, photoreactive probes to identify specific protein interaction partners of promiscuous, lipophilic signaling molecules and also showcase the power of chemical proteomics in guiding the discovery of novel biological insights in primary human cells.

## Experimental procedures

### General

Lipids were purchased from Cayman Chemicals and stored as ethanolic stocks under argon at -80 °C. Reagents and inhibitors used for biochemical experiments were purchased from Cayman Chemicals or Sigma Aldrich unless otherwise specified and stored at -20 °C, except Cy5-N<sub>3</sub> (Figure S3), which was synthesized according to previously published procedures. Biotin-N<sub>3</sub> (Figure S3) was purchased from Bio-Connect Life Sciences.

### Cloning

DNA oligos were purchased at Sigma Aldrich or Integrated DNA Technologies. Cloning reagents were from Thermo Fisher. Full-length cDNA encoding human PTGR1 or GFP was obtained from Source Bioscience. Expression constructs were generated by PCR amplification and restriction/ligation cloning into a pcDNA3.1 vector, in frame with a C-terminal FLAG tag. All plasmids were isolated from transformed XL10-Gold or DH10B competent cells (prepared using E. coli transformation buffer set, Zymo Research) using plasmid isolation kits following the supplier's protocol (Qiagen). All sequences were verified by Sanger sequencing (Macrogen).

### HEK-293-T culture

HEK-293-T cells were cultured at 37 °C under 7% CO<sub>2</sub> in DMEM (D6546, Merck) containing phenol red, stable glutamine, 10% (v/v) New Born Calf Serum (Thermo Fisher) and penicillin and streptomycin (200 µg/mL each, Duchefa). Cells were passaged twice a week at 80-90% confluence by resuspension in fresh medium. Cell lines were purchased from ATCC and were tested regularly for mycoplasma contamination. Cultures were discarded after 2-3 months of use.

### Transfection of HEK-293-T cells

GFP- or PTGR1-overexpressing HEK-293-T cells were generated by seeding HEK-293-T cells on 12-well plates ( $4.0 \times 10^4$  cells/cm<sup>2</sup>) 24 h before transfection. Culture medium was then aspirated and replaced with 400 µL fresh medium. A 3:1 (m/m) mixture of polyethylenimine (PEI) (1.875 µg/well) and plasmid DNA (0.625 µg/well) was prepared in serum-free culture medium (100 µL) and incubated for 15 min at rt. Transfection was performed by dropwise addition of the PEI/DNA mix to the cells. After 24 h, medium was refreshed. Cells were used 48 h post-transfection.

### Gel-based AfBPP of HEK-293-T cells

Confluent HEK-293-T cells on 12-well plates were treated with probe as follows: Growth medium was aspirated, the cells were washed with PBS (0.5 mL) and a solution of pac-DHA (**4**) or pac-17-HDHA (**5**) (10 µM from 10 mM ethanolic stock) in serum-free DMEM supplemented with 0.1% delipidated BSA (0.5 mL) was added. The cells were incubated for 30 min at 37 °C after which the medium was aspirated and the cells were irradiated ("UV") in 1 mL ice-cold PBS using a Caprobox™ (10 min, 4 °C, 350 nm) or exposed to ambient light ("No UV"). The cells were harvested by pipetting and pelleted by centrifugation (1,000 g, 10 min, 4 °C). The supernatant was removed and the cells were lysed by resuspension in lysis buffer (250 mM sucrose, 20 mM HEPES pH 7.5, 1 mM MgCl<sub>2</sub>) and sonication in a bath sonicator (0 °C, 10 s). Protein concentration was measured by Qubit™ assay (Invitrogen) and the samples were adjusted to 1.5 mg/mL and a volume of 100 µL, after which the samples were treated with 10.95 µL click mix (5.5 µL aq. 25 mM CuSO<sub>4</sub>, 3.25 µL aq. 250 mM NaAsc, 1.1 µL 25 mM THPTA in DMSO, 1.1 µL 0.9 mM Cy5-N<sub>3</sub> in DMSO) and left at rt for 1 h. Samples were then quenched by addition of 4X Laemmli buffer, boiled (5 min, 95 °C) and resolved by SDS-PAGE (10% acrylamide gel, ±80 min, 180 V) along with protein marker (PageRuler™ Plus, Thermo Fisher). In-gel fluorescence was measured in the Cy3- and Cy5-channel (Chemidoc™ MP, Bio-Rad).

Proteins were then transferred to a 0.2 µm polyvinylidene difluoride membrane by Trans-Blot Turbo™ Transfer system (Bio-Rad). Membranes were washed with TBS (50 mM Tris pH 7.5, 150 mM NaCl) and blocked with 5% (w/v) milk in TBS-T (50 mM Tris pH 7.5, 150 mM NaCl, 0.05% (w/v) Tween-20) for 1 h at rt. Membranes were then incubated with primary antibody mouse-anti-FLAG (F3156, Merck, 1:2,000 in 5% (w/v) BSA in TBS-T, 1 h, rt), washed three times with TBS-T, incubated with secondary goat-anti-mouse-HRP (sc-2005, Santa Cruz Biotechnologies, 1:5,000 in 5% (w/v) BSA in TBS-T, 1 h, rt) and washed three times with TBS-T and once with TBS. Luminol development solution (10 mL of 1.4 mM luminol in 100 mM Tris pH 8.8 + 100 µL of 6.7 mM *p*-coumaric acid in DMSO + 3 µL of 30% (v/v) H<sub>2</sub>O<sub>2</sub>) was added and chemiluminescence was detected on ChemiDoc™ MP (Bio-Rad) in the chemiluminescence channel and colorimetric channel for the protein marker.

### Macrophage and neutrophil isolation

This study was approved by the local medical ethical committee of the LUMC (METC), and written informed consent was given by all donors. Neutrophils were isolated from fresh 50 mL EDTA blood containers via DextranT500 sedimentation (Pharmacosmos). The upper layer was collected, followed by Ficoll density gradient separation. The remainder of the erythrocytes was removed by hypotonic lysis. Purity was checked by FACS (LSRIII, BD Biosciences) by staining the cells with CD3-AF700 (clone UCHT1)/CD15-APC (clone HI98)/CD16-PE (clone 3G8)/CD19-FITC (clone HIB19) and was typically above 97%. Isolated neutrophils were resuspended in Dulbecco's phosphate-buffered saline (DPBS) with MgCl<sub>2</sub> and CaCl<sub>2</sub> (D8662, Merck). Human peripheral blood mononuclear cells (PBMCs) were isolated by Ficoll density gradient from healthy donor buffy coats (Sanquin). Blood monocytes were isolated by positive selection from PBMCs using MACS CD14 Microbeads (Miltenyi Biotec) and purity was checked by FACS (LSRIII, BD Biosciences), by staining the cells with CD14-PE (clone MopP9). Purity was typical above >99%. Monocytes were differentiated for seven days in RPMI 1640 medium (Gibco) containing 8% FCS, 100 U/mL penicillin and streptomycin, 2 mM Glutamax (Thermo Fisher) and 50 ng/mL M-CSF (R&D Systems). 1/3rd of the medium was replenished containing 150 ng/mL M-CSF on day three and five. Phenotype was checked before experiments by visual inspection by assessing the typical morphology of M-CSF-treated monocyte-derived macrophages (elongated and spindle-like). Moreover, phenotype was also confirmed by performing IL-12 OptEIA (BD Biosciences), IL-10 PeliPair reagent set (Sanquin), and TNFa OptEIA (BD Biosciences) ELISA on supernatant of cells stimulated for 24 h with 10 ng/mL LPS (Merck). M-CSF-treated monocyte-derived macrophages secreted low IL-12 and TNFa and high IL-10 levels.

M-CSF-treated monocyte-derived macrophages (M2 macrophages) were harvested using Accutase (Merck) and for lipidomics experiments 2.5x10<sup>5</sup> cells were seeded in 24-well plates in 250 µL medium. All experiments were performed in phenol red-free RPMI 1640 medium (Gibco), supplemented with 0.1% (w/v) delipidated BSA (Merck), 100 U/mL penicillin and streptomycin, and 2 mM Glutamax. For lipidomics experiments, cells were pretreated with indicated amounts of 17(S)-HDHA (Cayman Chemicals) or vehicle, HPLC grade ethanol (Fischer Scientific), and indicated amount of inhibitor (Merck) or vehicle, 0.02% HPLC grade DMSO. Stimulation of both macrophages and neutrophils was done using 4 µM calcium ionophore A23178 (Merck) for 10 min.

### Lipid isolation and LC-MS/MS

After treatment, cells and supernatant were quenched using three volumes of MeOH (Honeywell, 349661L) and internal standard mix containing known concentrations of three internal standards: 5 ng/mL DHA-d5, 500 pg/mL LTB4-d4 and 500 pg/mL 15(S)-HETE-d8 (Cayman Chemicals) for subsequent quantification. All samples were stored at -80 °C under argon until analysis. Quenched samples were centrifuged (20,000 *g*, 5 min) and the supernatant was transferred into an autosampler vial containing an equal volume of H<sub>2</sub>O (Honeywell) before LC-MS/MS analysis, which was carried out as previously published.<sup>64</sup> The MS method was slightly adapted: it was extended with a MRM for 17-oxo-DHA (341 / 111). Lipid measurements were performed using a QTrap 6500 mass spectrometer in negative ESI mode (Sciex), coupled to a LC system employing LC-30AD pumps, a SIL-30AC auto sampler, and a CTO-20AC column oven (Shimadzu). A Kinetex C18 50 × 2.1 mm, 1.7 µm column

combined with a C8 precolumn (Phenomenex) was used and kept at 50 °C. A gradient of water and methanol with 0.01% acetic acid was used. The injection volume was 40 µL and a flow rate of 400 µL/min was used. MRM transitions used to identify LM were based on previous work by the group of M. Giera.<sup>64</sup> Peaks were integrated with manual supervision and retention time corrected to corresponding IS (RRT) with MultiQuant™ 2.1 (Sciex). Only peaks with a signal to noise (S/N) >10 were quantified. Calibration curves were constructed using authentic synthetic standards 17-HDHA, 17-oxo-DHA, AA, DHA, LTB4, 5-HETE, LTD4, LTE4, 15(S)-HETE-d8, LTB4-d4 and DHA-d5 which were purchased from Cayman Chemicals.

### AfBPP of M2 macrophages

M-CSF-treated monocyte-derived macrophages were plated on 6-well plates. The following day, they were washed with PBS (1 mL) and probe incubation was started by adding pac-DHA or pac-17-HDHA (10 µM from 10 mM ethanolic stock) in serum-free RPMI supplemented with 0.1% (w/v) delipidated BSA (1 mL). The cells were incubated for 30 min at 37 °C after which the medium was aspirated and replaced with ice-cold PBS. The cells were irradiated using a Caprobox™ (10 min, 4 °C, 350 nm, "UV") or exposed to ambient light (10 min, 4 °C, "No UV"). The PBS was collected in tubes and floating cells were spun down (1,000 g, 10 min, 4 °C) and the PBS was aspirated. The cells in the wells were lysed with lysis buffer (250 µL, 250 mM sucrose, 1X protease inhibitor cocktail (Roche), 20 mM HEPES pH 7.5, 1 mM MgCl<sub>2</sub>). The material was harvested by scraping and combined with the cell pellet. This was sonicated (Branson Sonifier probe sonicator, 10 x 1 s pulses, 10% amplitude). Protein concentration was measured by Qubit™ assay (Invitrogen) and the samples were adjusted to 0.5 mg/mL and a volume of 440 µL, of which 40 µL was reserved for gel analysis. For gel analysis, the 40 µL lysate was treated with freshly prepared click mix (4.37 µL per sample: 2.19 µL aq. 25 mM CuSO<sub>4</sub>, 1.3 µL aq. 250 mM NaAsc, 0.44 µL 25 mM THPTA in DMSO, 0.44 µL 0.9 mM Cy5-N<sub>3</sub> in DMSO) and left at rt for 1 h in the dark. Samples were then quenched by addition of 4X Laemmli buffer, boiled (5 min, 95 °C) and resolved by SDS-PAGE (10% acrylamide gel, ±80 min, 180 V) along with protein marker (PageRuler™ Plus, Thermo Fisher). In-gel fluorescence was measured in the Cy3- and Cy5-channel (Chemidoc™ MP, Bio-Rad) and gels were stained with Coomassie after scanning.

### Mass spectrometric analysis of tryptic peptides, identification and quantification

The pulldown experiment is performed as earlier described, with minor adjustments.<sup>65,66</sup> The lysates (400 µL) were subjected to a click reaction with freshly prepared click mix (43.7 µL per sample: 21.9 µL aq. 25 mM CuSO<sub>4</sub>, 13 µL aq. 250 mM NaAsc, 4.4 µL 25 mM THPTA in DMSO, 4.4 µL 2.25 mM biotin-N<sub>3</sub> in DMSO) at rt for 1 h. Proteins were precipitated by addition of HEPES buffer (50 µL, 50 mM, pH 7.5), MeOH (666 µL), CHCl<sub>3</sub> (166 µL) and MilliQ (150 µL), vortexing after each addition. After spinning down (1,500 g, 10 min) the upper and lower layer were aspirated and the protein pellet was resuspended in MeOH (600 µL) by sonication (Branson Sonifier probe sonicator, 10 x 0.5 s pulses, 10% amplitude). The proteins were spun down (20,000 g, 5 min) and the MeOH was aspirated. The proteins were then redissolved in 6 M urea (500 µL) with 25 mM NH<sub>4</sub>HCO<sub>3</sub> for 15 min, followed by reduction (65 °C, 15 min, 800 rpm shaking) with DTT (5 µL, 1 M). The samples were allowed to reach rt and proteins were alkylated (30 min) with IAA (40 µL, 0.5 M) in the dark. 140 µL SDS (10% w/v) was added and the samples were spun down (1,000 g, 5 min). They were transferred to 5 mL PBS containing 50 µL avidin agarose resin (Pierce, 100 µL of a 50% slurry, prewashed twice with 6 mL PBS + 0.5% SDS and once with 6 mL PBS) and incubated for 2 h while rotating. The beads were then spun down (2,000 g, 2 min) and washed (3 x PBS + 0.25% SDS, 2 x PBS, 1 x MilliQ). The beads were resuspended in digestion buffer (250 µL, 100 mM Tris pH 7.8, 100 mM NaCl, 1 mM CaCl<sub>2</sub>, 2% (v/v) acetonitrile, sequencing grade trypsin (Promega, 0.25 µg)) and transferred to low-binding tubes (Sarstedt) and incubated while shaking overnight (16 h, 37 °C, 1,000 rpm). Trypsin was quenched with 12.5 µL formic acid (LC-MS grade) and the beads were then filtered off over a Bio-Spin column (BioRad, 400 g, 5 min), collecting the flow-through in a new 2 mL tube. Samples were added on C18 stagetips<sup>67</sup> (preconditioned with 50 µL MeOH, then 50 µL of 0.5% (v/v) formic acid in 80% (v/v) acetonitrile/MilliQ (solution B) and then 50 µL 0.5% (v/v) formic acid in MilliQ (solution A) by centrifugation (600 g, 2 min)). The peptides were washed with

solution A (100 µL, 800 g, 3 min) and eluted into new low-binding tubes using solution B (100 µL, 800 g, 3 min). Samples were concentrated using an Eppendorf speedvac (Eppendorf Concentrator Plus 5301) and redissolved in LC-MS solution (30 µL per sample: 28.5 µL MilliQ, 2.85 µL acetonitrile, 0.095 µL formic acid, 600 fmol yeast enolase digest (Waters, 186002325)).

Samples were measured using a NanoACQUITY UPLC System coupled to a SYNAPT G2-Si high definition mass spectrometer (Waters). The peptides were separated using an analytical column (HSS-T3 C18 1.8 µm, 75 µm x 250 mm, Waters) with a concave gradient (5 to 40% acetonitrile in H<sub>2</sub>O with 0.1% formic acid). [Glu<sup>1</sup>]-fibrinopeptide B was used as lock mass. Mass spectra were acquired using the UDMS<sup>e</sup> method. The mass range was set from 50 to 2,000 Da with a scan time of 0.6 seconds in positive, resolution mode. The collision energy was set to 4 V in the trap cell for low-energy MS mode. For the elevated energy scan, the transfer cell collision energy was ramped using drift-time-specific collision energies. The lock mass is sampled every 30 seconds. For raw data processing, Progenesis QI for proteomics was used with the following parameters to search the human proteome from Uniprot (Table S1). Albumin was not included in the analysis of probe targets.

**Table S1 | Parameters used for Progenesis QI.**

Parameter	Value
Lock mass <i>m/z</i> value	785.8426
Low energy threshold	150 counts
Elevated energy threshold	30 counts
Digest reagent	Trypsin
Missed cleavages	Max 2
Modifications	Fixed carbamidomethyl C, variable oxidation M
FDR less than	1%
Minimum fragments/peptide	2
Minimum fragments/protein	5
Minimum peptides/protein	1
Minimum peptide score for quantification	5.5
Identified ion charges for quantification	2/3/4/5/6/7 <sup>+</sup>

### Statistical analysis

Unless otherwise noted, all data represent means ± SD. Statistical significance was determined using Student's t-tests (two-tailed, unpaired) or ANOVA with Dunnett's or Tukey's multiple comparisons correction. \*\*\* p <0.001; \*\* p <0.01; \* p <0.05; n.s. if p >0.05. All statistical analysis was conducted using Graphpad Prism 8.1.1 or Microsoft Excel.

## Synthesis

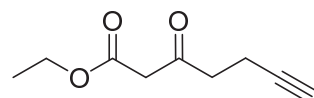
### General remarks

Dry solvents were prepared by storage on activated 4 Å molecular sieves for at least 24 hours. The reactions were performed under an inert atmosphere of nitrogen gas unless stated otherwise. All reagents were purchased from Alfa Aesar, Sigma Aldrich/Merck or Acros and used without further purification. Flash column chromatography was performed using SiliCycle silica gel type SiliaFlash P60 (230-400 mesh). TLC analysis was performed on Merck silica gel 60/Kieselguhr F254, 0.25 mm. Compounds were visualized using KMnO<sub>4</sub> stain (K<sub>2</sub>CO<sub>3</sub> (40 g), KMnO<sub>4</sub> (6 g), and water (600 mL)). <sup>1</sup>H NMR and <sup>13</sup>C NMR spectra were recorded on a Bruker AV-400 (400 MHz) or AV-500 (500 MHz) spectrometer. Chemical shift values are reported in ppm relative to the tetramethylsilane signal for <sup>1</sup>H NMR ( $\delta$  = 0 ppm) and relative to the solvent signal of CDCl<sub>3</sub> for <sup>13</sup>C NMR ( $\delta$  = 77.16 ppm). Data are reported as follows: Chemical shifts ( $\delta$ ), multiplicity (s = singlet, d = doublet, dd = doublet of doublets, ddt = doublet of doublet of triplets, td = triplet of doublets, t = triplet, q = quartet, p = pentet, bs = broad singlet, m = multiplet), coupling constants  $J$ (Hz), and integration. High resolution mass spectra (HRMS) were recorded by direct injection on a q-TOF mass spectrometer (Synapt G2-SI) equipped with an electrospray ion source in positive mode with Leu-enkephalin ( $m/z$  = 556.2771) as an internal lock mass. The instrument was calibrated prior to measurement using the MS/MS spectrum of [Glu<sup>1</sup>]-fibrinopeptide B.

Preparative HPLC separations were performed with an Agilent Technologies 1200 series HPLC system using a Gemini column (5 µm C18, pore size: 100 Å, 250 x 10.0 mm) or Nucleodur column (5 µm C18, pore size: 110 Å, 250 x 10.0 mm) using a specified linear gradient (Gradient of solvent B in solvent A in 12 min, flow rate of 5 mL/min, detection at 210 - 600 nm by a diode array and Agilent 6130 series quadrupole mass detector, solvent A: 0.2% (v/v) TFA in H<sub>2</sub>O, solvent B: acetonitrile). Analytical LC-MS was performed using a C18 column (50 x 4.6 mm, 3 µm; Nucleodur Gravity, Macherey-Nagel) connected to a Vanquish UHPLC system (Thermo Scientific) with a Vanquish Diode Array detector (Thermo Scientific) coupled to a LCQ™ Fleet (Thermo Scientific) via electrospray ionization (ESI). Acetonitrile and water containing TFA (0.1%) were used for chromatographic separation using an indicated gradient.

Fragmentation of pac-17-HDHA (**5**) was done after reduction of the double bonds, as LC-MS/MS fragmentation in negative mode was not successful, possibly due to activation of the diazirine during tandem MS. Pac-17-HDHA (**5**) was analyzed by complete hydrogenation of an analytical sample (50 nmol) in EtOH (1 mL) using catalytic PtO<sub>2</sub> and hydrogen gas, followed by the filtration of the catalyst by cotton, removal of the solvent under a stream of N<sub>2</sub> gas and redissolving in 100 µL acetonitrile, injecting 10 µL on a C18 column (50 x 4.6 mm, 3 µm; Gemini) connected to a Agilent Technologies 1260 Infinity system and eluting it with acetonitrile/H<sub>2</sub>O (70:30) with 10 mM NH<sub>4</sub>OAc onto a 6120 Quadrupole LC/MS (Agilent Technologies) equipped with an electrospray ion source in positive mode (source voltage 4 kV, sheath gas flow 10, capillary temperature 623 K).

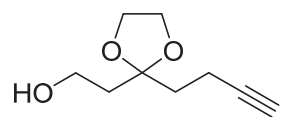
### Ethyl 3-oxohept-6-yneate (11)



Freshly distilled diisopropylamine (20.43 mL, 143 mmol) was dissolved in dry THF (60 mL) and cooled to -78 °C. *n*-BuLi (1.4 M in hexane, 102 mL, 143 mmol) was added dropwise and the reaction was stirred for 15 min.

The mixture was allowed to reach -40 °C after which ethyl 3-oxobutanoate (8.23 mL, 65.2 mmol) in dry THF (40 mL) was added dropwise. After 30 min of stirring, propargyl bromide (80 wt.% in toluene, 7.02 mL, 65.2 mmol) was added dropwise after which the reaction was allowed to reach 0 °C. After 1.5 h of stirring, it was quenched with 0.5 M aq. HCl (200 mL) and diluted with Et<sub>2</sub>O (200 mL). The organic layer was collected and the aq. layer extracted with Et<sub>2</sub>O (200 mL). The combined organic layers were washed with brine (100 mL), dried over MgSO<sub>4</sub>, filtered and concentrated under reduced pressure to afford a dark brown oil, which was distilled (105-110 °C, 6.8 mmHg) to afford the title compound as a clear oil (4.943 g, 29.4 mmol, 45%). R<sub>f</sub> = 0.60 (EtOAc/pentane = 1:4); <sup>1</sup>H NMR (400 MHz, CDCl<sub>3</sub>) δ 4.20 (q, *J* = 7.1 Hz, 2H), 3.48 (s, 2H), 2.82 (t, *J* = 7.2 Hz, 2H), 2.48 (td, *J* = 7.2, 2.7 Hz, 2H), 1.98 (t, *J* = 2.7 Hz, 1H), 1.29 (t, *J* = 7.1 Hz, 3H); <sup>13</sup>C NMR (101 MHz, CDCl<sub>3</sub>) δ 200.63, 166.95, 82.59, 69.05, 61.51, 49.23, 41.63, 14.13, 12.84. Spectra were consistent with previously reported data.<sup>68</sup>

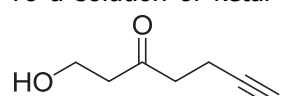
### 2-(2-(But-3-yn-1-yl)-1,3-dioxolan-2-yl)ethan-1-ol (12)

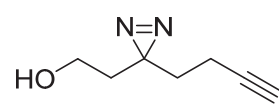


In a microwave vial, ketone **11** (0.8619 g, 5.12 mmol), ethylene glycol (2.143 mL, 38.4 mmol), *p*-TsOH·2H<sub>2</sub>O (0.049 g, 0.256 mmol) and triethyl orthoformate (2.56 mL, 15.37 mmol) were added, the vial was sealed and the reaction was stirred at 80 °C for 1.5 h. The mixture was diluted with Et<sub>2</sub>O (5 mL) and quenched with sat. aq. NaHCO<sub>3</sub> (5 mL). It was then diluted with Et<sub>2</sub>O (100 mL) and sat. aq. NaHCO<sub>3</sub> (100 mL). The layers were separated and the organic layer washed with brine (100 mL), dried over Na<sub>2</sub>SO<sub>4</sub> and concentrated under reduced pressure to afford crude ethyl 2-(2-(but-3-yn-1-yl)-1,3-dioxolan-2-yl)acetate. The residue was diluted with dry THF (20 mL) and added dropwise to a cold (0 °C) mixture of LiAlH<sub>4</sub> (0.389 g, 10.24 mmol) and dry THF (20 mL). The reaction was allowed to reach rt and after 0.5 h it was cooled to 0 °C and quenched with EtOAc (5 mL). After 15 min, 10% (w/v) aq. Rochelle's salt (40 mL) was added and the mixture was allowed to reach rt overnight. The mixture was then diluted with brine (40 mL) and extracted with Et<sub>2</sub>O (5 x 40 mL). The combined organic layers were washed with brine (100 mL), dried over Na<sub>2</sub>SO<sub>4</sub>, filtered, concentrated under reduced pressure and filtered over a plug of silica with EtOAc/pentane (1:1) to afford the title compound as a yellow oil (0.8204 g, 4.82 mmol, 94%). R<sub>f</sub> = 0.63 (EtOAc); <sup>1</sup>H NMR (400 MHz, CDCl<sub>3</sub>) δ 4.06 – 3.93 (m, 4H), 3.76 (q, *J* = 5.4 Hz, 2H), 2.72 (t, *J* = 5.5 Hz, 1H), 2.32 – 2.24 (m, 2H), 1.99 – 1.91 (m, 5H); <sup>13</sup>C NMR (101 MHz, CDCl<sub>3</sub>) δ 111.12, 84.04, 68.36, 65.03, 58.76, 38.35, 35.99, 13.22. Spectra were consistent with previously reported data.<sup>36</sup>

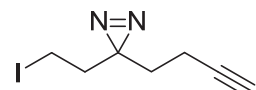
### 1-Hydroxyhept-6-yn-3-one (13)

To a solution of ketal **12** (0.8204 g, 4.82 mmol) in acetone (19 mL) and water (1 mL) was added *p*-TsOH·2H<sub>2</sub>O (0.229 g, 1.205 mmol) and the reaction was stirred for 1 h at 50 °C. It was quenched with sat. aq. NaHCO<sub>3</sub> (50 mL) and diluted with EtOAc (50 mL). The aq. layer was separated and extracted with EtOAc (50 mL). The combined organic layers were washed with brine (50 mL), dried over MgSO<sub>4</sub>, filtered, concentrated under reduced pressure and purified by column chromatography (EtOAc/pentane = 1:2 to 1:1) to afford the title compound as a yellow oil (0.565 g, 4.48 mmol, 93%). R<sub>f</sub> = 0.62 (EtOAc); <sup>1</sup>H NMR (400 MHz, CDCl<sub>3</sub>) δ 3.87 (t, *J* = 5.5 Hz, 2H), 2.76 – 2.68 (m, 5H), 2.46 (td, *J* = 7.1, 2.6 Hz, 2H), 1.98 (t, *J* = 2.7 Hz, 1H); <sup>13</sup>C NMR (101 MHz, CDCl<sub>3</sub>) δ 209.03, 82.89, 68.95, 57.62, 44.68, 41.81, 12.78. Spectra were consistent with previously reported data.<sup>36</sup>

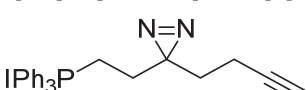


**2-(3-(But-3-yn-1-yl)-3*H*-diazirin-3-yl)ethan-1-ol (14)**

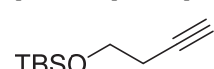
Ketone **13** (0.660 g, 5.23 mmol) was dried by coevaporation with toluene. It was dissolved in dry MeOH (15 mL) and cooled to 0 °C. NH<sub>3</sub> gas was bubbled through the solution for 30 min under stirring after which the reaction was stirred for 5 h. Then, hydroxylamine-*o*-sulfonic acid (0.887 g, 7.85 mmol) in dry MeOH (5 mL) was added dropwise and the reaction was allowed to reach rt overnight. It was filtered over celite and the filtrate was concentrated under reduced pressure. The residue was redissolved in dry MeOH (10 mL) and Et<sub>3</sub>N (1.094 mL, 7.85 mmol) was added. The reaction was cooled to 0 °C and a sat. solution of I<sub>2</sub> in dry MeOH was added dropwise until the color persisted for 20 min (8 mL). The reaction was diluted with EtOAc (100 mL) and quenched with 1 M aq. Na<sub>2</sub>S<sub>2</sub>O<sub>3</sub> (100 mL). The layers were separated, the aq. layer was extracted with EtOAc (100 mL) and the combined organic layers were washed with 1 M aq. HCl (100 mL) and brine (100 mL), dried over MgSO<sub>4</sub>, filtered and concentrated under reduced pressure. Column chromatography of the residue (EtOAc/pentane = 1:6 to 1:3) afforded the title compound as a yellow oil (0.2677 g, 1.937 mmol, 37%). R<sub>f</sub> = 0.59 (EtOAc/pentane = 1:1); <sup>1</sup>H NMR (400 MHz, CDCl<sub>3</sub>) δ 3.49 (t, J = 6.2 Hz, 2H), 2.10 – 2.01 (m, 2H), 1.99 (s, 1H), 1.77 – 1.65 (m, 4H); <sup>13</sup>C NMR (101 MHz, CDCl<sub>3</sub>) δ 82.95, 69.34, 57.36, 35.56, 32.68, 26.72, 13.31; HRMS: Calculated for [C<sub>7</sub>H<sub>10</sub>N<sub>2</sub>O+H]<sup>+</sup> 139.0866, found 139.0865.

**3-(But-3-yn-1-yl)-3-(2-iodoethyl)-3*H*-diazirine (15)**

To a cooled (0 °C) solution of alcohol **14** (0.6617 g, 4.79 mmol) dry DCM (24 mL) was added imidazole (0.978 g, 14.37 mmol), I<sub>2</sub> (1.459 g, 5.75 mmol) and PPh<sub>3</sub> (1.382 g, 5.27 mmol). The reaction was allowed to reach rt and stirred for 3 h. It was cooled to 0 °C and quenched with 10% aq. Na<sub>2</sub>S<sub>2</sub>O<sub>3</sub> (50 mL) and diluted with DCM (100 mL). The aq. layer was isolated and extracted with DCM (100 mL) and the combined organic layers were dried over MgSO<sub>4</sub>, filtered and concentrated under reduced pressure. Column chromatography of the residue (Et<sub>2</sub>O/pentane = 1:49 to 1:16) afforded the title compound as a yellow liquid (0.8609 g, 3.47 mmol, 73%). R<sub>f</sub> = 0.69 (EtOAc/pentane = 1:19); <sup>1</sup>H NMR (400 MHz, CDCl<sub>3</sub>) δ 2.90 (t, J = 7.6 Hz, 2H), 2.13 (t, J = 7.6 Hz, 2H), 2.07 – 2.00 (m, 3H), 1.72 – 1.67 (m, 2H); <sup>13</sup>C NMR (101 MHz, CDCl<sub>3</sub>) δ 82.50, 69.56, 37.54, 31.84, 28.67, 13.32, -3.76. Spectra were consistent with previously reported data.<sup>69</sup>

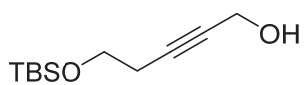
**(2-(3-(But-3-yn-1-yl)-3*H*-diazirin-3-yl)ethyl)triphenylphosphonium iodide (6)**

To a solution of iodide **15** (0.2621 g, 1.057 mmol) in dry acetonitrile (4.2 mL) in a microwave vial was added PPh<sub>3</sub> (1.386 g, 5.28 mmol) and the vial was sealed. The mixture was degassed and stirred at 70 °C overnight, concentrated under reduced pressure and purified by column chromatography (MeOH/DCM = 1:100 to 1:19) to afford the title compound as a white solid (0.539 g, 1.056 mmol, quant.). R<sub>f</sub> = 0.49 (MeOH/DCM = 1:9); <sup>1</sup>H NMR (400 MHz, CDCl<sub>3</sub>) δ 7.90 – 7.75 (m, 10H), 7.74 – 7.69 (m, 5H), 3.83 – 3.70 (m, 2H), 2.11 – 2.01 (m, 2H), 2.01 – 1.92 (m, 2H), 1.90 (t, J = 2.6 Hz, 1H), 1.85 – 1.72 (m, 2H); <sup>13</sup>C NMR (101 MHz, CDCl<sub>3</sub>) δ 135.52 (d, J = 2.9 Hz), 133.85 (d, J = 10.1 Hz), 130.79 (d, J = 12.7 Hz), 117.42 (d, J = 86.6 Hz), 83.03, 69.60, 31.16, 28.42, 27.22 (d, J = 2.9 Hz), 18.71 (d, J = 51.8 Hz), 13.55; HRMS: Calculated for [C<sub>25</sub>H<sub>24</sub>N<sub>2</sub>P]<sup>+</sup> 383.1672, found 383.1681.

**(But-3-yn-1-yloxy)(tert-butyl)dimethylsilane (17)**

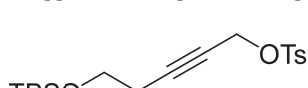
To a cooled (0 °C) solution of but-3-yn-1-ol (5.0 mL, 66 mmol) in dry DMF (150 mL) was added imidazole (6.75 g, 99 mmol) and subsequently TBSCl (11.95 g, 79 mmol) in portions. After 2 h, the reaction was quenched with H<sub>2</sub>O (100 mL) and diluted with Et<sub>2</sub>O (150 mL). The layers were separated and the aqueous layer extracted with Et<sub>2</sub>O (150 mL). The combined organic layers were washed with brine (4 x 100 mL), dried over MgSO<sub>4</sub>, filtered and concentrated under reduced pressure to afford the title compound as a clear liquid (11.95 g, 64.8 mmol, 98%). <sup>1</sup>H NMR (400 MHz, CDCl<sub>3</sub>) δ 3.74 (t, J = 7.1 Hz, 2H), 2.40 (td, J = 7.1, 2.7 Hz, 2H), 1.96 (t, J = 2.7 Hz, 1H), 0.89 (s, 9H), 0.07 (s, 6H); <sup>13</sup>C NMR (101 MHz, CDCl<sub>3</sub>) δ 81.66, 69.43, 61.87, 26.02, 22.98, -5.16. Spectra were consistent with previously reported data.<sup>70</sup>

**5-((*Tert*-butyldimethylsilyl)oxy)pent-2-yn-1-ol (18)**



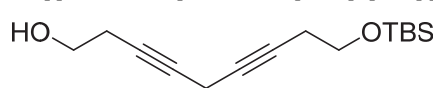
To a cooled (-40 °C) solution of alkyne **17** (26.76 g, 145 mmol) in dry THF (300 mL) under argon was added *n*-BuLi (61.0 mL, 152 mmol) dropwise over 10 min. After addition, it was stirred at -40 °C for 15 min and subsequently transferred through cannula to a flask containing a cooled (-40 °C) suspension of paraformaldehyde (13.08 g, 435 mmol) in dry THF (150 mL). After addition, the cooling bath was removed and the mixture was stirred for 1 h. It was then diluted with Et<sub>2</sub>O (500 mL) and quenched by addition of brine (50 mL). The mixture was then washed with brine (150 mL) after which the organic layer was collected, dried over MgSO<sub>4</sub>, filtered and concentrated under reduced pressure. The residue was purified through column chromatography (EtOAc/pentane = 1:19 to 1:4) to afford the title compound as a clear oil (25.46 g, 119 mmol, 82%). R<sub>f</sub> = 0.22 (EtOAc/pentane = 1:9); <sup>1</sup>H NMR (400 MHz, CDCl<sub>3</sub>) δ 4.23 (t, J = 2.2 Hz, 2H), 3.71 (t, J = 7.2 Hz, 2H), 2.42 (tt, J = 7.2, 2.1 Hz, 2H), 1.95 (bs, 1H), 0.89 (s, 9H), 0.06 (s, 6H); <sup>13</sup>C NMR (101 MHz, CDCl<sub>3</sub>) δ 83.43, 79.63, 61.95, 51.39, 26.00, 23.23, 18.47, -5.16. Spectra were consistent with previously reported data.<sup>71</sup>

**5-((*Tert*-butyldimethylsilyl)oxy)pent-2-yn-1-yl 4-methylbenzenesulfonate (19)**



To a cooled (0 °C) solution of alcohol **18** (8.220 g, 38.3 mmol) in Et<sub>2</sub>O (80 mL) was added TsCl (8.77 g, 46.0 mmol) followed by freshly pestled KOH (10.76 g, 192 mmol) in 10 portions over 5 min. The reaction was removed from the ice bath and after 45 min it was diluted with Et<sub>2</sub>O (120 mL), cooled to 0 °C and poured into ice water (200 mL). The layers were separated and the aq. layer extracted with Et<sub>2</sub>O (200 mL). The combined organic layers were washed with brine, dried over MgSO<sub>4</sub>, filtered and concentrated under reduced pressure to afford the crude product (12.9622 g) as a slightly orange oil which was used without further purification due to its instability. R<sub>f</sub> = 0.69 (EtOAc/pentane = 1:9); For NMR characterization an analytical sample was purified by column chromatography (EtOAc/pentane = 1:24); <sup>1</sup>H NMR (400 MHz, CDCl<sub>3</sub>) δ 7.80 (d, J = 8.4 Hz, 2H), 7.34 (d, J = 8.0 Hz, 2H), 4.67 (t, J = 2.2 Hz, 2H), 3.59 (t, J = 7.1 Hz, 2H), 2.44 (s, 3H), 2.29 (tt, J = 7.1, 2.2 Hz, 2H), 0.87 (s, 9H), 0.03 (s, 6H); <sup>13</sup>C NMR (101 MHz, CDCl<sub>3</sub>) δ 145.04, 133.37, 129.86, 128.24, 87.58, 73.03, 61.36, 58.66, 25.94, 23.17, 21.78, 18.40, -5.21. Spectra were consistent with previously reported data.<sup>72</sup>

**9-((*Tert*-butyldimethylsilyl)oxy)nona-3,6-diyne-1-ol (20)**



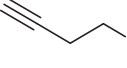
In a roundbottom flask, CuI (7.62 g, 40.0 mmol), NaI (6.00 g, 40.0 mmol) and Cs<sub>2</sub>CO<sub>3</sub> (13.04 g, 40.0 mmol) were dried under vacuum at 90 °C for 2 h. The flask was backfilled with nitrogen and allowed to reach rt. Dry degassed DMF (70 mL) was added and the mixture was stirred for 10 min. But-3-yn-1-ol (3.22 mL, 42.6 mmol) was added to the mixture which was then stirred for 10 min. Sulfonate ester **19** (13.08 g, 35.5 mmol) was then added dropwise and the reaction was stirred overnight in the dark. The reaction was quenched with sat. aq. NH<sub>4</sub>Cl (15 mL) and diluted with Et<sub>2</sub>O (150 mL). After 20 min of stirring, the mixture was filtered over pad of celite and sand. The pad was rinsed with Et<sub>2</sub>O (800 mL) and the resulting solution was washed with sat. aq. NH<sub>4</sub>Cl (200 mL) and water (200 mL). The combined aq. layers were extracted with Et<sub>2</sub>O (200 mL) and the combined organic layers were washed with brine (400 mL), dried over MgSO<sub>4</sub>, filtered and concentrated under reduced pressure. Column chromatography (Et<sub>2</sub>O/pentane = 1:10 to 1:4) afforded the title compound as a yellow oil (8.170 g, 30.7 mmol, 86%). R<sub>f</sub> = 0.36 (EtOAc/pentane = 1:4); <sup>1</sup>H NMR (400 MHz, CDCl<sub>3</sub>) δ 3.72 – 3.66 (m, 4H), 3.12 (p, J = 2.4 Hz, 2H), 2.43 (tt, J = 6.2, 2.4 Hz, 2H), 2.37 (tt, J = 7.2, 2.4 Hz, 2H), 0.88 (s, 9H), 0.06 (s, 6H); <sup>13</sup>C NMR (101 MHz, CDCl<sub>3</sub>) δ 77.80, 77.07, 76.74, 75.37, 62.08, 61.22, 26.02, 23.24, 23.22, 18.49, 9.89, -5.13; HRMS: Calculated for [C<sub>15</sub>H<sub>26</sub>O<sub>2</sub>Si+H]<sup>+</sup> 267.1775, found 267.1775.

**(3*Z*,6*Z*)-9-((*Tert*-butyldimethylsilyl)oxy)nona-3,6-dien-1-ol (9)**

In a Schlenk flask, nickel acetate hydrate (0.300 g, 1.206 mmol) was added to 96% EtOH (15.08 mL) and purged with nitrogen. In a vial, NaBH<sub>4</sub> (0.046 g, 1.206 mmol) was added to a mixture of 96% EtOH (0.2 mL) and aq. NaOH (2 M, 11  $\mu$ L) and the mixture was added dropwise to the Schlenk flask. The flask was

purged with H<sub>2</sub> and stirred for 20 min. Then, freshly distilled ethylenediamine (0.244 mL, 3.62 mmol) and alcohol **20** (1.6071 g, 6.03 mmol) were added and the reaction was stirred under H<sub>2</sub> atmosphere. After 2 h, additional catalyst was prepared in a Schlenk flask in 96% EtOH (5 mL) and added to the reaction via cannula. After 20 min of stirring the reaction was purged with N<sub>2</sub>, the mixture was diluted with Et<sub>2</sub>O (80 mL) and water (80 mL) and filtered over celite. The layers were separated, the organic layer was washed with water (80 mL) and the combined aq. layers were extracted with Et<sub>2</sub>O (100 mL). The combined organic layers were washed with water (100 mL) and brine (100 mL), dried over MgSO<sub>4</sub>, filtered and concentrated under reduced pressure. Column chromatography (EtOAc/pentane = 1:14.5 to 1:10.5) afforded the title compound (1.0363 g, 3.83 mmol, 64%) as a yellow oil. R<sub>f</sub> = 0.69 (EtOAc/pentane = 1:2); <sup>1</sup>H NMR (400 MHz, CDCl<sub>3</sub>) δ 5.58 – 5.49 (m, 1H), 5.47 – 5.35 (m, 3H), 3.65 (t, J = 6.5 Hz, 2H), 3.62 (t, J = 6.9 Hz, 2H), 2.84 (t, J = 5.7 Hz, 2H), 2.41 – 2.26 (m, 4H), 0.89 (s, 9H), 0.05 (s, 6H); <sup>13</sup>C NMR (101 MHz, CDCl<sub>3</sub>) δ 131.42, 129.52, 126.55, 125.67, 62.98, 62.35, 31.25, 30.97, 26.10, 26.02, -5.12; HRMS: Calculated for [C<sub>15</sub>H<sub>30</sub>O<sub>2</sub>Si+H]<sup>+</sup> 271.2088, found 271.2090.

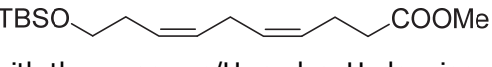
### Methyl pent-4-ynoate (22)

 To a cooled (0 °C) solution of pent-4-ynoic acid (5.14 g, 52.4 mmol) in dry MeOH (200 mL) was added SOCl<sub>2</sub> (4.21 mL, 57.6 mmol) dropwise after which the reaction was allowed to reach rt overnight. The reaction was diluted with DCM (250 mL) and sat. aq. NaHCO<sub>3</sub> (500 mL). The layers were separated and the aq. layer extracted with DCM (200 mL). The combined organic layers were washed with brine (200 mL), dried over MgSO<sub>4</sub>, filtered, concentrated under reduced pressure and coevaporated with DCM to afford the title compound as a clear oil (5.39 g, 48.1 mmol, 92%). R<sub>f</sub> = 0.47 (EtOAc/pentane 1:19); <sup>1</sup>H NMR (400 MHz, CDCl<sub>3</sub>) δ 3.71 (s, 3H), 2.60 – 2.54 (m, 2H), 2.54 – 2.48 (m, 2H), 1.99 (t, J = 2.5 Hz, 1H); <sup>13</sup>C NMR (101 MHz, CDCl<sub>3</sub>) δ 172.31, 82.55, 69.12, 51.92, 33.23, 14.44. Spectra were consistent with previously reported data.<sup>73</sup>

### Methyl 10-((tert-butyldimethylsilyl)oxy)deca-4,7-dynoate (23)

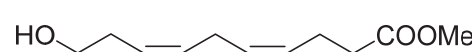
 In a roundbottom flask, CuI (7.29 g, 38.3 mmol), NaI (5.74 g, 38.3 mmol) and Cs<sub>2</sub>CO<sub>3</sub> (12.48 g, 38.3 mmol) were dried under vacuum for 6 h at 95 °C. The flask was refilled with nitrogen and allowed to cool to rt. Under stirring, dry degassed DMF (70 mL) was added and the mixture was stirred for 10 min. Then, alkyne **22** (5.389 g, 48.1 mmol) was added in one portion after which sulfonate ester **19** (12.97 g, 35.2 mmol) was added dropwise over 15 min and the reaction was stirred overnight. The reaction was diluted with Et<sub>2</sub>O (320 mL) and quenched with sat. aq. NH<sub>4</sub>Cl (12 mL) and stirred for 15 min. The mixture was filtered over celite and the filter was rinsed with Et<sub>2</sub>O (1.5 L). The mixture was washed with sat. aq. NH<sub>4</sub>Cl (100 mL) and water (100 mL), the combined aq. layers were extracted with Et<sub>2</sub>O (100 mL) and the combined organic layers were washed with brine (5 x 100 mL). The organic layer was dried over MgSO<sub>4</sub>, filtered and concentrated under reduced pressure. The residue was purified using neutralized silica (flushed with 0.5% Et<sub>3</sub>N in pentane, EtOAc/pentane = 1:99 to 1:24) to afford the title compound as a clear oil (8.050 g, 26.1 mmol, 74%). R<sub>f</sub> = 0.54 (EtOAc/pentane = 1:9); <sup>1</sup>H NMR (400 MHz, CDCl<sub>3</sub>) δ 3.73 – 3.65 (m, 5H), 3.09 (t, J = 2.3 Hz, 2H), 2.55 – 2.46 (m, 4H), 2.40 – 2.33 (m, 2H), 0.88 (s, 9H), 0.06 (s, 6H); <sup>13</sup>C NMR (101 MHz, CDCl<sub>3</sub>) δ 172.57, 78.55, 77.63, 75.45, 75.27, 62.09, 51.87, 33.49, 26.01, 23.22, 18.47, 14.76, 9.83, -5.15; HRMS: Calculated for [C<sub>17</sub>H<sub>28</sub>O<sub>3</sub>Si+H]<sup>+</sup> 309.1881, found 309.1882.

### Methyl (4Z,7Z)-10-((tert-butyldimethylsilyl)oxy)deca-4,7-dienoate (24)

 In a microwave vial, nickel acetate hydrate (0.169 g, 0.681 mmol) was dissolved in MeOH (2 mL) and purged with three vacuum/H<sub>2</sub> cycles. Under vigorous stirring, NaBH<sub>4</sub> (0.026 g, 0.681 mmol) was added in dry MeOH (1 mL). After 15 min, freshly distilled ethylenediamine (0.184 mL, 2.72 mmol) was added and the mixture was purged with a cycle of vacuum/H<sub>2</sub>. After 15 min a solution of methyl ester **23** in MeOH (1 mL) was added and the mixture was purged with a cycle of vacuum/H<sub>2</sub>. After 3 h, the mixture was purged with three vacuum/N<sub>2</sub> cycles, filtered over celite and concentrated under reduced pressure. The

residue was redissolved in Et<sub>2</sub>O (10 mL), washed with sat. aq. NH<sub>4</sub>Cl (5 mL) and brine (5 mL), dried over Na<sub>2</sub>SO<sub>4</sub>, filtered and concentrated under reduced pressure to afford the title compound as a yellow oil (0.0634 g, 0.203 mmol, 89%). R<sub>f</sub> = 0.62 (EtOAc/pentane = 1:24); <sup>1</sup>H NMR (400 MHz, CDCl<sub>3</sub>) δ 5.45 – 5.30 (m, 4H), 3.67 (s, 3H), 3.61 (t, J = 6.9 Hz, 2H), 2.81 (t, J = 5.8 Hz, 2H), 2.42 – 2.33 (m, 4H), 2.33 – 2.24 (m, 2H), 0.89 (s, 9H), 0.05 (s, 6H); <sup>13</sup>C NMR (101 MHz, CDCl<sub>3</sub>) δ 173.68, 129.63, 129.56, 127.87, 126.44, 62.98, 51.68, 34.15, 31.24, 26.09, 25.82, 22.92, 18.50, -5.13; HRMS: Calculated for [C<sub>17</sub>H<sub>32</sub>O<sub>3</sub>Si-TBS+2H]<sup>+</sup> 199.1329, found 199.1328.

### Methyl (4Z,7Z)-10-hydroxydeca-4,7-dienoate (25)

 To a cooled (0 °C) solution of methyl ester **24** (0.7420 g, 2.374 mmol) in THF (25 mL) was added TBAF (1 M in THF, 3.56 mL, 3.56 mmol) and the mixture was allowed to reach rt. After 2 h, additional TBAF (1 M in THF, 0.475 mL, 0.475 mmol) was added. After 0.5 h the reaction was cooled to 0 °C, diluted with sat. aq. NH<sub>4</sub>Cl (100 mL) and Et<sub>2</sub>O (100 mL). The organic phase was collected and the aq. phase extracted with Et<sub>2</sub>O (100 mL). The combined organic layers were washed with brine (2 x 100 mL), dried over MgSO<sub>4</sub>, filtered and concentrated under reduced pressure. Column chromatography (EtOAc/pentane = 1:9 to 1:1) afforded the title compound as a clear oil (0.3361 g, 1.695 mmol, 71%). R<sub>f</sub> = 0.52 (EtOAc/pentane = 1:1); <sup>1</sup>H NMR (500 MHz, CDCl<sub>3</sub>) δ 5.59 – 5.49 (m, 1H), 5.48 – 5.33 (m, 3H), 3.70 – 3.62 (m, 5H), 2.90 – 2.80 (m, 2H), 2.46 – 2.33 (m, 6H), 1.69 (s, 1H); <sup>13</sup>C NMR (126 MHz, CDCl<sub>3</sub>) δ 173.81, 130.99, 129.31, 128.07, 125.93, 62.31, 51.74, 34.08, 30.98, 25.84, 22.93; HRMS: Calculated for [C<sub>11</sub>H<sub>18</sub>O<sub>3</sub>+H]<sup>+</sup> 199.1329, found 199.1329.

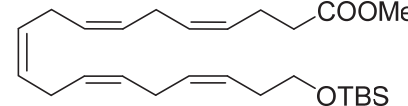
### Methyl (4Z,7Z)-10-bromodeca-4,7-dienoate (26)

 Alcohol **25** (0.4527 g, 2.283 mmol) was coevaporated three times with dry toluene, dissolved in dry DCM (10 mL) and cooled to -30 °C. CBr<sub>4</sub> (0.984 g, 2.97 mmol) was added and then PPh<sub>3</sub> (0.779 g, 2.97 mmol) was added in three portions over three min. After 30 min, the reaction was allowed to reach 0 °C and stirred for 1.5 h. The solvent was then removed under reduced pressure and the residue purified with column chromatography (Et<sub>2</sub>O/pentane = 1:19 to 1:9) to afford the title compound as a clear oil (0.6031 g, 2.309 mmol, quant.). R<sub>f</sub> = 0.71 (EtOAc/pentane = 1:19); <sup>1</sup>H NMR (400 MHz, CDCl<sub>3</sub>) δ 5.57 – 5.47 (m, 1H), 5.47 – 5.32 (m, 3H), 3.68 (s, 3H), 3.38 (t, J = 7.1 Hz, 2H), 2.83 (t, J = 5.9 Hz, 2H), 2.65 (q, J = 7.1 Hz, 2H), 2.39 (m, 4H); <sup>13</sup>C NMR (101 MHz, CDCl<sub>3</sub>) δ 173.58, 130.84, 128.94, 128.27, 126.53, 51.68, 34.03, 32.49, 30.86, 25.83, 22.90; HRMS: Calculated for [C<sub>11</sub>H<sub>17</sub>BrO<sub>2</sub>+H]<sup>+</sup> 261.0485, found 261.0486.

### ((3Z,6Z)-10-Methoxy-10-oxodeca-3,6-dien-1-yl)triphenylphosphonium bromide (8)

 In a microwave vial, bromide **26** (0.2803 g, 1.073 mmol) and dry PPh<sub>3</sub> (0.422 g, 1.610 mmol) were dissolved in dry acetonitrile (7 mL) and the vial was sealed. The solvent was purged with three vacuum/N<sub>2</sub> cycles and the reaction was stirred at 92 °C for 5 days in the dark. The reaction was concentrated under a flow of N<sub>2</sub> and purified with column chromatography (MeOH/DCM = 1:99 to 1:5) to afford the title compound as a clear syrup (0.5751 g, 1.099 mmol, quant.). R<sub>f</sub> = 0.19 (MeOH/DCM 1:9); <sup>1</sup>H NMR (500 MHz, CDCl<sub>3</sub>) δ 7.92 – 7.77 (m, 10H), 7.75 – 7.72 (m, 5H), 5.69 – 5.56 (m, 1H), 5.42 – 5.32 (m, 1H), 5.32 – 5.22 (m, 2H), 3.91 – 3.81 (m, 2H), 3.63 (s, 3H), 2.58 (t, J = 7.0 Hz, 2H), 2.54 – 2.39 (m, 2H), 2.30 (td, J = 7.2, 1.2 Hz, 2H), 2.26 – 2.18 (m, 2H); <sup>13</sup>C NMR (126 MHz, CDCl<sub>3</sub>) δ 173.41, 135.13 (d, J = 3.1 Hz), 133.68 (d, J = 10.1 Hz), 130.54 (d, J = 12.6 Hz), 130.17, 128.33 (d, J = 13.3 Hz), 126.54 (d, J = 14.7 Hz), 118.10 (d, J = 85.8 Hz) 51.53, 33.70, 25.49, 22.91 (d, J = 48.7 Hz), 22.69, 20.40 (d, J = 3.5 Hz). HRMS: Calculated for [C<sub>29</sub>H<sub>32</sub>O<sub>2</sub>P]<sup>+</sup> 443.2134, found 443.2132.

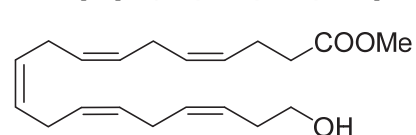
### Methyl (4Z,7Z,10Z,13Z,16Z)-19-((tert-butyldimethylsilyl)oxy)nonadeca-4,7,10,13,16-pentaenoate (29)

 To a cooled (0 °C) solution of alcohol **9** (0.2784 g, 1.029 mmol) in dry DCM (4 mL) was added DMP (0.655 g, 1.544 mmol) and the reaction was allowed to reach rt. After 30 min, the mixture was

cooled to 0 °C, diluted with Et<sub>2</sub>O (10 mL) and quenched with a mixture of sat. aq. NaHCO<sub>3</sub>/10% (w/v) aq. Na<sub>2</sub>S<sub>2</sub>O<sub>3</sub> (1:1 (v/v), 10 mL) under vigorous stirring. The layers were separated and the organic layer washed with water (3 x 10 mL) and brine (10 mL), dried over Na<sub>2</sub>SO<sub>4</sub>, filtered and concentrated under reduced pressure at rt. The generated aldehyde **28** was used in the next reaction immediately.

Phosphonium salt **8** (0.9028 g, 1.725 mmol) was dried by coevaporation with dry toluene four times and dissolved in dry THF (9 mL) and dry HMPA (1.7 mL). It was cooled to -60 °C after which LiHMDS (1 M in THF, 1.65 mL, 1.65 mmol) was added dropwise. The reaction was stirred for 40 min at -60 °C and then cooled to -100 °C. A solution of aldehyde **28** in dry THF (2 mL) was added dropwise to the reaction. The reaction was stirred at -100 °C for 30 min and then allowed to reach 0 °C over 3 h. It was cooled to -20 °C and quenched with sat. aq. NaHCO<sub>3</sub> (10 mL). It was diluted with Et<sub>2</sub>O (50 mL) and sat. aq. NaHCO<sub>3</sub> (20 mL), the aq. layer was isolated and extracted with Et<sub>2</sub>O (30 mL) and the combined organic layers were washed with brine (3 x 20 mL), dried over Na<sub>2</sub>SO<sub>4</sub>, filtered and concentrated under reduced pressure. Column chromatography (Et<sub>2</sub>O/pentane = 1:30 to 1:15) afforded the title compound as a clear oil (0.2529 g, 0.584 mmol, 57%). R<sub>f</sub> = 0.57 (EtOAc/pentane = 1:20); <sup>1</sup>H NMR (400 MHz, CDCl<sub>3</sub>) δ 5.50 – 5.29 (m, 10H), 3.67 (s, 3H), 3.62 (t, J = 7.0 Hz, 2H), 2.84 (dd, J = 7.0, 3.2 Hz, 8H), 2.38 (q, J = 3.1, 2.6 Hz, 4H), 2.30 (q, J = 6.9 Hz, 2H), 0.89 (s, 9H), 0.05 (s, 6H); <sup>13</sup>C NMR (101 MHz, CDCl<sub>3</sub>) δ 129.68, 129.46, 128.49, 128.38, 128.36, 128.25, 128.20, 128.18, 128.01, 126.36, 63.00, 51.70, 34.15, 31.26, 26.10, 25.90, 25.77, 25.71, 22.93, 18.51, -5.12; HRMS: Calculated for [C<sub>26</sub>H<sub>44</sub>O<sub>3</sub>Si+H]<sup>+</sup> 433.3133, found 433.3132.

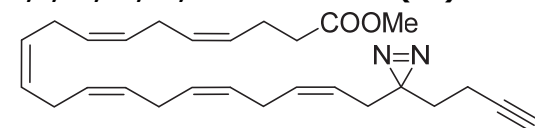
### Methyl (4Z,7Z,10Z,13Z,16Z)-19-hydroxynonadeca-4,7,10,13,16-pentaenoate (7)



To a cooled (0 °C) solution of methyl ester **29** (0.5385 g, 1.244 mmol) in THF (12 mL) was added TBAF (1 M in THF, 1.87 mL, 1.87 mmol) and the reaction was allowed to reach rt. After 2 h, the reaction was quenched with sat. aq. NH<sub>4</sub>Cl (100 mL)

and diluted with Et<sub>2</sub>O (100 mL). The layers were separated and the aq. layer was extracted with Et<sub>2</sub>O (2 x 50 mL). The combined organic layers were washed with brine (100 mL), dried over MgSO<sub>4</sub>, filtered and concentrated under reduced pressure. The residue was purified with column chromatography (EtOAc/pentane = 1:9 to 1:4) to afford the title compound (0.3453 g, 1.084 mmol, 87%) as a clear oil which was further purified with preparative HPLC (Gemini, 63 to 66% B in A over 12 min, 5 mL/min). R<sub>f</sub> = 0.70 (EtOAc/pentane = 1:1); <sup>1</sup>H NMR (500 MHz, CDCl<sub>3</sub>) δ 5.59 – 5.50 (m, 1H), 5.47 – 5.32 (m, 9H), 3.72 – 3.61 (m, 5H), 2.92 – 2.79 (m, 8H), 2.44 – 2.32 (m, 6H), 1.72 (bs, 1H); <sup>13</sup>C NMR (126 MHz, CDCl<sub>3</sub>) δ 173.77, 131.17, 129.46, 128.41, 128.36, 128.31, 128.26, 128.21, 128.15, 128.00, 125.82, 62.34, 51.73, 34.13, 30.97, 25.90, 25.79, 25.78, 25.71, 22.92; HRMS: Calculated for [C<sub>20</sub>H<sub>30</sub>O<sub>3</sub>+H]<sup>+</sup> 319.2268, found 319.2269.

### Methyl (4Z,7Z,10Z,13Z,16Z,19Z)-21-(3-(but-3-yn-1-yl)-3*H*-diazirin-3-yl)henicos-4,7,10,13,16,19-hexaenoate (31)



Alcohol **7** (0.0613 g, 0.192 mmol) was dissolved in dry DCM (2 mL), cooled to 0 °C and DMP (0.122 g, 0.289 mmol) was added. It was allowed to reach rt and stirred for 1 h, after which it was cooled to 0 °C, diluted with

Et<sub>2</sub>O (5 mL) and quenched by addition of a mixture of sat. aq. NaHCO<sub>3</sub>/10% (w/v) aq. Na<sub>2</sub>S<sub>2</sub>O<sub>3</sub> (1:1 (v/v), 4 mL). It was stirred at rt until two layers appeared, after which the layers were separated, the aq. layer was extracted with Et<sub>2</sub>O (10 mL) and the combined organic layers washed with brine (2 x 5 mL), dried over Na<sub>2</sub>SO<sub>4</sub>, filtered and concentrated under reduced pressure at rt. The formed aldehyde was dried by coevaporation with toluene at room temperature and used immediately. Phosphonium salt **6** (0.128 g, 0.250 mmol) was dried by coevaporation with toluene three times. It was suspended in dry THF (3 mL) and cooled to -70 °C after which KO*i*Bu (1.0 M in THF, 0.202 mL, 0.202 mmol) was added dropwise and the reaction was allowed to reach -50 °C over 1 h, then cooled to -105 °C. The aldehyde was dissolved in dry THF (2 mL) and added to the reaction via cannula dropwise. The reaction was allowed to reach -30 °C after which it was cooled to -80 °C. The reaction was diluted with dry Et<sub>2</sub>O (5

mL) and quenched with sat. aq. NaHCO<sub>3</sub> (2 mL) under vigorous stirring. The reaction was further diluted with Et<sub>2</sub>O (25 mL) and sat. aq. NaHCO<sub>3</sub> (25 mL), the layers were separated and the aq. layer extracted with Et<sub>2</sub>O (25 mL). The combined organic layers were washed with brine (50 mL), dried over MgSO<sub>4</sub>, filtered and concentrated under reduced pressure. Column chromatography of the residue (Et<sub>2</sub>O/pentane = 1:49 to 1:19) afforded the title compound as a yellow oil (0.0306 g, 0.073 mmol, 38%). R<sub>f</sub> = 0.68 (EtOAc/pentane = 1:9); <sup>1</sup>H NMR (500 MHz, CDCl<sub>3</sub>) δ 5.53 (dtt, J = 10.4, 2.0, 7.2, 1H), 5.45 – 5.30 (m, 10H), 5.24 (dtt, J = 10.4, 1.6, 7.6 Hz, 1H), 3.67 (s, 3H), 2.89 – 2.79 (m, 8H), 2.75 (t, J = 7.3 Hz, 2H), 2.43 – 2.35 (m, 4H), 2.17 (d, J = 7.6 Hz, 2H), 2.04 – 1.98 (m, 3H), 1.65 (t, J = 7.4 Hz, 2H); <sup>13</sup>C NMR (126 MHz, CDCl<sub>3</sub>) δ 173.66, 132.03, 129.43, 128.73, 128.42, 128.33, 128.25, 128.13, 128.03, 127.53, 121.94, 82.88, 69.26, 51.70, 34.13, 32.10, 31.27, 28.27, 25.86, 25.78, 25.71, 22.92, 13.45; HRMS: Calculated for [C<sub>27</sub>H<sub>36</sub>N<sub>2</sub>O<sub>2</sub>+H]<sup>+</sup> 421.2850, found 421.2849.

**(4Z,7Z,10Z,13Z,16Z,19Z)-21-(3-(But-3-yn-1-yl)-3*H*-diazirin-3-yl)henicos-4,7,10,13,16,19-hexaenoic acid (pac-DHA, 4)**

To a cooled (0 °C) solution of methyl ester **31** (0.0198 g, 0.047 mmol) in THF (2 mL) was added 1 M aq. LiOH (2 mL) and the reaction was allowed to reach rt overnight. It was then cooled to 0 °C, diluted with Et<sub>2</sub>O (5 mL) and acidified with 1 M aq. HCl to pH <2. NaCl was added until saturation and the organic layer was isolated. The aq. layer was extracted with Et<sub>2</sub>O (2 x 20 mL) and the combined organic layers were washed with brine (20 mL), dried over Na<sub>2</sub>SO<sub>4</sub>, filtered and concentrated under reduced pressure. Column chromatography of the residue (MeOH/DCM = 1:128 to 1:80) afforded the title compound as a slightly yellow oil (0.0159 g, 0.039 mmol, 83%). R<sub>f</sub> = 0.47 (MeOH/DCM = 1:11); <sup>1</sup>H NMR (400 MHz, CDCl<sub>3</sub>) δ 5.58 – 5.47 (m, 1H), 5.49 – 5.29 (m, 10H), 5.25 (dtt, J = 10.9, 7.6, 1.7 Hz, 1H), 2.84 (q, J = 6.9, 6.1 Hz, 8H), 2.75 (t, J = 7.0 Hz, 2H), 2.49 – 2.37 (m, 4H), 2.17 (dd, J = 7.6, 1.5 Hz, 2H), 2.05 – 1.96 (m, 3H), 1.65 (t, J = 7.3 Hz, 2H); <sup>13</sup>C NMR (101 MHz, CDCl<sub>3</sub>) δ 178.86, 132.06, 129.72, 128.75, 128.44, 128.42, 128.32, 128.29, 128.16, 127.70, 127.55, 121.96, 82.91, 69.29, 33.99, 32.11, 31.29, 28.31, 25.88, 25.80, 25.74, 22.63, 13.48; HRMS: Calculated for [C<sub>26</sub>H<sub>34</sub>N<sub>2</sub>O<sub>2</sub>+H]<sup>+</sup> 407.2693, found 407.2693.

**(4Z,7Z,10Z,13Z,15E,19Z)-21-(3-(But-3-yn-1-yl)-3*H*-diazirin-3-yl)-17-hydroxyhenicos-4,7,10,13,15,19-hexaenoic acid (pac-17-HDHA, 5)**

Carboxylic acid **4** (pac-DHA, 21 mg, 0.052 mmol) was dissolved in EtOH (5 mL) and added to a cooled (0 °C) borate buffer (50 mM boric acid in MilliQ, adjusted to pH 12 with NaOH, 500 mL). A solution of soy bean lipoxygenase (SBLOX, L7395, Sigma, 50 mg) in borate buffer was added under vigorous stirring and air bubbling, and the reaction was stirred for 20 min. Then, aq. NaBH<sub>4</sub> (10.33 mmol, 10.33 mL) was added and the reaction was stirred for 15 min. Then, acetic acid (2.63 mL, 45.9 mmol) was added dropwise and after 15 min the reaction was extracted with CHCl<sub>3</sub> (4 x 200 mL). The combined organic layers were dried over Na<sub>2</sub>SO<sub>4</sub>, filtered, concentrated under reduced pressure and purified with column chromatography (MeOH/DCM = 1:99) and preparative HPLC (Nucleodur, 66 to 72% B in A over 12 min, 5 mL/min) to afford the title compound as a clear oil (1.0 mg, 2.37 μmol, 4.6%). Aliquots were taken to analyze purity by LC-MS and NMR and regioselectivity was confirmed by the *m/z* 285 fragment ion after hydrogenation and LC-MS. <sup>1</sup>H NMR (500 MHz, CDCl<sub>3</sub>) δ 6.57 (dd, J = 15.1, 11.0 Hz, 1H), 5.98 (t, J = 10.9 Hz, 1H), 5.64 (dd, J = 15.2, 6.3 Hz, 1H), 5.58 – 5.32 (m, 9H), 4.16 – 4.09 (m, 1H), 2.97 (t, J = 7.0 Hz, 2H), 2.91 – 2.80 (m, 4H), 2.45 – 2.39 (m, 4H), 2.07 – 1.98 (m, 5H), 1.76 – 1.68 (m, 4H), 1.62 – 1.58 (m, 1H). HRMS: Calculated for [C<sub>26</sub>H<sub>34</sub>N<sub>2</sub>O<sub>3</sub>+Na]<sup>+</sup> 445.2462, found 445.2459.

## Supplementary data

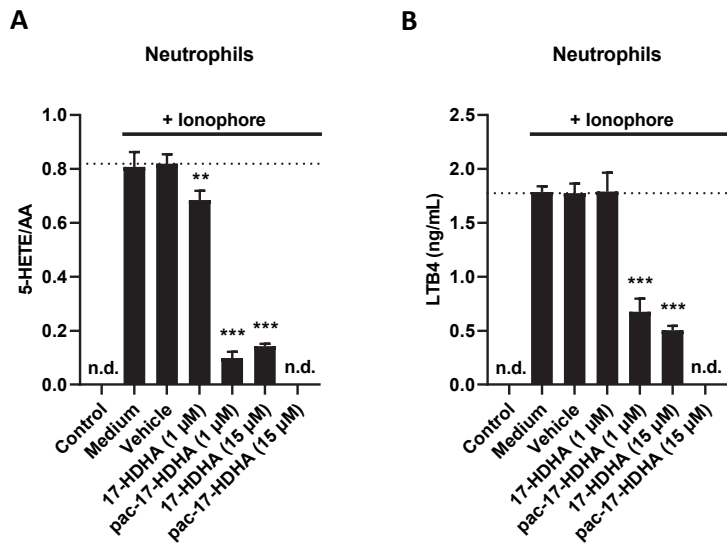


**Figure S1 | Effect of 17-HDHA and pac-17-HDHA (5) on neutrophils.** (A) 5-HETE/AA ratio and (B) LTB4 (LC-MS/MS) produced by ionophore-stimulated neutrophils. Data represent means  $\pm$  SD of representative donor ( $n = 3$ ). \*\*  $p < 0.01$ ; \*\*\*  $p < 0.001$  in comparison to ionophore-treated control (dotted line) using a one-way ANOVA with Dunnett's multiple comparisons correction. n.d.; not detected.

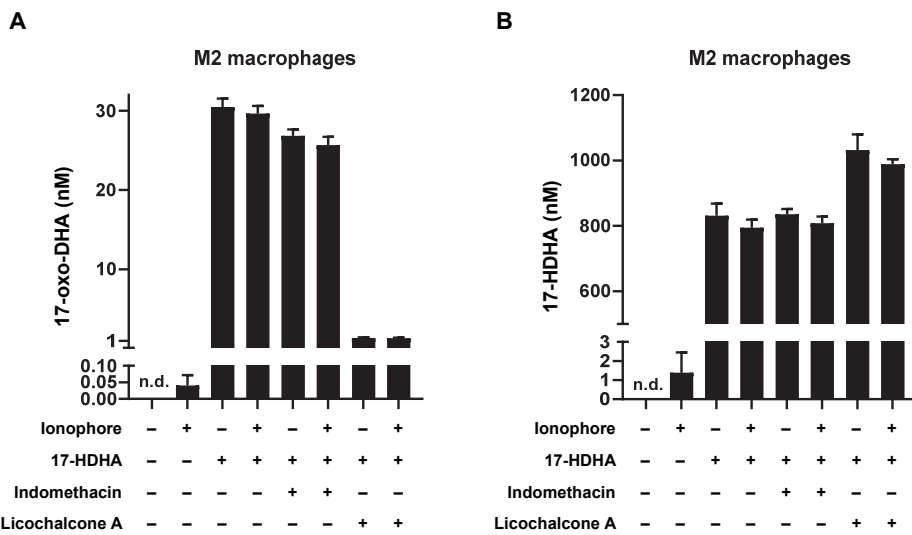


**Figure S2 | Stimulation of M2 macrophages results in detectable formation of 17-HDHA and 17-oxo-DHA.** (A) 17-oxo-DHA and (B) 17-HDHA measured in M2 macrophages shows that inhibition of PTGR1 by indomethacin and licochalcone A reduces conversion of 17-HDHA to 17-oxo-DHA. Cells were pretreated for 30 min with 10  $\mu$ M indomethacin, licochalcone A or vehicle before treatment with 17-HDHA (15  $\mu$ M) or vehicle for 2 h. Data represent means  $\pm$  SD of representative donor ( $n = 2-3$ ). One-way ANOVA between all conditions with Tukey's multiple comparisons correction: no significant difference between stimulated and unstimulated conditions.

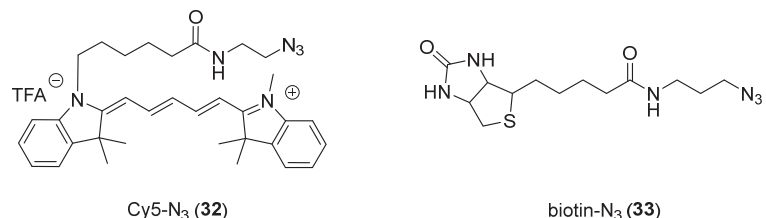


**Figure S3 | Structures of Cy5-N<sub>3</sub> (32) and biotin-N<sub>3</sub> (33).**

Print of window 80: MS Spectrum

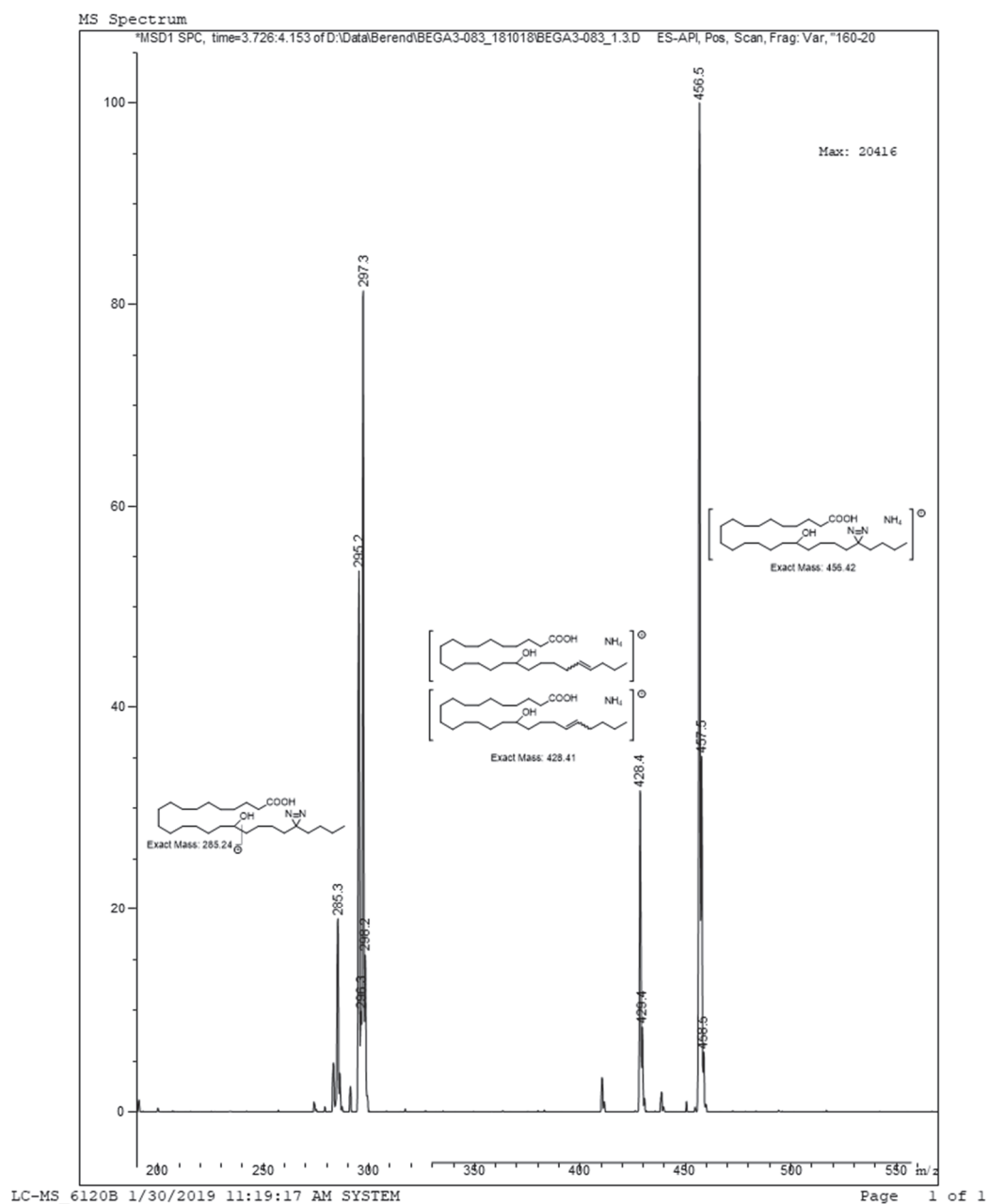


**Figure S4 | Fragmentation pattern of hydrogenated pac-17-HDHA (5).**

**Table S2 | Proteins significantly UV-enriched by pac-17-HDHA (5) in M2 macrophages.**

Gene name	Unique peptides	Description	UV/no HDHA (5)	UV pac-17-HDHA (5)	p-value	UV/ no UV pac-DHA (4)	Enrichment pac-17-HDHA/pac-DHA
DHRS4	10	Dehydrogenase/reductase SDR family member 4	56.45	0.0062	8.36	6.75	
HSD3B7	3	3 beta-hydroxysteroid dehydrogenase type 7	51.86	0.0361	4.36	11.88	
VDAC1	6	Voltage-dependent anion-selective channel protein 1	41.80	0.0025	27.96	1.50	
ECH1	14	Delta(3,5)-Delta(2,4)-dienoyl-CoA isomerase	19.25	0.0062	18.43	1.04	
ERAP1	20	Endoplasmic reticulum aminopeptidase 1	13.95	0.0109	1.28	10.94	
<b>PTGR1</b>	<b>11</b>	<b>Prostaglandin reductase 1</b>	<b>11.28</b>	<b>0.0038</b>	<b>1.47</b>	<b>7.67</b>	
APOL2	4	Apolipoprotein L2	9.97	0.0007	37.83	0.26	
CERS2	2	Ceramide synthase 2	8.46	0.0022	6.30	1.34	
SCP2	3	Non-specific lipid-transfer protein	7.60	0.0006	5.91	1.29	
PLIN2	11	Perilipin-2	6.62	0.0052	24.32	0.27	
PLIN3	2	Perilipin-3	6.22	0.0470	24.45	0.25	
DECR1	4	2,4-dienoyl-CoA reductase, mitochondrial	6.19	0.0017	1.66	3.72	
TMEM33	4	Transmembrane protein 33	4.95	0.0022	6.98	0.71	
RAB1C	2	Putative Ras-related protein Rab-1C	4.75	0.0252	15.33	0.31	
AGPS	2	Alkyldihydroxyacetonephosphate synthase peroxisomal	4.70	0.0087	2.90	1.62	
DHRS1	5	Dehydrogenase/reductase SDR family member 1	4.64	0.0037	2.50	1.85	
SRPRB	5	Signal recognition particle receptor subunit beta	4.04	0.0231	5.66	0.71	
VDAC2	7	Voltage-dependent anion-selective channel protein 2	3.99	0.0062	16.94	0.24	
METTL7A	2	Methyltransferase-like protein 7A	3.98	0.0067	23.57	0.17	
SNX5	2	Sorting nexin-5	3.90	0.0115	2.12	1.84	
FABP5	2	Fatty acid-binding protein epidermal	3.72	0.0328	1.00	3.72	
IFI30	3	Gamma-interferon-inducible lysosomal thiol reductase	3.56	0.0057	5.16	0.69	
HSD17B4	28	Peroxisomal multifunctional enzyme type 2	3.23	0.0073	2.47	1.31	
SCAMP2	2	Secretory carrier-associated membrane protein 2	2.85	0.0065	12.45	0.23	
HSD17B11	2	Estradiol 17-beta-dehydrogenase 11	2.65	0.0426	14.22	0.19	
IDH1	8	Isocitrate dehydrogenase [NADP] cytoplasmic	2.65	0.0195	0.87	3.03	
BCAP31	3	B-cell receptor-associated protein 31	2.64	0.0287	2.07	1.28	
SQOR	6	Sulfide:quinone oxidoreductase, mitochondrial	2.61	0.0036	0.95	2.75	
NCEH1	6	Neutral cholesterol ester hydrolase 1	2.59	0.0191	2.32	1.12	
TBXAS1	5	Thromboxane-A synthase	2.33	0.0099	2.61	0.89	
EPHX1	6	Epoxide hydrolase 1	2.26	0.0022	1.36	1.66	
ALDH1A1	17	Retinal dehydrogenase 1	2.24	0.0037	0.84	2.68	
ALDH2	16	Aldehyde dehydrogenase mitochondrial	2.03	0.0040	0.78	2.61	

## References

- (1) Calder, P. C. Omega-3 Fatty Acids and Inflammatory Processes: From Molecules to Man. *Biochem. Soc. Trans.* **2017**, *45* (5), 1105–1115.
- (2) Layé, S.; Nadjar, A.; Joffre, C.; Bazinet, R. P. Anti-Inflammatory Effects of Omega-3 Fatty Acids in the Brain: Physiological Mechanisms and Relevance to Pharmacology. *Pharmacol. Rev.* **2018**, *70* (1), 12–38.
- (3) Larrieu, T.; Layé, S. Food for Mood: Relevance of Nutritional Omega-3 Fatty Acids for Depression and Anxiety. *Front. Physiol.* **2018**, *9*, 1047.
- (4) Calder, P. C. Marine Omega-3 Fatty Acids and Inflammatory Processes: Effects, Mechanisms and Clinical Relevance. *Biochim. Biophys. Acta BBA - Mol. Cell Biol. Lipids* **2015**, *1851* (4), 469–484.
- (5) Proudman, S. M.; James, M. J.; Spargo, L. D.; Metcalf, R. G.; Sullivan, T. R.; Rischmueller, M.; Flabouris, K.; Wechalekar, M. D.; Lee, A. T.; Cleland, L. G. Fish Oil in Recent Onset Rheumatoid Arthritis: A Randomised, Double-Blind Controlled Trial within Algorithm-Based Drug Use. *Ann. Rheum. Dis.* **2015**, *74* (1), 89–95.
- (6) Gioxari, A.; Kaliora, A. C.; Marantidou, F.; Panagiotakos, D. P. Intake of ω-3 Polyunsaturated Fatty Acids in Patients with Rheumatoid Arthritis: A Systematic Review and Meta-Analysis. *Nutrition* **2018**, *45*, 114–124.e4.
- (7) Navarini, L.; Afeltra, A.; Gallo Afflitto, G.; Margiotta, D. P. E. Polyunsaturated Fatty Acids: Any Role in Rheumatoid Arthritis? *Lipids Health Dis.* **2017**, *16* (1), 197.
- (8) Serhan, C. N. Resolution Phase of Inflammation: Novel Endogenous Anti-Inflammatory and Proresolving Lipid Mediators and Pathways. *Annu. Rev. Immunol.* **2007**, *25* (1), 101–137.
- (9) Serhan, C. N. Pro-Resolving Lipid Mediators Are Leads for Resolution Physiology. *Nature* **2014**, *510* (7503), 92–101.
- (10) Barnig, C.; Bezema, T.; Calder, P. C.; Charloux, A.; Frossard, N.; Garssen, J.; Haworth, O.; Dilevskaya, K.; Levi-Schaffer, F.; Lonsdorfer, E.; Wauben, M.; Kraneveld, A. D.; te Velde, A. A. Activation of Resolution Pathways to Prevent and Fight Chronic Inflammation: Lessons From Asthma and Inflammatory Bowel Disease. *Front. Immunol.* **2019**, *10*, 1699.
- (11) Schett, G.; Neurath, M. F. Resolution of Chronic Inflammatory Disease: Universal and Tissue-Specific Concepts. *Nat. Commun.* **2018**, *9* (1), 1–8.
- (12) Tabas, I.; Glass, C. K. Anti-Inflammatory Therapy in Chronic Disease: Challenges and Opportunities. *Science* **2013**, *339* (6116), 166–172.
- (13) Serhan, C. N.; Fredman, G.; Yang, R.; Karamnov, S.; Belayev, L. S.; Bazan, N. G.; Zhu, M.; Winkler, J. W.; Petasis, N. A. Novel Proresolving Aspirin-Triggered DHA Pathway. *Chem. Biol.* **2011**, *18* (8), 976–987.
- (14) Weylandt, K. H.; Chiu, C.-Y.; Gomolka, B.; Waechter, S. F.; Wiedenmann, B. Omega-3 Fatty Acids and Their Lipid Mediators: Towards an Understanding of Resolvin and Protectin Formation. *Prostaglandins Other Lipid Mediat.* **2012**, *97* (3–4), 73–82.
- (15) Valdes, A. M.; Ravipati, S.; Menni, C.; Abhishek, A.; Metrstry, S.; Harris, J.; Nessa, A.; Williams, F. M. K.; Spector, T. D.; Doherty, M.; Chapman, V.; Barrett, D. A. Association of the Resolvin Precursor 17-HDHA, but Not D- or E- Series Resolvins, with Heat Pain Sensitivity and Osteoarthritis Pain in Humans. *Sci. Rep.* **2017**, *7* (1), 10748.
- (16) Bento, A. F.; Claudino, R. F.; Dutra, R. C.; Marcon, R.; Calixto, J. B. Omega-3 Fatty Acid-Derived Mediators 17(R)-Hydroxy Docosahexaenoic Acid, Aspirin-Triggered Resolvin D1 and Resolvin D2 Prevent Experimental Colitis in Mice. *J. Immunol.* **2011**, *187* (4), 1957–1969.
- (17) Duffield, J. S.; Hong, S.; Vaidya, V. S.; Lu, Y.; Fredman, G.; Serhan, C. N.; Bonventre, J. V. Resolvin D Series and Protectin D1 Mitigate Acute Kidney Injury. *J. Immunol.* **2006**, *177* (9), 5902–5911.
- (18) Lima-Garcia, J. F.; Dutra, R. C.; Silva, K. da; Motta, E. M.; Campos, M. M.; Calixto, J. B. The Precursor of Resolvin D Series and Aspirin-Triggered Resolvin D1 Display Anti-Hyperalgesic Properties in Adjuvant-Induced Arthritis in Rats. *Br. J. Pharmacol.* **2011**, *164* (2), 278–293.
- (19) González-Périz, A.; Planagumà, A.; Gronert, K.; Miquel, R.; López-Parra, M.; Titos, E.; Horrillo, R.; Ferré, N.; Deulofeu, R.; Arroyo, V.; Rodés, J.; Clària, J. Docosahexaenoic Acid (DHA) Blunts Liver Injury by Conversion to Protective Lipid Mediators: Protectin D1 and 17S-Hydroxy-DHA. *FASEB J.* **2006**, *20* (14), 2537–2539.
- (20) von Hegedus, J. H.; Kahnt, A. S.; Ebert, R.; Heijink, M.; Toes, R. E. M.; Giera, M.; Ioan-Facsinay, A. Toll-like Receptor Signaling Induces a Temporal Switch towards a Resolving Lipid Profile in Monocyte-Derived Macrophages. *Biochim. Biophys. Acta BBA - Mol. Cell Biol. Lipids* **2020**, *1865* (9), 158740.
- (21) Chiu, C.-Y.; Gomolka, B.; Dierkes, C.; Huang, N. R.; Schroeder, M.; Purschke, M.; Manstein, D.; Dangi, B.; Weylandt, K. H. Omega-6 Docosapentaenoic Acid-Derived Resolvins and 17-Hydroxydocosahexaenoic Acid Modulate Macrophage Function and Alleviate Experimental Colitis. *Inflamm. Res.* **2012**, *61* (9), 967–976.
- (22) Dalli, J.; Winkler, J. W.; Colas, R. A.; Arnardottir, H.; Cheng, C.-Y. C.; Chiang, N.; Petasis, N. A.; Serhan, C. N. Resolvin D3 and Aspirin-Triggered Resolvin D3 Are Potent Immunoresolvents. *Chem. Biol.* **2013**, *20* (2), 188–201.

- (23) Niphakis, M. J.; Lum, K. M.; Cognetta III, A. B.; Correia, B. E.; Ichu, T.-A.; Olucha, J.; Brown, S. J.; Kundu, S.; Piscitelli, F.; Rosen, H.; Cravatt, B. F. A Global Map of Lipid-Binding Proteins and Their Ligandability in Cells. *Cell* **2015**, *161* (7), 1668–1680.
- (24) Hulce, J. J.; Cognetta, A. B.; Niphakis, M. J.; Tully, S. E.; Cravatt, B. F. Proteome-Wide Mapping of Cholesterol-Interacting Proteins in Mammalian Cells. *Nat. Methods* **2013**, *10* (3), 259–264.
- (25) Rowland, M. M.; Bostic, H. E.; Gong, D.; Speers, A. E.; Lucas, N.; Cho, W.; Cravatt, B. F.; Best, M. D. Phosphatidylinositol 3,4,5-Trisphosphate Activity Probes for the Labeling and Proteomic Characterization of Protein Binding Partners. *Biochemistry* **2011**, *50* (51), 11143–11161.
- (26) Wang, D.; Du, S.; Cazenave-Gassiot, A.; Ge, J.; Lee, J.-S.; Wenk, M. R.; Yao, S. Q. Global Mapping of Protein–Lipid Interactions by Using Modified Choline-Containing Phospholipids Metabolically Synthesized in Live Cells. *Angew. Chem.* **2017**, *129* (21), 5923–5927.
- (27) Haberkant, P.; Rajmakers, R.; Wildwater, M.; Sachsenheimer, T.; Brügger, B.; Maeda, K.; Houweling, M.; Gavin, A.-C.; Schultz, C.; van Meer, G.; Heck, A. J. R.; Holthuis, J. C. M. In Vivo Profiling and Visualization of Cellular Protein–Lipid Interactions Using Bifunctional Fatty Acids. *Angew. Chem. Int. Ed.* **2013**, *52* (14), 4033–4038.
- (28) Höglinder, D.; Nadler, A.; Haberkant, P.; Kirkpatrick, J.; Schifferer, M.; Stein, F.; Hauke, S.; Porter, F. D.; Schultz, C. Trifunctional Lipid Probes for Comprehensive Studies of Single Lipid Species in Living Cells. *Proc. Natl. Acad. Sci.* **2017**, *114* (7), 1566–1571.
- (29) Haberkant, P.; Stein, F.; Höglinder, D.; Gerl, M. J.; Brügger, B.; Van Veldhoven, P. P.; Krijgsveld, J.; Gavin, A.-C.; Schultz, C. Bifunctional Sphingosine for Cell-Based Analysis of Protein-Sphingolipid Interactions. *ACS Chem. Biol.* **2016**, *11* (1), 222–230.
- (30) Zhuang, S.; Li, Q.; Cai, L.; Wang, C.; Lei, X. Chemoproteomic Profiling of Bile Acid Interacting Proteins. *ACS Cent. Sci.* **2017**, *3* (5), 501–509.
- (31) Macklin, T. K.; Micalizio, G. C. Convergent and Stereospecific Synthesis of Complex Skipped Polyenes and Polyunsaturated Fatty Acids. *Nat. Chem.* **2010**, *2* (8), 638–643.
- (32) Lum, K. M.; Sato, Y.; Beyer, B. A.; Plaisted, W. C.; Anglin, J. L.; Lairson, L. L.; Cravatt, B. F. Mapping Protein Targets of Bioactive Small Molecules Using Lipid-Based Chemical Proteomics. *ACS Chem. Biol.* **2017**, *12* (10), 2671–2681.
- (33) Koenders, S. T. A.; Gagestein, B.; van der Stelt, M. Opportunities for Lipid-Based Probes in the Field of Immunology. In *Activity-Based Protein Profiling*; Cravatt, B. F., Hsu, K.-L., Weerapana, E., Eds.; Current Topics in Microbiology and Immunology; Springer International Publishing: Cham, 2019; pp 283–319.
- (34) Bockelmann, S.; Mina, J. G. M.; Korneev, S.; Hassan, D. G.; Müller, D.; Hilderink, A.; Vlieg, H. C.; Rajmakers, R.; Heck, A. J. R.; Haberkant, P.; Holthuis, J. C. M. A Search for Ceramide Binding Proteins Using Bifunctional Lipid Analogs Yields CERT-Related Protein StarD7. *J. Lipid Res.* **2018**, *59* (3), 515–530.
- (35) Mbarik, M.; Biam, R. S.; Robichaud, P.-P.; Surette, M. E. The Impact of PUFA on Cell Responses: Caution Should Be Exercised When Selecting PUFA Concentrations in Cell Culture. *Prostaglandins Leukot. Essent. Fatty Acids* **2020**, 102083.
- (36) Li, Z.; Hao, P.; Li, L.; Tan, C. Y. J.; Cheng, X.; Chen, G. Y. J.; Sze, S. K.; Shen, H.-M.; Yao, S. Q. Design and Synthesis of Minimalist Terminal Alkyne-Containing Diazirine Photo-Crosslinkers and Their Incorporation into Kinase Inhibitors for Cell- and Tissue-Based Proteome Profiling. *Angew. Chem.* **2013**, *125* (33), 8713–8718.
- (37) Kleiner, P.; Heydenreuter, W.; Stahl, M.; Korotkov, V. S.; Sieber, S. A. A Whole Proteome Inventory of Background Photocrosslinker Binding. *Angew. Chem. Int. Ed.* **2017**, *56* (5), 1396–1401.
- (38) Sakurai, K. Photoaffinity Probes for Identification of Carbohydrate-Binding Proteins. *Asian J. Org. Chem.* **2015**, *4* (2), 116–126.
- (39) Vik, A.; Hansen, T. V. Synthetic Manipulations of Polyunsaturated Fatty Acids as a Convenient Strategy for the Synthesis of Bioactive Compounds. *Org. Biomol. Chem.* **2018**, *16* (48), 9319–9333.
- (40) Balas, L.; Durand, T.; Saha, S.; Johnson, I.; Mukhopadhyay, S. Total Synthesis of Photoactivatable or Fluorescent Anandamide Probes: Novel Bioactive Compounds with Angiogenic Activity. *J. Med. Chem.* **2009**, *52* (4), 1005–1017.
- (41) Heitz, M. P.; Wagner, A.; Mioskowski, C.; Noel, J. P.; Beaucourt, J. P. Synthesis of All-Cis-1-Bromo-4,7,10,13-Nonadecatetraene: A Precursor to C-1-Labeled Arachidonic Acid. *J. Org. Chem.* **1989**, *54* (2), 500–503.
- (42) Saha, G.; Basu, M. K.; Kim, S.; Jung, Y.-J.; Adiyaman, Y.; Adiyaman, M.; Powell, W. S.; FitzGerald, G. A.; Rokach, J. A Convenient Strategy for the Synthesis of  $\beta,\gamma$ -Unsaturated Aldehydes and Acids. A Construction of Skipped Dienes. *Tetrahedron Lett.* **1999**, *40* (40), 7179–7183.
- (43) Rosell, M.; Villa, M.; Durand, T.; Galano, J.-M.; Vercauteren, J.; Crauste, C. Total Syntheses of Two Bis-Allylic-Deuterated DHA Analogues. *Asian J. Org. Chem.* **2017**, *6* (3), 322–334.
- (44) Coffa, G.; Imber, A. N.; Maguire, B. C.; Laxmikanthan, G.; Schneider, C.; Gaffney, B. J.; Brash, A. R. On the Relationships of Substrate Orientation, Hydrogen Abstraction, and Product Stereochemistry in Single and Double Dioxygenations by Soybean Lipoxygenase-1 and Its Ala542Gly Mutant. *J. Biol. Chem.* **2005**, *280* (46), 38756–38766.

- (45) Chechetkin, I. R.; Osipova, E. V.; Tarasova, N. B.; Mukhitova, F. K.; Hamberg, M.; Gogolev, Y. V.; Grechkin, A. N. Specificity of Oxidation of Linoleic Acid Homologs by Plant Lipoxygenases. *Biochem. Mosc.* **2009**, *74* (8), 855–861.
- (46) Dobson, E. P.; Barrow, C. J.; Kralovec, J. A.; Adcock, J. L. Controlled Formation of Mono- and Dihydroxy-Resolvens from EPA and DHA Using Soybean 15-Lipoxygenase. *J. Lipid Res.* **2013**, *54* (5), 1439–1447.
- (47) Luo, Y.; Blex, C.; Baessler, O.; Glinski, M.; Dreger, M.; Sefkow, M.; Köster, H. The CAMP Capture Compound Mass Spectrometry as a Novel Tool for Targeting CAMP-Binding Proteins: FROM PROTEIN KINASE A TO POTASSIUM/SODIUM HYPERPOLARIZATION-ACTIVATED CYCLIC NUCLEOTIDE-GATED CHANNELS. *Mol. Cell. Proteomics* **2009**, *8* (12), 2843–2856.
- (48) Himo, F.; Lovell, T.; Hilgraf, R.; Rostovtsev, V. V.; Noddleman, L.; Sharpless, K. B.; Fokin, V. V. Copper(I)-Catalyzed Synthesis of Azoles. DFT Study Predicts Unprecedented Reactivity and Intermediates. *J. Am. Chem. Soc.* **2005**, *127* (1), 210–216.
- (49) Mellacheruvu, D.; Wright, Z.; Couzens, A. L.; Lambert, J. P.; St-Denis, N. A.; Li, T.; Miteva, Y. V.; Hauri, S.; Sardiu, M. E.; Low, T. Y.; Halim, V. A.; Bagshaw, R. D.; Hubner, N. C.; Al-Hakim, A.; Bouchard, A.; Faubert, D.; Fermin, D.; Dunham, W. H.; Goudreault, M.; Lin, Z. Y.; Badillo, B. G.; Pawson, T.; Durocher, D.; Coulombe, B.; Aebersold, R.; Superti-Furga, G.; Colinge, J.; Heck, A. J. R.; Choi, H.; Gstaiger, M.; Mohammed, S.; Cristea, I. M.; Bennett, K. L.; Washburn, M. P.; Raught, B.; Ewing, R. M.; Gingras, A. C.; Nesvizhskii, A. I. The CRAPome: A Contaminant Repository for Affinity Purification-Mass Spectrometry Data. *Nat. Methods* **2013**, *10* (8), 730–736.
- (50) Huang, D. W.; Sherman, B. T.; Lempicki, R. A. Systematic and Integrative Analysis of Large Gene Lists Using DAVID Bioinformatics Resources. *Nat. Protoc.* **2009**, *4* (1), 44–57.
- (51) Mesa, J.; Alsina, C.; Oppermann, U.; Parés, X.; Farrés, J.; Porté, S. Human Prostaglandin Reductase 1 (PGR1): Substrate Specificity, Inhibitor Analysis and Site-Directed Mutagenesis. *Chem. Biol. Interact.* **2015**, *234*, 105–113.
- (52) Kang, G.-J.; Lee, H.-J.; Byun, H. J.; Kim, E. J.; Kim, H. J.; Park, M. K.; Lee, C.-H. Novel Involvement of MiR-522-3p in High-Mobility Group Box 1-Induced Prostaglandin Reductase 1 Expression and Reduction of Phagocytosis. *Biochim. Biophys. Acta BBA - Mol. Cell Res.* **2017**, *1864* (4), 625–633.
- (53) Yamamoto, T.; Yokomizo, T.; Nakao, A.; Izumi, T.; Shimizu, T. Immunohistochemical Localization of Guinea-Pig Leukotriene B<sub>4</sub> 12-Hydroxydehydrogenase/15-Ketoprostaglandin 13-Reductase. *Eur. J. Biochem.* **2001**, *268* (23), 6105–6113.
- (54) Yokomizo, T.; Izumi, T.; Takahashi, T.; Kasama, T.; Kobayashi, Y.; Sato, F.; Taketani, Y.; Shimizu, T. Enzymatic Inactivation of Leukotriene B<sub>4</sub> by a Novel Enzyme Found in the Porcine Kidney. Purification and Properties of Leukotriene B<sub>4</sub> 12-Hydroxydehydrogenase. *J. Biol. Chem.* **1993**, *268* (24), 18128–18135.
- (55) Hori, T.; Ishijima, J.; Yokomizo, T.; Ago, H.; Shimizu, T.; Miyano, M. Crystal Structure of Anti-Configuration of Indomethacin and Leukotriene B<sub>4</sub> 12-Hydroxydehydrogenase/15-Oxo-Prostaglandin 13-Reductase Complex Reveals the Structural Basis of Broad Spectrum Indomethacin Efficacy. *J. Biochem. (Tokyo)* **2006**, *140* (3), 457–466.
- (56) Roberts, L. S.; Yan, P.; Bateman, L. A.; Nomura, D. K. Mapping Novel Metabolic Nodes Targeted by Anti-Cancer Drugs That Impair Triple-Negative Breast Cancer Pathogenicity. *ACS Chem. Biol.* **2017**, *12* (4), 1133–1140.
- (57) Yue, W. W.; Shafqat, N.; Krojer, T.; Pike, A. C. W.; von Delft, F.; Sethi, R.; Savitsky, P.; Johansson, C.; Arrowsmith, C.; Weigelt, J.; Edwards, A.; Bountra, C.; Oppermann, U. Crystal Structure of Human Leukotriene B<sub>4</sub> 12-Hydroxydehydrogenase in Complex with NADP and Raloxifene. No. RCS Protein Data Bank 2Y05.
- (58) Groeger, A. L.; Cipollina, C.; Cole, M. P.; Woodcock, S. R.; Bonacci, G.; Rudolph, T. K.; Rudolph, V.; Freeman, B. A.; Schopfer, F. J. Cyclooxygenase-2 Generates Anti-Inflammatory Mediators from Omega-3 Fatty Acids. *Nat. Chem. Biol.* **2010**, *6* (6), 433–441.
- (59) Cipollina, C.; Vincenzo, S. D.; Siena, L.; Sano, C. D.; Gjomarkaj, M.; Pace, E. 17-Oxo-DHA Displays Additive Anti-Inflammatory Effects with Fluticasone Propionate and Inhibits the NLRP3 Inflammasome. *Sci. Rep.* **2016**, *6* (1), 1–12.
- (60) Egawa, D.; Itoh, T.; Akiyama, Y.; Saito, T.; Yamamoto, K. 17-OxoDHA Is a PPAR $\alpha/\gamma$  Dual Covalent Modifier and Agonist. *ACS Chem. Biol.* **2016**, *11* (9), 2447–2455.
- (61) Jamil, M. U.; Kim, J.; Yum, H.-W.; Kim, S. H.; Kim, S.-J.; Kim, D.-H.; Cho, N.-C.; Na, H.-K.; Surh, Y.-J. 17-Oxo-Docosahexaenoic Acid Induces Nrf2-Mediated Expression of Heme Oxygenase-1 in Mouse Skin in Vivo and in Cultured Murine Epidermal Cells. *Arch. Biochem. Biophys.* **2020**, *679*, 108156.
- (62) Cipollina, C.; Di Vincenzo, S.; Gerbino, S.; Siena, L.; Gjomarkaj, M.; Pace, E. Dual Anti-Oxidant and Anti-Inflammatory Actions of the Electrophilic Cyclooxygenase-2-Derived 17-Oxo-DHA in Lipopolysaccharide- and Cigarette Smoke-Induced Inflammation. *Biochim. Biophys. Acta BBA - Gen. Subj.* **2014**, *1840* (7), 2299–2309.
- (63) Haeggström, J. Z.; Funk, C. D. Lipoxygenase and Leukotriene Pathways: Biochemistry, Biology, and Roles in Disease. *Chem. Rev.* **2011**, *111* (10), 5866–5898.
- (64) Jónasdóttir, H. S.; Ioan-Facsinay, A.; Kwekkeboom, J.; Brouwers, H.; Zuurmond, A.-M.; Toes, R.; Deelder, A. M.; Giera, M. An Advanced LC-MS/MS Platform for the Analysis of Specialized Pro-Resolving Lipid Mediators. *Chromatographia* **2015**, *78* (5), 391–401.

- (65) van Rooden, E. J.; Florea, B. I.; Deng, H.; Baggelaar, M. P.; van Esbroeck, A. C. M.; Zhou, J.; Overkleeft, H. S.; van der Stelt, M. Mapping *in Vivo* Target Interaction Profiles of Covalent Inhibitors Using Chemical Proteomics with Label-Free Quantification. *Nat. Protoc.* **2018**, *13*(4), 752–767.
- (66) Soethoudt, M.; Stolze, S. C.; Westphal, M. V.; van Stralen, L.; Martella, A.; van Rooden, E. J.; Guba, W.; Varga, Z. V.; Deng, H.; van Kasteren, S. I.; Grether, U.; IJzerman, A. P.; Pacher, P.; Carreira, E. M.; Overkleeft, H. S.; Ioan-Facsinay, A.; Heitman, L. H.; van der Stelt, M. Selective Photoaffinity Probe That Enables Assessment of Cannabinoid CB<sub>2</sub> Receptor Expression and Ligand Engagement in Human Cells. *J. Am. Chem. Soc.* **2018**, *140*(19), 6067–6075.
- (67) Rappsilber, J.; Mann, M.; Ishihama, Y. Protocol for Micro-Purification, Enrichment, Pre-Fractionation and Storage of Peptides for Proteomics Using StageTips. *Nat. Protoc.* **2007**, *2*(8), 1896–1906.
- (68) Morcillo, S. P.; Leboeuf, D.; Bour, C.; Gandon, V. Calcium-Catalyzed Synthesis of Polysubstituted 2-Alkenylfurans from β-Keto Esters Tethered to Propargyl Alcohols. *Chem. – Eur. J.* **2016**, *22*(47), 16974–16978.
- (69) Walko, M.; Hewitt, E.; E. Radford, S.; J. Wilson, A. Design and Synthesis of Cysteine-Specific Labels for Photo-Crosslinking Studies. *RSC Adv.* **2019**, *9*(14), 7610–7614.
- (70) Ravindar, K.; Sridhar Reddy, M.; Deslongchamps, P. A Highly Efficient Access to Spiroketal, Mono-Unsaturated Spiroketal, and Furans: Hg(II)-Catalyzed Cyclization of Alkyne Diols and Triols. *Org. Lett.* **2011**, *13*(12), 3178–3181.
- (71) Tang, W.; Prusov, E. V. Total Synthesis of RNA-Polymerase Inhibitor Ripostatin B and 15-Deoxyripostatin A. *Angew. Chem. Int. Ed.* **2012**, *51*(14), 3401–3404.
- (72) Köpfer, A.; Breit, B. Rhodium-Catalyzed Hydroformylation of 1,1-Disubstituted Allenes Employing the Self-Assembling 6-DPPon System. *Angew. Chem. Int. Ed.* **2015**, *54*(23), 6913–6917.
- (73) Ramella, V.; He, Z.; Daniliuc, C. G.; Studer, A. Palladium-Catalyzed Dearomatizing Difunctionalization of Indoles and Benzofurans. *Eur. J. Org. Chem.* **2016**, *2016*(13), 2268–2273.





# Chapter 4

## Exploring the neuroprotective role of DHEA in inflammation\*

### Introduction

Docosahexaenoic acid (DHA, 22:6 n-3, **1**) is an omega-3 fatty acid which is essential for brain development and function (Figure 1).<sup>1-4</sup> DHA and its metabolites are abundant in the brain, representing 13-14% of total fatty acids in the cerebral cortex of primates.<sup>5</sup> One of the DHA metabolites is *N*-docosahexaenylethanolamine (DHEA, **2**). DHEA is structurally related to the neurotransmitter anandamide (AEA) and is sometimes referred to as 'synaptamide', because it has been identified as a signaling lipid with potent neurotrophic and neuroprotective effects.<sup>6,7</sup> Inhibition of fatty acid amide hydrolase (FAAH), the main metabolic enzyme of DHEA, enhances some of the beneficial effects of DHA, which suggests that DHEA is involved in the physiological effects of DHA.<sup>8,9</sup> Despite their structural similarity, DHEA is much less active on the receptors of AEA, cannabinoid receptors type 1 and 2 (CB1R, CB2R). Instead, its neuronal effects are reported to be due to activation of GPR110.<sup>10</sup>

---

\*The data presented in this chapter was gathered in collaboration with Andrea Martella, Eva van Rooden, Kim Wals, Hans den Dulk, Thomas Bakkum, Tom van der Wel, Herman S. Overkleeft, Sander van Kasteren, Mario van der Stelt.

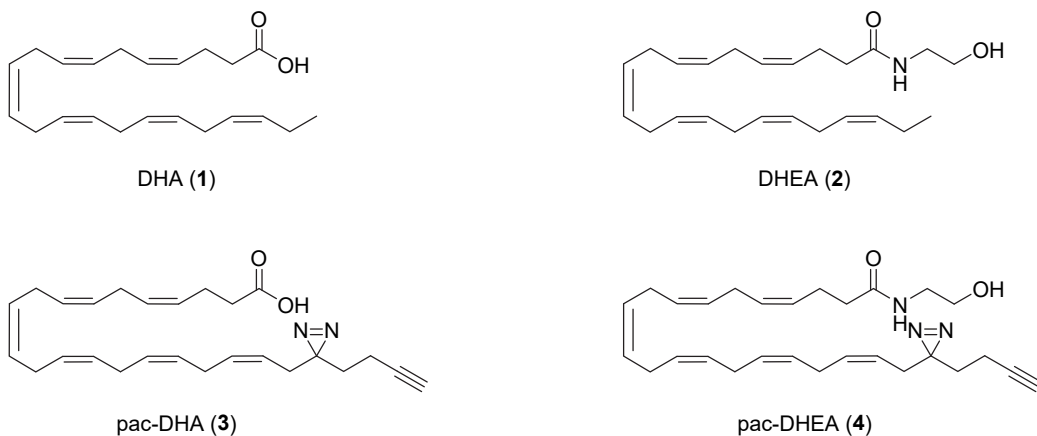


**Figure 1 |** DHA (**1**), DHEA (**2**) and their probe counterparts, photoaffinity-click (pac)-DHA (**3**) and pac-DHEA (**4**).

In addition to its role in neuronal growth, DHEA exerts neuroprotective effects by inhibiting the inflammatory response by immune cells in the central nervous system (CNS).<sup>6,11</sup> Although inflammation is a beneficial process to combat pathogens, persistent inflammation in the CNS is detrimental to neurons due to excessive production of pro-inflammatory cytokines and reactive oxygen and nitrogen species.<sup>12</sup> Chronic neuroinflammation is associated with many neurodegenerative diseases, such as multiple sclerosis (MS), Alzheimer's disease (AD) and Parkinson's disease (PD).<sup>12–14</sup> The inflammatory response in the CNS is regulated by microglia, which are a resident population of macrophage-like immune cells.<sup>15,16</sup> Microglia also modulate neuronal activity by releasing neurotrophic factors and removing immature synapses and excess neural precursor cells.<sup>17,18</sup> The pleiotropic effects of DHEA in the CNS indicate that it contributes to neuronal health through multiple pathways.

Activation of GPR110 by DHEA provides an anti-inflammatory signal.<sup>19</sup> Moreover, DHEA reduces COX-2-mediated production of pro-inflammatory eicosanoids in macrophages.<sup>20</sup> It is suggested that DHEA acts as a competitive or non-competitive inhibitor of COX-2, but it was also found to serve as a substrate of this enzyme, yielding oxidized metabolites.<sup>21</sup> This adds another level of complexity, as oxidative metabolism of DHEA introduces crosstalk between the epoxyeicosanoid and endocannabinoid signaling pathways.<sup>22</sup> Epoxyeicosanoids are synthesized from arachidonic acid by cytochrome P450 enzymes (CYP450) and have potent vasodilatory and anti-inflammatory effects.<sup>23,24</sup> DHEA can also serve as CYP450 substrate and the resulting metabolites act as cannabinoid receptor 2 (CB2R) agonists producing anti-inflammatory effects.<sup>22</sup> Another class of oxidized metabolites of DHEA, produced by lipoxygenase enzymes, are also potent agonists of the CB2R, which have organ-protective effects in an inflammatory model.<sup>25</sup> Finally, DHEA has been found to have additional cannabinoid receptor-independent anti-inflammatory effects.<sup>20,26</sup>

To further study the anti-inflammatory effects of DHEA and its metabolites, photoaffinity-based protein profiling (AfBPP) can be used to uncover protein interaction partners.<sup>27</sup> This approach, introduced in Chapter 3, uses bifunctional probes which consist of a ligand of interest modified with a photoreactive group and a bioorthogonal ligation handle. This combination allows for the discovery of probe-interacting proteins by sodium dodecyl sulfate polyacrylamide gel electrophoresis (SDS-PAGE) and fluorescence scanning, or alternatively, liquid chromatography-mass spectrometry (LC-MS, Figure 2).<sup>28</sup> Building on the methods and photoaffinity-click (pac)-DHA (**3**) developed in Chapter 3, the synthesis and application of photoaffinity probe pac-DHEA (**4**) is described in order to investigate the role of DHEA in neuroinflammation (Figure 1). This probe is used to map the lipid-protein interaction partners of DHEA in microglia using comparative AfBPP, which resulted in the discovery of novel protein interaction partners of DHEA. The role of these proteins in microglia was further investigated, which indicated that they may contribute to the anti-inflammatory effects of DHEA.

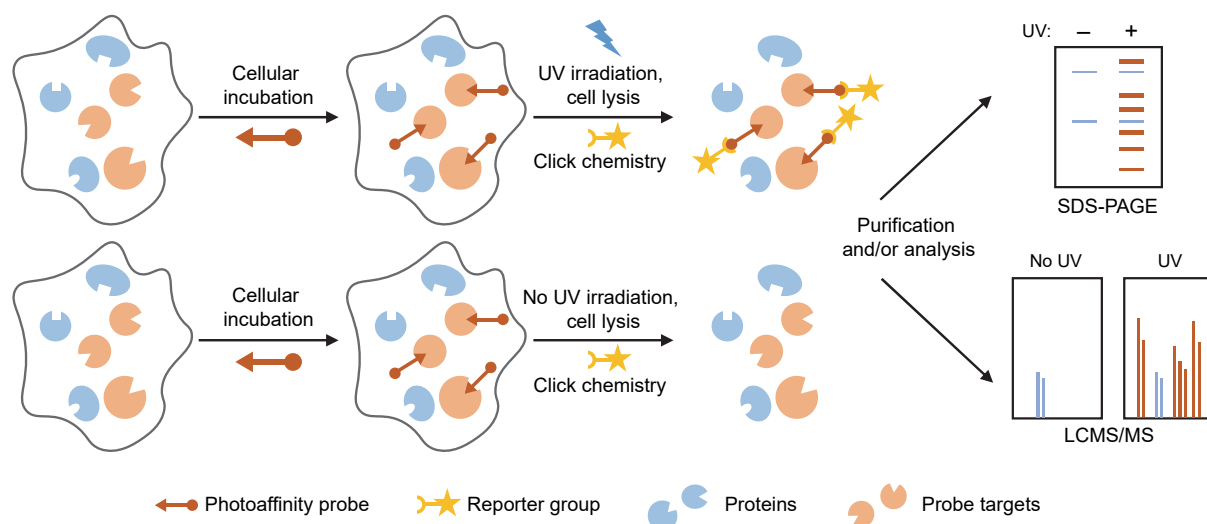


**Figure 2 | Schematic overview of AfBPP experiment.** Cells are incubated with a photoaffinity probe before UV irradiation or exposure to ambient light, followed by cell lysis and ligation of the probe-bound proteins to a fluorophore-azide or biotin-azide for SDS-PAGE or LC-MS/MS analysis respectively.

## Results

### Characterization of DHEA and pac-DHEA (**4**) in N9 microglia

To study the protein interaction partners of DHEA, pac-DHEA (**4**) was synthesized by condensation of pac-DHA (**3**) with ethanolamine (Figure 1). With both probes **3** and **4** in hand, it was investigated whether they showed similar anti-inflammatory properties as their parent lipids in lipopolysaccharide (LPS)-stimulated N9 microglia cells, which are widely used as an *in vitro* model of neuroinflammation.<sup>29</sup> The cells were incubated with DHA, DHEA, probe **3** or **4** at 10 µM for 4 h before addition of 25 ng/mL LPS. The effect of the lipids on a number of pro-inflammatory gene transcripts (*IL6*, *Ptgs2*, *Tlr2* and *CD86*) was quantified by qPCR (Figure 3). DHEA and pac-DHEA (**4**) were equipotent in their reduction of *IL6*, *Ptgs2*, *Tlr2* and *CD86* mRNA levels, which indicated that the photoaffinity probe retained the anti-inflammatory properties of DHEA. In line with previous reports, it was found that DHEA was more effective than DHA in suppressing the LPS-induced expression of pro-inflammatory genes, except of *Ptgs2*.<sup>11,30</sup> This result indicates that DHEA and DHA exert different biological activities and suggests that they have different interaction partners.

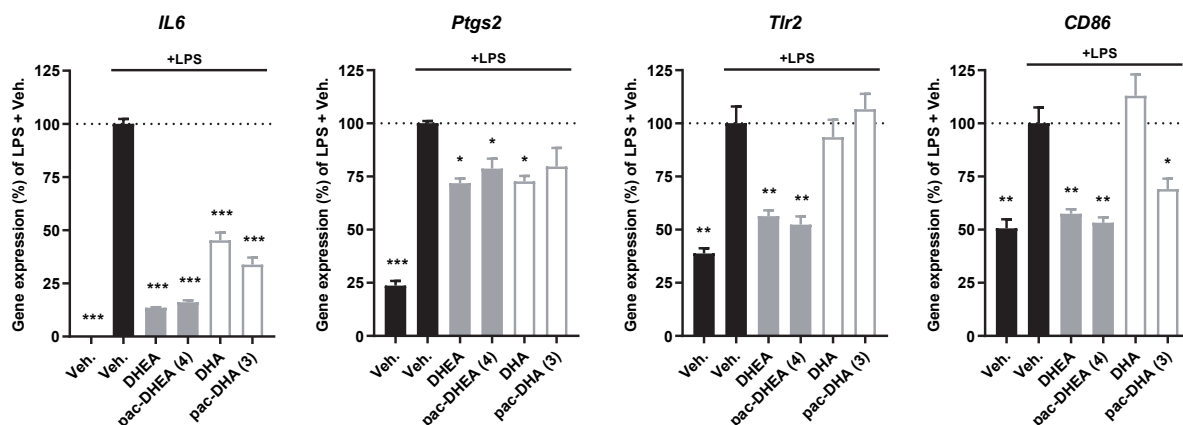


**Figure 3 | Effect of lipids on inflammatory markers of N9 microglia.** N9 microglia were pretreated with indicated lipid (10 µM) or vehicle for 4 h before LPS stimulation (25 ng/mL) for 24 h. Values reported are mRNA expression of inflammation-related genes as measured by qPCR and normalized to LPS-treated vehicle control. Data represent means ± SEM (n = 2). \* p < 0.05, \*\* p < 0.01, \*\*\* p < 0.001 in comparison to LPS-treated control (dotted line) using a one-way ANOVA with Dunnett's multiple comparisons correction.

### Photoaffinity labeling reveals pac-DHEA-interacting proteins

To discover DHEA-interacting proteins, the photoaffinity probes were used in an AfBPP experiment using N9 microglia. To capture the probe-interacting proteins, N9 microglia were treated with pac-DHA (**3**) or pac-DHEA (**4**) (10  $\mu$ M) and incubated for 24 h to simulate the qPCR experiments. After incubation, supernatant was removed and the cells were washed with PBS followed by irradiation (350 nm, 10 min, "UV") or exposure to ambient light ("no UV"). Cells were lysed and the probe-labeled proteins were conjugated to Cy5-N<sub>3</sub> under copper(I)-catalyzed azide-alkyne cycloaddition (CuAAC) conditions. Separation of the labeled proteins by SDS-PAGE and in-gel fluorescence scanning demonstrated UV-dependent labeling of proteins by probe **4** (Figure 4A).

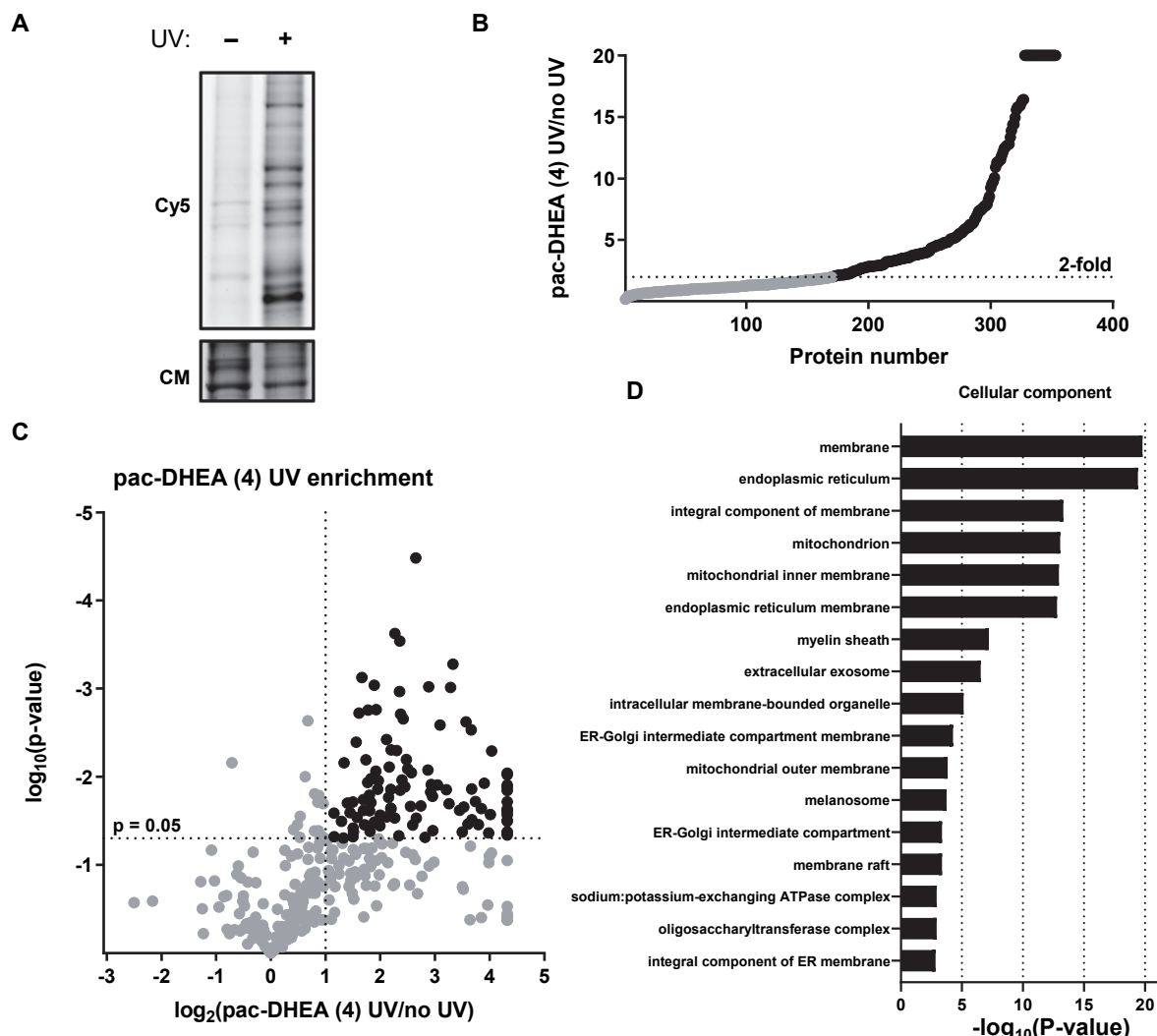


**Figure 4 | Pac-DHEA (4)-interacting proteins in N9 microglia.** **(A)** Gel-based AfBPP analysis of pac-DHEA (**4**)-interacting proteins in N9 microglia. **(B)** Waterfall plot of proteins identified in pulldown experiment with 10  $\mu$ M pac-DHEA (**4**). UV enrichment was capped at 20-fold and proteins with a ratio >2 are highlighted in black. **(C)** Volcano plot of proteins identified in pulldown experiment with 10  $\mu$ M pac-DHEA (**4**). UV enrichment was capped at 20-fold and proteins with a ratio >2 and p-value <0.05 are highlighted in black. **(D)** GO enrichment analysis of significantly UV-enriched pac-DHEA (**4**) targets.

## Chapter 4

To identify these targets, probe-bound proteins were ligated to biotin-N<sub>3</sub>, enriched using avidin-coated agarose beads, digested by trypsin and analyzed by LC-MS/MS.<sup>31</sup> Proteomic analysis resulted in 353 identified proteins with at least 2 unique peptides (Figure 4B). Out of these, 105 were designated as pac-DHEA (**4**)-interacting targets using >2-fold UV enrichment and a p-value <0.05 as cutoff criteria (Figure 4C). GO enrichment analysis of the cellular component annotation of these targets showed that mainly membrane proteins and proteins associated with the endoplasmic reticulum (ER) and mitochondria were enriched (Figure 4D).<sup>32,33</sup>

To distinguish between lipophilic, nonspecifically-interacting proteins and genuine probe targets, the probe **4**-interacting proteins were compared to the proteins identified by pac-DHA (**3**). To this end, label-free quantification (LFQ) values of pac-DHEA (**4**) targets were plotted against that of pac-DHA (**3**), which revealed eleven targets specific for probe **4** (Figure 5A, B and Table S3). These targets consisted in part of known lipid-metabolizing proteins and known AEA interaction partners previously found by AEA-based probes.<sup>34</sup> Of these targets, three proteins with unknown function or mechanism of action were chosen for further investigation, neudesin (NENF), adipocyte plasma membrane-associated protein (APMAP) and glutathione S-transferase Mu 1 (GSTM1). To confirm GSTM1 among the GSTM family, the identified peptides were compared to the known sequences. Of the peptides found for GSTM1, two were unique for GSTM1 within the family (Figure 5C).

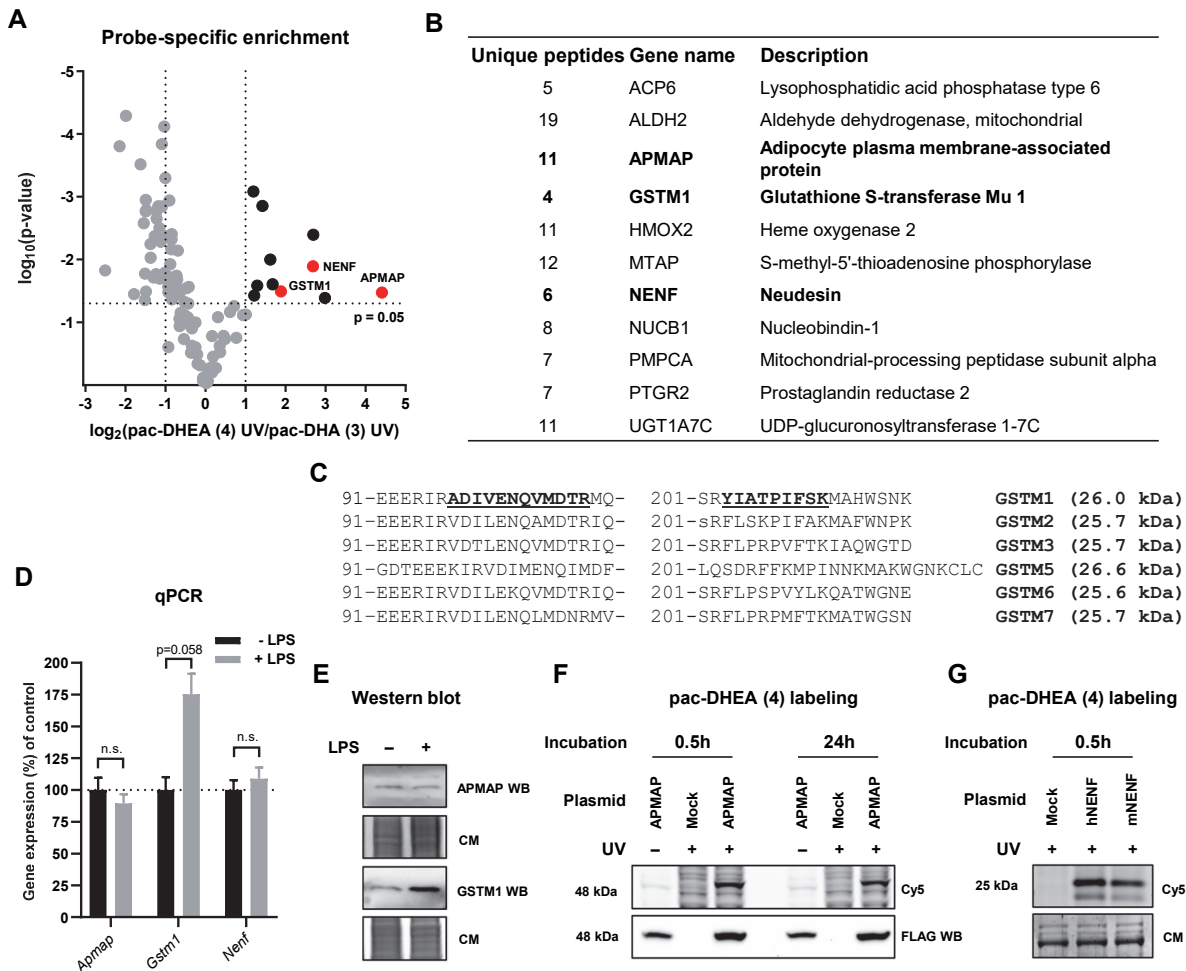


**Figure 5 | Specifically enriched pac-DHEA (4) targets.** **(A)** Volcano plot of LFQ values of pac-DHEA (4) versus pac-DHA (3) of probe 4 UV-enriched targets. Probe 4-specific targets are in black, NENF, GSTM1 and APMAP are highlighted in red. **(B)** List of all probe 4-specific targets. **(C)** Amino acid sequences for the GSTM family starting at amino acid 91 and 201 as per the mouse UNIPROT database with two identified peptides indicated in bold. **(D)** qPCR analysis of *Apmap*, *Gstm1* and *Nenf* genes in unstimulated or LPS-stimulated (25 ng/mL) N9 microglia. Data represent means  $\pm$  SEM ( $n = 2$ ). Student's t-tests were used to test for significance versus control. **(E)** Western blot of N9 microglia against APMAP and GSTM1 shows expression of both proteins and increased GSMT1 protein upon LPS stimulation (100 ng/mL). **(F)** Gel-based AfBPP with pac-DHEA (4) in APMAP-overexpressing HEK-293-T cells after 0.5 and 24 h probe incubation. **(G)** Gel-based AfBPP with pac-DHEA (4) on mouse or human NENF-expressing HEK-293-T supernatant. Coomassie served as a protein loading control.

The expression of NENF, APMAP and GSTM1 in N9 cells was further investigated by qPCR and western blot. *Apmap*, *Gstm1* and *Nenf* mRNA could be detected and APMAP and GSTM1 protein was detected by specific antibodies (Figure 5D/E). mRNA and protein levels of GSMT1 showed an increase upon LPS stimulation, which is consistent with its reported involvement in inflammatory signaling.<sup>35</sup> Next, the three proteins were overexpressed in HEK-293-T cells to confirm that they are targets of probe 4. Gel-based AfBPP revealed that APMAP could be labeled by the probe after a short (0.5 h) or long (24 h) incubation time (Figure 5F). Probe labeling of NENF, an extracellular protein, was observed in the supernatant of NENF-overexpressing HEK-293-T cells (Figure 5G). GSTM1 was overexpressed in HEK-293-T cells, but could not be labeled at any incubation time. This indicated that APMAP and NENF, but not GSTM1, are direct protein targets of pac-DHEA (4).

## Characterization of NENF, GSMT1 and APMAP in N9 microglia

The three proteins were further investigated for their role in inflammatory response by measuring secreted pro-inflammatory markers interleukin-6 (IL-6) and nitric oxide (NO). NO is rapidly oxidized in cells to form nitrite, which can be detected and quantified through its reactivity towards 2,3-diaminonaphthalene (DAN).<sup>36,37</sup> Incubation of N9 cells with LPS induced the formation of IL-6 as measured by ELISA and nitrite as measured using a DAN assay (Figure 6A, B, Figure S1, S2).<sup>38</sup> DHEA reduced both NO and IL-6 production in a dose-dependent manner (Figure 6A, B, Figure S2). In contrast to previously published results, which indicated that CYP450-derived epoxide metabolites of DHEA play a critical role in microglial inflammatory response,<sup>22</sup> the broad-spectrum CYP inhibitor ketoconazole and a soluble epoxide hydrolase inhibitor did not affect the anti-inflammatory effects of DHEA (Figure S3).

Next, the effect of the three proteins on LPS-induced inflammatory response by N9 cells was investigated. NENF acts as an extracellular signaling factor, and recombinant NENF has been shown to have neurotrophic effects on neuronal cells under serum-free conditions.<sup>39</sup> Therefore, N9 cells were incubated with or without fetal calf serum and supplemented with recombinant NENF protein or bovine serum albumin (BSA) as control. Under these conditions, NENF reduced LPS-induced NO production slightly in serum-free medium, but not in combination with DHEA (Figure 6C, D).

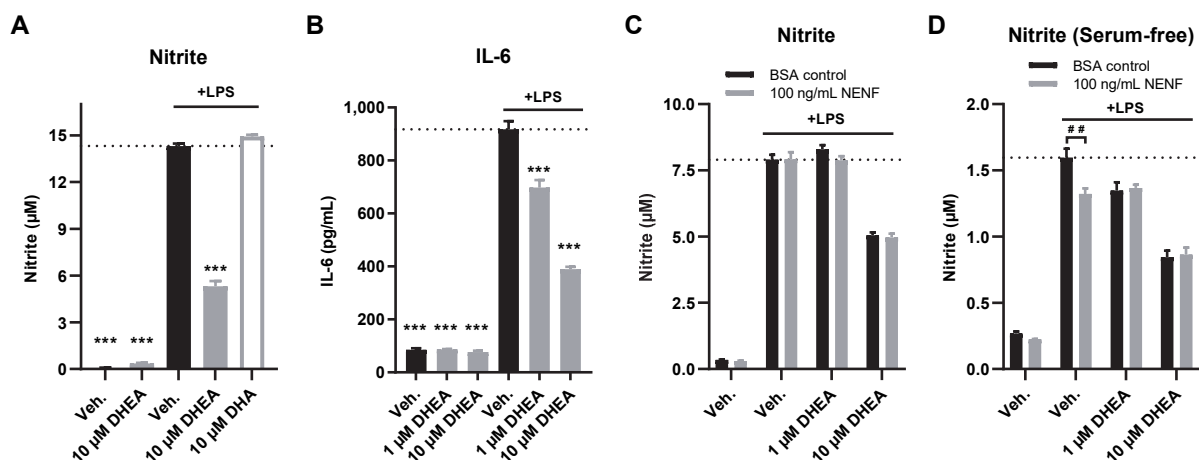


**Figure 6 | Effect of DHA, DHEA and NENF on inflammatory markers.** N9 microglia were pretreated with indicated lipid or vehicle for 4 h before LPS stimulation (100 ng/mL) for 24 h. Supernatant was collected for (**A, C, D**) DAN assay or (**B**) IL-6 ELISA and viability was tested by MTT assay (Figure S1). For the NENF treatment, N9 microglia were cultured in full medium or serum-free medium supplemented with 0.1% delipidated BSA for 3 h, after which they were treated with indicated combination of recombinant human NENF or BSA, and DHEA or vehicle for 4 h before LPS stimulation (100 ng/mL) in the corresponding medium. Data represent means  $\pm$  SEM ( $n = 3-6$ ). \*\*\*  $p < 0.001$  in comparison to LPS-treated control (dotted line) using a one-way ANOVA with Dunnett's multiple comparisons correction. ##  $p < 0.01$  using a one-way ANOVA between all conditions with Tukey's multiple comparisons correction.

Next, since GSTM1 and APMAP have no known function or inhibitors, the role of these proteins in inflammatory response was studied by overexpression in N9 cells. Since most traditional methods of introduction of foreign DNA in microglial cells result in cell death or premature activation, stable expressing N9 cells were made using lentiviral vectors.<sup>40,41</sup>

To follow incorporation of the genetic material during the selection procedure, GFP fusions of GSTM1 and APMAP were used. HEK-293-T cells were transfected to obtain lentiviral particles carrying vectors encoding GFP, GSMT1-GFP and APMAP-GFP, which were subsequently used to infect N9 microglia. Selection for cells which incorporated the DNA of interest afforded populations with good (>90% of cells) expression of GFP and acceptable (50-75% of cells) expression of GSTM1-GFP and APMAP-GFP based on fluorescent signal. Expression of GSTM1-GFP and APMAP-GFP was confirmed by western blot (Figure S4A, B) and localization was investigated by confocal microscopy of live cells (Figure S4C). This showed homogeneous localization of GFP and GSTM1-GFP throughout the cell, whereas APMAP-GFP showed exclusion from the nucleus, which was consistent with literature.<sup>42</sup>

Next, IL-6 and nitrite levels in LPS-stimulated GFP-, GSTM1-GFP- and APMAP-GFP-expressing cells were determined (Figure 7). Both GSTM1-GFP and APMAP-GFP overexpression did not elicit an immune response or affect cell viability (Figure S5), but upon LPS stimulation the NO and IL-6 response was strongly and significantly increased compared to control cells expressing GFP. The increased nitrite and IL-6 levels in both GSTM1-GFP- and APMAP-GFP-expressing cells were reduced by pretreatment with DHEA. Of note, DHA only partly reduced levels of IL-6, but not nitrite, in GSTM1-GFP- and APMAP-GFP-expressing cells.

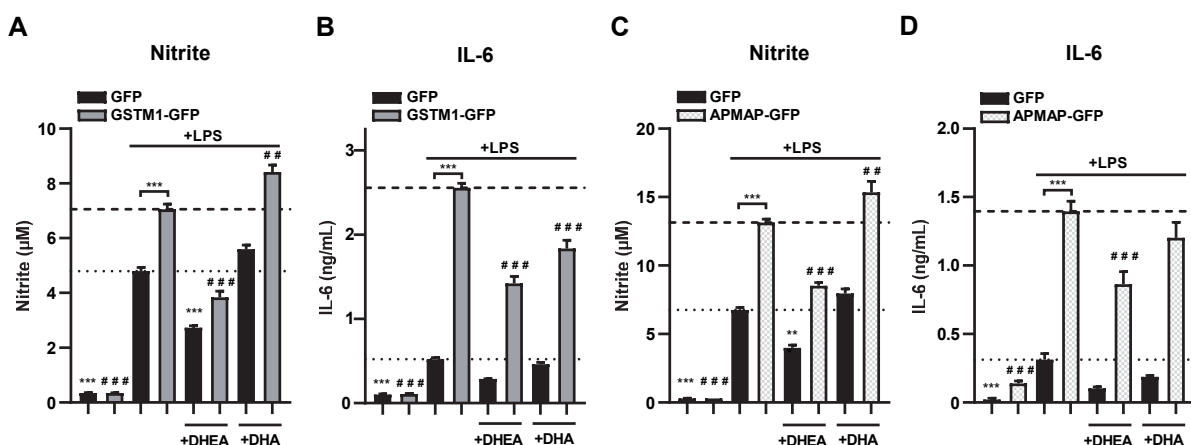


**Figure 7 | Effect of expression of GFP, GSTM1-GFP or APMAP-GFP on inflammatory markers. (A,B)** GSTM1-GFP-, **(C,D)** APMAP-GFP- or GFP-expressing N9 microglia were pretreated with indicated lipid or vehicle for 4 h before LPS stimulation (100 ng/mL) for 24 h. Supernatant was collected for DAN assay or IL-6 ELISA and viability was tested by MTT assay (Figure S5). Data represent means  $\pm$  SEM ( $n = 4$ ). \*\*\*  $p < 0.001$ ; \*\*  $p < 0.01$  in comparison to LPS-treated GFP-expressing cells (dotted line), #####  $p < 0.001$ ; ##  $p < 0.01$  in comparison to LPS-treated GSTM1-GFP- or APMAP-GFP-expressing cells (dashed line) using a one-way ANOVA between all conditions followed by Tukey's multiple comparisons correction.

## Discussion and conclusion

DHEA is an omega-3 fatty acid derivative with pleiotropic effects in the brain. It is known to have a role in neurogenesis, neuritogenesis and synaptogenesis, but also to reduce the inflammatory response of immune cells. Although large improvements have been made to detect and quantify DHEA and its metabolites, this does not allow for the discovery of novel protein targets that bestow their anti-inflammatory properties. This is enabled by photoaffinity probes, which have been successfully used to characterize lipid-protein interactions of several lipid classes.<sup>34,43–45</sup> In this chapter, the role of DHEA in neuroinflammation was investigated by characterization of its anti-inflammatory effects in a microglial cell line and the protein interaction landscape was investigated using a DHEA-based photoaffinity probe. DHEA dose-dependently reduced inflammatory response to a greater extent than DHA. Inhibition of CYP450 and sEH enzymes did not alter this effect, indicating that epoxide metabolites of DHEA were not involved in LPS-stimulated N9 microglia. Photoaffinity probe **4** had the same anti-inflammatory capacity as its parent lipid, which indicated that the introduction of the minimalist bifunctional photoreactive linker with an alkyne ligation tag was tolerated. Probe **4** was used to identify 105 pac-DHEA-interacting proteins. Of these, 11 were deemed DHEA-specific after deselection, of which three were further investigated.

NENF is a 171 amino acid secreted protein expressed abundantly in the central nervous system and was identified as a heme-binding neurotrophic factor.<sup>46–48</sup> It signals for neuronal differentiation and survival through the mitogen-activated protein kinase (MAPK) and phosphatidylinositol 3-kinase (PI3K) pathways.<sup>39,47</sup> Specific receptors remain unknown.<sup>49</sup> Recombinant NENF did not alter NO production in complete medium upon LPS stimulation, however, the NO response was reduced by NENF when N9 microglia were cultured in serum-free medium. In line with previously reported neuroprotective properties of NENF<sup>39</sup> and interaction with AEA,<sup>34</sup> NENF could act as a facilitator for the intercellular exchange of signaling lipids like DHEA and AEA in the brain.

GSTM1 is part of a family of enzymes responsible for the metabolism of a broad range of xenobiotics and carcinogens.<sup>50</sup> GSTM1 was found to promote pro-inflammatory signaling in mice and to be required in astrocytes for the activation of nuclear factor κB and stimulated the formation of pro-inflammatory mediators.<sup>35</sup> Knockdown of GSMT1 in astrocytes resulted in attenuated activation of microglia in the prefrontal cortex of mice in response to LPS stimulation.<sup>35</sup> The results presented here show that GSTM1 is also present in microglia and its expression is increased upon LPS stimulation. Overexpression of GSTM1-GFP in N9 microglia exacerbated the inflammatory response to LPS. DHEA could partially reverse this effect, while DHA was less effective. Since probe **4** did not directly label recombinant GSMT1 in HEK-293-T cells, an oxidative metabolite of DHEA produced by lipoxygenases or cyclooxygenases may be responsible for the interaction with GSMT1. Previously, GSMT1 has been implicated in neuroinflammation<sup>35</sup> and its null polymorphism is associated with increased risk of

inflammatory disease<sup>51</sup> and cancer.<sup>52,53</sup> Based on the results reported in this study, it can be speculated that GSTM1 inactivates not only toxic metabolites, but also anti-inflammatory lipids, thereby exacerbating the inflammatory response.

APMAP was identified as an integral plasma membrane protein with a large extracellular C-terminal domain.<sup>54</sup> It induces differentiation of 3T3-L1 cells into adipocytes,<sup>54</sup> but it is also expressed in non-adipose tissues, like liver, central nervous system, blood vessels and on the cell surface of CD14+ monocytes and endothelial cells.<sup>42</sup> It has esterase activity and its sequence homology with paraoxonase family members indicates that it might be involved in detoxification processes.<sup>42</sup> Here, it was shown to interact with pac-DHEA and to increase the inflammatory response to LPS in N9 microglia, which could be partially prevented by DHEA. The interaction of APMAP with pac-DHEA (**4**) and its homology to paraoxonases suggests that it could be involved in metabolism of immunomodulatory lipids.

In conclusion, lipid photoaffinity probes can be used to investigate protein-lipid interactions that infer the anti-inflammatory properties of omega-3 fatty acids and metabolites. Control probes are needed to distinguish between specific and nonspecific interactions. Applying DHA- and DHEA-based photoaffinity probes provided an overview of the interaction landscape in microglial cells and provide a basis for further investigation of the role of these omega-3 fatty acids in neuroinflammation.

## Experimental procedures

### General

Lipids were purchased from Cayman Chemicals and stored as 10 mM ethanolic stocks under nitrogen at -80 °C. Inhibitors were purchased from Cayman Chemicals or Sigma Aldrich and stored as 10 mM DMSO stocks at -20 °C. LPS from *Escherichia coli* (O111:B4, Sigma Aldrich) was dissolved in PBS and stored at 200 µg/mL at -20 °C. Human recombinant NENF was obtained from R&D Systems (6714-ND-050), reconstituted to 100 µg/mL in PBS and stored at -80 °C. FP-TAMRA was purchased from Thermo Fisher. MB064 was synthesized in-house as previously described.<sup>55</sup> All other reagents were purchased from Sigma Aldrich or Cayman Chemicals unless otherwise specified.

### Cloning

DNA oligos were purchased at Sigma Aldrich or Integrated DNA Technologies. Cloning reagents were from Thermo Fisher. Full-length cDNA encoding human NENF or murine APMAP, NENF and GSTM1 was obtained from Source Bioscience. Expression constructs were generated by PCR amplification and restriction/ligation cloning into a pcDNA3.1 vector, in frame with a C-terminal FLAG tag or, in case of GFP fusion constructs, a C-terminal GFP-FLAG tag. Lentiviral vectors (pLenti6.3/V5-DEST, pMD2.G, pRSV-Rev and pMDLg/pRRE) were kind gifts from Dr. Rolf Boot (Leiden University). Lentiviral expression constructs were generated by PCR amplification of the GFP, APMAP-GFP-FLAG or GSTM1-GFP-FLAG sequence and restriction/ligation cloning into a pLenti6.3/V5-DEST vector. All plasmids were isolated from transformed XL10-Gold or DH10B competent cells (prepared using *E. coli* transformation buffer set, Zymo Research) using plasmid isolation kits following the supplier's protocol (Qiagen). All sequences were verified by Sanger sequencing (Macrogen).

### General cell culture

HEK-293-T cells were cultured at 37 °C under 7% CO<sub>2</sub> in DMEM (Sigma Aldrich, D6546) containing phenol red, stable glutamine, 10% (v/v) New Born Calf Serum (Thermo Fisher) and penicillin and streptomycin (200 µg/mL each, Duchefa). Cells were passaged twice a week at 80-90% confluence by resuspension in fresh medium.

N9 microglia were cultured at 37 °C under 5% CO<sub>2</sub> in RPMI 1640 (Sigma) containing phenol red, stable glutamine, 10% (v/v) sterile-filtered Fetal Calf Serum (Thermo Fisher) and penicillin and streptomycin (200 µg/mL each, Duchefa). Cells were passaged every two days by washing with PBS and trypsinization, subsequently quenching the trypsin with medium and removal of the trypsin by spinning down the cell suspension (200 g, 5 min). The resulting pellet was resuspended in culture medium by vortexing and subsequently seeded on new plates. Cells were tested regularly for mycoplasma contamination. Cultures were discarded after 2-3 months of use.

### N9 lentivirus infection

To produce lentiviral particles, HEK-293-T cells were seeded on 10 cm dishes 24 h prior to transfection. Culture medium (DMEM) was then aspirated and replaced with 5 mL fresh medium. A 3:1 (m/m) mixture of PEI (30 µg/dish) and plasmid DNA (10 µg/dish, 1:1:2:4 ratio (m/m) of pMD2.G, pRSV-Rev, pMDLg/pRRE, and pLenti6.3/V5-DEST encoding GFP, GSMT1-GFP or APMAP-GFP) was prepared in serum-free culture medium (1 mL) and incubated for 15 min at rt. Transfection was performed by dropwise addition of the PEI/DNA mix to the cells. After 24 h, medium was replaced with fresh medium supplemented with HEPES pH 7.4 (20 mM final). After 24 h, the supernatant was collected in a 15 mL tube, spun down (10,000 g, 5 min) and filtered over a 0.45 µm sterile filter and used immediately.

For the infection,  $1.0 \times 10^5$  N9 cells were plated on 6-well plates 24 h prior to infection. The medium (RPMI) was aspirated and replaced with 1 mL fresh medium. This was supplemented with 1 mL of HEK-293-T supernatant containing the lentiviral particles and the cells were cultured for 24 h. The medium was removed and replaced with 4 mL culture medium (RPMI). After 24 h, the medium was replaced with 4 mL medium containing 2  $\mu$ g/mL blasticidin S and the cells were maintained on 2  $\mu$ g/mL blasticidin S for two weeks, splitting cells when confluent and replacing the medium at least every two days. For subsequent experiments, the cells were plated in medium without blasticidin S.

### RNA extraction and cDNA synthesis

Cells were lysed in Invitrogen TRIzol reagent (Thermo Fisher) in a total volume of 500  $\mu$ L and frozen at -80 °C. RNA extraction was performed following the supplier's protocol with minor modifications. In short, 100  $\mu$ L CHCl<sub>3</sub> was added to the lysates and the sample was thoroughly vortexed and centrifuged (12,000 *g*, 15 min). The clear lysate was transferred to a new vial and isopropanol was added (1:1 v/v). This was vortexed, incubated for 10 min and centrifuged (7,500 *g*, 10 min). The RNA pellet was then washed twice with 750  $\mu$ L of 75% ethanol and dried by evaporation. The pellet was resuspended in 10  $\mu$ L of RNase free DEPC water (BioSphere) and the RNA concentration and purity were determined using a DeNovix DS-11 spectrophotometer. RNA with an A<sub>260</sub>/A<sub>280</sub>-ratio between 1.95 and 2.05 was considered to be of sufficient quality. The samples were brought to equal concentration by diluting with DEPC water. RNA was then mixed with dNTPs (0.5 mM) and oligodT (5  $\mu$ M), and shortly heated up to 85 °C. Subsequently, RT-buffer (ThermoFisher), Reverse transcriptase (Thermo Fisher, EP0752) and RiboLock (2 units, Thermo Fisher, O0381) was added in a total volume of 10  $\mu$ L and the cDNA was generated in 30 min at 50 °C in a thermal cycler.

### Quantitative real-time polymerase chain reaction

Quantitative real-time polymerase chain reaction (qPCR) was performed with 10 ng of RNA as a template. Forward and reverse primers for the indicated gene were added both at 0.3  $\mu$ M final concentration, with 7.5  $\mu$ L of 2\*SYBR Green Master mix (BioTools, B21202) in a total volume of 15  $\mu$ L. Amplification was performed in a BioRad CFX96 Touch Real-time PCR. 5 min at 95 °C was done to heat-start the polymerase-activity. 40 cycles were then performed consisting of 15 seconds of denaturation at 95 °C, followed by 45 seconds of annealing and elongation at 60 °C. Afterwards, the melting temperature was measured to assess amplicon integrity by performing 60 cycles of 65 °C + 0.5 °C/cycle for 5 seconds/cycle. Used primers sets are listed in Table S1.

**Table S1 | Primers used in qPCR experiments.**

Gene	Forward primer	Reverse primer
<i>Hprt</i>	TTGACACTGGTAAAACAATGC	GCCTGTATCCAACACTTCG
<i>Il6</i>	TAGTCCTTCCTACCCCAATTCC	TTGGTCCTTAGCCACTCCTTC
<i>Ptgs2</i>	TGAGCAACTATTCAAACCCAGC	GCACGTAGTCTCGATCACTATC
<i>Cd86</i>	TGTTTCCGTGGAGACGCAAG	TTGAGCCTTGAAATGGGCA
<i>Tlr2</i>	AGGTGCCGACTGTTCCCTC	AGATTGACGCTTGCTGAGG
<i>Apmip</i>	GAGGTCAAGGAGGGCAGTTC	GGGTTCTTGAAGCTGAAACTCT
<i>Gstm1</i>	TAATTGGGATTGGTGCAGGGT	CTGGTGCTGTGGCTTCTCAA
<i>Nenf</i>	GAAGGGAGTGGTTCGATGT	GTGTCGTGAGTGAGGTCTGC

Data was analyzed with CFX Manager software (BioRad) and Ct-values were averaged and normalized to the expression of *Hprt*, as this gene was found to be among the more stable reference genes for LPS-stimulated microglia. Data are expressed as relative mRNA levels with standard errors of the mean of duplicate reactions, which was calculated with the REST 2009 software.<sup>56</sup>

### Enzyme-linked immunosorbent assay (ELISA)

ELISA was performed using an IL-6 Mouse uncoated ELISA KIT (Thermo Fisher, 88-7064-88) following the manufacturers protocol with minor modifications. In short, half-area high-binding 96 well plates (Greiner) were coated with 25 µL of coating antibody in PBS (1:250) overnight at 4 °C. The wells were blocked with 100 µL of diluent buffer for 2 h at rt. Incubation with 25 µL (diluted) supernatant and provided standard was done for 2 h at rt. The plates were then washed five times with PBS-T (PBS supplemented with 0.05% (w/v) Tween-20). 25 µL of the biotinylated detection antibody in diluent was incubated for 1 hour at rt, after which the plate was washed again five times with PBST. The secondary antibody in diluent was incubated 30 min at rt and the plate was washed seven times with PBST. Detection was done by reacting 25 µL of TMB solution in each well for 10-20 min before quenching with 12.5 µL of 1M aq. HCl. Absorption was measured at 450 nm using a CLARIOstar plate reader (BMG Labtech) and analyzed with Graphpad Prism 8.1.1.

### DAN assay

To 100 µL of freshly isolated supernatant in a black 96-well plate was added 10 µL of 0.05 mg/mL 2,3-diethylaminonaphthalene (DAN) in 0.62 M aq. HCl. This was mixed and incubated for 30 min in the dark. The reaction was quenched with 10 µL of 1.4 M aq. NaOH. The solution was subsequently scanned for fluorescence at 365 nm excitation and 450 nm emission in a CLARIOstar plate reader (BMG Labtech). The concentration was determined using a standard curve of a freshly prepared dilution of NaNO<sub>2</sub> in medium.

### Viability assay

Cells were seeded at 2.0x10<sup>4</sup> or 3.0x10<sup>4</sup> cells per well in a 96-well plate in 0.1 mL medium per well 24 h before treatment. The cells were then treated with the indicated stimuli in fresh complete medium. Afterwards, the culture medium was collected for DAN assay or ELISA. For the MTT assay, the medium was replaced with 90 µL fresh medium supplemented with 10 µL PBS with 5 mg/mL 3-(4,5-dimethylthiazol-2-yl)-2,5-diphenyltetrazolium (0.5 mg/mL final) and the plate was incubated at 37 °C for 3 h. The medium was removed and the formed formazan crystals were dissolved in 100 µL DMSO by shaking the plates at 800 rpm for 5 min. Absorbance was measured at 450 nm in a CLARIOstar plate reader (BMG Labtech) and data was analyzed using Graphpad Prism 8.1.1.

### AfBPP of N9 microglia

#### *Probe labeling and gel-based AfBPP*

N9 microglia were grown to ~70% confluence on 6-well plates. They were washed with PBS (2 mL) and pac-DHA (**3**) or pac-DHEA (**4**) (10 µM from 10 mM ethanolic stock) was added in serum-free medium. The cells were incubated for 30 min at 37 °C after which the medium was aspirated and replaced with fresh medium and the cells were incubated for 4 or 24 h. Medium was aspirated, the cells were washed with PBS (1 mL) and ice-cold PBS (1 mL) was added. The cells were irradiated using a Caprobox™ (10 min, 4 °C, 350 nm, "UV") or exposed to ambient light (10 min, 4 °C, "No UV"). The PBS was collected in tubes and floating cells were spun down (1,000 g, 10 min, 4 °C) and the PBS aspirated. The cells in the wells were collected by scraping into ice-cold PBS (0.5 mL) and combined with the cell pellet. The cells were lysed with lysis buffer (250 µL, 250 mM sucrose, 1X protease inhibitor cocktail (Roche), 20 mM HEPES pH 7.5, 1 mM MgCl<sub>2</sub>). This was sonicated (Branson Sonifier probe sonicator, 10 x 2 s pulses, 10% amplitude). Protein concentration was measured by Qubit™ assay (Invitrogen) and the samples were adjusted to 0.27 mg/mL and a volume of 440 µL, of which 40 µL was reserved for gel analysis. For gel analysis, 40 µL lysate was treated with freshly prepared click mix (4.37 µL per sample: 2.19 µL aq. 25 mM CuSO<sub>4</sub>, 1.3 µL aq. 250 mM NaAsc, 0.44 µL 25 mM THPTA in DMSO, 0.44 µL 0.9 mM Cy5-N<sub>3</sub> in DMSO) and left at rt for 1 h in the dark. Samples were then quenched by addition of 4X Laemmli buffer, boiled (5 min, 95 °C) and resolved by SDS-PAGE (10% acrylamide gel, ±80 min, 180 V) along with protein marker (PageRuler™ Plus, Thermo Fisher). In-gel fluorescence was measured in the Cy3- and Cy5-channel (Chemidoc™ MP, Bio-Rad) and gels were stained with Coomassie after scanning.

*Mass spectrometric analysis of tryptic peptides, identification and quantification*

The pulldown experiment was performed as earlier described, with minor adjustments.<sup>31,57</sup> The lysates (400 µL) were subjected to a click reaction with freshly prepared click mix (43.7 µL per sample: 21.9 µL aq. 25 mM CuSO<sub>4</sub>, 13 µL aq. 250 mM NaAsc, 4.4 µL 25 mM THPTA in DMSO, 4.4 µL 2.25 mM biotin-N<sub>3</sub> in DMSO) at rt for 1 h. Proteins were precipitated by addition of HEPES buffer (50 µL, 50 mM, pH 7.5), MeOH (666 µL), CHCl<sub>3</sub> (166 µL) and MilliQ (150 µL), vortexing after each addition. After spinning down (1,500 g, 10 min) the upper and lower layer were aspirated and the protein pellet was resuspended in MeOH (600 µL) by sonication (Branson Sonifier probe sonicator, 10 x 0.5 s pulses, 10% amplitude). The proteins were spun down (20,000 g, 5 min) and the MeOH was aspirated. The proteins were then redissolved in 6 M urea (500 µL) with 25 mM NH<sub>4</sub>HCO<sub>3</sub> for 15 min, followed by reduction (65 °C, 15 min, 800 rpm shaking) with DTT (5 µL, 1 M). The samples were allowed to reach rt and proteins were alkylated (30 min) with IAA (40 µL, 0.5 M) in the dark. 140 µL SDS (10% w/v) was added and the samples were spun down (1,000 g, 5 min). They were transferred to 5 mL PBS containing 50 µL avidin agarose resin (Pierce, 100 µL of a 50% slurry, prewashed twice with 6 mL PBS + 0.5% SDS and once with 6 mL PBS) and incubated for 2 h while rotating. The beads were spun down (2,000 g, 2 min) and washed (3 x PBS + 0.5% SDS, 2 x PBS, 1 x MilliQ). The beads were resuspended in digestion buffer (250 µL, 100 mM Tris pH 7.8, 100 mM NaCl, 1 mM CaCl<sub>2</sub>, 2% (v/v) acetonitrile, sequencing grade trypsin (Promega, 0.25 µg)) and transferred to low-binding tubes (Sarstedt) and incubated while shaking overnight (16 h, 37 °C, 1,000 rpm). Trypsin was quenched with 12.5 µL formic acid (LC-MS grade) and the beads were filtered off over a Bio-Spin column (BioRad, 400 g, 5 min), collecting the flow-through in a new 2 mL tube. Samples were added on C18 stagetips<sup>58</sup> (preconditioned with 50 µL MeOH, then 50 µL of 0.5% (v/v) formic acid in 80% (v/v) acetonitrile/MilliQ (solution B) and then 50 µL 0.5% (v/v) formic acid in MilliQ (solution A) by centrifugation (600 g, 2 min)). The peptides were washed with solution A (100 µL, 800 g, 3 min) and eluted into new low-binding tubes using solution B (100 µL, 800 g, 3 min). Samples were concentrated using an Eppendorf speedvac (Eppendorf Concentrator Plus 5301) and redissolved in LC-MS solution (30 µL per sample: 28.5 µL MilliQ, 2.85 µL acetonitrile, 0.095 µL formic acid, 600 fmol yeast enolase peptide digest (Waters, 186002325)). Samples were measured using a NanoACQUITY UPLC System coupled to a SYNAPT G2-Si high definition mass spectrometer (Waters). The peptides were separated using an analytical column (HSS-T3 C18 1.8 µm, 75 µm x 250 mm, Waters) with a concave gradient (5 to 40% acetonitrile in H<sub>2</sub>O with 0.1% formic acid). [Glu<sup>1</sup>]-fibrinopeptide B was used as lock mass. Mass spectra were acquired using the UDMS<sup>e</sup> method. The mass range was set from 50 to 2,000 Da with a scan time of 0.6 seconds in positive, resolution mode. The collision energy was set to 4 V in the trap cell for low-energy MS mode. For the elevated energy scan, the transfer cell collision energy was ramped using drift-time-specific collision energies. The lock mass is sampled every 30 seconds. For raw data processing, Progenesis QI for proteomics was used with the following parameters to search the murine proteome from Uniprot (Table S2).

**Table S2 | Parameters used for Progenesis QI.**

Parameter	Value
Lock mass m/z value	785.8426
Low energy threshold	150 counts
Elevated energy threshold	30 counts
Digest reagent	Trypsin
Missed cleavages	Max 2
Modifications	Fixed carbamidomethyl C, variable oxidation M
FDR less than	1%
Minimum fragments/peptide	2
Minimum fragments/protein	5
Minimum peptides/protein	1
Minimum peptide score for quantification	5.5
Identified ion charges for quantification	2/3/4/5/6/7 <sup>+</sup>

### Transfection of HEK-293-T for gel-based AfBPP

HEK-293-T cells expressing hNENF, mNENF or mAPMAP were generated by seeding HEK-293-T cells on 12-wells plates ( $4.0 \times 10^4$  cells/cm $^2$ ) 24 h before transfection. Culture medium was aspirated and replaced with 400  $\mu$ L fresh medium. A 3:1 (m/m) mixture of polyethylenimine (PEI) (1.875  $\mu$ g/well) and plasmid DNA (0.625  $\mu$ g/well) was prepared in serum-free culture medium (100  $\mu$ L) and incubated for 15 min at rt. Transfection was performed by dropwise addition of the PEI/DNA mix to the cells. After 24 h, medium was refreshed. Cells were used 48 h post-transfection. Growth medium was aspirated and a solution of pac-DHEA (10  $\mu$ M from a 10 mM stock) in serum-free DMEM supplemented with 0.1% (w/v) delipidated BSA (0.5 mL) was added and the cells were incubated for indicated time at 37 °C. Medium was aspirated and replaced with 1 mL ice-cold DPBS and the cells were irradiated using a Caprobox™ (10 min, 4 °C, 350 nm, "UV") or exposed to ambient light (10 min, 4 °C, "No UV"). The cells were harvested by pipetting and pelleted by centrifugation (1,000  $g$ , 10 min, 4 °C). The supernatant was removed and the cells were lysed by resuspension in lysis buffer (250 mM sucrose, 20 mM HEPES pH 7.5, 1 mM MgCl<sub>2</sub>, 1X protease inhibitor cocktail (Roche), 25 U/mL benzonase) and sonication in a bath sonicator (0 °C, 5 min). Protein concentration was measured by Qubit™ assay (Invitrogen) and the samples were adjusted to 1.5 mg/mL and a volume of 100  $\mu$ L. For hNENF- and mNENF-transfected cells, 24 h post-transfection the medium was replaced with serum-free medium and after 24 h the supernatant was collected in tubes, spun down (1,000  $g$ , 5 min) and concentrated on 10 kDa Amicon MW cutoff filters (Sigma) to 100  $\mu$ L. The supernatant was then treated with pac-DHEA (10  $\mu$ M from a 10 mM stock) for 30 min at rt and irradiated using a Caprobox™ (10 min, 4 °C, 350 nm).

All samples were treated with 10.4  $\mu$ L click mix (5.5  $\mu$ L aq. 25 mM CuSO<sub>4</sub>, 3.25  $\mu$ L aq. 250 mM NaAsc, 1.1  $\mu$ L 25 mM THPTA in DMSO, 0.55  $\mu$ L 0.9 mM Cy5-N<sub>3</sub> in DMSO) and left at r.t. for 1 h. Samples were then quenched by addition of 4X Laemmli buffer, boiled (5 min, 95 °C) and resolved by SDS-PAGE (10% acrylamide gel, ±80 min, 180 V) along with protein marker (PageRuler™ Plus, Thermo Fisher). In-gel fluorescence was measured in the Cy3- and Cy5-channel (Chemidoc™ MP, Bio-Rad) and the gels were subsequently stained with Coomassie and imaged as a loading control for normalization of fluorescence intensity. Alternatively, proteins were transferred to a 0.2  $\mu$ m polyvinylidene difluoride membrane by Trans-Blot Turbo™ Transfer system (Bio-Rad). Membranes were washed with TBS (50 mM Tris pH 7.5, 150 mM NaCl) and blocked with 5% (w/v) milk in TBS-T (50 mM Tris pH 7.5, 150 mM NaCl, 0.05% (w/v) Tween-20) for 1 h at rt. Membranes were incubated with primary antibody mouse-anti-FLAG (F3156, Sigma Aldrich, 1:2,000, 1 h, rt) in the blocking solution. The membranes were then washed three times with TBS-T (5 min) and incubated with secondary goat-anti-mouse-HRP (sc-2005, Santa Cruz, 1:5,000 in 5% (w/v) milk in TBS-T, 1 h, rt) and washed three times with TBS-T and once with TBS. Membranes were developed in luminol development solution (10 mL of 1.4 mM luminol in 100 mM Tris pH 8.8 + 100  $\mu$ L of 6.7 mM *p*-coumaric acid in DMSO + 3  $\mu$ L of 30% (v/v) H<sub>2</sub>O<sub>2</sub>) and chemiluminescence was detected on ChemiDoc™ MP (Bio-Rad) in the chemiluminescence channel and colorimetric channel for the protein marker. Images were processed using Image Lab 6.0.1 (BioRad).

### Western blot of N9 microglia

Expression of GSTM1-GFP and APMAP-GFP was checked by washing WT, GFP-, GSMT1-GFP- and APMAP-GFP-expressing cells with PBS and harvesting the cells in ice-cold PBS by scraping. Expression of endogenous GSMT1 and APMAP was checked by treatment of the cells with PBS or LPS (100 ng/mL) for 24 h, washing with PBS and harvesting the cells in ice-cold PBS by scraping. The cells were pelleted by centrifugation (1,000  $g$ , 5 min) and lysed by resuspension in lysis buffer (250 mM sucrose, 20 mM HEPES pH 7.5, 1 mM MgCl<sub>2</sub>, 1X protease inhibitor cocktail (Roche), 25 U/mL benzonase) and sonication in a bath sonicator (0 °C, 5 min). Protein concentration was measured by Qubit™ assay (Invitrogen) and the samples were adjusted to 1.5 mg/mL. Proteins were then denatured by adding 4X Laemmli buffer, boiled (5 min, 95 °C) and resolved by SDS-PAGE (10% acrylamide gel, ±80 min, 180 V) along with protein marker (PageRuler™ Plus, Thermo Fisher). Part of the gel was stained with Coomassie and imaged as a loading control. The rest of the gel was transferred to a 0.2  $\mu$ m polyvinylidene difluoride membrane by Trans-Blot Turbo™ Transfer system (Bio-Rad). Membranes were washed with TBS (50

mM Tris pH 7.5, 150 mM NaCl) and blocked with 5% (w/v) milk in TBS-T (50 mM Tris pH 7.5, 150 mM NaCl, 0.05% (w/v) Tween-20) for 1 h at rt.

For endogenous protein, membranes were washed three times with TBS-T, followed by incubation with primary antibody in 5% (w/v) BSA in TBS-T (GSTM1, 13289748, 1:1,000, o/n, 4 °C or APMAP, 15985444, Fisher Scientific, 1:500, o/n, 4 °C). Membranes were then washed three times with TBS-T and incubated with matching secondary antibody in 5% (w/v) milk in TBS-T (1:5,000, 1 h at rt), then washed three times with TBS-T and once with TBS before developing.

For lentivirus-infected lysates, membranes were either directly incubated in the blocking solution with primary antibody (APMAP, 15985444, Fisher Scientific, 1:2,000, 1 h, rt) or washed three times with TBS-T, followed by incubation with primary antibody in 5% (w/v) BSA in TBS-T (GSTM1, 13289748, 1:1,000, 1 h, rt). Membranes were washed three times with TBS-T and incubated with matching secondary antibody in 5% (w/v) milk in TBS-T (1:4,000, 1 h at rt), then washed three times with TBS-T and once with TBS before developing.

Membranes were developed in luminol development solution (10 mL of 1.4 mM luminol in 100 mM Tris pH 8.8 + 100 µL of 6.7 mM *p*-coumaric acid in DMSO + 3 µL of 30% (v/v) H<sub>2</sub>O<sub>2</sub>) and chemiluminescence was detected on ChemiDoc™ MP (Bio-Rad) in the chemiluminescence channel and colorimetric channel for the protein marker. Images were processed using Image Lab 6.0.1 (BioRad). Secondary antibodies: goat anti-mouse-HRP (Santa Cruz, sc-2005), goat anti-rabbit-HRP (Santa Cruz, sc-2030).

### Confocal microscopy

Cells were grown on an ibidi 8 well µ-Slide (1.5 polymer coverslip, ibiTreat) and mounted in a Okolab cage incubator warmed to 37 °C, supplied with 5% CO<sub>2</sub>. For live cell microscopy, RPMI containing 2 mM GlutaMAX, 100 I.U./mL penicillin and 50 µg/mL streptomycin was used during image acquisition. For fixed samples, mounting medium of 9:1 glycerol:PBS containing 1% DABCO anti-bleaching agent was used. All images were collected using an Andor DragonFly 505 spinning disk confocal system, containing an 8-line integrated laser engine, on a Leica DMi8 inverted microscope equipped with a 63X/1.40-0.60 HCX PL APO oil objective. Hoechst 33342 was excited with the 405 line and collected with the 450/50 BP emission filter. GFP-fusion proteins were excited with the 488 line and collected with the 525/50 BP emission filter. Images were acquired with the Zyla 2048x2048 sCMOS camera and 2x2 camera binning controlled with the integrated Fusion software. Z-series optical sections were collected with a system-optimized step-size of 0.13 microns and deconvolved using the integrated ClearView-GPU™ deconvolution software. Z-series are displayed as maximum z-projections, and gamma, brightness and contrast were adjusted using FIJI.<sup>59</sup>

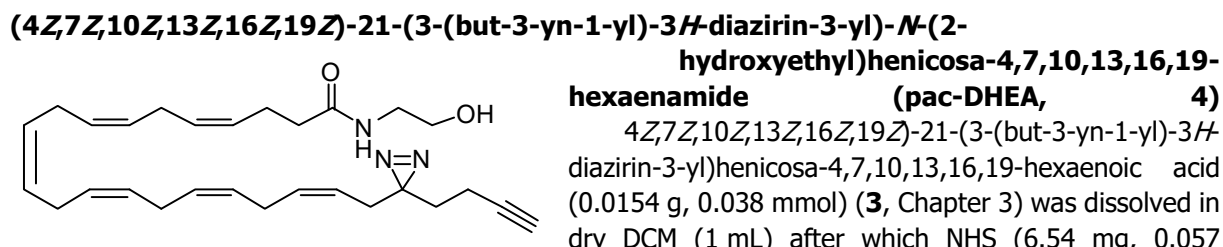
### Statistical analysis

Unless otherwise noted, all replicates represent biological replicates and all data represent means ± SEM. Statistical significance between two conditions was determined using Student's t-tests (two-tailed, unpaired). Statistical significance between multiple conditions was tested using a one-way ANOVA with Dunnett's multiple comparisons correction, or when all conditions were compared, Tukey's multiple comparisons correction. \*\*\* p <0.001; \*\* p <0.01; \* p <0.05; n.s. if p >0.05. All statistical analysis was conducted using Graphpad Prism 8.1.1 or Microsoft Excel.

## Synthesis

### General remarks

Dry DCM was prepared by storage on activated 4 Å molecular sieves for at least 24 hours. All reagents were purchased from Alfa Aesar, Sigma Aldrich/Merck or Acros and used without further purification. Flash column chromatography was performed using SiliCycle silica gel type SiliaFlash P60 (230-400 mesh). TLC analysis was performed on Merck silica gel 60/Kieselguhr F254, 0.25 mm. Compounds were visualized using KMnO<sub>4</sub> stain (K<sub>2</sub>CO<sub>3</sub> (40 g), KMnO<sub>4</sub> (6 g), and water (600 mL)). <sup>1</sup>H NMR and <sup>13</sup>C NMR spectra were recorded on a Bruker AV-400 (400 MHz) spectrometer. Chemical shift values are reported in ppm relative to the tetramethylsilane signal for <sup>1</sup>H NMR ( $\delta$  = 0 ppm) and relative to the solvent signal of CDCl<sub>3</sub> for <sup>13</sup>C NMR ( $\delta$  = 77.16 ppm). Data are reported as follows: Chemical shifts ( $\delta$ ), multiplicity (s = singlet, d = doublet, dd = doublet of doublets, ddt = doublet of doublet of triplets, td = triplet of doublets, t = triplet, q = quartet, p = pentet, bs = broad singlet, m = multiplet), coupling constants  $J$  (Hz), and integration. High resolution mass spectra (HRMS) were recorded by direct injection on a q-TOF mass spectrometer (Synapt G2-SI) equipped with an electrospray ion source in positive mode with Leu-enkephalin ( $m/z$  = 556.2771) as an internal lock mass. The instrument was calibrated prior to measurement using the MS/MS spectrum of [Glu<sup>1</sup>]-fibrinopeptide B.



## Supplementary data

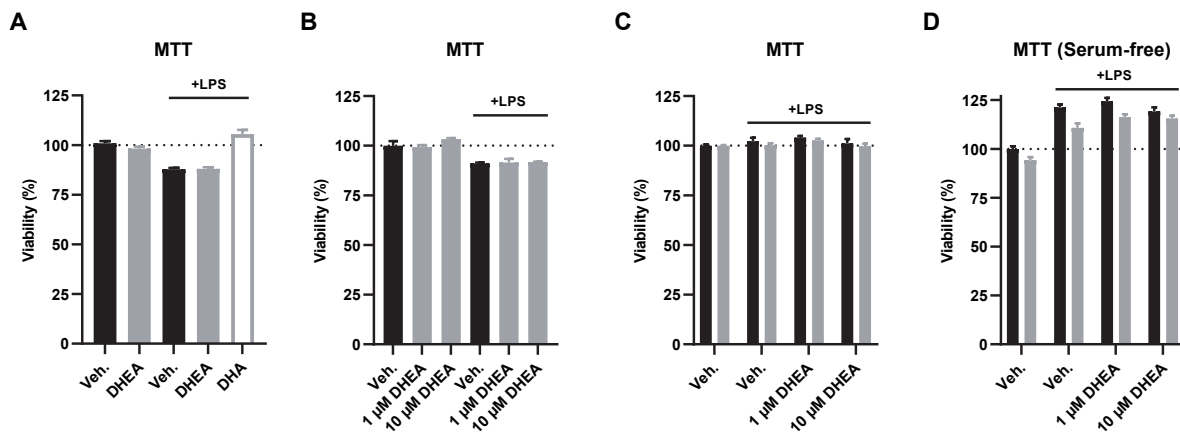


**Figure S1 | Viability assay of N9 microglia corresponding to Figure 6A/B/C/D.** The supernatant of treated N9 microglia was collected for DAN assay or IL-6 ELISA and viability was tested by MTT assay. Data represent means  $\pm$  SEM (n = 3-6).

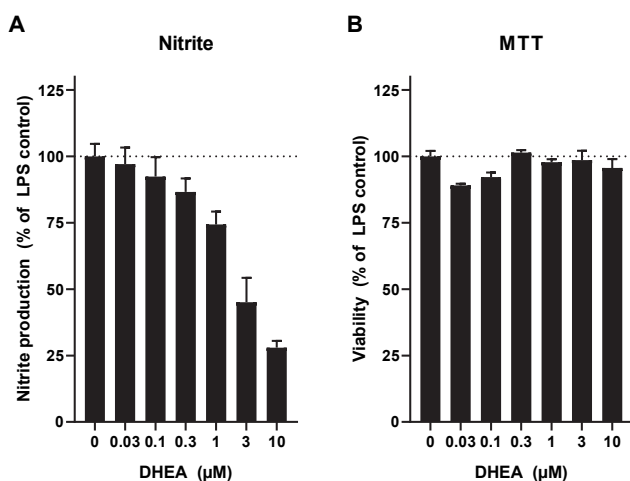


**Figure S2 | DHEA dose-dependently decreases NO production of N9 microglia after LPS stimulation.** N9 microglia were pretreated with DHEA or vehicle for 4 h before LPS stimulation (100 ng/mL) for 24 h. Supernatant was collected for **(A)** DAN assay and viability was tested by **(B)** MTT assay. Data represent means  $\pm$  SEM (n = 3).

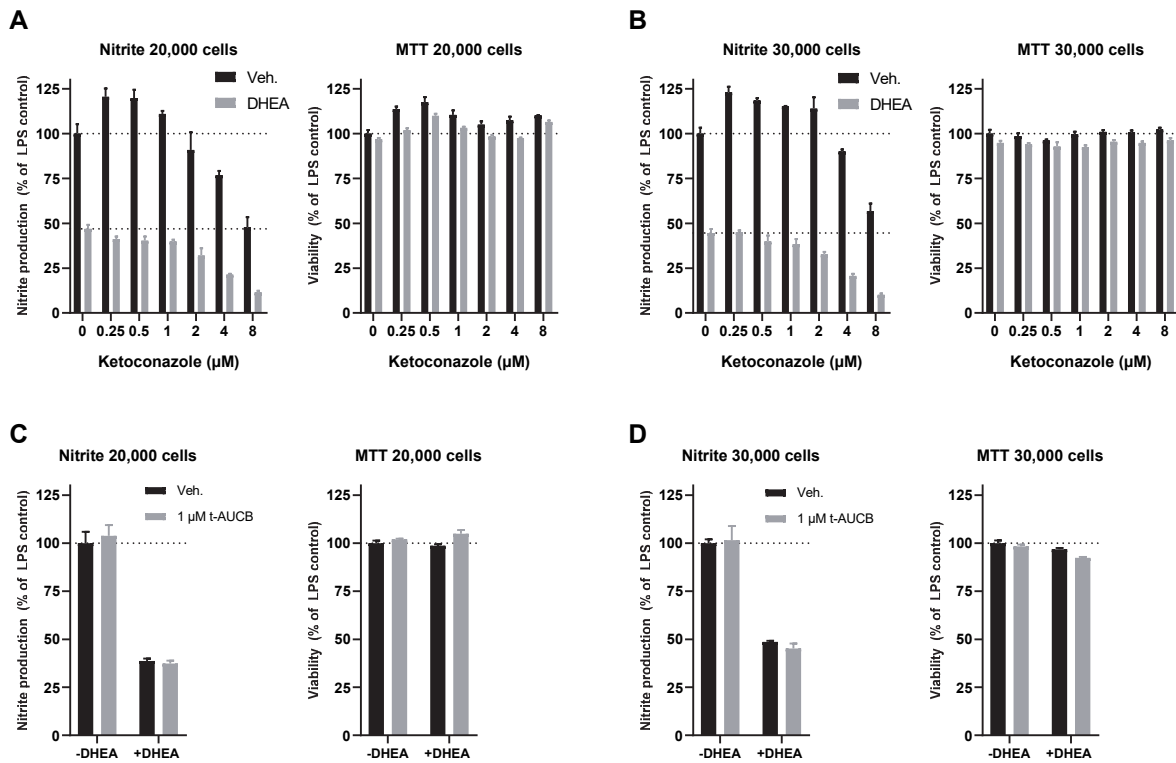


**Figure S3 | Ketoconazole or t-AUCB do not influence the anti-inflammatory effects of DHEA. (A, C)** 20,000 or **(B, D)** 30,000 N9 microglia were pretreated with indicated combination of ketoconazole, t-AUCB, 10  $\mu\text{M}$  DHEA or vehicle for 4 h before LPS stimulation (100 ng/mL) for 24 h. Supernatant was collected for DAN assay and viability was tested by MTT assay. Data represent means  $\pm$  SEM ( $n = 3$ ).

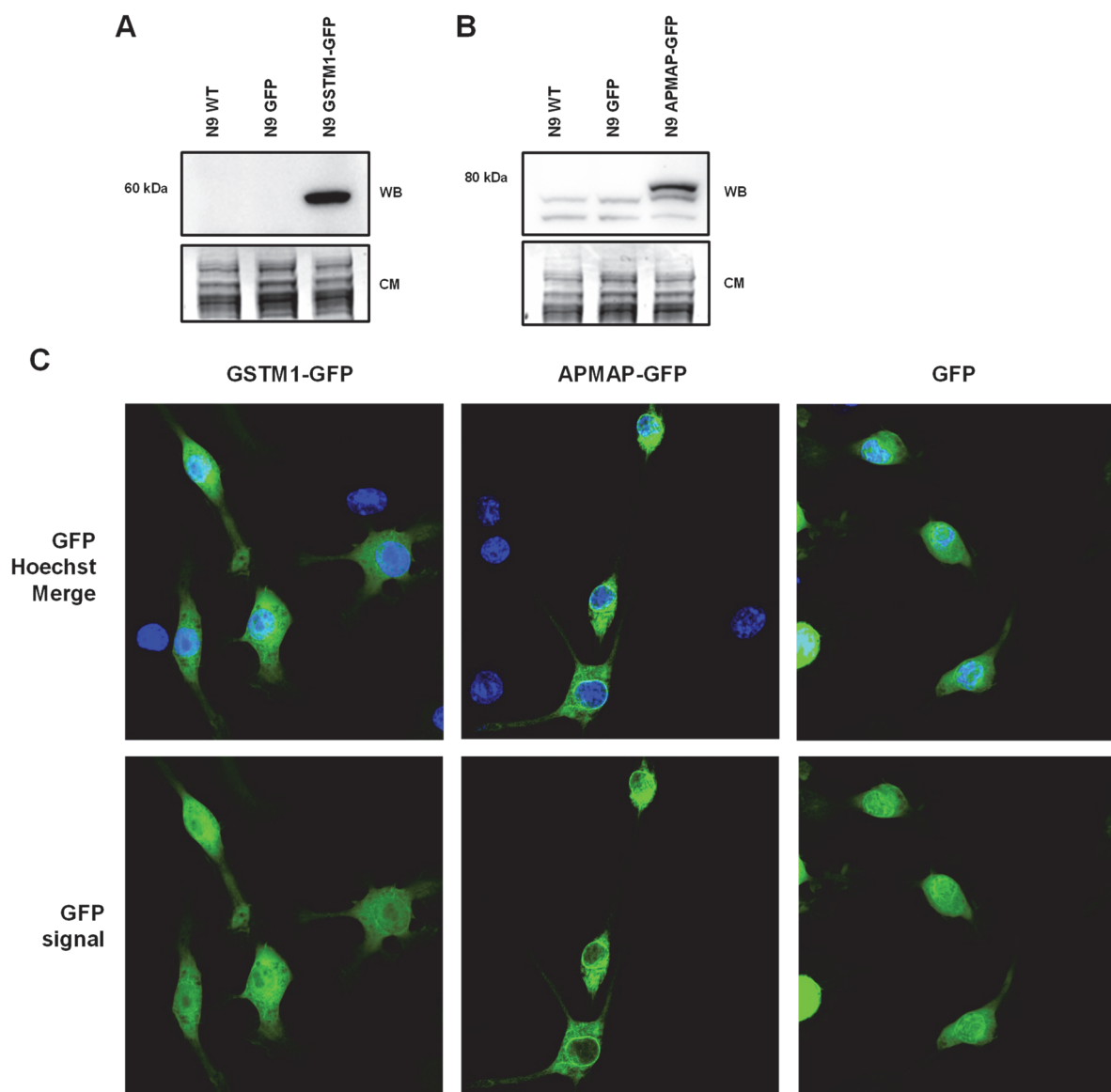


**Figure S4 | Expression of GFP, GSTM1-GFP and APMAP-GFP in N9 microglia.** **(A)** GSMT1 and **(B)** APMAP western blot of N9 microglia lysate confirms expression of the GFP fusion proteins. Coomassie served as loading control. **(C)** Live-cell confocal microscopy shows GSMT1-GFP is homogeneously localized in the cell whereas APMAP-GFP is excluded from the nucleus in N9 microglia.

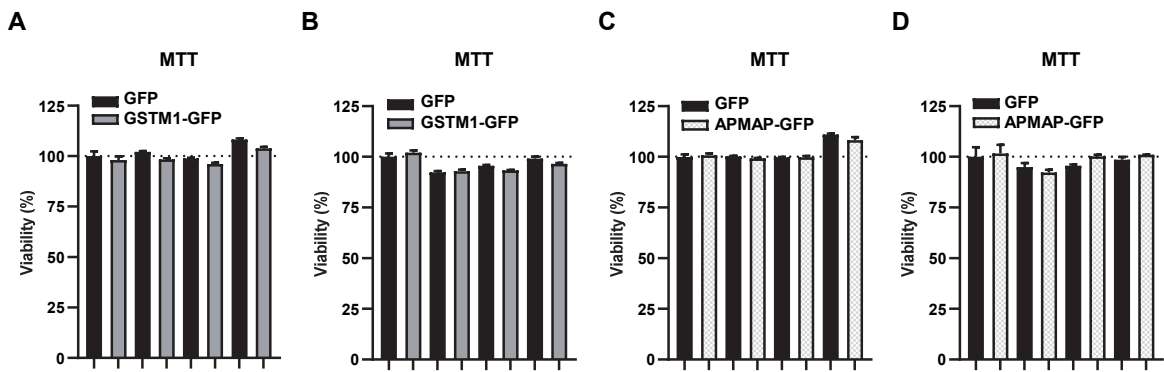


**Figure S5 | Viability assay of N9 microglia corresponding to Figure 7A/B/C/D.** The supernatant of treated N9 microglia was collected for DAN assay or IL-6 ELISA and viability was tested by MTT assay. Data represent means  $\pm$  SEM ( $n = 4$ ).

**Table S3 | Proteins significantly and specifically UV-enriched by pac-DHEA (4) in N9 microglia.**

Gene name	Unique peptides	Description	UV/no (4)	UV pac-DHEA	p-value	UV/UV pac-DHEA (4) vs pac-DHA (3), 24h	p-value	UV/UV pac-DHEA (4) vs pac-DHA (3), 4h
APMAP	11	Adipocyte plasma membrane-associated protein	47.47	0.0319	21.27	0.0334	4.85	
PMPCA	7	Mitochondrial-processing peptidase subunit alpha	7.78	0.0405	7.92	0.0408	6.67	
NUCB1	8	Nucleobindin-1	5.57	0.0064	6.48	0.0040	5.17	
NENF	6	Neudesin	69.34	0.0094	6.43	0.0128	2.69	
GSTM1	4	Glutathione S-transferase Mu 1	5.88	0.0216	3.70	0.0321	2.83	
PTGR2	7	Prostaglandin reductase 2	22.54	0.0132	3.19	0.0248	2.83	
ACP6	5	Lysophosphatidic acid phosphatase type 6	5.35	0.0022	3.07	0.0100	1.82	
HMOX2	11	Heme oxygenase 2	2.53	0.0069	2.68	0.0014	2.17	
MTAP	12	S-methyl-5'-thioadenosine phosphorylase	6.70	0.0214	2.45	0.0260	10.20	
ALDH2	19	Aldehyde dehydrogenase 2	4.48	0.0077	2.33	0.0372	1.40	
UGT1A7C	11	UDP-glucuronosyltransferase 1-7C	3.43	0.0017	2.30	0.0008	0.87	

## References

- (1) Salem, N.; Litman, B.; Kim, H.-Y.; Gawrisch, K. Mechanisms of Action of Docosahexaenoic Acid in the Nervous System. *Lipids* **2001**, *36* (9), 945–959.
- (2) Kawakita, E.; Hashimoto, M.; Shido, O. Docosahexaenoic Acid Promotes Neurogenesis in Vitro and in Vivo. *Neuroscience* **2006**, *139* (3), 991–997.
- (3) Calderon, F.; Kim, H.-Y. Docosahexaenoic Acid Promotes Neurite Growth in Hippocampal Neurons. *J. Neurochem.* **2004**, *90* (4), 979–988.
- (4) Guemez-Gamboa, A.; Nguyen, L. N.; Yang, H.; Zaki, M. S.; Kara, M.; Ben-Omran, T.; Akizu, N.; Rosti, R. O.; Rosti, B.; Scott, E.; Schroth, J.; Copeland, B.; Vaux, K. K.; Cazenave-Gassiot, A.; Quek, D. Q. Y.; Wong, B. H.; Tan, B. C.; Wenk, M. R.; Gunel, M.; Gabriel, S.; Chi, N. C.; Silver, D. L.; Gleeson, J. G. Inactivating Mutations in MFSD2A, Required for Omega-3 Fatty Acid Transport in Brain, Cause a Lethal Microcephaly Syndrome. *Nat. Genet.* **2015**, *47* (7), 809–813.
- (5) Hsieh, A. T.; Anthony, J. C.; Diersen-Schade, D. A.; Rumsey, S. C.; Lawrence, P.; Li, C.; Nathanielsz, P. W.; Brenna, J. T. The Influence of Moderate and High Dietary Long Chain Polyunsaturated Fatty Acids (LCPUFA) on Baboon Neonate Tissue Fatty Acids. *Pediatr. Res.* **2007**, *61* (5), 537–545.
- (6) Park, T.; Chen, H.; Kevala, K.; Lee, J.-W.; Kim, H.-Y. N-Docosahexaenoylethanolamine Ameliorates LPS-Induced Neuroinflammation via cAMP/PKA-Dependent Signaling. *J. Neuroinflammation* **2016**, *13* (1), 284.
- (7) Rashid, M. A.; Kim, H.-Y. N-Docosahexaenoylethanolamine Ameliorates Ethanol-Induced Impairment of Neural Stem Cell Neurogenic Differentiation. *Neuropharmacology* **2016**, *102*, 174–185.
- (8) Kim, H.-Y.; Moon, H.-S.; Cao, D.; Lee, J.; Kevala, K.; Jun, S. B.; Lovinger, D. M.; Akbar, M.; Huang, B. X. N-Docosahexaenoylethanolamide Promotes Development of Hippocampal Neurons. *Biochem. J.* **2011**, *435* (2), 327–336.
- (9) Kharebava, G.; Rashid, M. A.; Lee, J.-W.; Sarkar, S.; Kevala, K.; Kim, H.-Y. N-Docosahexaenoylethanolamine Regulates Hedgehog Signaling and Promotes Growth of Cortical Axons. *Biol. Open* **2015**, *4* (12), 1660–1670.
- (10) Watson, J. E.; Kim, J. S.; Das, A. Emerging Class of Omega-3 Fatty Acid Endocannabinoids & Their Derivatives. *Prostaglandins Other Lipid Mediat.* **2019**, *143*, 106337.
- (11) Meijerink, J.; Plastina, P.; Vincken, J.-P.; Poland, M.; Attya, M.; Balvers, M.; Gruppen, H.; Gabriele, B.; Witkamp, R. F. The Ethanolamide Metabolite of DHA, Docosahexaenoylethanolamine, Shows Immunomodulating Effects in Mouse Peritoneal and RAW264.7 Macrophages: Evidence for a New Link between Fish Oil and Inflammation. *Br. J. Nutr.* **2011**, *105* (12), 1798–1807.
- (12) Heneka, M. T.; Kummer, M. P.; Latz, E. Innate Immune Activation in Neurodegenerative Disease. *Nat. Rev. Immunol.* **2014**, *14* (7), 463–477.
- (13) Lull, M. E.; Block, M. L. Microglial Activation and Chronic Neurodegeneration. *Neurotherapeutics* **2010**, *7* (4), 354–365.
- (14) Morales, I.; Guzmán-Martínez, L.; Cerdá-Troncoso, C.; Farías, G. A.; Maccioni, R. B. Neuroinflammation in the Pathogenesis of Alzheimer's Disease. A Rational Framework for the Search of Novel Therapeutic Approaches. *Front. Cell. Neurosci.* **2014**, *8*.
- (15) Lawson, L. J.; Perry, V. H.; Dri, P.; Gordon, S. Heterogeneity in the Distribution and Morphology of Microglia in the Normal Adult Mouse Brain. *Neuroscience* **1990**, *39* (1), 151–170.
- (16) Cherry, J. D.; Olschowka, J. A.; O'Banion, M. K. Neuroinflammation and M2 Microglia: The Good, the Bad, and the Inflamed. *J. Neuroinflammation* **2014**, *11* (1), 98.
- (17) Leyrolle, Q.; Layé, S.; Nadjar, A. Direct and Indirect Effects of Lipids on Microglia Function. *Neurosci. Lett.* **2019**, *708*, 134348.
- (18) Ekdahl, C. T. Microglial Activation – Tuning and Pruning Adult Neurogenesis. *Front. Pharmacol.* **2012**, *3*.
- (19) Park, T.; Chen, H.; Kim, H.-Y. GPR110 (ADGRF1) Mediates Anti-Inflammatory Effects of N-Docosahexaenoylethanolamine. *J. Neuroinflammation* **2019**, *16* (1), 225.
- (20) Meijerink, J.; Poland, M.; Balvers, M. G. J.; Plastina, P.; Lute, C.; Dwarkasing, J.; van Norren, K.; Witkamp, R. F. Inhibition of COX-2-Mediated Eicosanoid Production Plays a Major Role in the Anti-Inflammatory Effects of the Endocannabinoid N-Docosahexaenoylethanolamine (DHEA) in Macrophages. *Br. J. Pharmacol.* **2015**, *172* (1), 24–37.
- (21) Bus, I. de; Zuilhof, H.; Witkamp, R.; Balvers, M.; Albada, B. Novel COX-2 Products of n-3 Polyunsaturated Fatty Acid-Ethanolamine-Conjugates Identified in RAW264.7 Macrophages. *J. Lipid Res.* **2019**, *60* (11), 1829–1840.
- (22) McDougle, D. R.; Watson, J. E.; Abdeen, A. A.; Adili, R.; Caputo, M. P.; Krapf, J. E.; Johnson, R. W.; Kilian, K. A.; Holinstat, M.; Das, A. Anti-Inflammatory ω-3 Endocannabinoid Epoxides. *Proc. Natl. Acad. Sci.* **2017**, *114* (30), E6034–E6043.
- (23) Spector, A. A.; Fang, X.; Snyder, G. D.; Weintraub, N. L. Epoxyeicosatrienoic Acids (EETs): Metabolism and Biochemical Function. *Prog. Lipid Res.* **2004**, *43* (1), 55–90.
- (24) Deng, Y.; Theken, K. N.; Lee, C. R. Cytochrome P450 Epoxigenases, Soluble Epoxide Hydrolase, and the Regulation of Cardiovascular Inflammation. *J. Mol. Cell. Cardiol.* **2010**, *48* (2), 331–341.

## Chapter 4

- (25) Yang, R.; Fredman, G.; Krishnamoorthy, S.; Agrawal, N.; Irimia, D.; Piomelli, D.; Serhan, C. N. Decoding Functional Metabolomics with Docosahexaenoyl Ethanolamide (DHEA) Identifies Novel Bioactive Signals. *J. Biol. Chem.* **2011**, *286* (36), 31532–31541.
- (26) Alhouayek, M.; Bottemanne, P.; Makriyannis, A.; Muccioli, G. G. N-Acylethanolamine-Hydrolyzing Acid Amidase and Fatty Acid Amide Hydrolase Inhibition Differentially Affect N-Acylethanolamine Levels and Macrophage Activation. *Biochim. Biophys. Acta BBA - Mol. Cell Biol. Lipids* **2017**, *1862* (5), 474–484.
- (27) Lapinsky, D. J.; Johnson, D. S. Recent Developments and Applications of Clickable Photoprobes in Medicinal Chemistry and Chemical Biology. *Future Med. Chem.* **2015**, *7* (16), 2143–2171.
- (28) Hein, J. E.; Fokin, V. V. Copper-Catalyzed Azide–Alkyne Cycloaddition (CuAAC) and beyond: New Reactivity of Copper(I) Acetylides. *Chem. Soc. Rev.* **2010**, *39* (4), 1302–1315.
- (29) Stansley, B.; Post, J.; Hensley, K. A Comparative Review of Cell Culture Systems for the Study of Microglial Biology in Alzheimer’s Disease. *J. Neuroinflammation* **2012**, *9*, 115.
- (30) Weldon, S. M.; Mullen, A. C.; Loscher, C. E.; Hurley, L. A.; Roche, H. M. Docosahexaenoic Acid Induces an Anti-Inflammatory Profile in Lipopolysaccharide-Stimulated Human THP-1 Macrophages More Effectively than Eicosapentaenoic Acid. *J. Nutr. Biochem.* **2007**, *18* (4), 250–258.
- (31) van Rooden, E. J.; Florea, B. I.; Deng, H.; Baggelaar, M. P.; van Esbroeck, A. C. M.; Zhou, J.; Overkleft, H. S.; van der Stelt, M. Mapping *in Vivo* Target Interaction Profiles of Covalent Inhibitors Using Chemical Proteomics with Label-Free Quantification. *Nat. Protoc.* **2018**, *13* (4), 752–767.
- (32) Huang, D. W.; Sherman, B. T.; Lempicki, R. A. Systematic and Integrative Analysis of Large Gene Lists Using DAVID Bioinformatics Resources. *Nat. Protoc.* **2009**, *4* (1), 44–57.
- (33) Huang, D. W.; Sherman, B. T.; Lempicki, R. A. Bioinformatics Enrichment Tools: Paths toward the Comprehensive Functional Analysis of Large Gene Lists. *Nucleic Acids Res.* **2009**, *37* (1), 1–13.
- (34) Niphakis, M. J.; Lum, K. M.; Cognetta III, A. B.; Correia, B. E.; Ichu, T.-A.; Olucha, J.; Brown, S. J.; Kundu, S.; Piscitelli, F.; Rosen, H.; Cravatt, B. F. A Global Map of Lipid-Binding Proteins and Their Ligandability in Cells. *Cell* **2015**, *161* (7), 1668–1680.
- (35) Kano, S.; Choi, E. Y.; Dohi, E.; Agarwal, S.; Chang, D. J.; Wilson, A. M.; Lo, B. D.; Rose, I. V. L.; Gonzalez, S.; Imai, T.; Sawa, A. Glutathione S-Transferases Promote Proinflammatory Astrocyte-Microglia Communication during Brain Inflammation. *Sci Signal* **2019**, *12* (569), eaar2124.
- (36) Ignarro, L. J.; Fukuto, J. M.; Griscavage, J. M.; Rogers, N. E.; Byrns, R. E. Oxidation of Nitric Oxide in Aqueous Solution to Nitrite but Not Nitrate: Comparison with Enzymatically Formed Nitric Oxide from L-Arginine. *Proc. Natl. Acad. Sci.* **1993**, *90* (17), 8103–8107.
- (37) Bryan, N. S.; Grisham, M. B. Methods to Detect Nitric Oxide and Its Metabolites in Biological Samples. *Free Radic. Biol. Med.* **2007**, *43* (5), 645–657.
- (38) Luo, Y.; Zheng, S. G. Hall of Fame among Pro-Inflammatory Cytokines: Interleukin-6 Gene and Its Transcriptional Regulation Mechanisms. *Front. Immunol.* **2016**, *7*.
- (39) Kimura, I.; Nakayama, Y.; Zhao, Y.; Konishi, M.; Itoh, N. Neurotrophic Effects of Neudesin in the Central Nervous System. *Front. Neurosci.* **2013**, *7*.
- (40) Burke, B.; Sumner, S.; Maitland, N.; Lewis, C. E. Macrophages in Gene Therapy: Cellular Delivery Vehicles and *In Vivo* Targets. *J. Leukoc. Biol.* **2002**, *72* (3), 417–428.
- (41) Carrillo-Jimenez, A.; Puigdellívol, M.; Vilalta, A.; Venero, J. L.; Brown, G. C.; StGeorge-Hyslop, P.; Burguillos, M. A. Effective Knockdown of Gene Expression in Primary Microglia With SiRNA and Magnetic Nanoparticles Without Cell Death or Inflammation. *Front. Cell. Neurosci.* **2018**, *12*.
- (42) Ilhan, A.; Gartner, W.; Nabokikh, A.; Daneva, T.; Majdic, O.; Cohen, G.; Böhmig, G. A.; Base, W.; Hörl, W. H.; Wagner, L. Localization and Characterization of the Novel Protein Encoded by C20orf3. *Biochem. J.* **2008**, *414* (3), 485–495.
- (43) Hulce, J. J.; Cognetta, A. B.; Niphakis, M. J.; Tully, S. E.; Cravatt, B. F. Proteome-Wide Mapping of Cholesterol-Interacting Proteins in Mammalian Cells. *Nat. Methods* **2013**, *10* (3), 259–264.
- (44) Haberkant, P.; Stein, F.; Höglinger, D.; Gerl, M. J.; Brügger, B.; Van Veldhoven, P. P.; Krijgsveld, J.; Gavin, A.-C.; Schultz, C. Bifunctional Sphingosine for Cell-Based Analysis of Protein-Sphingolipid Interactions. *ACS Chem. Biol.* **2016**, *11* (1), 222–230.
- (45) Bockelmann, S.; Mina, J. G. M.; Korneev, S.; Hassan, D. G.; Müller, D.; Hilderink, A.; Vlieg, H. C.; Raijmakers, R.; Heck, A. J. R.; Haberkant, P.; Holthuis, J. C. M. A Search for Ceramide Binding Proteins Using Bifunctional Lipid Analogs Yields CERT-Related Protein StarD7. *J. Lipid Res.* **2018**, *59* (3), 515–530.
- (46) Kimura, I.; Nakayama, Y.; Yamauchi, H.; Konishi, M.; Miyake, A.; Mori, M.; Ohta, M.; Itoh, N.; Fujimoto, M. Neurotrophic Activity of Neudesin, a Novel Extracellular Heme-Binding Protein, Is Dependent on the Binding of Heme to Its Cytochrome B5-like Heme/Steroid-Binding Domain. *J. Biol. Chem.* **2008**, *283* (7), 4323–4331.
- (47) Kimura, I.; Yoshioka, M.; Konishi, M.; Miyake, A.; Itoh, N. Neudesin, a Novel Secreted Protein with a Unique Primary Structure and Neurotrophic Activity. *J. Neurosci. Res.* **2005**, *79* (3), 287–294.
- (48) Kimura, I.; Konishi, M.; Miyake, A.; Fujimoto, M.; Itoh, N. Neudesin, a Secreted Factor, Promotes Neural Cell Proliferation and Neuronal Differentiation in Mouse Neural Precursor Cells. *J. Neurosci. Res.* **2006**, *83* (8), 1415–1424.

- (49) Ohta, H.; Konishi, M.; Kobayashi, Y.; Kashio, A.; Mochiyama, T.; Matsumura, S.; Inoue, K.; Fushiki, T.; Nakao, K.; Kimura, I.; Itoh, N. Deletion of the Neurotrophic Factor Neudesin Prevents Diet-Induced Obesity by Increased Sympathetic Activity. *Sci. Rep.* **2015**, *5*(1), 1–12.
- (50) Mannervik, B. The Isoenzymes of Glutathione Transferase. In *Advances in Enzymology and Related Areas of Molecular Biology*; John Wiley & Sons, Ltd, 2006; pp 357–417.
- (51) Wu, W.; Peden, D.; Diaz-Sanchez, D. Role of GSTM1 in Resistance to Lung Inflammation. *Free Radic. Biol. Med.* **2012**, *53*(4), 721–729.
- (52) Cotton, S. C.; Sharp, L.; Little, J.; Brockton, N. Glutathione S-Transferase Polymorphisms and Colorectal Cancer: A HuGE Review. *Am. J. Epidemiol.* **2000**, *151*(1), 7–32.
- (53) Saitou, M.; Satta, Y.; Gokcumen, O.; Ishida, T. Complex Evolution of the GSTM Gene Family Involves Sharing of GSTM1 Deletion Polymorphism in Humans and Chimpanzees. *BMC Genomics* **2018**, *19*(1), 293.
- (54) Albrektsen, T.; Richter, H. E.; Clausen, J. T.; Fleckner, J. Identification of a Novel Integral Plasma Membrane Protein Induced during Adipocyte Differentiation. *Biochem. J.* **2001**, *359*(2), 393–402.
- (55) Baggelaar, M. P.; Janssen, F. J.; van Esbroeck, A. C. M.; den Dulk, H.; Allarà, M.; Hoogendoorn, S.; McGuire, R.; Florea, B. I.; Meeuwenoord, N.; van den Elst, H.; van der Marel, G. A.; Brouwer, J.; Di Marzo, V.; Overkleef, H. S.; van der Stelt, M. Development of an Activity-Based Probe and In Silico Design Reveal Highly Selective Inhibitors for Diacylglycerol Lipase- $\alpha$  in Brain. *Angew. Chem. Int. Ed.* **2013**, *52*(46), 12081–12085.
- (56) Pfaffl, M. W.; Horgan, G. W.; Dempfle, L. Relative Expression Software Tool (REST $\circledcirc$ ) for Group-Wise Comparison and Statistical Analysis of Relative Expression Results in Real-Time PCR. *Nucleic Acids Res.* **2002**, *30*(9), e36–e36.
- (57) Soethoudt, M.; Stolze, S. C.; Westphal, M. V.; van Stralen, L.; Martella, A.; van Rooden, E. J.; Guba, W.; Varga, Z. V.; Deng, H.; van Kasteren, S. I.; Grether, U.; IJzerman, A. P.; Pacher, P.; Carreira, E. M.; Overkleef, H. S.; Ioan-Facsinay, A.; Heitman, L. H.; van der Stelt, M. Selective Photoaffinity Probe That Enables Assessment of Cannabinoid CB2 Receptor Expression and Ligand Engagement in Human Cells. *J. Am. Chem. Soc.* **2018**, *140*(19), 6067–6075.
- (58) Rappaport, J.; Mann, M.; Ishihama, Y. Protocol for Micro-Purification, Enrichment, Pre-Fractionation and Storage of Peptides for Proteomics Using StageTips. *Nat. Protoc.* **2007**, *2*(8), 1896–1906.
- (59) Schindelin, J.; Arganda-Carreras, I.; Frise, E.; Kaynig, V.; Longair, M.; Pietzsch, T.; Preibisch, S.; Rueden, C.; Saalfeld, S.; Schmid, B.; Tinevez, J.-Y.; White, D. J.; Hartenstein, V.; Eliceiri, K.; Tomancak, P.; Cardona, A. Fiji: An Open-Source Platform for Biological-Image Analysis. *Nat. Methods* **2012**, *9*(7), 676–682.



# Chapter 5

## An expeditious synthesis of DHA-alkyne\*

### Introduction

Docosahexaenoic acid (DHA, 22:6 n-3, **1**) is a polyunsaturated fatty acid (PUFA) which is found to be particularly enriched in the brain (Figure 1).<sup>1</sup> In mammals, DHA can be synthesized from α-linolenic acid (ALA, 18:3 n-3) via sequential desaturation and elongation steps. However, as this process is quite inefficient, most mammalian DHA is obtained from dietary sources.<sup>2–4</sup> DHA has a beneficial role in neuronal development<sup>5</sup> and neuroprotection,<sup>6</sup> as well as in chronic inflammatory conditions like rheumatoid arthritis.<sup>7,8</sup> Recent advances in mass spectrometry have allowed the accurate detection and quantification of PUFAAs and their metabolites.<sup>9</sup> This led to the discovery of anti-inflammatory metabolites of DHA produced via oxidative pathways. Several oxygenated metabolites of DHA are involved in the resolution of inflammation and are called specialized pro-resolving mediators (SPMs).<sup>10–12</sup>

---

\*The data presented in this chapter was gathered in collaboration with Hugo Minnee, Joost von Hegedus, Joanneke C. Kwekkeboom, Hans van den Elst, Remco Peter, Herman S. Overkleeft, René E. M. Toes, Andreea Ioan-Facsinay, Mario van der Stelt.

To date, investigation of PUFA metabolites, their cellular localization and role in inter-cellular signaling remains a difficult process. To aid this process, the labeling of fatty acids using (radioactive) isotopes<sup>13</sup> and fluorophores<sup>14,15</sup> has proven an invaluable tool. Isotopically labeled lipids have been used primarily in the investigation of the metabolism of many lipid species,<sup>16,17</sup> while fluorescently labeled lipids have been used extensively to visualize lipid localization and trafficking.<sup>15,18</sup> However, these tools have several drawbacks. Radioactive isotopes require special equipment and procedures, while non-radioactive isotopes do not allow for investigation of the localization of the lipids. Fluorescent tags can be introduced to study localization of lipids, but they are relatively large and rigid compared to the labeled molecules, affecting their metabolism and distribution.<sup>19,20</sup> Thus, to trace metabolism and localization of PUFAs, new tools are required.

The discovery of the copper(I)-catalyzed azide-alkyne cycloaddition (CuAAC) has led to the development of a large toolbox of 'click' chemistry reagents.<sup>21</sup> Alkyne moieties are synthetically accessible and minimally intrusive when placed on the terminal alkyl chain of a lipid. Terminal alkyne analogues for lipid families such as fatty acids,<sup>22,23</sup> sterols<sup>24,25</sup> and sphingolipids, have already been developed.<sup>26,27</sup> Alkyne lipids have several benefits over radio-labeled lipids. For example, no special equipment or permissions are needed to handle alkyne lipids. After conjugation to a reporter group, alkyne lipids can be used to identify metabolites by liquid chromatography-mass spectrometry (LC-MS) analysis or thin-layer chromatography (TLC).<sup>28</sup> Importantly, alkyne-tagged lipids have outperformed established radiolabeled lipids tracers in sensitivity and linearity of detection.<sup>22</sup> Moreover, alkyne lipids can also be used to study localization by *in situ* click ligation to a fluorophore, followed by fluorescence microscopy.<sup>25,29</sup>

A wide range of fluorophore azides are available for the detection of alkyne-modified lipids.<sup>29,30</sup> With these tools, an alkyne-tagged lipid can be used in different types of experiments, allowing parallel investigation on metabolism and distribution of the same molecule.<sup>29</sup> However, the availability of chemical tools based on PUFAs is limited due to their synthetic difficulty. PUFAs and modified derivatives can be synthesized through a number of strategies. The synthetic challenge lies in the double bonds, which for most natural PUFAs are in *cis* configuration. The two main strategies for the synthesis of PUFAs are linking together skipped alkynes followed by partial hydrogenation,<sup>31</sup> or sequential Wittig reactions.<sup>32</sup> However, skipped alkynes are prone to isomerization to reactive allenes and their partial hydrogenation often affords inseparable mixtures of under- and overreduced products.<sup>33</sup> Total synthesis by Wittig reactions suffers from the severe instability of the multiple  $\beta,\gamma$ -unsaturated aldehyde intermediates whose purity is essential for a successful reaction.<sup>34,35</sup>

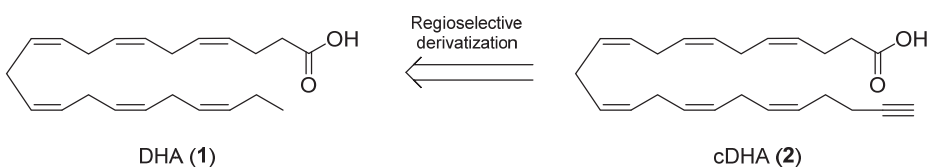


**Figure 1 |** Structures of DHA (**1**) and alkyne-modified derivative, cDHA (**2**)

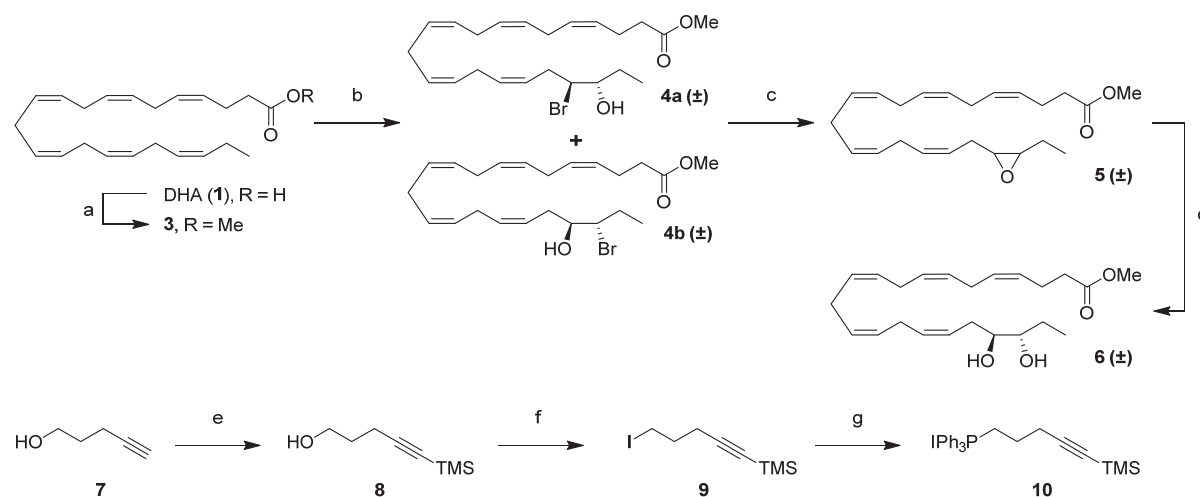
In Chapter 3, the synthesis of a diazirine- and alkyne-modified DHA derivative was achieved by a combination of Wittig reactions and partial hydrogenation of skipped alkynes. However, this was a strenuous process that required HPLC purification of a late-stage intermediate. Here, a concise synthesis of click-DHA (cDHA, **2**) is described which starts from commercially available DHA (Figure 1). Regioselective hydrobromination allowed chemical derivatization of the terminal double bond after which the alkyne was installed using a Wittig reaction. This strategy greatly reduces the number of steps and avoids the use of unstable skipped alkynes, which makes it attractive for the synthesis of other DHA derivatives. As an application cDHA **2** was used to visualize its incorporation into cells using a fluorogenic azidocoumarin and to follow its exchange between primary human cells using flow cytometry.

## Results

### Synthesis of cDHA (**2**) from DHA

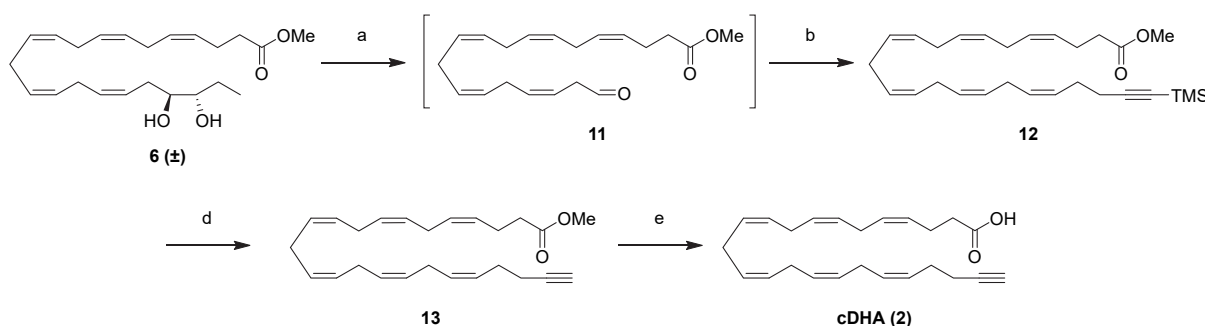
For the introduction of an alkyne moiety to the tail of the molecule, the use of commercially available DHA as a starting point was investigated. The terminal double bond of DHA has a different reactivity compared to the other alkenes in aqueous medium, which makes it available for chemical derivatization. This difference is hypothesized to be due to a coiled conformation of DHA in solution.<sup>36</sup> The design of click lipid **2** was chosen to keep all double bonds intact and to have the minimal space required between the last double bond and alkyne to afford a stable click lipid.<sup>37</sup>

Starting from commercially available DHA (**1**), the carboxylate was protected by methylation to afford ester **3**, which was used in a hydrobromination reaction (Scheme 1).<sup>36</sup> Following a reported procedure, 1.3 eq. *N*-bromosuccinimide (NBS) was added in portions over 8 h to a cooled (0 °C) solution of **3** in dimethoxyethane (DME)/H<sub>2</sub>O (4:1), which afforded a mixture of brominated and hydrobrominated products. The hydrobrominated products accounted for a low yield of 16%, of which 70% consisted of the desired regioisomers **4a/b** as judged by <sup>1</sup>H-NMR. To obtain a higher yield and improve the reproducibility, a syringe pump was used to add a solution of recrystallized NBS in DME/H<sub>2</sub>O (4:1) over 24 h. After complete addition the reaction was stirred for another 2 h and quenched by adding Na<sub>2</sub>S<sub>2</sub>O<sub>3</sub>. This resulted in a mixture of monohydrobromins **4a/b** with a 27% yield, as well as recovery of 34% starting material **3**, which could be reused. The selectivity for the desired hydrobrominated alkene remained 70%, but formation of brominated DHA and other unwanted products was greatly reduced.



**Scheme 1 | Synthesis of dihydroxide **6** and phosphonium salt **10**.** Reagents and conditions: (a) DHA, oxalyl chloride, DCM, 0 °C to rt, 5 h, then NaOMe, MeOH, 1 h, 98%; (b) NBS, DME/H<sub>2</sub>O (3:1), 0 °C, 26 h, 27% (41% based on recovered starting material); (c) NaOMe, MeOH, rt, 45 min; (d) HClO<sub>4</sub>, THF/H<sub>2</sub>O (4:3), rt, 7 h, 69% over 2 steps; (e) *n*-BuLi, TMSCl, THF, -78 °C to rt, 16 h, 82%; (f) I<sub>2</sub>, PPh<sub>3</sub>, imidazole, THF, rt, 1 h, 93%; (g) PPh<sub>3</sub>, acetonitrile, reflux, 3 d, 88%.

The mixture of bromohydrins **4a/b** was treated with anhydrous sodium methoxide in methanol to afford epoxide **5** without hydrolysis of the methyl ester. Epoxide **5** was hydrolyzed with perchloric acid to obtain **6** in 69% yield over two steps. To introduce the terminal alkyne, butynol (**7**) was protected as the trimethylsilyl alkyne to form alcohol **8** in 82% yield. Compound **8** was converted into iodide **9** using an Appel reaction in 93% yield. Subsequently, phosphonium salt **10** was obtained in 88% yield by reacting **9** with PPh<sub>3</sub> in refluxing ACN for 72 h. Phosphonium salt **10** was used in a Wittig reaction to install the terminal double bond of the DHA scaffold. To this end, **6** was oxidatively cleaved by sodium periodate at 0 °C to afford unstable the β,γ-unsaturated aldehyde (**11**) (Scheme 2).<sup>35,38</sup> After a workup, it was immediately added to a cooled (-110 °C) solution of phosphonium salt **10** pretreated with potassium *tert*-butoxide. The reaction temperature was raised to -90 °C over 1 h and subsequently to 0 °C in 2 h after which the mixture was quenched at -78 °C by addition of a suspension of silica in Et<sub>2</sub>O. This resulted in the formation of **12** in 19% yield from the dihydroxylated **6**. At this stage, shorter side products resulting from regioisomers in the hydrobromination reaction could be removed by silica gel purification.



**Scheme 2 | Synthesis of cDHA (2).** Reagents and conditions: (a) NaIO<sub>4</sub>, MeOH/H<sub>2</sub>O (10:3), 0 °C, 4 h; (b) **10**, KO*t*Bu, THF, -78 °C, 1 h, then **11**, -110 °C to 0 °C, 3 h, 19% over two steps; (c) TBAF, THF, rt, 30 min, 95%; (d) LiOH, H<sub>2</sub>O/THF (1:1), rt, 16 h, 82%.

Next, the silyl group of **12** was deprotected with TBAF providing terminal alkyne **13** in 95% yield. Final product **2** was obtained by hydrolysis of the methyl ester in aqueous LiOH in a total of 4.2% yield over 6 steps from DHA.

Investigation of metabolism of cDHA (**2**) on HPTLC

To investigate the incorporation of clickable lipids into cells, cDHA (**2**) was compared to a saturated palmitic acid-alkyne (cPA, **14**),<sup>39</sup> which was previously used for this application.<sup>22</sup> The lipids (20  $\mu$ M, 40 nmol) were incubated with mouse neuroblastoma Neuro-2a cells for 2 h. Cellular lipids were extracted and conjugated to fluorogenic hydroxycoumarin azide (**15**) under CuAAC conditions.<sup>27</sup> As a reference, 1 nmol of the free fatty acids were also reacted with **15**. All lipids were then separated on high-performance thin layer chromatography (HPTLC) and visualized by capturing the fluorescent signal (Figure 2B). This showed that cDHA (**2**) could be incorporated in a similar manner to cPA (**14**) into higher-running hydrophobic species, as well as lower-running, hydrophilic species. Interestingly, the labeling pattern indicated that cDHA (**2**), as well as cPA (**14**) were also incorporated in non-overlapping, lipid-specific metabolites.

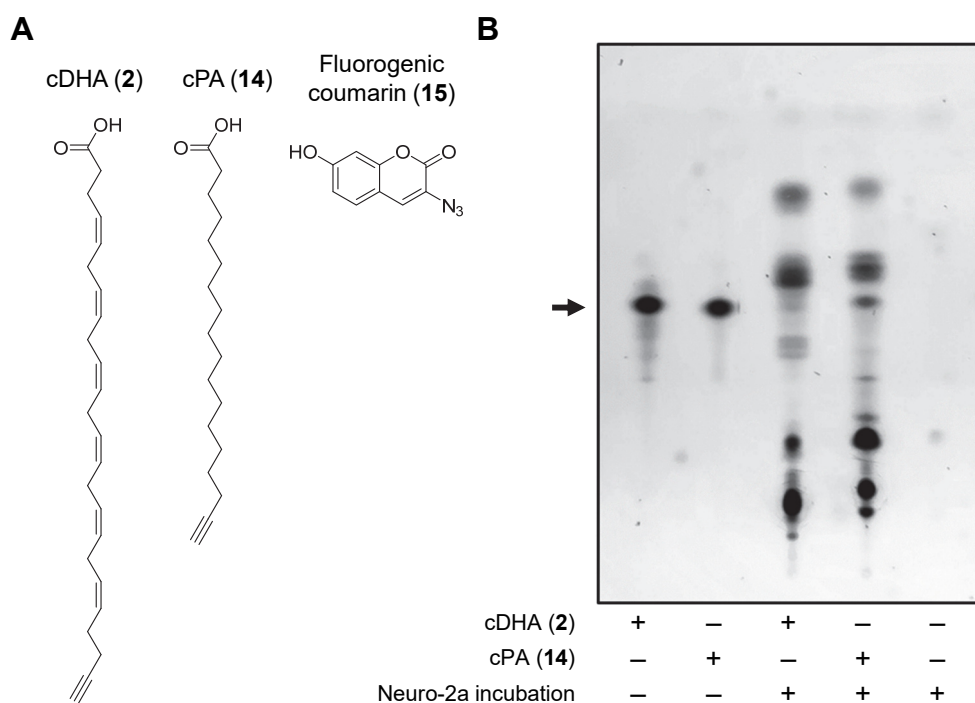


**Figure 2 | cDHA (**2**) and cPA (**14**) can be used to follow lipid metabolism. (A)** Structures of clickable lipids **2** and **14** and hydroxycoumarin azide (**15**). **(B)** Fluorescent signal of hydroxycoumarin-labeled lipids. Neuro-2a cells were incubated for 2 h with 20  $\mu$ M cPA (**14**), cDHA (**2**) or vehicle (EtOH) and the total lipid extracts or 1 nmol of indicated click lipid were subjected to a click reaction with hydroxycoumarin azide, separated on HPTLC and the fluorescent signal was imaged. The arrow indicates the elution height of the coumarin-conjugated free acids.

### Uptake and exchange of cDHA (**2**) by macrophages and fibroblasts

Next, the cellular uptake and exchange of clickable lipids was studied using flow cytometry. First, fibroblasts isolated from synovial membrane of osteoarthritis patients and expanded *in vitro*, as well as GM-CSF-stimulated macrophages differentiated from healthy donor peripheral blood monocytes were separately incubated with clickable lipid **2** (10 nM, 0.5 pmol) or unlabeled DHA for 24 h. The cells were fixed and subjected to click chemistry with AlexaFluor-647-N<sub>3</sub> (AF647) and analyzed by flow cytometry.<sup>40</sup> Over 90% of macrophages (Figure 3A) and fibroblasts (Figure 3B) were successfully labeled using cDHA (**2**).

To study if cDHA (**2**) can be used to visualize lipid exchange between macrophages and fibroblasts, macrophages were treated with cDHA (**2**) (10 nM, 0.5 pmol) or DHA for 4 h, washed thoroughly and subsequently cocultured with unlabeled fibroblasts for an additional 24 h. Detection of the alkyne handle using AF647 showed that 97% of the fibroblasts were fluorescently labeled by AF647, indicating that these cells have incorporated cDHA (**2**) or cDHA derivatives transferred from the macrophages (Figure 3C).

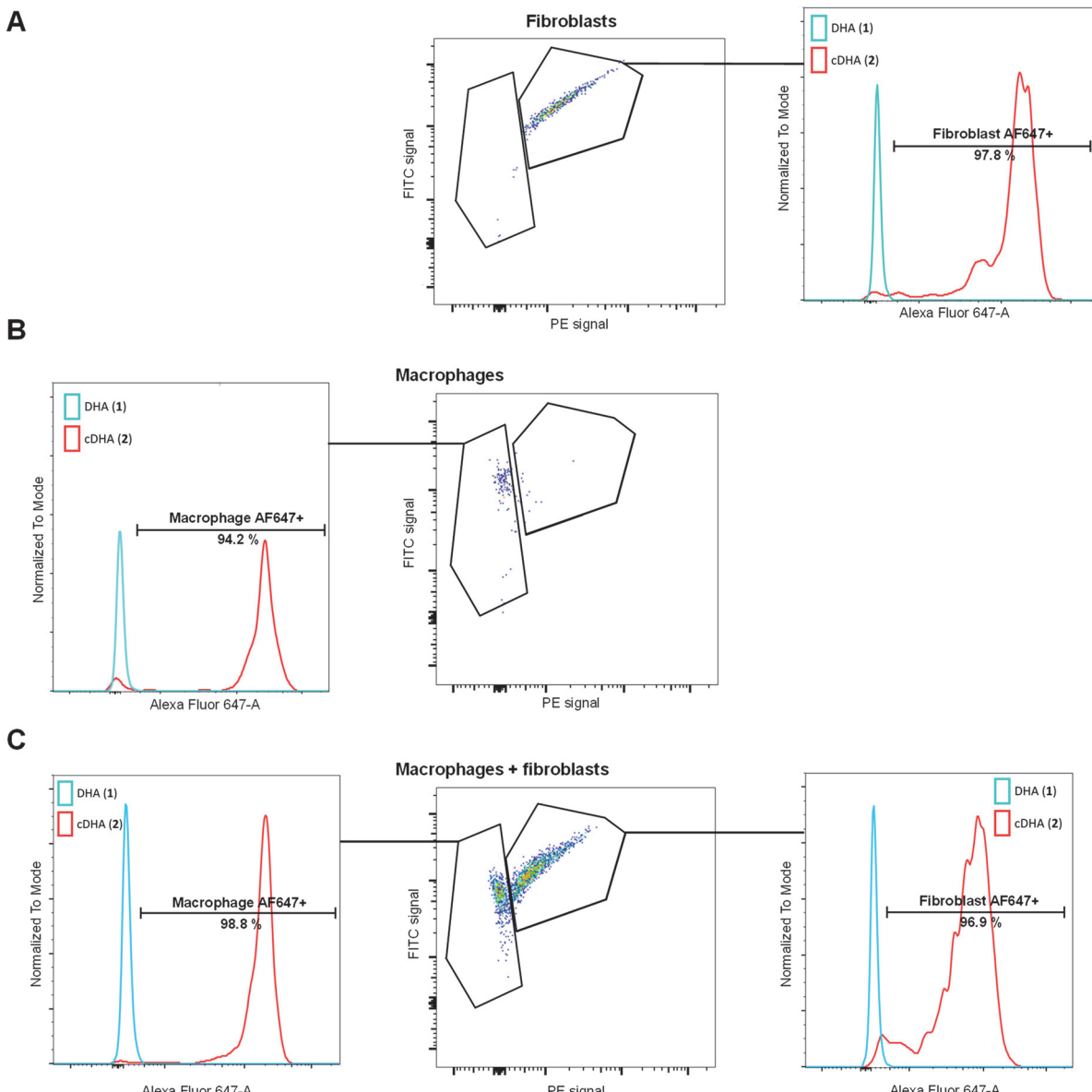


**Figure 3 | cDHA (2) exchange is detectable between macrophages and fibroblast.** Cells were incubated with indicated lipid, harvested and treated with AlexaFluor-647-N<sub>3</sub> under CuAAC conditions and analyzed using flow cytometry. **(A)** Treatment of fibroblasts with clickable lipid **2** results in labeling of 97.8% of cells compared to control. **(B)** Treatment of macrophages with clickable lipid **2** results in labeling of 94.2% of cells compared to control. **(C)** Coculturing fibroblasts with macrophages that had been pretreated with cDHA (**2**) results in detectable exchange of the clickable lipid between the different cell types. Gating strategy included the exclusion of debris and doublets based on FSC/SSC and separation of macrophages and fibroblasts in the coculture was based on the autofluorescence observed in both the PE and FITC channel (Figure S1).

## Conclusion

Alkyne-modified lipids such as clickable fatty acids, sphingolipids and cholesterol are versatile tools to study localization, metabolism and exchange of these diverse biomolecules. In recent years, innovative methods to use these tools have been developed, many of which from the lab of Dr. Thiele.<sup>22,27-29</sup> Importantly, these methods to study alkyne lipids require no specialized equipment and use commercially available reagents. However, alkyne-modified PUFAs are scarcely available, due to their synthetic difficulty. This difficulty arises from many inseparable side products, as well as the instability of many intermediates.<sup>33</sup> In this work, a concise synthetic route for an alkyne-modified DHA derivative is reported starting from commercially available DHA. Regioselective hydrobromination allowed chemical derivatization of the terminal double bond after which the alkyne was installed using a Wittig reaction. cDHA was obtained in 6 steps from DHA without making use of unstable skipped alkynes. It is envisioned that this new synthetic route enables the synthesis of other DHA derivatives through Wittig reactions with synthetically accessible phosphonium salts.

As an application, cDHA (**2**) was used to visualize of its incorporation into cells using a fluorogenic azidocoumarin, as well as its exchange between primary human cells using flow cytometry. As little as 0.5 picomoles of cDHA (**2**) was demonstrated to efficiently label cells and to allow for visualization of lipid exchange between human macrophages and fibroblasts using flow cytometry. Quantification and identification of the exchanged lipids under pro-inflammatory or pro-resolution conditions could provide information on the role of PUFA metabolites as lipid signaling molecules.<sup>41</sup>

## Experimental procedures

### General

Solvents were dried over activated 4 Å molecular sieves for at least 24 hours. Reactions were monitored by TLC using silica gel 60 F254 coated aluminum sheets from Merck. DHA was obtained from Cayman chemicals (90310). 3-Azido-7-hydroxycoumarin azide (**15**) and cPA (**14**) were prepared as previously reported in literature.<sup>39,42</sup> The hydroxycoumarin azide was unstable, therefore small aliquots (44.5 mM in DMSO) were stored under nitrogen at -20 °C and discarded after a single use. NBS was recrystallized from H<sub>2</sub>O at 90 °C and dried under reduced pressure. Phosphate buffer A was prepared by dissolving KH<sub>2</sub>PO<sub>4</sub> (0.5 M) in Milli-Q and adjusting the pH value to 7.0 with aq. NaOH. All other reagents were purchased from Alfa Aesar, Sigma Aldrich/Merck or Acros and used without further purification.

### Cell culture

#### *Neuro-2a culture*

Neuro-2a cells were cultured at 37 °C under 7% CO<sub>2</sub> in DMEM (Sigma Aldrich, D1145) containing stable glutamine, 10% (v/v) New Born Calf Serum (Thermo Fisher) and penicillin and streptomycin (200 µg/mL each, Duchefa). Cells were passaged twice a week at 80-90% confluence by resuspension in fresh medium. Cell lines were purchased from ATCC and were tested regularly for mycoplasma contamination. Cultures were discarded after 2-3 months of use.

#### *Primary cell culture*

This study was approved by the local medical ethical committee of the LUMC (METC), and written informed consent was given by all donors. Human peripheral blood mononuclear cells (PBMCs) were isolated by Ficoll density gradient from healthy donor buffy coats (Sanquin). Blood monocytes were isolated by positive selection from PBMCs using MACS CD14 Microbeads (Miltenyi Biotec) and purity was checked by FACS (LSRIII, BD Biosciences), by staining the cells with CD14-PE (clone MpP9). Monocytes were differentiated for seven days in RPMI 1640 medium (Gibco) containing 8% FCS, 100 U/mL penicillin and streptomycin, 2 mM Glutamax (Thermo Fisher) and 5 ng/mL GM-CSF (Miltenyi Biotec). Medium was replenished on day three and five. Phenotype was checked before experiments by visual inspection by assessing the typical morphology of GM-CSF cultured macrophages ('egg sunny-side up-like'). Phenotype was also confirmed by performing IL-12 OptEIA (BD Biosciences), IL-10 PeliPair reagent set (Sanquin), and TNF $\alpha$  OptEIA (BD Biosciences) ELISA on supernatant of cells stimulated for 24 hours with 10 ng/mL LPS (Merck). GM-CSF monocyte-derived macrophages (MDM) secreted high IL-12 and TNF $\alpha$  and low IL-10. Cells were harvested using Accutase (Merck) and 2.5x10<sup>5</sup> cells were seeded in 24-well plates in 250 µL medium. Lipids were added in phenol red-free RPMI 1640 medium (Gibco), supplemented with 0.1% (w/v) fatty acid free BSA (A7030, Sigma). For isolation of fibroblasts, left-over synovial tissue was collected anonymously from patients undergoing total knee replacement surgery in the context of standard clinical care at the Departments of Orthopedic Surgery in the LUMC or Alrijne Hospital in Leiderdorp. Preparation of synovial tissue cells was performed less than 6 hours after the surgical procedure. The tissue was kept in PBS at room temperature. All tissue material was obtained with permission from the ethical committee and with patient approval. Whole synovial tissue was cut into small pieces and digested for 1.5 - 3 h at 37 °C under constant roller movement with 6.47 mg (245 U/mg) collagenase type 2 (Worthington Biochemical Corporation) in 5 mL serum-free IMDM medium (Lonza). To remove remaining undigested tissue and collect synovial tissue cells, the cell suspension was filtered and mashed using a 70 µm cell strainer (Falcon, Corning Incorporated). The cell suspension was washed 3 times with 10 mL warm serum-free IMDM medium (Lonza) through centrifugation at 195 g for 10 minutes. Cells were cultured at a density of 2.5x10<sup>4</sup> cells/cm<sup>2</sup> at 37 °C with 5% CO<sub>2</sub> in appropriate culture dishes in DMEM-F12 complete medium. Synovium cells were harvested with 2 mL 0.25% trypsin for a T75 flask (Thermo Fisher) for 4-5 min at 37 °C for further passaging to obtain fibroblast-like cells.

## HPTLC

HPTLC experiments were performed according to published procedure<sup>22</sup> with adjustments. Neuro-2a cells were plated on a 6-well plate and grown to confluence. They were washed with PBS (1 mL) and subsequently DMEM (2 mL) supplemented with 0.1% (w/v) fatty acid free BSA (A7030, Sigma) was added containing indicated click lipid (from 10 mM ethanolic stock, 20 µM final) or vehicle. After 2 h incubation, the medium was aspirated and the cells were washed with PBS with 0.1% (w/v) fatty acid free BSA, then PBS, after which they were harvested by pipetting in PBS (0.3 mL). Cells were transferred to 2 mL tubes and methanol (600 µL) and CHCl<sub>3</sub> (150 µL) were added, after which the tubes are vortexed (10 s) and centrifuged (14,000 g, 2 min). The supernatant was transferred to new 2 mL tubes and CHCl<sub>3</sub> (300 µL) and 0.1% (v/v) aq. acetic acid (600 µL) were added, followed by vortexing (10 s) and centrifugation (14,000 g, 5 min). The lower organic layer was transferred to 1.5 mL eppendorfs and concentrated in a speed-vac. The lipid pellet was redissolved in 7 µL CHCl<sub>3</sub> and 30 µL click mix was added (click mix: 5 µL of 44.5 mM 3-azido-7-hydroxycoumarin in DMSO, 500 µL of 10 mM [acetonitrile]<sub>4</sub>CuBF<sub>4</sub> in acetonitrile, 2 mL ethanol) after which the tube was left in a heating block at 42 °C for 3 h until all solvent condensed under the cap. The tubes were briefly centrifuged and vortexed and 3 µL was applied to a HPTLC silica gel 60 plate (Merck). The plate was developed with a solvent system consisting of CHCl<sub>3</sub>/MeOH/H<sub>2</sub>O/AcOH = 65:25:4:1 until 50% of the length of the plate, which was then dried under a stream of nitrogen in the dark and developed again in hexane/EtOAc = 1:1 for 90% of the length of the plate. The plate was dried under a stream of nitrogen in the dark and then dipped in a solution of 4% (v/v) DIPEA in hexane. After allowing most solvent to evaporate in the dark it was then imaged by placing it over a UV-lamp and capturing the fluorescent signal through a Perspex plate. Images were processed using FIJI.<sup>43</sup>

## Flow cytometry

Upon differentiation/expansion, fibroblasts and macrophages were washed with PBS, enzymatically harvested (fibroblasts using trypsin, macrophages using accutase) and resuspended in PBS. They were spun down and resuspended in DMEM/F12 (Sigma) supplemented with 0.5% (w/v) fatty acid free BSA (A7030, Sigma), 2 mM Glutamax (Thermo Fisher), and penicillin and streptomycin (200 µg/mL each). The cells were counted and 2.5x10<sup>4</sup> cells were plated on a 96-well plate in 50 µL medium. After 24 h, DHA or cDHA was added (5 µL of a 11X concentrated solution in medium, 10 nM final) and the cells were incubated for 4 h. For the monocultures (Figure 3A/B), cells were then washed twice with DMEM/F12 and cultured for 24 h before FACS analysis. For the coculture (Figure 3C), the macrophages were washed twice with DMEM/F12 and then 2.5x10<sup>4</sup> fibroblasts were added and then incubated for 24 h. Flow cytometry analysis of macrophages and fibroblasts was performed following previously reported procedure with minor modifications.<sup>40</sup> In brief, the cells were washed with PBS (100 µL) and accutase (30 µL) was added and incubated at 37 °C for 10 min. The cell suspension was then placed in V-bottom plates and the wells washed with PBS (100 µL). The plate containing the harvested cells was centrifuged (2,000 g, 3 min) and the supernatant was removed. The cells were fixed in 100 µL 4% (w/v) paraformaldehyde (PFA) in PBS (10 min, rt). The cells were spun down (2,000 g, 3 min) and washed with PBS (100 µL) and nonspecific binding sites were blocked by incubation with 1% (w/v) BSA in PBS (100 µL) for 30 min. Cells were then washed with PBS and resuspended in 50 µL click mix (2.5 µL 100 mM CuSO<sub>4</sub>, 1.5 µL 1 M NaAsc, 0.5 µL 100 mM THPTA and 1 µL 2 mM AF647-N<sub>3</sub> (Invitrogen), 44.5 µL 100 mM HEPES). After incubation for 1 h at rt, the cells were pelleted (2,000 g, 3 min) and washed with PBS and 1% (w/v) BSA in PBS. The cells were resuspended in 1% (w/v) BSA in PBS with 400 nM DAPI (Molecular Probes, D1306) and analyzed with a LSRIII (BD Biosciences, with lasers: 405 nm, 488 nm and 633 nm). Gating strategy included the exclusion of dead cells and doublets based on FSC/SSC (Figure S1). Separation of macrophages and fibroblasts in the co-culture was based on the autofluorescence observed in both the PE and FITC channel. Analysis was preformed using BD FACSDiva™ software.

## Chemistry

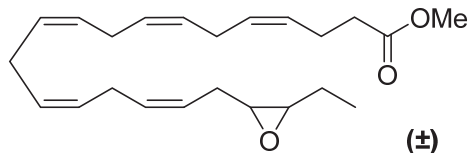
A NE-1000G Future Chemistry syringe pump was used in combination with BD Discardit II plastic syringes. For a 10 mm syringe, the diameter setting was 15.6 mm. The reactions were performed under an inert atmosphere of nitrogen gas unless stated otherwise.  $^1\text{H}$  NMR and  $^{13}\text{C}$  NMR spectra were recorded on a Bruker AV-400 (400 MHz) or AV-500 (500 MHz) spectrometer. Chemical shift values are reported in ppm relative to the tetramethylsilane signal for  $^1\text{H}$  NMR ( $\delta = 0$  ppm) and relative to the solvent signal of  $\text{CDCl}_3$  for  $^{13}\text{C}$  NMR ( $\delta = 77.16$  ppm). Data are reported as follows: Chemical shifts ( $\delta$ ), multiplicity (s = singlet, d = doublet, dd = doublet of doublets, ddt = doublet of doublet of triplets, td = triplet of doublets, t = triplet, q = quartet, p = pentet, bs = broad singlet, m = multiplet), coupling constants  $J$ (Hz), and integration. Flash column chromatography was performed using SiliCycle silica gel type SiliaFlash P60 (230–400 mesh). TLC analysis was performed on Merck silica gel 60/Kieselguhr F254, 0.25 mm. Compounds were visualized using  $\text{KMnO}_4$  stain ( $\text{K}_2\text{CO}_3$  (40 g),  $\text{KMnO}_4$  (6 g), and water (600 mL)). High resolution mass spectra (HRMS) were recorded by direct injection on a q-TOF mass spectrometer (Synapt G2-SI) equipped with an electrospray ion source in positive mode with Leu-enkephalin ( $m/z = 556.2771$ ) as an internal lock mass. The instrument was calibrated prior to measurement using the MS/MS spectrum of [ $\text{Glu}^1$ ]-fibrinopeptide B.

### Methyl (4Z,7Z,10Z,13Z,16Z,19Z)-docosa-4,7,10,13,16,19-hexaenoate (3).

DHA (0.888 g, 2.70 mmol) was coevaporated with toluene thrice and dissolved in DCM (44 mL). Oxalyl chloride (0.75 mL, 8.75 mmol) was added dropwise to the reaction mixture at 0 °C. The reaction was allowed to reach room temperature over 5 h. Then, a methanolic solution of NaOMe (1.3 M, 4.5 mL, 2.70 mmol) was added and the reaction was stirred for 5 min. The reaction mixture was diluted with  $\text{Et}_2\text{O}$  (450 mL) and washed with  $\text{H}_2\text{O}$  (2 x 200 mL) and brine (200 mL). The combined aq. layers were extracted with  $\text{Et}_2\text{O}$  (2 x 150 mL) and the combined organic fractions were dried over  $\text{MgSO}_4$ , filtered and concentrated under reduced pressure to afford the title compound as a yellow oil (0.904 g, 2.64 mmol, 98%).  $R_f = 0.5$  (pentane/ $\text{Et}_2\text{O}$  = 96:4).  $^1\text{H}$  NMR (400 MHz,  $\text{CDCl}_3$ ):  $\delta$  5.47 – 5.26 (m, 12H), 3.67 (s, 3H), 2.92 – 2.75 (m, 10H), 2.46 – 2.32 (m, 4H), 2.08 (m, 2H), 0.97 (t,  $J = 7.5$  Hz, 3H).  $^{13}\text{C}$  NMR (100 MHz,  $\text{CDCl}_3$ ):  $\delta$  173.6, 132.1, 129.4, 128.7, 128.4, 128.4, 128.3, 128.2, 128.2, 128.0, 127.1, 51.7, 34.1, 25.8, 25.7, 25.7, 22.9, 20.7, 14.4. Spectra were consistent with previously reported data.<sup>44</sup>

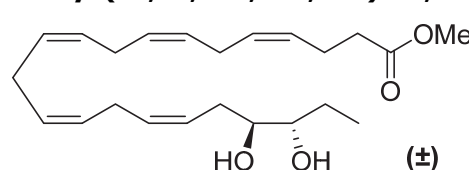
### Methyl (4Z,7Z,10Z,13Z,16Z)-19-bromo-20-hydroxydocosa-4,7,10,13,16-pentaenoate (4a) & Methyl (4Z,7Z,10Z,13Z,16Z)-20-bromo-19-hydroxydocosa-4,7,10,13,16-pentaenoate (4b).

Methyl ester **3** (0.534 g, 1.56 mmol) was dissolved in dimethoxyethane/ $\text{H}_2\text{O}$  (22.9 mL, 4:1 (v/v)) and cooled to 0 °C. A solution of freshly recrystallized NBS (0.399 g, 2.42 mmol) in dimethoxyethane/ $\text{H}_2\text{O}$  (5.5 mL, 4:1 (v/v)) was added over 24 hours with the use of a syringe pump. After an additional 2 h of stirring, aq.  $\text{Na}_2\text{S}_2\text{O}_3$  (6.0 mL, 10 wt%) was added dropwise and the reaction mixture was allowed to reach room temperature. The mixture was diluted with  $\text{Et}_2\text{O}$  (250 mL), washed with  $\text{H}_2\text{O}$  (3 x 125 mL) and brine (100 mL), dried over  $\text{MgSO}_4$ , filtered and concentrated under reduced pressure. The residue was purified by silica gel column chromatography (pentane/ $\text{Et}_2\text{O}$  = 96:4 to 74:26) to afford the starting material **3** as a colorless oil (0.183 g, 0.53 mmol, 34%) and a mixture of monobromohydrins including **4a** and **4b** as a colorless oil (0.183 g, 0.42 mmol, 27%).  $R_f = 0.3$  (pentane/ $\text{Et}_2\text{O}$  = 4:1).  $^1\text{H}$  NMR (400 MHz,  $\text{CDCl}_3$ ):  $\delta$  5.62 – 5.28 (m, 10H), 4.13 – 3.99 (m, 1H), 3.68 (s, 3H), 3.60 – 3.38 (m, 1H), 2.91 – 2.71 (m, 10H), 2.45 – 2.33 (m, 4H), 1.68 – 1.54 (m, 2H), 0.98 (t,  $J = 7.4$  Hz, 3H).  $^{13}\text{C}$  NMR (100 MHz,  $\text{CDCl}_3$ ):  $\delta$  173.7, 132.2, 131.4, 131.2, 129.4, 128.7, 128.6, 128.6, 128.3, 128.2, 128.1, 128.0, 128.0, 127.8, 127.1, 126.2, 125.9, 124.8, 74.4, 73.4, 72.3, 66.1, 63.1, 51.7, 34.1, 34.0, 33.8, 29.3, 29.1, 26.1, 26.0, 25.8, 25.7, 22.9, 12.7, 10.1. HRMS: Calculated for  $[\text{C}_{23}\text{H}_{35}\text{BrO}_3+\text{H}]^+$  439.1842, found 439.1842.

**Methyl (4Z,7Z,10Z,13Z,16Z)-18-(3-ethyloxiran-2-yl)octadeca-4,7,10,13,16-pentaenoate (5).**

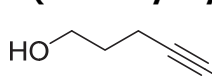
The mixture of **4a** and **4b** (0.116 g, 0.26 mmol) was coevaporated thrice with toluene and dissolved in a methanolic solution of NaOMe (0.2 M, 6.6 mL, 1.3 mmol). After stirring for 45 min at room temperature, the reaction mixture was diluted with Et<sub>2</sub>O (100 mL) and 0.2 M HCl (7 mL)

was added dropwise. The organic layer was washed with H<sub>2</sub>O (2 x 50 mL) and brine (50 mL), dried over MgSO<sub>4</sub>, filtered and concentrated under reduced pressure. The crude **5** was used in the next reaction without further purification. R<sub>f</sub> = 0.5 (pentane/Et<sub>2</sub>O = 4:1). <sup>1</sup>H NMR (400 MHz, CDCl<sub>3</sub>): δ 5.52 – 5.34 (m, 10H), 3.68 (s, 3H), 2.98 – 2.85 (m, 10H), 2.43 – 2.35 (m, 4H), 2.30 – 2.20 (m, 2H), 1.61 – 1.53 (m, 2H), 1.04 (t, J = 7.5 Hz, 3H). <sup>13</sup>C NMR (100 MHz, CDCl<sub>3</sub>): δ 173.69, 130.53, 129.43, 128.53, 128.36, 128.32, 128.26, 128.22, 128.04, 127.98, 124.65, 58.48, 56.66, 51.73, 34.15, 26.32, 25.95, 25.79, 25.72, 22.94, 21.22, 10.79. HRMS: Calculated for [C<sub>23</sub>H<sub>34</sub>O<sub>3</sub>+H]<sup>+</sup> 359.2581, found 359.2583.

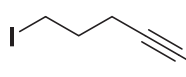
**Methyl (4Z,7Z,10Z,13Z,16Z)-19,20-dihydroxydocosa-4,7,10,13,16-pentaenoate (6).**

To a cooled (0 °C) solution of crude **5** in THF (4.3 mL) was added dropwise aq. HClO<sub>4</sub> (0.4 M, 3.3 mL) and the resulting suspension was stirred for 4 h at rt. Phosphate buffer A (8 mL) was added and the reaction mixture was diluted with H<sub>2</sub>O (80 mL). The aq. layer was extracted with EtOAc (3 x 50

mL) and the combined organic layers were washed with brine (50 mL), dried over MgSO<sub>4</sub>, filtered and concentrated under reduced pressure. The residue was purified by silica gel column chromatography (pentane/EtOAc = 4:1) to afford the title compound as a colorless oil (0.068 g, 0.181 mmol, 69% over 2 steps). R<sub>f</sub> = 0.4 (pentane/EtOAc = 3:2). <sup>1</sup>H NMR (400 MHz, CDCl<sub>3</sub>): δ 5.63 – 5.30 (m, 10H), 3.68 (s, 3H), 3.50 (dd, J = 12.0, 8.0 Hz, 1H), 3.39 (dt, J = 8.0, 4.0 Hz, 1H), 2.90 – 2.79 (m, 8H), 2.42 – 2.30 (m, 6H), 1.65 – 1.45 (m, 2H), 1.00 (t, J = 7.5 Hz, 3H). <sup>13</sup>C NMR (100 MHz, CDCl<sub>3</sub>): δ 173.81, 131.39, 129.46, 128.53, 128.36, 128.23, 128.01, 125.51, 75.31, 73.53, 51.77, 34.14, 31.93, 29.86, 26.68, 25.93, 25.80, 25.73, 22.94, 10.20. HRMS: Calculated for [C<sub>23</sub>H<sub>36</sub>O<sub>4</sub>+Na]<sup>+</sup> 399.2506, found 399.2508.

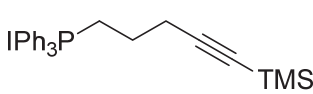
**5-(Trimethylsilyl)pent-4-yn-1-ol (8).**

To a cooled (-78 °C) solution of pent-4-yn-1-ol (1.1 mL, 12 mmol) in THF (45 mL) was added dropwise n-BuLi (1.6 M solution in hexanes, 16.3 mL, 26.1 mmol) over a period of 20 min affording a light yellow suspension. After stirring for 50 min at rt, the solution was cooled to -78 °C and TMSCl (3.3 mL, 28 mmol) was added dropwise. The reaction mixture was allowed to reach room temperature overnight. 3 M HCl (16.7 mL) was added and after 40 min the solution was diluted with H<sub>2</sub>O (60 mL) and extracted with Et<sub>2</sub>O (2 x 30 mL). The combined organic fractions were washed with brine (30 mL), dried over MgSO<sub>4</sub>, filtered and concentrated under reduced pressure. Purification of the residue by silica gel column chromatography (pentane/EtOAc = 9:1) afforded the title compound as a colorless oil (1.52 g, 9.75 mmol, 82%). Spectra were consistent with previously reported data.<sup>45</sup>

**5-(Trimethylsilyl)pent-4-ynyl-1-iodide (9).**

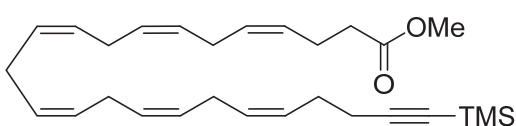
To a cooled (0 °C) solution of **8** (0.179 g, 1.15 mmol) in THF (7.8 mL) was added PPh<sub>3</sub> (0.45 g, 1.72 mmol), imidazole (0.12 g, 1.72 mmol) and I<sub>2</sub> (0.44 g, 1.72 mmol). The reaction mixture was stirred for 1 h at room temperature and diluted with Et<sub>2</sub>O (20 mL) and an aq. Na<sub>2</sub>S<sub>2</sub>O<sub>3</sub> solution (10 wt%, 30 mL).

The aq. layer was extracted with Et<sub>2</sub>O (20 mL) and the combined organic fractions were washed with brine (20 mL), dried over MgSO<sub>4</sub>, filtered and concentrated under reduced pressure. The residue was triturated in pentane (4 mL) overnight and the resulting suspension was filtered over a glass frit. The filtrate was concentrated under reduced pressure and the residue was purified by silica gel column chromatography (pentane) to afford the title compound as a yellow oil (0.283 g, 1.06 mmol, 93%). Spectra were consistent with previously reported data.<sup>45</sup>

**5-Trimethylsilylpent-4-ynyltriphenylphosphineiodide (10).**

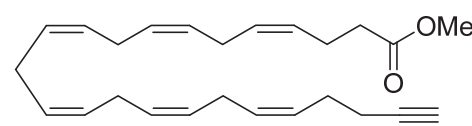
To a solution of **9** (2.45 g, 9.19 mmol) in acetonitrile (46 mL) was added PPh<sub>3</sub> (3.62 g, 13.8 mmol) and the suspension heated to reflux for 72 h. After cooling to room temperature, the reaction mixture was

concentrated under reduced pressure and the residue was purified by silica gel column chromatography (DCM/MeOH = 95:5) to afford the title compound as a white foam (4.27 g, 8.07 mmol, 88%). R<sub>f</sub> = 0.3 (DCM/MeOH = 95:5). <sup>1</sup>H NMR (400 MHz, CDCl<sub>3</sub>): δ 7.76 – 7.65 (m, 9H), 7.65 – 7.57 (m, 6H), 3.73 – 3.61 (m, 2H), 2.54 (td, J = 6.6, 1.3 Hz, 2H), 1.82 – 1.70 (m, 2H), 0.00 (s, 9H). <sup>13</sup>C NMR (100 MHz, CDCl<sub>3</sub>): δ 135.03 (d, J = 3 Hz), 133.32 (d, J = 10 Hz), 130.37 (d, J = 13 Hz) 117.48 (d, J = 87 Hz), 104.83, 86.46, 21.70 (d, J = 5 Hz), 21.42 (d, J = 44 Hz), 20.33 (d, J = 18 Hz), -0.14. HRMS: Calculated for [C<sub>26</sub>H<sub>30</sub>PSi]<sup>+</sup> 401.1849, found 401.1855.

**Methyl (4Z,7Z,10Z,13Z,16Z,19Z)-24-(trimethylsilyl)tetracosa-4,7,10,13,16,19-hexaen-23-ynoate (12).**

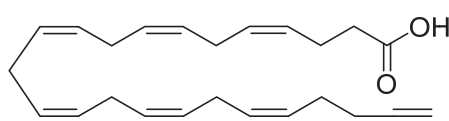
To a cooled (0 °C) solution of **6** (0.085 g, 0.226 mmol) in MeOH (4.4 mL) was added a solution of NaIO<sub>4</sub> (0.072 g, 0.339 mmol) in H<sub>2</sub>O (1.3 mL). After 3.5 h, the mixture was diluted with Et<sub>2</sub>O (50 mL), washed with H<sub>2</sub>O (3 x 25 mL) and brine (20 mL), dried over Na<sub>2</sub>SO<sub>4</sub>, filtered and

concentrated under reduced pressure. Phosphonium salt **10** (0.300 g, 0.564 mmol) was coevaporated with benzene/CHCl<sub>3</sub> (1:1 (v/v)) and twice with benzene, and subsequently suspended in THF (5 mL). The suspension was cooled to -78 °C and KOtBu (1.0 M in THF, 0.56 mL, 0.56 mmol) was added dropwise. The solution was stirred for 1 h and then cooled down to -110 °C. Then, the aldehyde was coevaporated with benzene twice and added to the reaction via cannula in THF (1 mL). The reaction mixture was stirred at -90 °C for 1 h, warmed to 0 °C over 2 h and then cooled to -78 °C. It was diluted with Et<sub>2</sub>O (7 mL) and quenched with a suspension of silica (5 mL) in Et<sub>2</sub>O (7 mL). The reaction was allowed to reach room temperature and filtered. The silica plug was rinsed with Et<sub>2</sub>O (20 mL) and the solvents were concentrated under reduced pressure. The residue was purified by silica gel column chromatography (pentane/Et<sub>2</sub>O = pentane to 49:1) to afford the title compound as a clear oil (0.0184 g, 0.042 mmol, 19%). R<sub>f</sub> = 0.6 (pentane/Et<sub>2</sub>O = 96:4). <sup>1</sup>H NMR (400 MHz, CDCl<sub>3</sub>): δ 5.50 – 5.31 (m, 12H), 3.68 (s, 3H), 2.85 (m, 10H), 2.48 – 2.34 (m, 4H), 2.27 (m, 4H), 0.15 (s, 9H). <sup>13</sup>C NMR (100 MHz, CDCl<sub>3</sub>): δ 173.68, 129.45, 129.25, 128.41, 128.36, 128.31, 128.24, 128.22, 128.02, 107.00, 84.77, 51.73, 34.15, 26.75, 25.84, 25.78, 25.72, 22.93, 20.30, 0.28. HRMS: Calculated for [C<sub>28</sub>H<sub>42</sub>O<sub>2</sub>Si+H]<sup>+</sup> 439.3027, found 439.3024.

**Methyl (4Z,7Z,10Z,13Z,16Z,19Z)-tetracosa-4,7,10,13,16,19-hexaen-23-ynoate (13).**

To a cooled (0 °C) solution of **12** (0.0232 g, 0.052 mmol) in THF (3 mL) was added dropwise TBAF (1 M in THF, 0.079 mL, 0.079 mmol) and the reaction was stirred at rt for 30 min. Then, aq. sat. NH<sub>4</sub>Cl (1 mL) and Et<sub>2</sub>O (30 mL) were added

and the layers were separated. The organic layer was washed with H<sub>2</sub>O (3 x 15 mL) and brine (10 mL), dried over MgSO<sub>4</sub>, filtered and concentrated under reduced pressure. The residue was purified by silica gel column chromatography (pentane/Et<sub>2</sub>O = 49:1) to afford the title compound as a clear oil (0.0183 g, 0.050 mmol, 95%). R<sub>f</sub> = 0.6 (pentane/EtOAc = 19:1). <sup>1</sup>H NMR (400 MHz, CDCl<sub>3</sub>): δ 5.50 – 5.32 (m, 12H), 3.68 (s, 3H), 2.86 (dd, J = 11.1, 6.6 Hz, 3H), 2.44 – 2.35 (m, 1H), 2.35 – 2.27 (m, 1H), 2.28 – 2.20 (m, 1H), 1.96 (t, J = 2.5 Hz, 1H). <sup>13</sup>C NMR (100 MHz, CDCl<sub>3</sub>): δ 173.63, 129.50, 129.44, 128.36, 128.31, 128.28, 128.22, 128.09, 128.02, 84.09, 68.60, 51.72, 34.14, 26.52, 25.84, 25.78, 25.71, 22.93, 18.88. HRMS: Calculated for [C<sub>25</sub>H<sub>34</sub>O<sub>2</sub>+H]<sup>+</sup> 367.2632, found 367.2632.

**(4Z,7Z,10Z,13Z,16Z,19Z)-Tetracosa-4,7,10,13,16,19-hexaen-23-ynoic acid (cDHA, 2).**

To a cooled (0 °C) solution of **13** (0.0183 g, 0.050 mmol) in THF (1.6 mL) was added 1 M aq. LiOH (1.6 mL, 1.6 mmol) and the solution was allowed to reach rt overnight. After cooling the reaction mixture to 0 °C, 1 M aq. HCl (1.6 mL) was added and the solution was diluted with H<sub>2</sub>O (15 mL). The aq. layer

was extracted with EtOAc (3 x 6 mL) and the combined organic fractions were dried over MgSO<sub>4</sub>, filtered and concentrated under reduced pressure. Purification of the residue by silica gel column chromatography (DCM/MeOH = 199:1) afforded the title compound as a clear oil (0.0145 g, 0.041 mmol, 82%). R<sub>f</sub> = 0.6 (DCM/MeOH = 19:1). <sup>1</sup>H NMR (500 MHz, CDCl<sub>3</sub>): δ 5.51 – 5.30 (m, 12H), 2.81 (d, J = 38.1 Hz, 10H), 2.46 – 2.36 (m, 4H), 2.32 (dt, J = 11.3, 7.4 Hz, 2H), 2.28 – 2.21 (m, 2H), 1.96 (t, J = 2.6 Hz, 1H). <sup>13</sup>C NMR (125 MHz, CDCl<sub>3</sub>): δ 177.77, 152.67, 129.88, 129.71, 129.52, 128.44, 128.34, 128.30, 128.15, 128.11, 127.71, 84.21, 68.61, 33.89, 26.53, 25.86, 25.80, 25.75, 22.67, 18.90. HRMS: Calculated for [C<sub>24</sub>H<sub>32</sub>O<sub>2</sub>+Na]<sup>+</sup> 375.2295, found 375.2302.

## Supplementary data

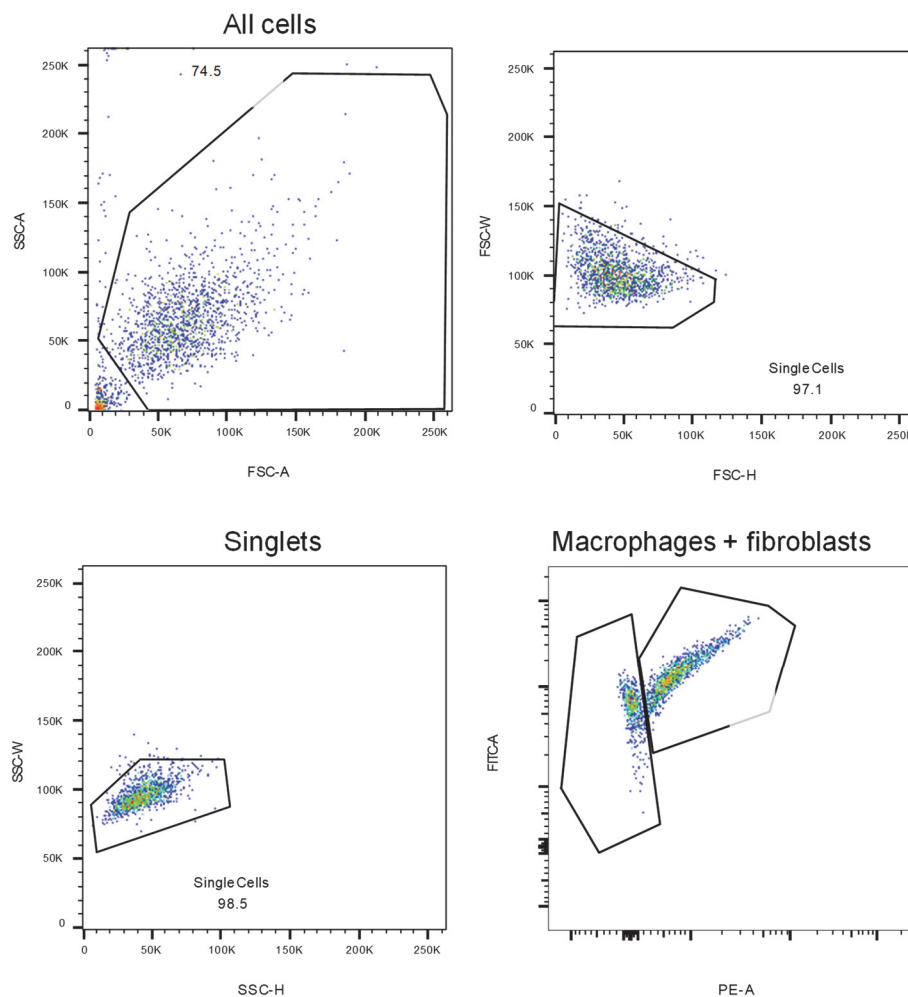


**Figure S1 | Gating strategy and example of coculture of fibroblasts with macrophages pretreated with cDHA.** Gating strategy included the exclusion of debris and doublets based on FSC/SSC. Separation of macrophages and fibroblasts in the coculture was based on the autofluorescence observed in both the PE and FITC channel.

## References

- (1) Bazinet, R. P.; Layé, S. Polyunsaturated Fatty Acids and Their Metabolites in Brain Function and Disease. *Nat. Rev. Neurosci.* **2014**, *15*(12), 771–785.
- (2) Spector, A. A. Essentiality of Fatty Acids. *Lipids* **1999**, *34*(1), S1–S3.
- (3) Guesnet, P.; Alessandri, J.-M. Docosahexaenoic Acid (DHA) and the Developing Central Nervous System (CNS) – Implications for Dietary Recommendations. *Biochimie* **2011**, *93*(1), 7–12.
- (4) Burdge, G. C.; Calder, P. C. Dietary α-Linolenic Acid and Health-Related Outcomes: A Metabolic Perspective. *Nutr. Res. Rev.* **2006**, *19*(1), 26–52.
- (5) Weiser, M. J.; Butt, C. M.; Mohajeri, M. H. Docosahexaenoic Acid and Cognition throughout the Lifespan. *Nutrients* **2016**, *8*(2), 99.
- (6) Dyall, S. C.; Michael-Titus, A. T. Neurological Benefits of Omega-3 Fatty Acids. *NeuroMolecular Med.* **2008**, *10*(4), 219–235.
- (7) Calder, P. C. N-3 Polyunsaturated Fatty Acids, Inflammation, and Inflammatory Diseases. *Am. J. Clin. Nutr.* **2006**, *83*(6), 1505S–1519S.
- (8) Wall, R.; Ross, R. P.; Fitzgerald, G. F.; Stanton, C. Fatty Acids from Fish: The Anti-Inflammatory Potential of Long-Chain Omega-3 Fatty Acids. *Nutr. Rev.* **2010**, *68*(5), 280–289.
- (9) Saliba, A.-E.; Vonkova, I.; Gavin, A.-C. The Systematic Analysis of Protein–Lipid Interactions Comes of Age. *Nat. Rev. Mol. Cell Biol.* **2015**, *16*(12), 753.
- (10) Serhan, C. N.; Yacoubian, S.; Yang, R. Anti-Inflammatory and Pro-Resolving Lipid Mediators. *Annu. Rev. Pathol.* **2008**, *3*, 279–312.
- (11) Serhan, C. N. Pro-Resolving Lipid Mediators Are Leads for Resolution Physiology. *Nature* **2014**, *510*(7503), 92–101.
- (12) Dalli, J.; Serhan, C. N. Identification and Structure Elucidation of the Pro-Resolving Mediators Provides Novel Leads for Resolution Pharmacology. *Br. J. Pharmacol.* **2019**, *176*(8), 1024–1037.
- (13) Brown, M. S.; Goldstein, J. L. Cholesterol Feedback: From Schoenheimer’s Bottle to Scap’s MELADL. *J. Lipid Res.* **2009**, *50*(Supplement), S15–S27.
- (14) Wüstner, D. Fluorescent Sterols as Tools in Membrane Biophysics and Cell Biology. *Chem. Phys. Lipids* **2007**, *146*(1), 1–25.
- (15) Gimpl, G.; Gehrig-Burger, K. Probes for Studying Cholesterol Binding and Cell Biology. *Steroids* **2011**, *76*(3), 216–231.
- (16) Emken, E. A. Stable Isotope Approaches, Applications, and Issues Related to Polyunsaturated Fatty Acid Metabolism Studies. *Lipids* **2001**, *36*(9), 965–973.
- (17) Ecker, J.; Liebisch, G. Application of Stable Isotopes to Investigate the Metabolism of Fatty Acids, Glycerophospholipid and Sphingolipid Species. *Prog. Lipid Res.* **2014**, *54*, 14–31.
- (18) McIntosh, A. L.; Atshaves, B. P.; Huang, H.; Gallegos, A. M.; Kier, A. B.; Schroeder, F. Fluorescence Techniques Using Dehydroergosterol to Study Cholesterol Trafficking. *Lipids* **2008**, *43*(12), 1185–1208.
- (19) Laguerre, A.; Schultz, C. Novel Lipid Tools and Probes for Biological Investigations. *Curr. Opin. Cell Biol.* **2018**, *53*, 97–104.
- (20) Sezgin, E.; Can, F. B.; Schneider, F.; Clausen, M. P.; Galiani, S.; Stanly, T. A.; Waithe, D.; Colaco, A.; Honigmann, A.; Wüstner, D.; Platt, F.; Eggeling, C. A Comparative Study on Fluorescent Cholesterol Analogs as Versatile Cellular Reporters. *J. Lipid Res.* **2016**, *57*(2), 299–309.
- (21) Rostovtsev, V. V.; Green, L. G.; Fokin, V. V.; Sharpless, K. B. A Stepwise Huisgen Cycloaddition Process: Copper(I)-Catalyzed Regioselective “Ligation” of Azides and Terminal Alkynes. *Angew. Chem. Int. Ed.* **2002**, *41*(14), 2596–2599.
- (22) Thiele, C.; Papan, C.; Hoelper, D.; Kusserow, K.; Gaebler, A.; Schoene, M.; Piotrowitz, K.; Lohmann, D.; Spandl, J.; Stevanovic, A.; Shevchenko, A.; Kuerschner, L. Tracing Fatty Acid Metabolism by Click Chemistry. *ACS Chem. Biol.* **2012**, *7*(12), 2004–2011.
- (23) Raghavan, A.; Charron, G.; Flexner, J.; Hang, H. C. Chemical Probes for Profiling Fatty Acid-Associated Proteins in Living Cells. *Bioorg. Med. Chem. Lett.* **2008**, *18*(22), 5982–5986.
- (24) Hulce, J. J.; Cognetta, A. B.; Niphakis, M. J.; Tully, S. E.; Cravatt, B. F. Proteome-Wide Mapping of Cholesterol-Interacting Proteins in Mammalian Cells. *Nat. Methods* **2013**, *10*(3), 259–264.
- (25) Hofmann, K.; Thiele, C.; Schött, H.-F.; Gaebler, A.; Schoene, M.; Kiver, Y.; Friedrichs, S.; Lütjohann, D.; Kuerschner, L. A Novel Alkyne Cholesterol to Trace Cellular Cholesterol Metabolism and Localization. *J. Lipid Res.* **2014**, *55*(3), 583–591.
- (26) Sandbhor, M. S.; Key, J. A.; Strelkov, I. S.; Cairo, C. W. A Modular Synthesis of Alkynyl-Phosphocholine Headgroups for Labeling Sphingomyelin and Phosphatidylcholine. *J. Org. Chem.* **2009**, *74*(22), 8669–8674.
- (27) Gaebler, A.; Milan, R.; Straub, L.; Hoelper, D.; Kuerschner, L.; Thiele, C. Alkyne Lipids as Substrates for Click Chemistry-Based in Vitro Enzymatic Assays. *J. Lipid Res.* **2013**, *54*(8), 2282–2290.
- (28) Thiele, C.; Wunderling, K.; Leyendecker, P. Multiplexed and Single Cell Tracing of Lipid Metabolism. *Nat. Methods* **2019**, *16*(11), 1123–1130.

- (29) Gaebler, A.; Penno, A.; Kuerschner, L.; Thiele, C. A Highly Sensitive Protocol for Microscopy of Alkyne Lipids and Fluorescently Tagged or Immunostained Proteins. *J. Lipid Res.* **2016**, *57*(10), 1934–1947.
- (30) Neef, A. B.; Schultz, C. Selective Fluorescence Labeling of Lipids in Living Cells. *Angew. Chem. Int. Ed.* **2009**, *48*(8), 1498–1500.
- (31) Goto, T.; Urabe, D.; Masuda, K.; Isobe, Y.; Arita, M.; Inoue, M. Total Synthesis of Four Stereoisomers of (4Z,7Z,10Z,12E,16Z,18E)-14,20-Dihydroxy-4,7,10,12,16,18-Docosahexaenoic Acid and Their Anti-Inflammatory Activities. *J. Org. Chem.* **2015**, *80*(15), 7713–7726.
- (32) Sandri, J.; Viala, J. Syntheses of All-(Z)-5,8,11,14,17-Eicosapentaenoic Acid and All-(Z)-4,7,10,13,16,19-Docosahexaenoic Acid from (Z)-1,1,6,6-Tetraisopropoxy-3-Hexene. *J. Org. Chem.* **1995**, *60*(20), 6627–6630.
- (33) Vik, A.; Hansen, T. V. Synthetic Manipulations of Polyunsaturated Fatty Acids as a Convenient Strategy for the Synthesis of Bioactive Compounds. *Org. Biomol. Chem.* **2018**, *16*(48), 9319–9333.
- (34) Saha, G.; Basu, M. K.; Kim, S.; Jung, Y.-J.; Adiyaman, Y.; Adiyaman, M.; Powell, W. S.; FitzGerald, G. A.; Rokach, J. A Convenient Strategy for the Synthesis of  $\beta,\gamma$ -Unsaturated Aldehydes and Acids. A Construction of Skipped Dienes. *Tetrahedron Lett.* **1999**, *40*(40), 7179–7183.
- (35) Rosell, M.; Villa, M.; Durand, T.; Galano, J.-M.; Vercauteran, J.; Crauste, C. Total Syntheses of Two Bis-Allylic-Deuterated DHA Analogues. *Asian J. Org. Chem.* **2017**, *6*(3), 322–334.
- (36) Kato, T.; Hirukawa, T.; Namiki, K. Selective Terminal Olefin Oxidation of N-3 Polyunsaturated Fatty Acids. *Tetrahedron Lett.* **1992**, *33*(11), 1475–1478.
- (37) Tokunaga, T.; Watanabe, B.; Sato, S.; Kawamoto, J.; Kurihara, T. Synthesis and Functional Assessment of a Novel Fatty Acid Probe,  $\omega$ -Ethynyl Eicosapentaenoic Acid Analog, to Analyze the in Vivo Behavior of Eicosapentaenoic Acid. *Bioconjug. Chem.* **2017**, *28*(8), 2077–2085.
- (38) Yu, M.; Alonso-Galicia, M.; Sun, C.-W.; J. Roman, R.; Ono, N.; Hirano, H.; Ishimoto, T.; Reddy, Y. K.; Katipally, K. R.; Reddy, K. M.; Gopal, V. R.; Yu, J.; Takhi, M.; Falck, J. R. 20-Hydroxyeicosatetraenoic Acid (20-HETE): Structural Determinants for Renal Vasoconstriction. *Bioorg. Med. Chem.* **2003**, *11*(13), 2803–2821.
- (39) Menger, F. M.; Chen, X. Y.; Brocchini, S.; Hopkins, H. P.; Hamilton, D. Synthesis and Thermotropic Properties of Macroyclic Lipids Related to Archaeabacterial Membranes. *J. Am. Chem. Soc.* **1993**, *115*(15), 6600–6608.
- (40) Soethoudt, M.; Stolze, S. C.; Westphal, M. V.; van Stralen, L.; Martella, A.; van Rooden, E. J.; Guba, W.; Varga, Z. V.; Deng, H.; van Kasteren, S. I.; Grether, U.; IJzerman, A. P.; Pacher, P.; Carreira, E. M.; Overkleef, H. S.; Ioan-Facsinay, A.; Heitman, L. H.; van der Stelt, M. Selective Photoaffinity Probe That Enables Assessment of Cannabinoid CB2 Receptor Expression and Ligand Engagement in Human Cells. *J. Am. Chem. Soc.* **2018**, *140*(19), 6067–6075.
- (41) Poulcharidis, D.; Belfor, K.; Kros, A.; Kasteren, S. I. van. A Flow Cytometry Assay to Quantify Intercellular Exchange of Membrane Components. *Chem. Sci.* **2017**, *8*(8), 5585–5590.
- (42) Sivakumar, K.; Xie, F.; Cash, B. M.; Long, S.; Barnhill, H. N.; Wang, Q. A Fluorogenic 1,3-Dipolar Cycloaddition Reaction of 3-Azidocoumarins and Acetylenes. *Org. Lett.* **2004**, *6*(24), 4603–4606.
- (43) Schindelin, J.; Arganda-Carreras, I.; Frise, E.; Kaynig, V.; Longair, M.; Pietzsch, T.; Preibisch, S.; Rueden, C.; Saalfeld, S.; Schmid, B.; Tinevez, J.-Y.; White, D. J.; Hartenstein, V.; Eliceiri, K.; Tomancak, P.; Cardona, A. Fiji: An Open-Source Platform for Biological-Image Analysis. *Nat. Methods* **2012**, *9*(7), 676–682.
- (44) Wright, S. W.; Kuo, E. Y.; Corey, E. J. An Effective Process for the Isolation of Docosahexaenoic Acid in Quantity from Cod Liver Oil. *J. Org. Chem.* **1987**, *52*(19), 4399–4401.
- (45) Baldwin, J. E.; Adlington, R. M.; Singh, R. Carbocyclic Ring Expansion Reactions via Free Radical Pathways - Part III. *Tetrahedron* **1992**, *48*(16), 3385–3412.



# Chapter 6

## Profiling the anandamide reuptake inhibitor WOBE437\*

### Introduction

Anandamide (AEA) is a lipid signaling molecule that belongs to the endocannabinoid system (ECS). It modulates neurotransmitter release via activation of the cannabinoid CB1 receptor (CB1R).<sup>1</sup> AEA is produced by hydrolysis of phospholipids, mainly by *N*-acylphosphatidylethanolamine phospholipase D (NAPE-PLD), after which it is released to activate the CB1R. AEA-induced CB1R signaling is terminated by a two-step process, i.e. cellular uptake and hydrolysis of the amide bond by fatty acid amide hydrolase (FAAH). The ECS is responsible for regulation of a large number of physiological processes, including energy balance, pain, inflammation and neurotransmission.<sup>2</sup> Consequently, modulation of ECS signaling may have therapeutic benefits for a number of diseases, including neurodegenerative,<sup>3,4</sup> inflammatory<sup>5</sup> and cardiovascular diseases,<sup>6–8</sup> pain,<sup>9,10</sup> psychiatric disorders,<sup>2,11</sup> obesity,<sup>12</sup> and others.<sup>13</sup> Activation of CB1R signaling has been achieved by direct and indirect methods, through the application of CB1R agonists and through altering endocannabinoid metabolism, respectively.<sup>13</sup> The latter strategy may lead to fewer side effects that are usually associated with direct CB1R activation.<sup>14</sup>

---

\*The data presented in this chapter was gathered in collaboration with Floor Stevens, Domenico Fazio, Bogdan I. Florea, Alexander Bakker, Hans den Dulk, Kim Wals, Aron Smids, Herman S. Overkleeft, Mauro Maccarrone, Mario van der Stelt.

Elevation of AEA levels can be achieved by inhibiting its cellular reuptake, or by inhibiting FAAH. While inhibition of FAAH is well-characterized and selective inhibitors are currently tested in phase 2 clinical trials, the mechanism of AEA reuptake remains unclear. Small lipophilic molecules may diffuse freely through the lipid bilayer, but AEA reuptake can be saturated.<sup>15</sup> This indicates that a protein facilitator for transport across the membrane may exist. Numerous candidates for a purported endocannabinoid membrane transporter and their inhibitors (AM404,<sup>16</sup> VDM11,<sup>17</sup> UCM707,<sup>18</sup> OMDM-1/2<sup>19</sup>) have been reported, but the existence of such a transporter remains subject of intense scientific debate.<sup>20–25</sup> One of the difficulties encountered in the field is the technical challenge of reliably measuring AEA uptake in short timeframes.<sup>24</sup> Moreover, FAAH inhibition results in an intracellular accumulation of AEA, which disrupts the concentration gradient across the cellular membrane that normally drives AEA uptake.<sup>25</sup> Consequently, many AEA uptake inhibitors have been revealed to act through inhibition of FAAH.<sup>25,26</sup> Another confounding factor is inhibition of intracellular transport of AEA, which can also reduce AEA reuptake. For example, inhibition of FABP5, which is an intracellular binding protein that transports AEA to FAAH at the endoplasmic reticulum,<sup>27</sup> blocks AEA uptake.<sup>28</sup> Other intracellular AEA binding proteins are Hsp70,<sup>29</sup> albumin and potentially FLAT, a catalytically inactive version of FAAH.<sup>30</sup>

Recently, WOBE437 (**1**, Figure 1) has been reported by Dr. Gertsch and co-workers as a novel, natural product-based AEA uptake inhibitor, which is selective over FAAH, FABP5, Hsp70, and FLAT.<sup>31</sup> WOBE437 reduced AEA uptake in mouse neuroblastoma Neuro-2a cells and in primary neurons in a concentration-dependent manner. In BALB/c mice, WOBE437 was orally bioavailable and induced CB1R-dependent anxiolytic, anti-inflammatory and analgesic effects.<sup>32</sup> Absence of FAAH inhibition was demonstrated in different assay systems, including recombinant FAAH, cell lysates and brain homogenates. Moreover, WOBE437 retained activity in FAAH-deficient HMC-1 human mast cells.<sup>33</sup> Although its pharmacological properties have been well-studied, the identity of its primary target remains unknown.

To identify targets of WOBE437, photoaffinity-based protein profiling (AfBPP) may be of use.<sup>34</sup> AfBPP makes use of bifunctional photoaffinity probes, which consist of a ligand of interest functionalized with a photoreactive group and a bioorthogonal ligation handle. After administration of the probe to intact cells, the photoreactive group is activated by UV light. This results in the formation of a reactive intermediate that may form a covalent bond with amino acids that interact with the probe. An alkyne group in the probe serves as a ligation handle to introduce reporter groups by copper(I)-catalyzed azide-alkyne cycloaddition (CuAAC) chemistry. A fluorophore-azide can be conjugated to visualize interacting proteins by sodium dodecyl sulfate polyacrylamide gel electrophoresis (SDS-PAGE) and fluorescence scanning, or alternatively, a biotin-azide can be ligated for protein isolation and identification using liquid chromatography-mass spectrometry (LC-MS).<sup>35</sup> Previously, a photoactivatable WOBE437 derivative was reported.<sup>31</sup> This derivative, RX-055 (**2**, Figure 1), showed similar activity to WOBE437 and retained activity after UV-irradiation in washout experiments, whereas

WOBE437 did not. This indicated that WOBE437 binds reversibly to a protein target, which can be irreversibly blocked by RX-055. However, as this probe only contains a photoreactive group, it cannot be used in AfBPP experiments to identify the targeted proteins. Therefore, the aim of the current study was to develop an alternative photoaffinity-based probe (pac)-WOBE (**3**) to map the protein interaction landscape of WOBE437 (Figure 1).

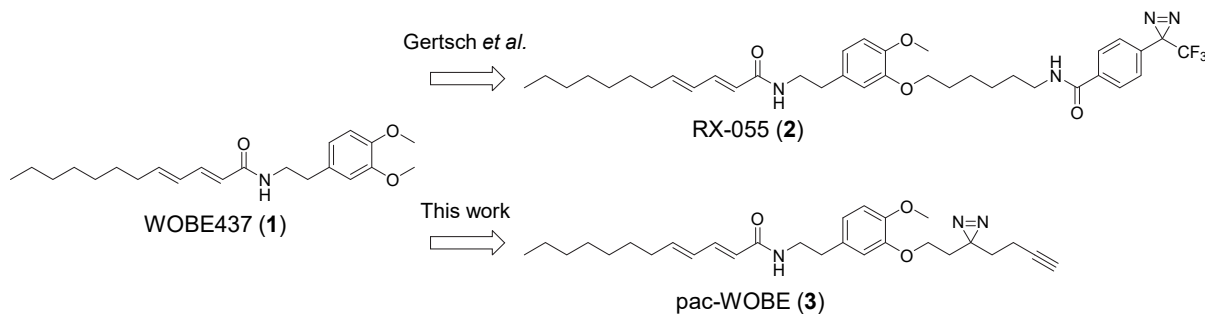


**Figure 1 | Structures of WOBE437 and its probe derivatives.**

## Results

### WOBE437 increases anandamide uptake by disrupting NAE levels

First, WOBE437 was synthesized according to previously reported procedure (Figure 2A).<sup>31</sup> A Horner–Wadsworth–Emmons reaction with (*E*)-dec-2-enal (**4**) and ethyl 2-(diethoxyphosphoryl)acetate resulted in ester **5**, which was saponified to afford carboxylic acid **6**. A subsequent peptide coupling with 2-(3,4-dimethoxyphenyl)ethan-1-amine gave WOBE437 in 49% yield over three steps. The compound was characterized in a [<sup>3</sup>H]-AEA uptake assay in Neuro-2a cells following a previously published method.<sup>36</sup> In brief, Neuro-2a cells were treated with vehicle, WOBE437 or positive control OMDM-1 for 10 min in serum-free medium, which was replaced with PBS containing AEA (400 nM) spiked with [<sup>3</sup>H]AEA. After 15 min, the cells were thoroughly washed and resuspended in aq. NaOH for measurement in a scintillation counter. Passive uptake at 4 °C was subtracted and uptake of OMDM-1-treated cells was set as baseline. In contrast to previous reports,<sup>31</sup> WOBE437 resulted in a concentration-dependent increase in uptake of anandamide when compared to the positive control OMDM-1 (Figure 2B).

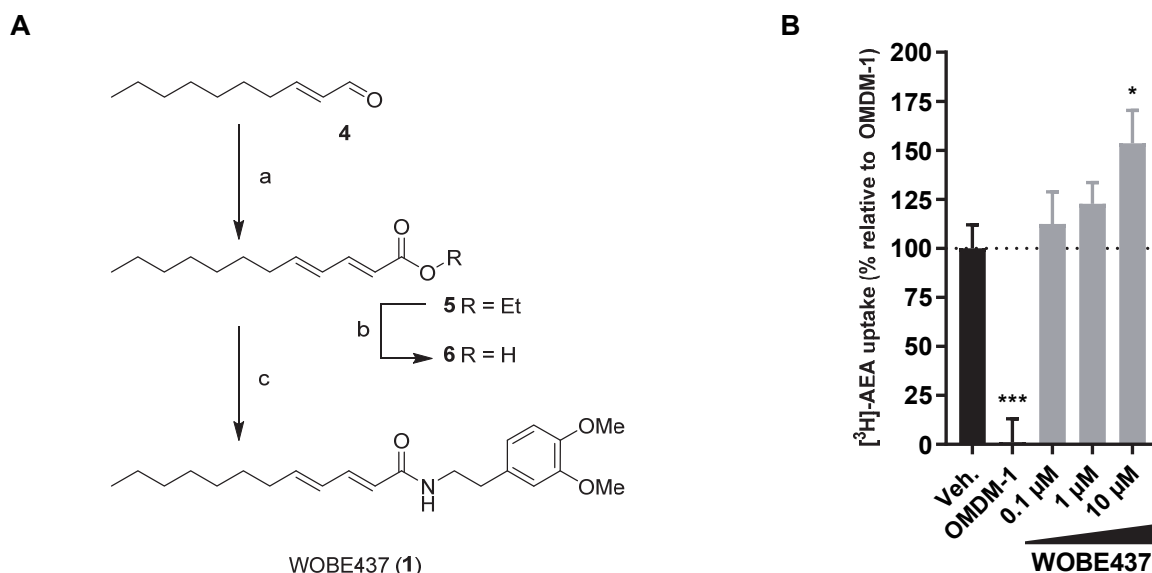


**Figure 2 | Synthesis and characterization of WOBE437.** **(A)** Reagents and conditions: (a) Ethyl 2-(diethoxyphosphoryl)acetate, NaH, 0 °C, then (*E*)-dec-2-enal, -78 °C to rt, 63%; (b) NaOH, 60 °C, quant.; (c) 2-(3,4-dimethoxyphenyl)ethan-1-amine, HOAt, EDC, rt, 78%. **(B)** Endocannabinoid uptake was assayed in Neuro-2a cells, which were preincubated with OMDM-1 (40 μM) as a positive control or different concentrations of WOBE437 for 10 min. [<sup>3</sup>H]-AEA was added and cells were incubated for an additional 15 min, washed and harvested to measure radioactivity. Control experiments were also carried out under the same conditions at 4 °C in order to subtract passive diffusion from active uptake. Data are expressed as means ± SEM of three independent experiments, each performed in triplicate. \* p < 0.05; \*\*\* p < 0.001 in comparison to vehicle-treated control (Dotted line) using a one-way ANOVA with Dunnett's multiple comparisons correction.

To investigate the cellular effects of WOBE437 in more detail, *N*-acylethanolamines (NAEs), free fatty acids and monoacylglycerides were measured using a LC-MS-based assay (Table S2). Neuro-2a cells were incubated for different time periods with either WOBE437 or vehicle, washed and lipids were extracted. Compared to vehicle-treated Neuro-2a cells,

WOBE437 induced a time-dependent decrease in all NAE levels, except SEA, PDEA and DHEA (Figure 3, Figure S1). The largest decrease was observed after 30 min. No effect on free fatty acids or monoacylglycerols was found (Figure S2C). Previously, the inhibition of AEA uptake by WOBE437 was shown to be dependent on the passage number of Neuro-2a cells, but no effect of passage number was found in the current study (Figure S2A, B).

The decrease in NAE levels is consisted with increased AEA uptake, as the transport is driven by the concentration gradient across the plasma membrane.<sup>21</sup> To investigate whether the reduction of NAEs was due to inhibition of NAPE-PLD, WOBE437 was tested in a surrogate substrate-based fluorescence assay using purified enzyme (Figure S3A). WOBE437 did not inhibit NAPE-PLD activity, nor was any serine hydrolase inhibited as indicated by activity-based protein profiling (Figure S3B).<sup>37</sup>

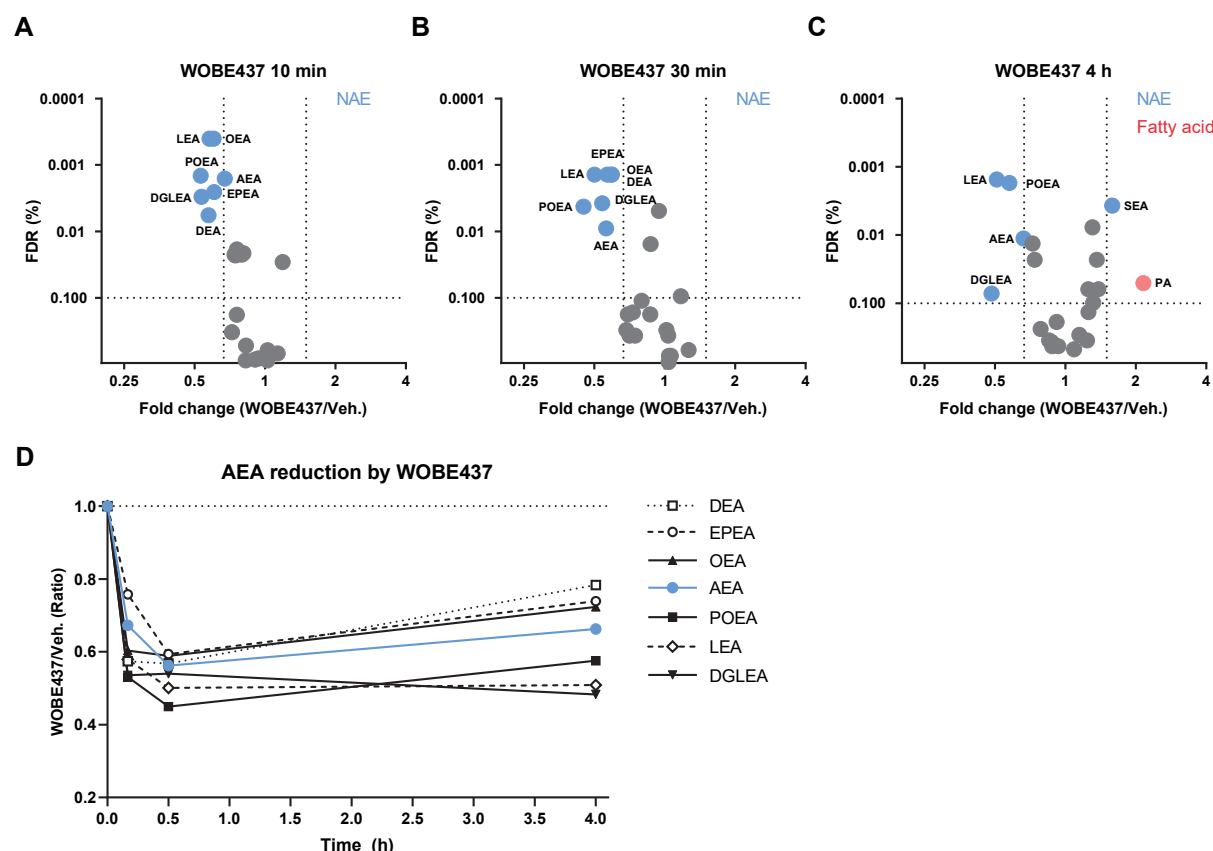


**Figure 3 | WOBE437 disrupts NAEs within 10 minutes of treatment.** Neuro-2a cells were treated with 10  $\mu$ M WOBE437 or vehicle and harvested at the indicated time points to be analyzed by MS-based lipidomics. **(A, B, C)** Lipidomic data are presented as a volcano plot and lipids with a fold-change threshold of  $\geq 1.50$  or  $\leq 0.67$  and a Benjamini-Hochberg false-discovery rate (FDR)  $\leq 10\%$  following a Student's t-test are represented by colored circles indicating lipid class. **(D)** Fold-change of altered NAEs are represented as a function of time. The complete list of ratios at 30 min are depicted in Figure S1.

## Synthesis and characterization of pac-WOBE (3)

To profile the protein interaction landscape of WOBE437, a photoaffinity probe (**3**) was designed, guided by the reported structure-activity relationship.<sup>31</sup> A minimalist diazirine and alkyne-containing moiety<sup>38</sup> was introduced on the phenyl ring of WOBE437 by peptide coupling 5-(2-aminoethyl)-2-methoxyphenol with **6** after which an S<sub>N</sub>2 substitution on 3-(but-3-yn-1-yl)-3-(2-iodoethyl)-3*H*-diazirine afforded pac-WOBE (**3**) in 12% yield over 2 steps (Figure 4A).

To visualize the protein targets of WOBE437 by gel-based AfBPP, Neuro-2a cells were incubated with **3** and irradiated with UV light (350 nm, 10 min, "UV") or exposed to ambient light ("no UV"). The cells were harvested, lysed and the probe-bound proteins were conjugated to Cy5-N<sub>3</sub> under CuAAC conditions. The protein samples were resolved by SDS-PAGE and visualized by in-gel fluorescence scanning (Figure 4B). This showed that **3** could UV-dependently label several proteins. Pretreatment of the cells with WOBE437 resulted in a reduced labeling intensity of two bands around 50 kDa, which suggested that these proteins specifically interact with WOBE437.

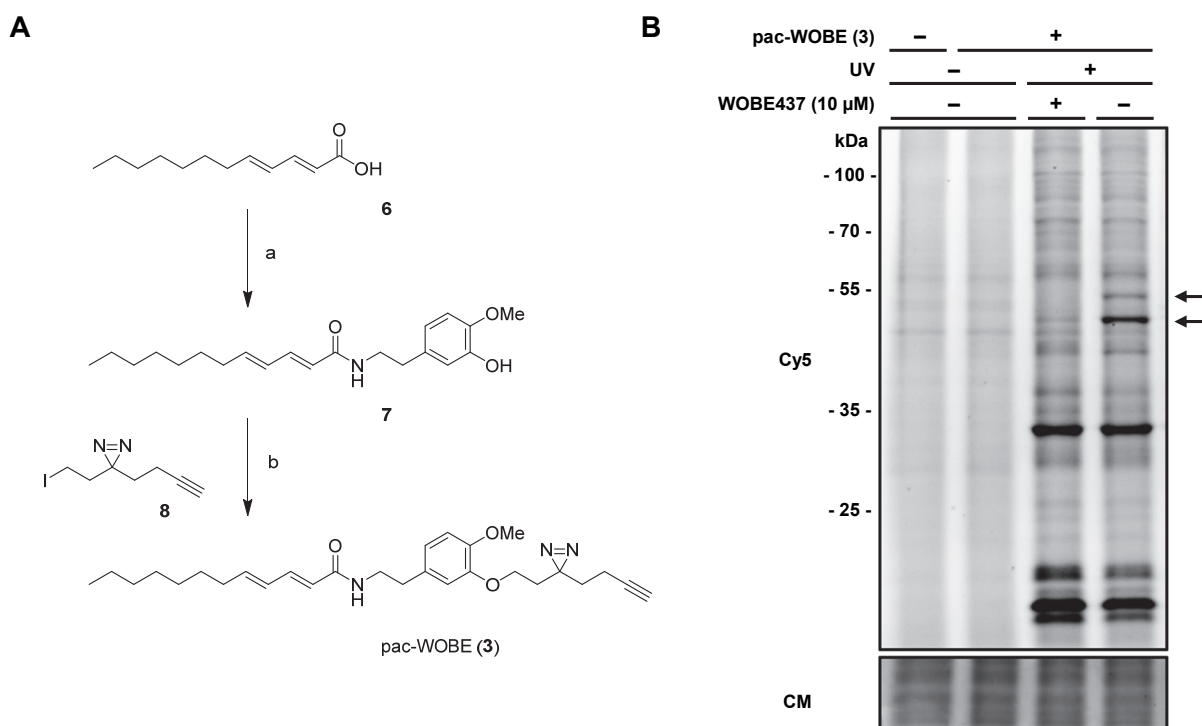


**Figure 4 | Synthesis and characterization of pac-WOBE (3).** **(A)** Reagents and conditions: (a) 5-(2-aminoethyl)-2-methoxyphenol, HOBr, EDC, 0 °C to rt, 43%; (b) 3-(but-3-yn-1-yl)-3-(2-iodoethyl)-3*H*-diazirine, K<sub>2</sub>CO<sub>3</sub>, 60 °C, 29%. **(B)** Neuro-2a cells were treated with 10 μM WOBE437 or vehicle and subsequently with 0.1 μM pac-WOBE (**3**) or vehicle, irradiated, lysed and proteomes were conjugated to Cy5-N<sub>3</sub> using CuAAC chemistry and analyzed by SDS-PAGE and in-gel fluorescence scanning. Coomassie served as a protein loading control. Arrows indicate WOBE437-competed targets.

## Identification and characterization of WOBE437 targets

Next, a label-free chemical proteomics experiment was performed to identify the WOBE437-interacting proteins.<sup>39</sup> Neuro-2a cells were pretreated with WOBE437 (10 µM) or vehicle, after which they were incubated with 1.0 or 0.1 µM pac-WOBE (**3**) with or without UV exposure. Cells were lysed and treated with biotin-N<sub>3</sub> under CuAAC conditions. Probe-bound proteins were enriched using avidin-coated agarose beads, digested by trypsin and analyzed by LC-MS/MS. Proteins displaying >2-fold UV enrichment with a p-value <0.05 were designated as pac-WOBE-interacting targets. This afforded 39 and 8 significantly UV-enriched targets for the two probe concentrations, respectively (Figure 5A, S4A, Table S4). Three of these probe targets (i.e. Saccharopine dehydrogenase-like oxidoreductase (SCCPDH), Vesicle Amine Transport 1 (VAT1) and Ferrochelatase (FECH)) could be outcompeted by preincubation with WOBE437 (Figure 5B, S4A, Table S4).

Mouse and human orthologues of these three targets were recombinantly expressed in HEK-293-T cells and target engagement with AEA was investigated using gel-based AfBPP (Figure 5C, D). AEA engaged in a dose-dependent manner with SCCPDH and VAT1. Of note, AEA binding was most potent on the mouse orthologue of SCCPDH (Figure 5D, E). AEA did not compete with pac-WOBE (**3**) labeling of FECH, a mitochondrial enzyme extensively studied for its role in heme biosynthesis, and a common off-target of kinase inhibitors<sup>40</sup> and lipid probes.<sup>41</sup>

In view of these results, further experiments were conducted with mouse SCCPDH and mouse VAT1. VAT1 has previously been shown to be involved in lipid binding and transport.<sup>42,43</sup> To investigate whether SCCPDH and VAT1 were selective for WOBE437 and AEA, competitive AfBPP was performed with a selection of other closely related lipids, such as 2-arachidonoylglycerol (2-AG), palmitoylethanolamide (PEA), arachidonic acid (AA), and the FAAH inhibitor URB597 (Figure 5F-I). WOBE437 was the most potent competitor of mSCCPDH labeling followed by AEA > URB597 > AA> 2-AG > PEA. Mouse VAT1 was much more selective since its labeling was only significantly inhibited by WOBE437, AEA and PEA (Figure 5G-I).

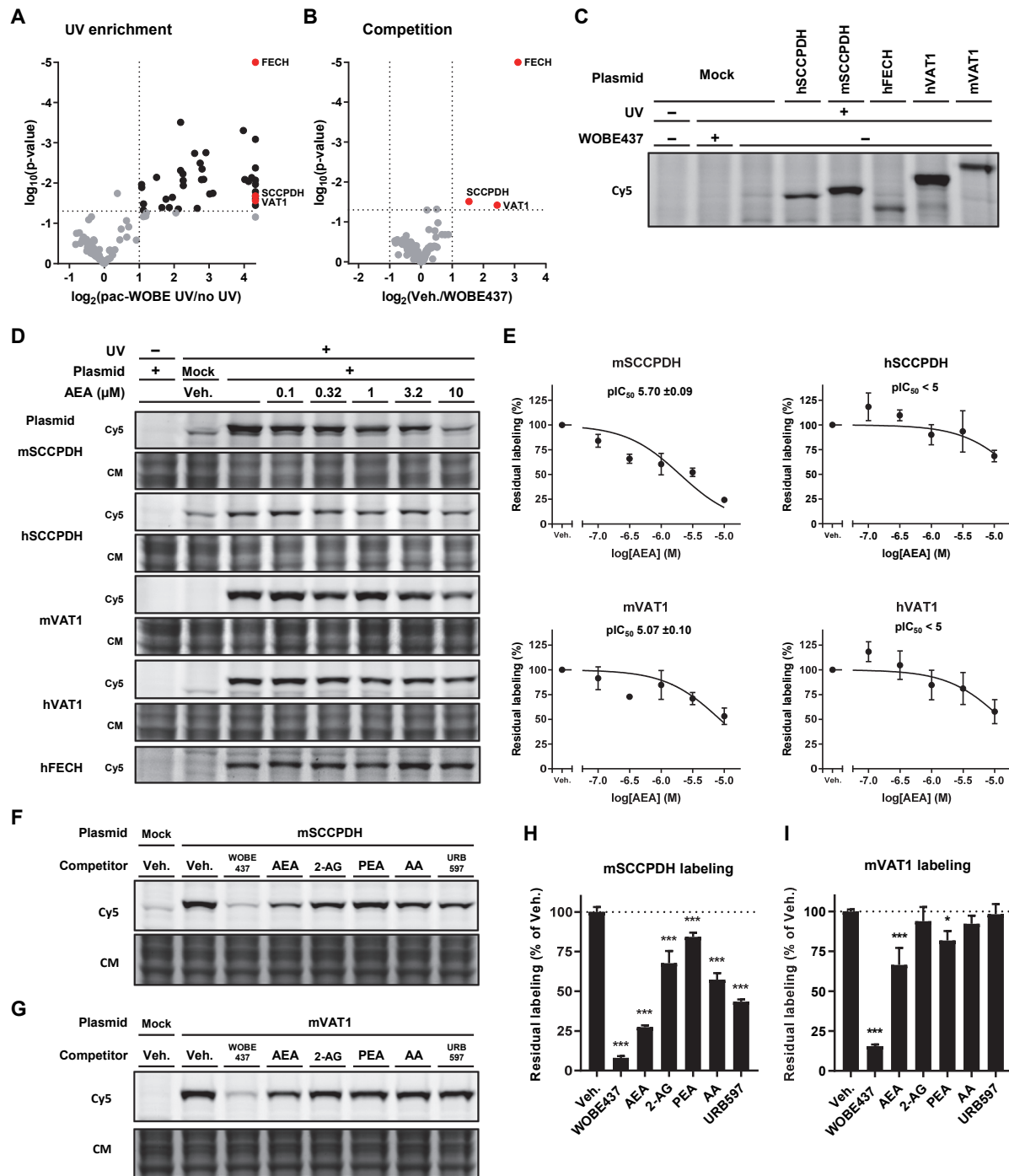


**Figure 5 | Identification and characterization of WOBE437 targets using pac-WOBE (3).** Volcano plot depicting (A) UV enrichment and (B) WOBE437 competition of proteins labeled by *in situ* AfBPP in Neuro-2a cells using 1  $\mu$ M pac-WOBE (3). UV enrichment is capped at 20-fold, p-value at 0.00001. A complete list of targets are listed in Table S4. (C) Gel-based AfBPP profiling of overexpressing HEK-293-T cells using 0.1  $\mu$ M pac-WOBE (3). (D) Representative gels of AEA competition of 0.1  $\mu$ M pac-WOBE (3) labeling of overexpressing HEK-293-T cells. (E) Quantified residual labeling of indicated protein by 0.1  $\mu$ M pac-WOBE (3) after AEA preincubation. Fluorescent signal was quantified, corrected by Coomassie and expressed as remaining labeling compared to vehicle. Data represent means  $\pm$  SD of three separate experiments and  $pIC_{50} \pm$  SD. (F, G) Representative gels of competition of 0.1  $\mu$ M pac-WOBE (3) labeling of overexpressing HEK-293-T cells. (H, I) Quantified residual labeling of indicated protein by 0.1  $\mu$ M pac-WOBE (3) after preincubation with indicated compound. Data represent means  $\pm$  SD of three biological replicates. \*  $p < 0.05$ , \*\*\*  $p < 0.001$  in comparison to vehicle-treated control (dotted line) using a one-way ANOVA with Dunnett's multiple comparisons correction.

Next, a genetic approach was used to investigate whether SCCPDH or VAT1 is responsible for WOBE437-induced decrease in NAE levels in Neuro-2a cells, since no selective SCCPDH or VAT1 inhibitors are available. Of note, single cell heterogeneity in NAE production prevented the unequivocal analysis of single cell clone knockouts.<sup>44</sup> Therefore, disruption of SCCPDH and VAT1 genes was performed by three sequential rounds of transfection of Cas9 and single guide RNAs (sgRNA) in Neuro-2a cell populations. SCCPDH and VAT1 expression in these cell populations was significantly, albeit not completely, decreased as determined by gel-based AfBPP and western blot for VAT1 (Figure 6A, C). The residual expression of SCCPDH and VAT1 can be explained by a transfection efficiency below 100% and by insertion or deletion of a full codon upon Cas9-mediated DNA modification, thus preventing the frameshift that generally results in an early STOP-codon. Next, the cellular NAE levels of these genetically modified Neuro-2a populations were determined using LC-MS and serine hydrolase activity by ABPP. No change in NAE levels or serine hydrolase activity was observed for these knockdown populations compared to wild type cells (Figure 6B, D and Figure S5, S6). Notably, WOBE437 was still able to significantly reduce NAE levels in these genetically modified cells (Figure 6E). This indicated that other targets than SCCPDH or VAT1 are responsible for the WOBE437-mediated reduction in NAE levels.

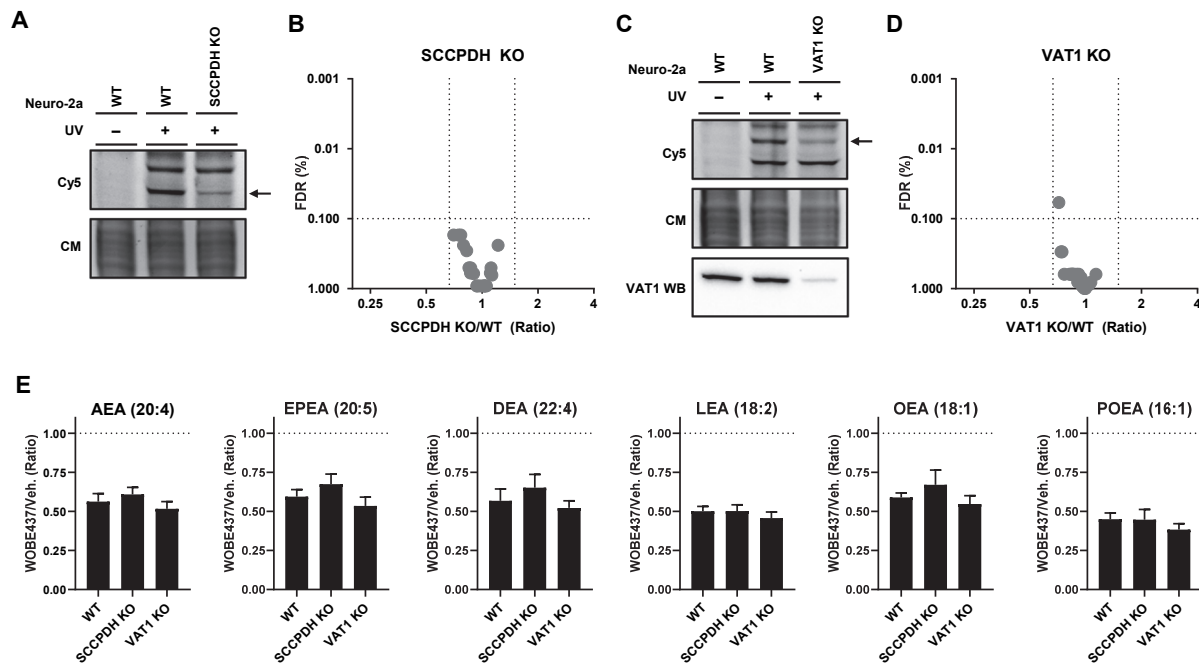


**Figure 6 | Partial SCCPDH and VAT1 knockouts were generated by CRISPR-Cas9.** (A) SCCPDH and (C) VAT1 KO Neuro-2a lines were generated and checked by gel-based AfBPP using 0.1  $\mu$ M pac-WOBE (3) for residual expression. VAT1 protein was tested by VAT1 western blot. Coomassie served as a protein loading control. Lipid levels were tested by lipidomics on (B) SCCPDH KO and (D) VAT1 KO cells and compared to WT cells. Further characterization and the complete list of ratios are depicted in Figure S5 and S6. (E) Neuro-2a cells were treated with 10  $\mu$ M WOBE437 or vehicle for 30 min and harvested to be analyzed by MS-based lipidomics. Lipid levels are displayed as ratio against the same type of cells treated with vehicle. Data represent means  $\pm$  SEM ( $n = 4$ ). One-way ANOVA with Dunnett's multiple comparisons correction: not significant when compared to WT.

## Conclusion

WOBE437 has been reported as an AEA-uptake inhibitor that shows various *in vivo* effects that are consistent with indirect cannabinoid CB<sub>1</sub> receptor activation by elevated AEA levels. However, the molecular target of WOBE437 is unknown. In this chapter, a photoaffinity-based approach was employed to identify the protein targets of WOBE437 in Neuro-2a cells. Surprisingly, WOBE437 increased AEA uptake and decreased endogenous NAE levels in Neuro-2a cells. Although the WOBE437-induced time-dependent decrease in endogenous AEA levels appears in keeping with the increased AEA uptake in Neuro-2a cells, it is unclear why the current results are in contrast to the previous findings of the laboratory of Dr. Gertsch.<sup>31</sup> Differences in the experimental protocol of AEA-uptake experiments or heterogeneity of Neuro-2a cells may be contributing factors. It should be noted that the positive control OMDM-1 did reduce AEA uptake in Neuro-2a cells under the same conditions. At the very least, this suggests that OMDM-1 and WOBE437 have different molecular modes of action, although both compounds are reported as AEA uptake inhibitors.

AfBPP using a WOBE437-based photoaffinity probe identified SCCPHD, VAT1 and FECH as WOBE437-interacting proteins in Neuro-2a cells. Competitive gel-based AfBPP demonstrated that SCCPHD and VAT1, but not FECH, could bind AEA preferentially over related lipids. Further genetic studies indicated, however, that SCCPDH and VAT1 were not responsible for the WOBE437-induced reduction in endogenous NAE levels in Neuro-2a cells. It remains to be investigated whether FECH is involved in this process. Regardless of the exact mechanism of action of WOBE437, the current study identified SCCPDH, VAT1 and FECH as off-targets of WOBE437, which may confound the interpretation of the biological effects obtained with this compound.

## Experimental procedures

### General

Lipids were purchased from Cayman Chemicals and stored as 10 mM ethanolic stocks under nitrogen at -80 °C, except glycerides, which were dissolved in acetonitrile. Inhibitors were purchased from Cayman Chemicals or Sigma Aldrich and stored as 10 mM DMSO stocks at -20 °C. FP-TAMRA was purchased from Thermo Fisher. MB064<sup>37</sup> and 3-(but-3-yn-1-yl)-3-(2-iodoethyl)-3*H*-diazirine<sup>38</sup> were prepared as previously reported in literature. All other reagents were purchased from Sigma Aldrich or Cayman Chemicals unless otherwise specified.

### Cloning

DNA oligos were purchased at Sigma Aldrich or Integrated DNA Technologies. Cloning reagents were from Thermo Fisher. Full-length cDNA encoding human and murine SCCPDH and VAT1, as well as human FECH was obtained from Source Bioscience. Expression constructs were generated by PCR amplification and restriction/ligation cloning into a pcDNA3.1 vector, in frame with a C-terminal FLAG tag. All plasmids were isolated from transformed XL10-Gold or DH10B competent cells (prepared using *E. coli* transformation buffer set, Zymo Research) using plasmid isolation kits following the supplier's protocol (Qiagen). All sequences were verified by Sanger sequencing (Macrogen).

### Cell culture

#### *General cell culture*

Neuro-2a and HEK-293-T cells were cultured at 37 °C under 7% CO<sub>2</sub> in DMEM (Sigma Aldrich, HEK-293-T: D6546, Neuro-2a: D1145) containing stable glutamine, 10% (v/v) New Born Calf Serum (Thermo Fisher) and penicillin and streptomycin (200 µg/mL each, Duchefa). Cells were passaged twice a week at 80-90% confluence by resuspension in fresh medium. Cell lines were purchased from ATCC and were tested regularly for mycoplasma contamination. Cultures were discarded after 2-3 months of use.

#### *Transfection*

SCCPDH/VAT1/FECH-overexpressing Neuro-2a or HEK-293-T cells were generated by seeding cells on 12-well plates (4.0x10<sup>4</sup> cells/cm<sup>2</sup>) 24 h prior to transfection. Culture medium was aspirated and replaced with 400 µL fresh medium. A mixture of polyethylenimine (PEI, Neuro-2a: 5:1 (m/m), HEK-293-T: 3:1 (m/m)) and plasmid DNA (0.625 µg/well) was prepared in serum-free culture medium (100 µL) and incubated for 15 min at rt. Transfection was performed by dropwise addition of the PEI/DNA mix to the cells. After 24 h, medium was refreshed. Cells were used 48 h post-transfection.

#### *Viability assay*

2.0x10<sup>5</sup> Neuro-2a cells were seeded in 500 µL medium on a 24-well plate 24 h prior. Then, 55 µL PBS supplemented with 5 mg/mL 3-(4,5-dimethylthiazol-2-yl)-2,5-diphenyltetrazolium bromide was added for 0.5 mg/mL final and the plate was incubated at 37 °C for 3 h. The medium was aspirated and the formed formazan crystals were dissolved in 200 µL DMSO by shaking the plates at 800 rpm for 5 min. Absorbance was measured at 450 nm in a CLARIOstar plate reader (BMG Labtech) and data was analyzed using Graphpad Prism 8.1.1.

#### *AEA uptake assay*

The uptake of AEA was measured in Neuro-2a cells (seeded in triplicate in 12-well plates) according to literature protocol with minor modifications.<sup>36</sup> Neuro-2a cells were pre-incubated in serum-free medium with OMDM-1 (40 µM) for 15 min or different concentrations of WOBE437 (0.1, 1, and 10 µM) or vehicle for 10 min by adding the substance directly to the incubation medium. Medium was aspirated and the cells were incubated with PBS at 37 °C containing AEA (400 nM) supplemented with [<sup>3</sup>H]AEA (30,000 cpm, ARC, St. Louis, MO, USA) for 15 min. PBS was then aspirated and the cells were washed three

## Chapter 6

times with PBS supplemented with 1% (w/v) BSA (1 mL) and resuspended in aq. NaOH (0.5 M, 0.5 mL) and measured in a scintillation counter. Control experiments were also carried out at 4 °C in order to subtract passive diffusion from active uptake.

### Photoaffinity-based protein profiling

#### Gel-based AfBPP

For gel-based profiling, transfected HEK-293-T or Neuro-2a (WT or KO) on 12-well plates were treated with probe as follows:

Growth medium was aspirated and a solution of indicated competitor (2X, 10 µM final) or vehicle in serum-free DMEM supplemented with 0.1% (w/v) delipidated BSA (0.5 mL) was added and the cells were incubated for 30 min at 37 °C. Then, a solution of pac-WOBE (**3**, 2X, 100 nM final) in serum-free DMEM supplemented with 0.1% (w/v) delipidated BSA (0.5 mL) was added and the cells were incubated for 30 min at 37 °C. Medium was aspirated and replaced with 1 mL ice-cold DPBS and the cells were irradiated using a Caprobox™ (10 min, 4 °C, 350 nm, "UV") or exposed to ambient light (10 min, 4 °C, "No UV").

The cells were harvested by pipetting and pelleted by centrifugation (1,000 *g*, 10 min, 4 °C). The supernatant was removed and the cells were lysed by resuspension in lysis buffer (250 mM sucrose, 20 mM HEPES pH 7.5, 1 mM MgCl<sub>2</sub>, 1X protease inhibitor cocktail (Roche), 25 U/mL benzonase) and sonication in a bath sonicator (0 °C, 5 min). Protein concentration was measured by Qubit™ assay (Invitrogen) and the samples were adjusted to 1.5 mg/mL and a volume of 100 µL, after which the samples were treated with 10.4 µL click mix (5.5 µL aq. 25 mM CuSO<sub>4</sub>, 3.25 µL aq. 250 mM NaAsc, 1.1 µL 25 mM THPTA in DMSO, 0.55 µL 0.9 mM Cy5-N<sub>3</sub> in DMSO) and left at rt for 1 h. Samples were then quenched by addition of 4X Laemmli buffer, boiled (5 min, 95 °C) and resolved by SDS-PAGE (10% acrylamide gel, ±80 min, 180 V) along with protein marker (PageRuler™ Plus, Thermo Fisher). In-gel fluorescence was measured in the Cy3- and Cy5-channel (Chemidoc™ MP, Bio-Rad) and the gels were subsequently stained with Coomassie and imaged as a loading control for normalization of fluorescence intensity. Band intensities were quantified using Image Lab 6.0.1 (BioRad).

For VAT-1 western blot, part of the gel was stained with Coomassie and imaged for loading control. The rest of the gel was transferred to a 0.2 µm polyvinylidene difluoride membrane by Trans-Blot Turbo™ Transfer system (Bio-Rad). Membranes were washed with TBS (50 mM Tris pH 7.5, 150 mM NaCl) and blocked with 5% (w/v) milk in TBS-T (50 mM Tris pH 7.5, 150 mM NaCl, 0.05% (w/v) Tween-20) for 1 h at rt. Membranes were then washed three times with TBS-T, followed by incubation with primary antibody in 5% (w/v) BSA in TBS-T (VAT1, PA5-43777, Thermo Fisher, 1:1,000, 1 h, rt). Membranes were then washed three times with TBS-T and incubated with secondary goat-anti-rabbit-HRP (sc-2030, Santa Cruz, 1:5,000 in 5% (w/v) milk in TBS-T, 1 h, rt), then washed three times with TBS-T and once with TBS before developing. Membranes were developed in luminol development solution (10 mL of 1.4 mM luminol in 100 mM Tris pH 8.8 + 100 µL of 6.7 mM *p*-coumaric acid in DMSO + 3 µL of 30% (v/v) H<sub>2</sub>O<sub>2</sub>) and chemiluminescence was detected on ChemiDoc™ MP (Bio-Rad) in the chemiluminescence channel and colorimetric channel for the protein marker. Images were processed using Image Lab 6.0.1 (BioRad).

#### Chemical proteomics-based AfBPP

Neuro-2a cells were plated on 6-well plates and grown to near confluence (90%). The supernatant was aspirated and serum-free DMEM supplemented with 0.1% (w/v) delipidated BSA (1 mL) and WOBE-437 or vehicle was added and the cells were incubated for 30 min at 37 °C. After this period, pac-WOBE (**3**) was added and the cells were incubated for 30 min at 37 °C. Subsequently, medium was aspirated and replaced with 1 mL ice-cold DPBS and the cells were irradiated using a Caprobox™ (10 min, 4 °C, 350 nm, "UV") or exposed to ambient light (10 min, 4 °C, "No UV"). The cells were harvested by pipetting and pelleted by centrifugation (1,000 *g*, 10 min, 4 °C). The supernatant was removed and the cells were lysed by resuspension in lysis buffer (250 µL, 250 mM sucrose, 20 mM HEPES pH 7.5, 1 mM MgCl<sub>2</sub>,

1X protease inhibitor cocktail (Roche)) and sonication (Branson Sonifier probe sonicator, 10 x 2 s pulses, 10% amplitude). Protein concentration was measured by Qubit™ assay (Invitrogen) and the samples were adjusted using 50 mM HEPES pH 7.5 to a protein concentration of 1.0 mg/mL and a volume of 400 µL. The pulldown experiment was performed as earlier described, with minor adjustments.<sup>39,45</sup> The lysates (400 µL) were subjected to a click reaction with freshly prepared click mix (43.7 µL per sample: 21.9 µL aq. 25 mM CuSO<sub>4</sub>, 13 µL aq. 250 mM NaAsc, 4.4 µL 25 mM THPTA in DMSO, 4.4 µL 2.25 mM biotin-N<sub>3</sub> in DMSO) at rt for 1 h. Proteins were precipitated by addition of HEPES buffer (50 µL, 50 mM, pH 7.5), MeOH (666 µL), CHCl<sub>3</sub> (166 µL) and MilliQ (150 µL), vortexing after each addition. After spinning down (1,500 g, 10 min) the upper and lower layer were aspirated and the protein pellet was resuspended in MeOH (600 µL) by sonication (Branson Sonifier probe sonicator, 10 x 0.5 s pulses, 10% amplitude). The proteins were spun down (20,000 g, 5 min) and the MeOH was aspirated. The proteins were redissolved in 6 M urea (500 µL) with 25 mM NH<sub>4</sub>HCO<sub>3</sub> for 15 min, followed by reduction (65 °C, 15 min, 800 rpm shaking) with DTT (5 µL, 1 M). The samples were allowed to reach rt and proteins were alkylated (30 min) with IAA (40 µL, 0.5 M) in the dark. 140 µL SDS (10% w/v) was added and the samples were spun down (1,000 g, 5 min). They were transferred to 5 mL PBS containing 50 µL avidin agarose resin (Pierce, 100 µL of a 50% slurry, prewashed twice with 6 mL PBS + 0.5% SDS and once with 6 mL PBS) and incubated for 2 h while rotating. The beads were spun down (2,000 g, 2 min) and washed (3 x PBS + 0.5% SDS, 2 x PBS, 1 x MilliQ). The beads were resuspended in digestion buffer (250 µL, 100 mM Tris pH 7.8, 100 mM NaCl, 1 mM CaCl<sub>2</sub>, 2% (v/v) acetonitrile, sequencing grade trypsin (Promega, 0.25 µg)) and transferred to low-binding tubes (Sarstedt) and incubated while shaking overnight (16 h, 37 °C, 1,000 rpm). Trypsin was quenched with 12.5 µL formic acid (LC-MS grade) and the beads were filtered off over a Bio-Spin column (BioRad, 400 g, 5 min), collecting the flow-through in a new 2 mL tube. Samples were added on C18 stagetips<sup>46</sup> (preconditioned with 50 µL MeOH, then 50 µL of 0.5% (v/v) formic acid in 80% (v/v) acetonitrile/MilliQ (solution B) and then 50 µL 0.5% (v/v) formic acid in MilliQ (solution A) by centrifugation (600 g, 2 min)). The peptides were washed with solution A (100 µL, 800 g, 3 min) and eluted into new low-binding tubes using solution B (100 µL, 800 g, 3 min). Samples were concentrated using an Eppendorf speedvac (Eppendorf Concentrator Plus 5301) and redissolved in LC-MS solution (30 µL per sample: 28.5 µL MilliQ, 2.85 µL acetonitrile, 0.095 µL formic acid, 600 fmol yeast enolase peptide digest (Waters, 186002325)).

Samples were measured using a NanoACQUITY UPLC System coupled to a SYNAPT G2-Si high definition mass spectrometer (Waters). The peptides were separated using an analytical column (HSS-T3 C18 1.8 µm, 75 µm x 250 mm, Waters) with a concave gradient (5 to 40% acetonitrile in H<sub>2</sub>O with 0.1% formic acid). [Glu<sup>1</sup>]-fibrinopeptide B was used as lock mass. Mass spectra were acquired using the UDMS<sup>e</sup> method. The mass range was set from 50 to 2,000 Da with a scan time of 0.6 seconds in positive, resolution mode. The collision energy was set to 4 V in the trap cell for low-energy MS mode. For the elevated energy scan, the transfer cell collision energy was ramped using drift-time-specific collision energies. The lock mass is sampled every 30 seconds. For raw data processing, Progenesis QI for proteomics was used with the following parameters to search the murine proteome from Uniprot (Table S1).

**Table S1 | Parameters used for Progenesis QI.**

Parameter	Value
Lock mass <i>m/z</i> value	785.8426
Low energy threshold	150 counts
Elevated energy threshold	30 counts
Digest reagent	Trypsin
Missed cleavages	Max 2
Modifications	Fixed carbamidomethyl C, variable oxidation M
FDR less than	1%
Minimum fragments/peptide	2
Minimum fragments/protein	5
Minimum peptides/protein	1
Minimum peptide score for quantification	5.5
Identified ion charges for quantification	2/3/4/5/6/7 <sup>+</sup>

### Activity-based protein profiling

To perform comparative ABPP, 39 µL of lysate (39 µg protein) was mixed with 1 µL of indicated compound (40X stock in DMSO) before probe addition. Final concentration of probes were 500 nM for FP-TAMRA and 2 µM for MB064. The probes were incubated for 30 min at rt before quenching the reaction with 4X Laemmli buffer for 30 min at rt. Labelled proteins were resolved by SDS-PAGE (10% acrylamide gel, ±80 min, 180 V) along with protein marker (PageRuler™ Plus, Thermo Fisher). In-gel fluorescence was measured in the Cy3- and Cy5-channel (Chemidoc™ MP, Bio-Rad) and the gels were subsequently stained with Coomassie and imaged as a loading control for normalization of fluorescence intensity. Band intensities were quantified using Image Lab 6.0.1 (BioRad).

### Lipidomics

A targeted analysis of 23 compounds, including endocannabinoids and related *N*-acylethanolamines (NAEs) and free fatty acids (Table S2), was measured using an Acquity UPLC I class binary solvent manager pump in conjugation with a tandem quadrupole mass spectrometer as mass analyzer (Waters Corporation). The separation was performed with an Acquity HSS T3 column (2.1 × 100 mm, 1.8 µm) maintained at 45 °C. The aqueous mobile phase A consisted of 2 mM ammonium formate and 10 mM formic acid, and the organic mobile phase B was acetonitrile. The flow rate was set to 0.55 mL/min; initial gradient conditions were 55% B held for 2 min and linearly ramped to 100% B over 6 min and held for 2 min; after 10 s the system returned to initial conditions and held 2 min before next injection. Electrospray ionization-MS and a selective Multiple Reaction Mode (sMRM) was used for lipid quantification. Individually optimized MRM transitions using their synthetic standards for target compounds and internal standards are described in Table S2. Peak area integration was performed with MassLynx 4.1 software (Waters Corporation). The obtained peak areas of targets were corrected by appropriate internal standards. Calculated response ratios, determined as the peak area ratios of the target analyte to the peak area of the respective internal standard, were used to obtain absolute concentrations from their respective calibration curves. Concentrations were normalized to the amount of protein in the sample as determined by Bradford assay.

**Table S2 | LC-MS standards and internal standards for lipidomics analysis.** The target list includes fatty acids, endocannabinoids, N-acylethanolamines (NAEs) and deuterated labeled internal standards. The compound ID is the abbreviation of metabolite name along with number of carbon atoms and number of double bonds in the fatty acid chain of the molecule, respectively. All compounds are analyzed in positive mode except fatty acids in negative mode. Q1 and Q3 are optimized precursor ion and product ion respectively, expressed as m/z. DP and CE are declustering potential (V) and collision energy (V).

<b>Standards</b>						
<b>Abbreviation</b>	<b>Metabolite</b>	<b>Q1</b>	<b>Q3</b>	<b>DP, CE</b>	<b>Polarity</b>	
<b>1 &amp; 2-AG (20:4)</b>	1-Arachidonoyl Glycerol	379.21	287.20	45, 10	+	
<b>2-LG (18:2)</b>	2-Linoleoyl Glycerol	357.34	247.50	48, 10	+	
<b>2-OG (18:1)</b>	2-Oleoyl Glycerol	357.34	247.50	40, 12	+	
<b>AEA (20:4)</b>	Arachidonoyl Ethanolamide	348.40	62.02	35, 16	+	
<b>DEA (22:4)</b>	Docosatetraenoyl Ethanolamide	376.38	61.92	55, 18	+	
<b>DGLEA (18:3)</b>	Dihomo-γ-Linolenoyl Ethanolamide	350.38	61.98	40, 14	+	
<b>DHEA (22:6)</b>	Docosahexaenoyl Ethanolamide	372.38	62.01	50, 14	+	
<b>EPEA (20:5)</b>	Eicosapentaenoyl Ethanolamide	346.34	61.98	36.16	+	
<b>LEA (18:2)</b>	Linoleoyl Ethanolamide	324.34	61.98	35, 14	+	
<b>OEA (18:1)</b>	Oleoyl Ethanolamide	326.4	62.01	45, 16	+	
<b>PDEA (15:0)</b>	Pentadecanoyl Ethanolamide	286.34	62.01	45, 12	+	
<b>PEA (16:0)</b>	Palmitoyl Ethanolamide	300.34	61.98	42, 14	+	
<b>POEA (16:1)</b>	Palmitoleoyl Ethanolamide	298.34	62.01	45, 14	+	
<b>SEA (18:0)</b>	Stearoyl Ethanolamide	328.38	61.98	45, 16	+	
<b>AA (20:4)</b>	Arachidonic Acid	302.28	259.30	-40, -12	-	
<b>PA (FA 16:0)</b>	Palmitic Acid	255.33	237.24	-50, -20	-	
<b>OA (FA 18:1)</b>	Oleic Acid	281.34	263.31	-50, -20	-	
<b>LA (FA 18:2)</b>	Linoleic Acid	279.34	261.25	-64, -16	-	
<b>GLA (FA 18:3)</b>	γ-Linolenic Acid	277.30	58.00	-60, -20	-	
<b>ETA (FA 20:3, (ω-3))</b>	Eicosatrienoic Acid	305.28	306.09	-60, -18	-	
<b>DGLA (FA 20:3, (ω-6))</b>	Dihomo-γ-Linolenic Acid (20:3)	305.28	306.03	-66, -18	-	
<b>EPA (FA 20:5,(ω-3))</b>	Eicosapentaenoic Acid	301.34	257.30	-60, -10	-	
<b>DHA (FA 22:6, (ω-3))</b>	Docosahexaenoic Acid	327.28	283.31	-60, -10	-	
<b>Internal standards</b>						
<b>Abbreviation</b>	<b>Metabolite</b>	<b>Q1</b>	<b>Q3</b>	<b>DP, CE</b>	<b>Polarity</b>	
<b>2-AG-d8 (20:4)</b>	2-Arachidonoyl Glycerol-d8	387.38	294.20	45, 10	+	
<b>AEA-d8 (20:4)</b>	Arachidonoyl Ethanolamide-d8	356.38	62.79	35, 16	+	
<b>DHEA-d4 (22:6)</b>	Docosahexaenoyl Ethanolamide-d4	376.38	66.01	50, 14	+	
<b>LEA-d4 (18:2)</b>	Linoleoyl Ethanolamide-d4	328.34	66.01	35, 16	+	
<b>OEA-d4 (18:1)</b>	Oleoyl Ethanolamide-d4	330.38	66.01	45, 16	+	
<b>PEA-d5 (16:0)</b>	Palmitoyl Ethanolamide-d5	305.34	61.98	42, 16	+	
<b>SEA-d3 (18:0)</b>	Stearoyl Ethanolamide-d3	331.38	61.91	45, 16	+	
<b>EPEA-d4 (20:5)</b>	Eicosapentaenoyl Ethanolamide-d4	350.34	66.08	36, 18	+	
<b>AA-d8 (20:4)</b>	Arachidonic Acid-d8	311.34	267.30	-40, -12	-	
<b>PA (16:0)-d31</b>	Palmitic Acid-d31	286.50	266.37	-40, -22	-	

## CRISPR/Cas9 KO generation

### Guide design & constructs

Two sgRNAs, in early exons of the *Vat1* and *Sccpdh* genes, with high efficiency and specificity as predicted by CHOPCHOP v2 online web tool were selected.<sup>47</sup> Guides were cloned into the *BbsI* restriction site of plasmid px330-U6-Chimeric\_BB-CBh-hSpCas9 (a kind gift from Feng Zhang, Addgene plasmid #42230) as previously described.<sup>48,49</sup> Primers are annotated in Table S3.

### CRISPR/Cas9-mediated knockout population generation

*Note: Neuro-2a cells display high level of heterogeneity upon clonal isolation.<sup>44</sup> To circumvent this issue, sequential transfections were used to generate a high efficiency knockout cell population.*

Neuro-2a cells were transfected sequentially (3 times within the course of 10 days) to yield populations with a high knockout efficiency. Cells were seeded at day 1, 4, and 7 and transfected at day 2, 5, and 8. Samples for T7E1 assays were harvested at day 4, 7, and 10 and after several weeks of culturing the cells. One day prior to the first transfection, Neuro-2a cells were seeded to a 6-well plate to reach 80% confluence at the time of transfection. Prior to transfection, culture medium was aspirated and 2 mL of fresh medium was added. A 5:1 (m/m) mixture of PEI (17.5 µg per well) and plasmid DNA (total 3.5 µg per well) was prepared in serum-free culture medium (250 µL each) and incubated (15 min, rt). Transfection was performed by dropwise addition of the PEI/DNA mixture to the cells. 24 h post-transfection the culture medium was refreshed. 48 h post-transfection a small amount of cells was harvested for analysis by T7E1 assay and ABPP, while the remainder was kept in culture under standard conditions for following transfections. After three transfection rounds, the cells were cultured according to standard protocol. Ampoules of knockdown populations were prepared (complete DMEM, 10% DMSO) and stored at -150 °C. Efficiency of knockdown was checked over time. Cells were discarded after 3 months of culture.

### T7E1 assay

Genomic DNA was obtained by mixing 50 µL QuickExtract™ (Epicentre) with cell pellet (~10% of a well from a 6-well plate). The samples were incubated at 65 °C for 6 min, mixed by vortexing and incubated at 98 °C for 2 min. Genomic DNA extracts were diluted in sterile water and directly used in PCR reactions. Genomic PCR reactions were performed on 5 µL isolated genomic DNA extract using Phusion High-Fidelity DNA Polymerase (Thermo Fisher) in Phusion GC buffer Green (Thermo Fisher) in a final volume of 45 µL, primers are annotated in Table S3.

For the T7E1 assay, genomic PCR products (20 µL) were denatured and reannealed in a thermocycler using the following program: 5 min at 95 °C, 95 to 85 °C using a ramp rate of -2 °C/s, 85 °C to 25 °C using a ramp rate of -0.2 °C/s. Annealed PCR product (8.5 µL) was mixed with NEB2 buffer (1 µL) and T7 endonuclease I (5 U, 0.5 µL; New England Biolabs), followed by a 30 min incubation at 37 °C. Digested PCR products were analyzed using agarose gel electrophoresis with ethidium bromide staining. A sample without T7 endonuclease I was taken along as control. Agarose gels were analyzed using Image Lab 6.0.1 (BioRad).

**Table S3 | sgRNA targets, sgRNA oligos (top, bottom) and T7E1 primers (forward, reverse).**

<b>sgRNA Target</b>	<b>Construct</b>	<b>Primer Sequences</b>
<b><i>Vat1</i> – Exon 1</b>	1162	Top: CACCGTTCGCAGCCCCCGACAGTCG Bottom: AAACCGACTGTCGGGGCTGCGAAC Forward: TCAGGGTACCTATCAGTCACACGACGTACAC Reverse: CCATGGGCCGTAGTCGGTCGTACAGCCCTT
	– Exon 2 1163	Top: CACCGAGACCGGGCATAGCGTCT Bottom: AAACAGACGCTATGGCCCGGTCTC Forward: TCAGGGTACCGCTGTGAGGACTGACTGAACAC Reverse: CCATGGGCCGTCTAAATGTTACCACGGCA
<b><i>Sccdph</i> – Exon 1</b>	1164	Top: CACCGAGGCCGAACACCAACAGG Bottom: AAACCTGGTGGTGGTACCGCCCTC Forward: TCAGGGTACCGCTTCAGGGGAACCAAGAG Reverse: CCATGGGCCCGCCGTGTTACCCAGTTCTG
	– Exon 2 1165	Top: CACCGTTACCGGTCTACGCAGTTG Bottom: AAACCAACTGCGTAGGACCGGTAAC Forward: TCAGGGTACCCCACACTGACCACATAGGCA Reverse: CCATGGGCCACTGAACAAAATTGTCGGGTT

### NAPE-PLD surrogate substrate-based fluorescence assay

The NAPE-PLD activity assay was performed according to a previously reported method with minor adjustments.<sup>50,51</sup> Purified recombinant MBP-tagged (N-terminal) and His<sub>6</sub>-tagged (C-terminal) human Δ47-NAPE-PLD from *Escherichia coli*, a kind gift from Dr. Piomelli, was diluted to 25 nM in assay buffer (50 mM Tris pH 7.5, 150 mM NaCl, 0.02% Triton X-100).<sup>52</sup> The substrate PED6 (Invitrogen, D23739, 1 mM stock in DMSO) was consecutively diluted in DMSO (5X) and in assay buffer (10X), to make a 20 μM working solution. Inhibitor solutions (50X) were prepared in DMSO. The assay was performed in a dark 96-well plate (flat bottom, Greiner), in a final volume of 50 μL. Inhibitor or DMSO was incubated with enzyme (2.5 nM final) for 30 min at 37 °C. Then, PED6 was added (2 μM final) and the measurement was started immediately on a CLARIOstar plate reader (BMG Labtech) at 37 °C (excitation 474–490 nm, emission 510–550 nm), scanning every 2 min for 1 hour. Negative control wells containing no enzyme were used for background subtraction. The measurements were performed in n = 4.

### Statistical analysis

Unless otherwise noted, all replicates represent biological replicates and all data represent means ± SEM. Statistical significance was determined using Student's t-tests (two-tailed, unpaired) or one-way ANOVA with Dunnett multiple comparisons correction. \*\*\* p <0.001; \*\* p <0.01; \* p <0.05; n.s. if p >0.05. All statistical analysis were conducted using Graphpad Prism 8.1.1 or Microsoft Excel.

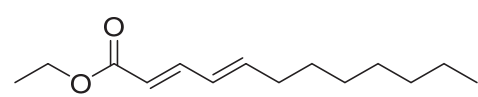
## Synthesis

### General remarks

Dry solvents were prepared by storage on activated 4 Å molecular sieves for at least 24 hours. The reactions were performed under an inert atmosphere of nitrogen gas unless stated otherwise. All reagents were purchased from Alfa Aesar, Sigma Aldrich/Merck or Acros and used without further purification. Flash column chromatography was performed using SiliCycle silica gel type SiliaFlash P60 (230-400 mesh). TLC analysis was performed on Merck silica gel 60/Kieselguhr F254, 0.25 mm. Compounds were visualized using KMnO<sub>4</sub> stain (K<sub>2</sub>CO<sub>3</sub> (40 g), KMnO<sub>4</sub> (6 g), and water (600 mL)).

<sup>1</sup>H NMR and <sup>13</sup>C NMR spectra were recorded on a Bruker AV-400 (400 MHz) or AV-500 (500 MHz) spectrometer. Chemical shift values are reported in ppm relative to the tetramethylsilane signal for <sup>1</sup>H NMR ( $\delta$  = 0 ppm) and relative to the solvent signal of CDCl<sub>3</sub> for <sup>13</sup>C NMR ( $\delta$  = 77.16 ppm). Data are reported as follows: Chemical shifts ( $\delta$ ), multiplicity (s = singlet, d = doublet, dd = doublet of doublets, ddt = doublet of doublet of triplets, td = triplet of doublets, t = triplet, q = quartet, p = pentet, bs = broad singlet, m = multiplet), coupling constants  $J$ (Hz), and integration. High resolution mass spectra (HRMS) were recorded by direct injection on a q-TOF mass spectrometer (Synapt G2-SI) equipped with an electrospray ion source in positive mode with Leu-enkephalin ( $m/z$  = 556.2771) as an internal lock mass. The instrument was calibrated prior to measurement using the MS/MS spectrum of [Glu<sup>1</sup>]-fibrinopeptide B.

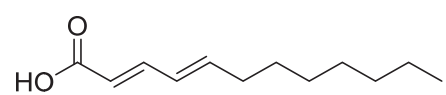
### Ethyl (2E,4E)-dodeca-2,4-dienoate (5)



To a cooled (0 °C) suspension of sodium hydride (0.518 g, 12.94 mmol) in dry THF (30 mL) was added a solution of ethyl 2-(diethoxyphosphoryl)acetate (2.90 g, 12.94 mmol in dry THF (10 mL)) dropwise and the reaction was stirred for 10 min. It was then cooled to -78 °C and a

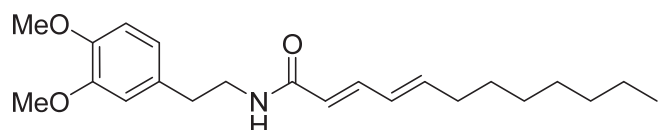
solution of (*E*)-dec-2-enal (1.98 mL, 10.8 mmol) in dry THF (10 mL) was added dropwise and the reaction was allowed to reach rt overnight. The reaction was quenched with water (150 mL) and the mixture was extracted with EtOAc (2 x 150 mL). The combined organic layers were washed with brine (100 mL), dried over MgSO<sub>4</sub>, filtered and concentrated under reduced pressure. Purification of the residue by column chromatography (pentane/Et<sub>2</sub>O = pentane to 9:1) afforded the title compound as a clear oil (1.5281 g, 6.81 mmol, 63%). R<sub>f</sub> = 0.4 (pentane/Et<sub>2</sub>O = 19:1); <sup>1</sup>H NMR (400 MHz, CDCl<sub>3</sub>)  $\delta$  7.35 – 7.19 (m, 1H), 6.23 – 6.06 (m, 2H), 5.78 (d,  $J$  = 15.4 Hz, 1H), 4.20 (q,  $J$  = 7.1 Hz, 2H), 2.16 (q,  $J$  = 7.1 Hz, 2H), 1.48 – 1.38 (m, 2H), 1.38 – 1.19 (m, 11H), 0.88 (t,  $J$  = 6.7 Hz, 3H); <sup>13</sup>C NMR (101 MHz, CDCl<sub>3</sub>)  $\delta$  167.48, 145.27, 144.96, 128.44, 119.25, 60.30, 33.14, 31.91, 29.28, 29.24, 28.85, 22.78, 14.46, 14.23. Spectra were consistent with previously reported data.<sup>31</sup>

### (2E,4E)-dodeca-2,4-dienoic acid (6)



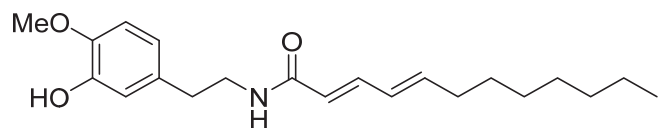
To a solution of ester **5** (1.514 g, 6.75 mmol) in MeOH (17 mL) was added 2 M aq. NaOH (6.75 mL, 13.50 mmol) and the reaction was stirred at 60 °C for 30 min. Solvent was removed under reduced pressure and the reaction was diluted with water

(10 mL), washed with Et<sub>2</sub>O (20 mL), acidified with 1 M aq. HCl to pH <4 and extracted with EtOAc (2 x 20 mL). The combined organic layers were washed with brine (20 mL), dried over MgSO<sub>4</sub>, filtered and concentrated under reduced pressure to afford the title compound as an off-white solid (1.324 g, 6.75 mmol, quant.). R<sub>f</sub> = 0.6 (pentane/EtOAc = 1:1 + 0.5% AcOH); <sup>1</sup>H NMR (400 MHz, CDCl<sub>3</sub>)  $\delta$  7.40 – 7.30 (m, 1H), 6.23 – 6.16 (m, 2H), 5.78 (d,  $J$  = 15.3 Hz, 1H), 2.23 – 2.13 (m, 2H), 1.48 – 1.39 (m, 2H), 1.37 – 1.19 (m, 8H), 0.87 (t,  $J$  = 6.7 Hz, 3H); <sup>13</sup>C NMR (101 MHz, CDCl<sub>3</sub>)  $\delta$  172.81, 147.77, 146.56, 128.33, 118.27, 33.22, 31.91, 29.29, 29.24, 28.76, 22.78, 14.24. Spectra were consistent with previously reported data.<sup>31</sup>

**(2E,4E)-N-(3,4-dimethoxyphenethyl)dodeca-2,4-dienamide (WOBE437, 1)**

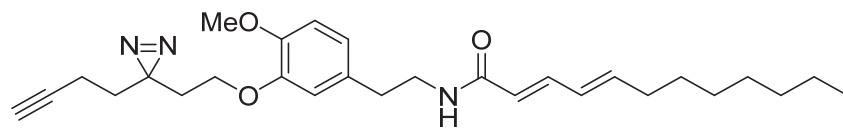
To a solution of carboxylic acid **6** (0.2500 g, 1.274 mmol) and 2-(3,4-dimethoxyphenyl)ethan-1-amine (0.254 g, 1.401 mmol) in DCM (2.5 mL) was added HOAt (0.087 g, 0.637 mmol) and EDC (0.293

g, 1.528 mmol) and the reaction was stirred for 45 min. Then, it was diluted with DCM (100 mL) and sat. aq. NaHCO<sub>3</sub> (100 mL). The layers were separated and the aq. layer was extracted with DCM (2 x 100 mL). The combined organic layers were dried over MgSO<sub>4</sub>, filtered and concentrated under reduced pressure. Purification of the residue by column chromatography (pentane/EtOAc = 1:4 to 1:1) afforded the title compound (WOBE437, **1**) as a white solid (0.3585 g, 0.997 mmol, 78%). R<sub>f</sub> = 0.5 (pentane/EtOAc = 1:1 + 0.5% AcOH); <sup>1</sup>H NMR (400 MHz, DMSO-*d*<sub>6</sub>) δ 8.00 (t, J = 5.7 Hz, 1H), 6.97 (dd, J = 15.1, 10.6 Hz, 1H), 6.85 (d, J = 8.2 Hz, 1H), 6.79 (d, J = 2.0 Hz, 1H), 6.70 (dd, J = 8.2, 2.0 Hz, 1H), 6.17 (dd, J = 15.2, 10.7 Hz, 1H), 6.06 (dt, J = 15.1, 6.7 Hz, 1H), 5.89 (d, J = 15.1 Hz, 1H), 3.72 (s, 3H), 3.70 (s, 3H), 3.33 – 3.28 (m, 2H), 2.66 (t, J = 7.3 Hz, 2H), 2.11 (q, J = 7.1 Hz, 2H), 1.43 – 1.32 (m, 2H), 1.32 – 1.17 (m, 8H), 0.89 – 0.82 (t, J = 6.7 Hz, 3H); <sup>13</sup>C NMR (101 MHz, DMSO) δ 165.21, 148.57, 147.20, 141.69, 139.12, 131.93, 128.60, 123.29, 120.42, 112.47, 111.83, 55.49, 55.34, 40.42, 34.72, 32.26, 31.25, 28.59, 28.53, 28.38, 22.10, 13.97. Spectra were consistent with previously reported data.<sup>31</sup>

**(2E,4E)-N-(3-hydroxy-4-methoxyphenethyl)dodeca-2,4-dienamide (7)**

To a cooled (0 °C) solution of 5-(2-aminoethyl)-2-methoxyphenol hydrochloride (0.0836 g, 0.408 mmol) in dry DMF (1.5 mL) was added carboxylic acid **6** (0.088 g, 0.449

mmol), EDC (0.094 g, 0.490 mmol), HOEt (0.066 g, 0.490 mmol) and Et<sub>3</sub>N (0.114 mL, 0.817 mmol) after which the reaction was allowed to reach rt. After 3 hours, the reaction was diluted with water (25 mL) and the mixture was extracted with Et<sub>2</sub>O (2 x 30 mL). The combined organic layers were washed with brine (4 x 10 mL), dried over Na<sub>2</sub>SO<sub>4</sub>, filtered and concentrated under reduced pressure. Purification of the residue by column chromatography (pentane/EtOAc/CHCl<sub>3</sub> = 4/1/2 + 0.5% AcOH to 2/1/1 + 0.5% AcOH) afforded the title compound as an off-white solid (0.0611 g, 0.177 mmol, 43%). R<sub>f</sub> = 0.5 (pentane/EtOAc/CHCl<sub>3</sub> = 2/2/1 + 0.5% AcOH); <sup>1</sup>H NMR (400 MHz, CDCl<sub>3</sub>) δ 7.19 (dd, J = 15.0, 10.0 Hz, 1H), 6.82 – 6.75 (m, 2H), 6.67 (dd, J = 8.1, 2.2 Hz, 1H), 6.12 – 6.03 (m, 2H), 5.68 (d, J = 15.0 Hz, 1H), 5.56 (bs, 1H), 3.87 (s, 3H), 3.56 (q, J = 6.6 Hz, 2H), 2.75 (t, J = 6.8 Hz, 2H), 2.17 – 2.12 (m, 2H), 1.47 – 1.35 (m, 2H), 1.35 – 1.21 (m, 8H), 0.88 (t, J = 6.4 Hz, 3H); <sup>13</sup>C NMR (101 MHz, CDCl<sub>3</sub>) δ 166.72, 145.82, 145.43, 143.74, 141.83, 132.19, 128.26, 121.47, 120.32, 115.01, 110.99, 56.12, 40.85, 35.09, 33.10, 31.90, 29.26, 29.23, 28.90, 22.77, 14.22. Spectra were consistent with previously reported data.<sup>31</sup>

**(2E,4E)-N-(3-(2-(3-(but-3-yn-1-yl)-3H-diazirin-3-yl)ethoxy)-4-methoxyphenethyl)dodeca-2,4-dienamide (pac-WOBE, 3)**

A solution of phenol **7** (16.8 mg, 0.049 mmol), 3-(but-3-yn-1-yl)-3-(2-iodoethyl)-3H-diazirine **8** (19.3 mg, 0.078

mmol) and K<sub>2</sub>CO<sub>3</sub> (13.4 mg, 0.097 mmol) in dry DMF (0.5 mL) was purged with N<sub>2</sub> and stirred at 60 °C overnight. The mixture was quenched with water (4 mL), extracted with Et<sub>2</sub>O (3 x 5 mL), dried over Na<sub>2</sub>SO<sub>4</sub>, filtered and concentrated under reduced pressure. Phenol **7** and the title compound were separated by column chromatography (MeOH/DCM = 1:1,000 to 1:100) and the recovered phenol **7** was dissolved in dry DMF (0.5 mL) with 3-(but-3-yn-1-yl)-3-(2-iodoethyl)-3H-diazirine **8** (19.3 mg, 0.078 mmol) and K<sub>2</sub>CO<sub>3</sub> (13.4 mg, 0.097 mmol), purged with N<sub>2</sub> and stirred at 60 °C overnight. The mixture was quenched with water (4 mL), extracted with Et<sub>2</sub>O (3 x 5 mL), dried over Na<sub>2</sub>SO<sub>4</sub> and concentrated under reduced pressure. It was combined with previously isolated title compound and purified with

## Chapter 6

column chromatography twice (pentane/EtOAc = 9:1 to 2:1 followed by MeOH/DCM = 1:1,000 to 1:100) to afford the title compound (pac-WOBE, **3**) as a white solid (0.0065 g, 0.014 mmol, 29%).  $R_f$  = 0.7 (pentane/EtOAc = 1:1 + 0.5% AcOH);  $^1\text{H}$  NMR (500 MHz,  $\text{CDCl}_3$ )  $\delta$  7.18 (dd,  $J$  = 15.0, 9.7 Hz, 1H), 6.82 (d,  $J$  = 8.2 Hz, 1H), 6.76 (dd,  $J$  = 8.1, 2.0 Hz, 1H), 6.71 (d,  $J$  = 2.0 Hz, 1H), 6.17 – 6.02 (m, 2H), 5.68 (d,  $J$  = 15.0 Hz, 1H), 5.43 (bs, 1H), 3.89 – 3.84 (m, 5H), 3.57 (q,  $J$  = 6.7 Hz, 2H), 2.78 (t,  $J$  = 6.9 Hz, 2H), 2.14 (q,  $J$  = 6.9 Hz, 2H), 2.09 (td,  $J$  = 7.6, 2.6 Hz, 2H), 1.98 (t,  $J$  = 2.7 Hz, 1H), 1.89 (t,  $J$  = 6.4 Hz, 2H), 1.76 (t,  $J$  = 7.6 Hz, 2H), 1.44 – 1.37 (m, 2H), 1.28 (m, 8H), 0.88 (t,  $J$  = 6.9 Hz, 3H);  $^{13}\text{C}$  NMR (126 MHz,  $\text{CDCl}_3$ )  $\delta$  166.45, 148.51, 148.22, 143.63, 141.67, 131.67, 128.30, 121.70, 121.63, 114.55, 112.36, 83.06, 69.20, 63.96, 56.26, 40.90, 35.31, 33.28, 33.11, 32.85, 31.92, 29.29, 29.25, 28.95, 26.86, 22.78, 14.23, 13.45. HRMS: Calculated for  $[\text{C}_{28}\text{H}_{39}\text{N}_3\text{O}_3+\text{H}]^+$  466.3064, found 466.3073.

## Supplementary data

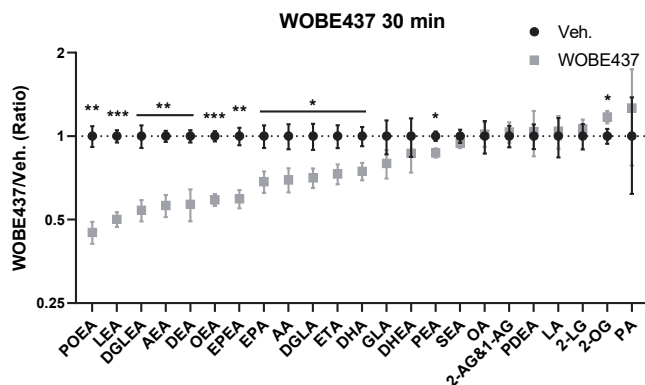


**Figure S1 | Lipid levels of Neuro-2a cells after 30 min of WOBE437 treatment corresponding to Figure 3.** Neuro-2a cells were treated with 10  $\mu$ M WOBE437 or vehicle and harvested after 30 min to be analyzed by MS-based lipidomics. Lipid levels are relative to vehicle-treated control. Data represent means  $\pm$  SEM ( $n = 4$ ), t-test with Benjamini-Hochberg correction: \*  $p < 0.05$ , \*\*  $p < 0.01$ , \*\*\*  $p < 0.001$ .

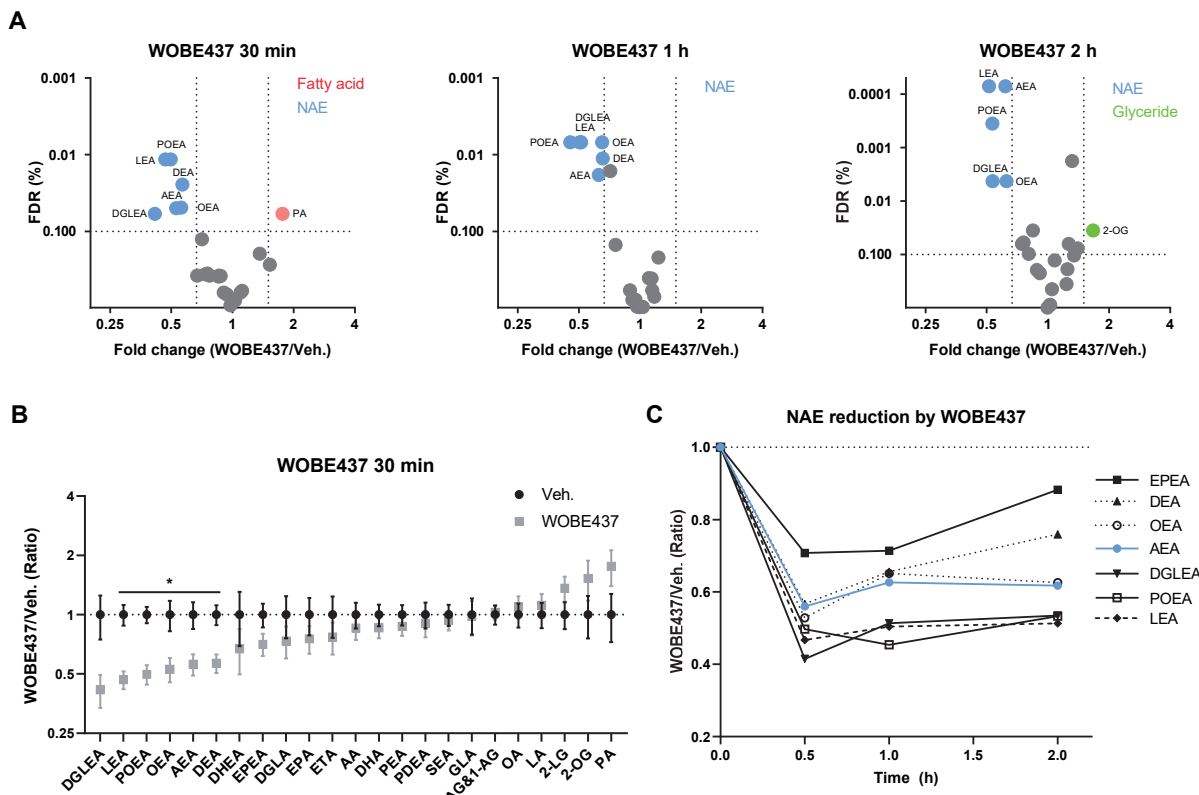


**Figure S2 | NAE disruption of WOBE437 on different passage of Neuro-2a.** Neuro-2a cells kept in culture for over 2.5 months were treated with 10  $\mu$ M WOBE437 or vehicle and harvested at the indicated time points to be analyzed by MS-based lipidomics. **(A)** Lipidomic data are presented as a volcano plot and lipids with a fold-change threshold of  $\geq 1.50$  or  $\leq 0.67$  and a Benjamini-Hochberg false-discovery rate (FDR)  $\leq 10\%$  are represented by colored circles indicating lipid class ( $n = 4$ ). **(B)** All ratios of measured lipids after 30 min of WOBE437 treatment. Lipid levels are relative to vehicle-treated control. Data represent means  $\pm$  SEM ( $n = 4$ ), t-test with Benjamini-Hochberg correction: \*  $p < 0.05$ . **(C)** Selected NAE ratios over time after WOBE437 incubation.

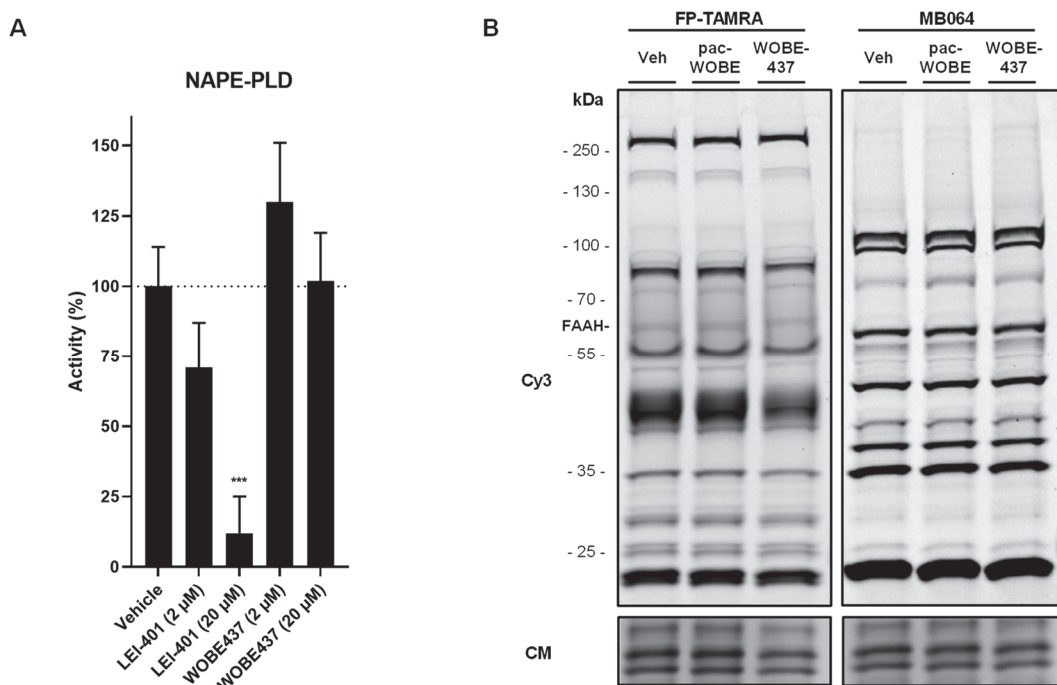


**Figure S3 | NAPE-PLD activity assay and serine hydrolase ABPP.** (A) Activity of recombinant human NAPE-PLD as tested in a PED6 surrogate substrate assay using LEI-401 as positive control.<sup>51</sup> Data represent means  $\pm$  SD ( $n = 4$ ), one-way ANOVA with Dunnett's multiple comparisons correction: \*\*\*  $p < 0.001$  in comparison to vehicle-treated control (Dotted line). (B) Neuro-2a lysate was preincubated with 10  $\mu$ M of indicated compound or vehicle followed by FP-TAMRA or MB064 after which the labeled proteins were resolved by SDS-PAGE and in-gel fluorescence was detected. Coomassie served as a protein loading control.

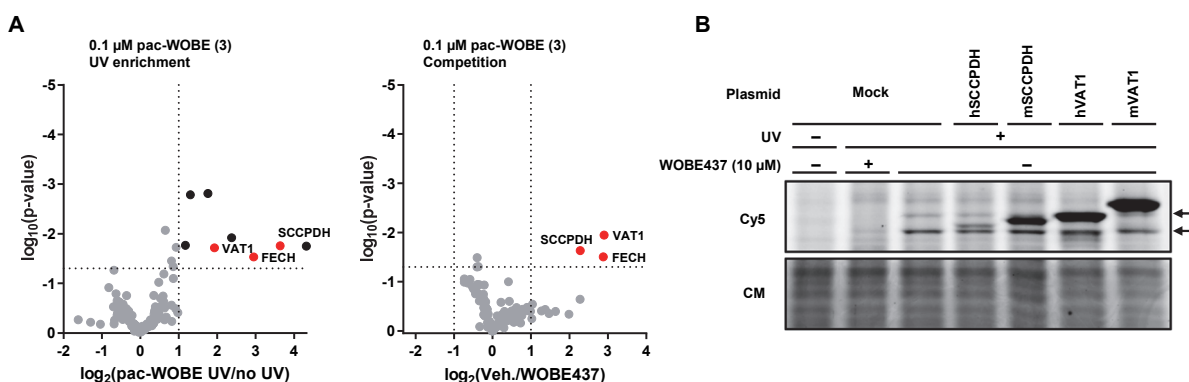


**Figure S4 | Pulldown and overexpression of pac-WOBE (3) targets in Neuro-2a.** (A) Volcano plots of pulldown experiment using 0.1  $\mu$ M pac-WOBE (3) and 10  $\mu$ M WOBE437 corresponding to Figure 5, Table S4. (B) Neuro-2a cells were transfected with indicated plasmid and treated with 10  $\mu$ M WOBE437 or vehicle and subsequently with 0.1  $\mu$ M pac-WOBE (3), irradiated, lysed and proteomes were conjugated to Cy5-N<sub>3</sub> using CuAAC chemistry and analyzed by SDS-PAGE and in-gel fluorescence scanning. Coomassie served as a protein loading control. Arrows indicate endogenous WOBE437 targets.

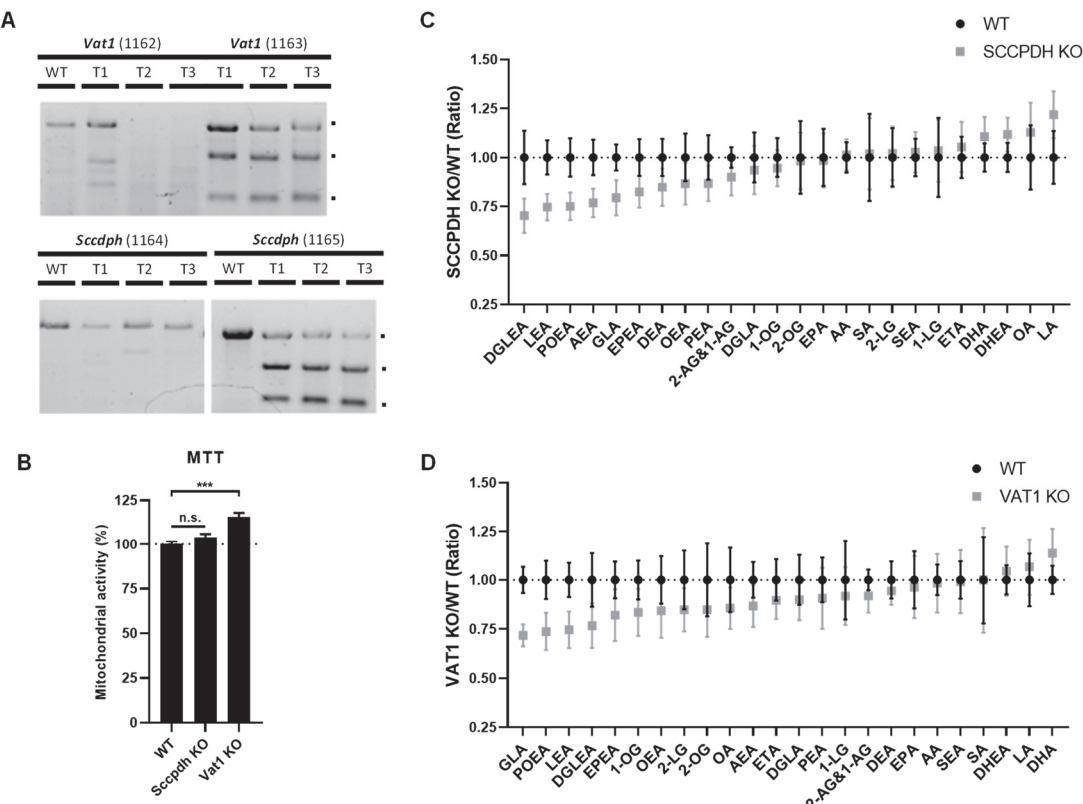


**Figure S5 | Characterization of CRISPR/Cas9-mediated knockouts in Neuro-2a.** **(A)** Knockout populations were generated by three sequential transfections (T1-T3) with Cas9 and two different separate guides for each target. Knockdown efficiency was determined by a T7E1 assay on genomic DNA, which was analyzed after each round of transfection for *Vat1* and *Sccdpdh* knockouts. **(B)**  $2.0 \times 10^5$  Neuro-2a cells were plated and after 24 h checked for mitochondrial activity by MTT assay. Values shown are mean mitochondrial activity relative to WT Neuro-2a  $\pm$  SEM ( $n = 6$ ), one-way ANOVA with Dunnett's multiple comparisons correction: \*\*\*  $p < 0.001$  in comparison to WT. **(C)** SCCPDH KO and **(D)** VAT1 KO lipid ratios corresponding to Figure 6. Lipid levels relative to WT Neuro-2a. Data represent means  $\pm$  SEM ( $n = 4$ ), t-test with Benjamini-Hochberg correction: not significant.

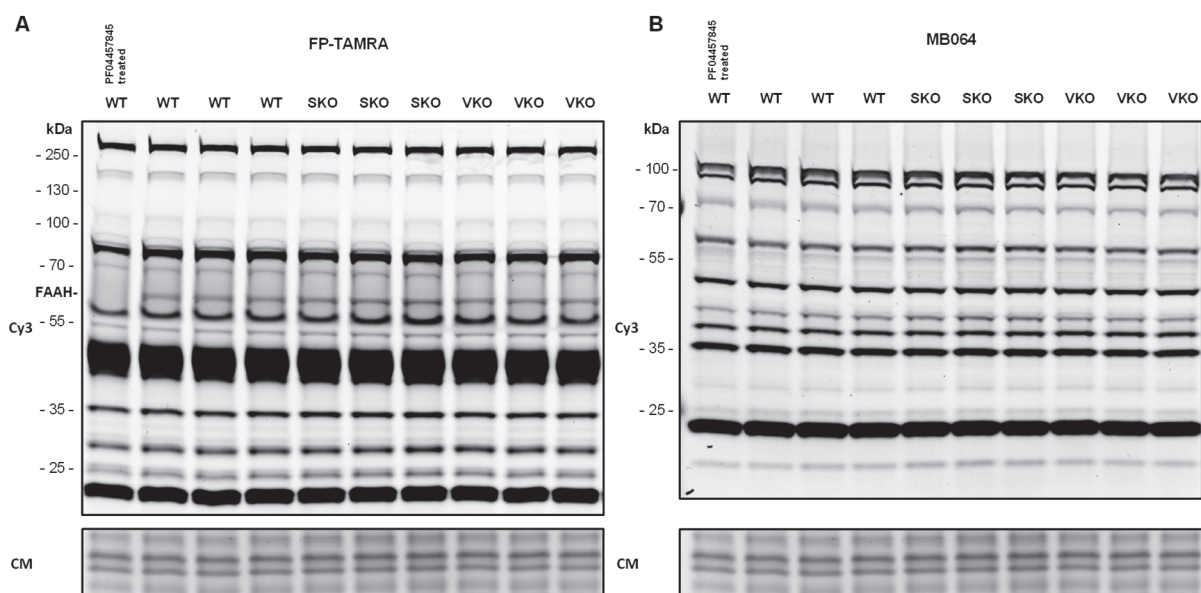


**Figure S6 | SCCPDH (SKO) or VAT1 (VKO) knockdown does not affect serine hydrolases labeled by FP-TAMRA or MB064.** Neuro-2a serine hydrolases were labeled with **(A)** FP-TAMRA or **(B)** MB064 in triplicate and the labeled proteins were resolved by SDS-PAGE and in-gel fluorescence was detected. Coomassie served as a protein loading control.

## Chapter 6

**Table S4 | All proteins significantly UV-enriched by 1 µM pac-WOBE (3).**

Gene name	Unique peptides	Description	1 µM pac-WOBE (3)				0.1 µM pac-WOBE (3)			
			UV/noUV	p-value	Veh/WOBE	p-value	UV/noUV	p-value	Veh/WOBE	p-value
TOMM22	3	Mitochondrial import receptor subunit TOM22 homolog	∞	0.0108	1.02	0.9209	995	0.0176	1.62	0.4054
SRPRB	5	Signal recognition particle receptor subunit beta	83.6	0.0354	0.56	0.2953	3.26	0.0832	1.00	0.9937
TIMM17B	3	Mitochondrial import inner membrane translocase subunit Tim17-B	72.3	0.0165	0.75	0.3197	5.18	0.0119	0.85	0.4630
<b>FECH</b>	<b>20</b>	<b>Ferrochelatase mitochondrial</b>	<b>68.9</b>	<b>0.0000</b>	<b>8.62</b>	<b>0.0000</b>	<b>7.71</b>	<b>0.0293</b>	<b>7.37</b>	<b>0.0310</b>
<b>VAT1</b>	<b>12</b>	<b>Synaptic vesicle membrane protein VAT-1 homolog</b>	<b>53.8</b>	<b>0.0272</b>	<b>5.44</b>	<b>0.0379</b>	<b>3.80</b>	<b>0.0191</b>	<b>7.48</b>	<b>0.0112</b>
HSD17B12	16	Very-long-chain 3-oxoacyl-CoA reductase	47.6	0.0084	1.01	0.9378	7.96	0.0794	1.42	0.3886
LSS	14	Lanosterol synthase	44.6	0.0210	1.13	0.5565	3.53	0.1759	1.40	0.5063
CYB5B	2	Cytochrome b5 type B	36.2	0.0246	0.79	0.6025	∞	0.3910	176. 1	0.3932
<b>SCCPDH</b>	<b>10</b>	<b>Saccharopine dehydrogenase-like oxidoreductase</b>	<b>30.5</b>	<b>0.0208</b>	<b>2.91</b>	<b>0.0308</b>	<b>12.5</b>	<b>0.0175</b>	<b>4.87</b>	<b>0.0230</b>
EMB	2	Emarginate	21.1	0.0042	0.67	0.2760	2.25	0.1379	1.20	0.5608
TMEM199	2	Transmembrane protein 199	20.5	0.0008	0.69	0.2993	2.16	0.3167	1.80	0.3856
PHB2	2	Prohibitin-2	18.6	0.0073	1.10	0.6037	4.83	0.3220	1.46	0.6590
PCYOX1	5	Prenylcysteine oxidase	17.5	0.0091	0.99	0.9770	2.46	0.0016	1.16	0.2582
TMEM33	7	Transmembrane protein 33	16.2	0.0082	0.83	0.3693	3.39	0.0015	0.92	0.6712
SGPL1	3	Sphingosine-1-phosphate lyase 1	15.8	0.0005	1.01	0.9108	1.41	0.4232	1.23	0.4534
EPHX1	3	Epoxide hydrolase 1	8.61	0.0178	0.74	0.4935	1.57	0.0084	0.94	0.6247
BSG	6	Basigin	8.08	0.0186	0.57	0.3377	1.81	0.0456	0.96	0.7915
IAP	17	IgE-binding protein	7.51	0.0018	0.59	0.2785	1.53	0.0647	0.75	0.1173
LRRC59	4	Leucine-rich repeat-containing protein 59	7.17	0.0081	0.80	0.5381	2.75	0.0655	1.19	0.4612
LBR	2	Lamin-B receptor	6.94	0.0045	0.66	0.3621	1.81	0.0792	0.94	0.6368
SEC61A1	2	Protein transport protein Sec61 subunit alpha isoform 1	6.88	0.0082	0.64	0.3321	2.04	0.1468	0.85	0.1786
TMX1	3	Thioredoxin-related transmembrane protein 1	6.69	0.0032	0.80	0.3149	3.17	0.0614	1.18	0.5139
RPN1	14	Dolichyl-diphosphooligosaccharide-protein glycosyltransferase subunit 1	6.31	0.0423	0.70	0.3664	1.75	0.0351	0.93	0.4492
VDAC1	12	Voltage-dependent anion-selective channel protein 1	6.00	0.0018	0.77	0.4955	1.53	0.2356	1.33	0.0992
ATP2A2	12	Sarcoplasmic/endoplasmic reticulum calcium ATPase 2	4.79	0.0115	0.71	0.2963	1.27	0.1740	0.96	0.7365
VDAC2	5	Voltage-dependent anion-selective channel protein 2	4.78	0.0086	0.73	0.4201	2.25	0.0170	0.95	0.7329
DHRS1	2	Dehydrogenase/reductase SDR family member 1	4.76	0.0059	1.46	0.1048	1.24	0.6531	2.06	0.2849
STT3A	5	Dolichyl-diphosphooligosaccharide-protein glycosyltransferase subunit STT3A	4.54	0.0049	0.79	0.3747	1.50	0.1787	0.77	0.0488
PDIA3	2	Protein disulfide-isomerase A3	4.54	0.0003	1.23	0.4045	3.01	0.3298	2.59	0.3620
RTN4	2	Reticulon-4	4.34	0.0439	0.88	0.4041	3.90	0.2232	1.51	0.5317
SLC25A3	8	Phosphate carrier protein mitochondrial	3.86	0.0224	0.81	0.5785	1.91	0.0187	0.96	0.6610
HSPA9	3	Stress-70 protein mitochondrial	3.63	0.0403	1.84	0.2066	4.36	0.2304	4.85	0.2252
VDAC3	5	Voltage-dependent anion-selective channel protein 3	3.39	0.0251	0.96	0.8860	1.39	0.0945	0.99	0.9584
RAB1A	2	Ras-related protein Rab-1A	3.14	0.0403	0.84	0.6040	1.29	0.3577	1.02	0.9054
ATP5F1B	6	ATP synthase subunit beta mitochondrial	2.81	0.0072	0.94	0.7622	2.76	0.3547	2.42	0.3870
HNRNPA1	2	Heterogeneous nuclear ribonucleoprotein A1	2.17	0.0329	1.71	0.2078	2.78	0.2948	1.98	0.3933
HSPD1	2	60 kDa heat shock protein mitochondrial	2.17	0.0465	0.90	0.7459	1.55	0.3124	1.01	0.9522
PRPH	5	Peripherin	2.10	0.0129	1.19	0.1558	1.75	0.2736	1.49	0.3740
UBA52	6	Ubiquitin-60S ribosomal protein L40	2.09	0.0108	0.72	0.2937	1.12	0.7069	0.96	0.7858

## References

- (1) Pacher, P.; Bátkai, S.; Kunos, G. The Endocannabinoid System as an Emerging Target of Pharmacotherapy. *Pharmacol. Rev.* **2006**, *58* (3), 389–462.
- (2) Mechoulam, R.; Parker, L. A. The Endocannabinoid System and the Brain. *Annu. Rev. Psychol.* **2013**, *64* (1), 21–47.
- (3) Centonze, D.; Finazzi-Agrò, A.; Bernardi, G.; Maccarrone, M. The Endocannabinoid System in Targeting Inflammatory Neurodegenerative Diseases. *Trends Pharmacol. Sci.* **2007**, *28* (4), 180–187.
- (4) Skaper, S. D.; Di Marzo, V. Endocannabinoids in Nervous System Health and Disease: The Big Picture in a Nutshell. *Philos. Trans. R. Soc. B Biol. Sci.* **2012**, *367* (1607), 3193–3200.
- (5) Klein, T. W. Cannabinoid-Based Drugs as Anti-Inflammatory Therapeutics. *Nat. Rev. Immunol.* **2005**, *5* (5), 400–411.
- (6) Pacher Pál; Mukhopadhyay Partha; Mohanraj Rajesh; Godlewski Grzegorz; Bátkai Sándor; Kunos George. Modulation of the Endocannabinoid System in Cardiovascular Disease. *Hypertension* **2008**, *52* (4), 601–607.
- (7) Steffens, S.; Pacher, P. Targeting Cannabinoid Receptor CB2 in Cardiovascular Disorders: Promises and Controversies. *Br. J. Pharmacol.* **2012**, *167* (2), 313–323.
- (8) Montecucco, F.; Di Marzo, V. At the Heart of the Matter: The Endocannabinoid System in Cardiovascular Function and Dysfunction. *Trends Pharmacol. Sci.* **2012**, *33* (6), 331–340.
- (9) Guindon, J.; Hohmann, A. G. Cannabinoid CB2 Receptors: A Therapeutic Target for the Treatment of Inflammatory and Neuropathic Pain. *Br. J. Pharmacol.* **2008**, *153* (2), 319–334.
- (10) Guindon, J.; Hohmann, A. G. The Endocannabinoid System and Pain. *CNS Neurol. Disord. Drug Targets* **2009**, *8* (6), 403–421.
- (11) Hillard, C. J.; Weinlander, K. M.; Stuhr, K. L. Contributions of Endocannabinoid Signaling to Psychiatric Disorders in Humans: Genetic and Biochemical Evidence. *Neuroscience* **2012**, *204*, 207–229.
- (12) Pacher, P.; Mechoulam, R. Is Lipid Signaling through Cannabinoid 2 Receptors Part of a Protective System? *Prog. Lipid Res.* **2011**, *50* (2), 193–211.
- (13) Pacher, P.; Kunos, G. Modulating the Endocannabinoid System in Human Health and Disease – Successes and Failures. *FEBS J.* **2013**, *280* (9), 1918–1943.
- (14) Marzo, V. D.; Bifulco, M.; Petrocellis, L. D. The Endocannabinoid System and Its Therapeutic Exploitation. *Nat. Rev. Drug Discov.* **2004**, *3* (9), 771–784.
- (15) Sandberg, A.; Fowler, C. J. Measurement of Saturable and Non-Saturable Components of Anandamide Uptake into P19 Embryonic Carcinoma Cells in the Presence of Fatty Acid-Free Bovine Serum Albumin. *Chem. Phys. Lipids* **2005**, *134* (2), 131–139.
- (16) Beltramo, M.; Stella, N.; Calignano, A.; Lin, S. Y.; Makriyannis, A.; Piomelli, D. Functional Role of High-Affinity Anandamide Transport, as Revealed by Selective Inhibition. *Science* **1997**, *277* (5329), 1094–1097.
- (17) Petrocellis, L. D.; Bisogno, T.; Davis, J. B.; Pertwee, R. G.; Marzo, V. D. Overlap between the Ligand Recognition Properties of the Anandamide Transporter and the VR1 Vanilloid Receptor: Inhibitors of Anandamide Uptake with Negligible Capsaicin-like Activity. *FEBS Lett.* **2000**, *483* (1), 52–56.
- (18) López-Rodríguez, M. L.; Viso, A.; Ortega-Gutiérrez, S.; Fowler, C. J.; Tiger, G.; de Lago, E.; Fernández-Ruiz, J.; Ramos, J. A. Design, Synthesis, and Biological Evaluation of New Inhibitors of the Endocannabinoid Uptake: Comparison with Effects on Fatty Acid Amidohydrolase. *J. Med. Chem.* **2003**, *46* (8), 1512–1522.
- (19) Ortar, G.; Ligresti, A.; De Petrocellis, L.; Morera, E.; Di Marzo, V. Novel Selective and Metabolically Stable Inhibitors of Anandamide Cellular Uptake. *Biochem. Pharmacol.* **2003**, *65* (9), 1473–1481.
- (20) Maccarrone, M. Metabolism of the Endocannabinoid Anandamide: Open Questions after 25 Years. *Front. Mol. Neurosci.* **2017**, *10*.
- (21) Deutsch, D. G. A Personal Retrospective: Elevating Anandamide (AEA) by Targeting Fatty Acid Amide Hydrolase (FAAH) and the Fatty Acid Binding Proteins (FABPs). *Front. Pharmacol.* **2016**, *7*.
- (22) Fowler, C. J. Anandamide Uptake Explained? *Trends Pharmacol. Sci.* **2012**, *33* (4), 181–185.
- (23) Nicolussi, S.; Gertsch, J. Chapter Fourteen - Endocannabinoid Transport Revisited. In *Vitamins & Hormones*; Litwack, G., Ed.; Hormones and Transport Systems; Academic Press, 2015; Vol. 98, pp 441–485.
- (24) Glaser, S. T.; Kaczocha, M.; Deutsch, D. G. Anandamide Transport: A Critical Review. *Life Sci.* **2005**, *77* (14), 1584–1604.
- (25) Glaser, S. T.; Abumrad, N. A.; Fatake, F.; Kaczocha, M.; Studholme, K. M.; Deutsch, D. G. Evidence against the Presence of an Anandamide Transporter. *Proc. Natl. Acad. Sci.* **2003**, *100* (7), 4269–4274.
- (26) Kaczocha, M.; Hermann, A.; Glaser, S. T.; Bojesen, I. N.; Deutsch, D. G. Anandamide Uptake Is Consistent with Rate-Limited Diffusion and Is Regulated by the Degree of Its Hydrolysis by Fatty Acid Amide Hydrolase. *J. Biol. Chem.* **2006**, *281* (14), 9066–9075.
- (27) Cravatt, B. F.; Giang, D. K.; Mayfield, S. P.; Boger, D. L.; Lerner, R. A.; Gilula, N. B. Molecular Characterization of an Enzyme That Degrades Neuromodulatory Fatty-Acid Amides. *Nature* **1996**, *384* (6604), 83–87.
- (28) Kaczocha, M.; Glaser, S. T.; Deutsch, D. G. Identification of Intracellular Carriers for the Endocannabinoid Anandamide. *Proc. Natl. Acad. Sci.* **2009**, *106* (15), 6375–6380.

## Chapter 6

- (29) Oddi, S.; Fezza, F.; Pasquariello, N.; D'Agostino, A.; Catanzaro, G.; De Simone, C.; Rapino, C.; Finazzi-Agrò, A.; Maccarrone, M. Molecular Identification of Albumin and Hsp70 as Cytosolic Anandamide-Binding Proteins. *Chem. Biol.* **2009**, *16* (6), 624–632.
- (30) Fu, J.; Bottegoni, G.; Sasso, O.; Bertorelli, R.; Rocchia, W.; Masetti, M.; Guijarro, A.; Lodola, A.; Armirotti, A.; Garau, G.; Bandiera, T.; Reggiani, A.; Mor, M.; Cavalli, A.; Piomelli, D. A Catalytically Silent FAAH-1 Variant Drives Anandamide Transport in Neurons. *Nat. Neurosci.* **2012**, *15* (1), 64–69.
- (31) Chicca, A.; Nicolussi, S.; Bartholomäus, R.; Blunder, M.; Rey, A. A.; Petrucci, V.; Reynoso-Moreno, I. del C.; Viveros-Paredes, J. M.; Gens, M. D.; Lutz, B.; Schiöth, H. B.; Soeberdt, M.; Abels, C.; Charles, R.-P.; Altmann, K.-H.; Gertsch, J. Chemical Probes to Potently and Selectively Inhibit Endocannabinoid Cellular Reuptake. *Proc. Natl. Acad. Sci.* **2017**, *114* (25), E5006–E5015.
- (32) Reynoso-Moreno, I.; Chicca, A.; Flores-Soto, M. E.; Viveros-Paredes, J. M.; Gertsch, J. The Endocannabinoid Reuptake Inhibitor WOBE437 Is Orally Bioavailable and Exerts Indirect Polypharmacological Effects via Different Endocannabinoid Receptors. *Front. Mol. Neurosci.* **2018**, *11*.
- (33) Maccarrone, M.; Fiorucci, L.; Erba, F.; Bari, M.; Finazzi-Agrò, A.; Ascoli, F. Human Mast Cells Take up and Hydrolyze Anandamide under the Control of 5-Lipoxygenase and Do Not Express Cannabinoid Receptors. *FEBS Lett.* **2000**, *468* (2–3), 176–180.
- (34) Lapinsky, D. J.; Johnson, D. S. Recent Developments and Applications of Clickable Photoprobes in Medicinal Chemistry and Chemical Biology. *Future Med. Chem.* **2015**, *7* (16), 2143–2171.
- (35) Hein, J. E.; Fokin, V. V. Copper-Catalyzed Azide-Alkyne Cycloaddition (CuAAC) and beyond: New Reactivity of Copper(I) Acetylides. *Chemical Society Reviews*. 2010, pp 1302–1315.
- (36) Fezza, F.; Oddi, S.; Tommaso, M. D.; Simone, C. D.; Rapino, C.; Pasquariello, N.; Dainese, E.; Finazzi-Agrò, A.; Maccarrone, M. Characterization of Biotin-Anandamide, a Novel Tool for the Visualization of Anandamide Accumulation. *J. Lipid Res.* **2008**, *49* (6), 1216–1223.
- (37) Baggelaar, M. P.; Janssen, F. J.; van Esbroeck, A. C. M.; den Dulk, H.; Allarà, M.; Hoogendoorn, S.; McGuire, R.; Florea, B. I.; Meeuwenhoord, N.; van den Elst, H.; van der Marel, G. A.; Brouwer, J.; Di Marzo, V.; Overkleeft, H. S.; van der Stelt, M. Development of an Activity-Based Probe and In Silico Design Reveal Highly Selective Inhibitors for Diacylglycerol Lipase- $\alpha$  in Brain. *Angew. Chem. Int. Ed.* **2013**, *52* (46), 12081–12085.
- (38) Li, Z.; Hao, P.; Li, L.; Tan, C. Y. J.; Cheng, X.; Chen, G. Y. J.; Sze, S. K.; Shen, H.-M.; Yao, S. Q. Design and Synthesis of Minimalist Terminal Alkyne-Containing Diazirine Photo-Crosslinkers and Their Incorporation into Kinase Inhibitors for Cell- and Tissue-Based Proteome Profiling. *Angew. Chem.* **2013**, *125* (33), 8713–8718.
- (39) van Rooden, E. J.; Florea, B. I.; Deng, H.; Baggelaar, M. P.; van Esbroeck, A. C. M.; Zhou, J.; Overkleeft, H. S.; van der Stelt, M. Mapping *in Vivo* Target Interaction Profiles of Covalent Inhibitors Using Chemical Proteomics with Label-Free Quantification. *Nat. Protoc.* **2018**, *13* (4), 752–767.
- (40) Klaeger, S.; Gohlke, B.; Perrin, J.; Gupta, V.; Heinzelmeir, S.; Helm, D.; Qiao, H.; Bergamini, G.; Handa, H.; Savitski, M. M.; Bantscheff, M.; Médard, G.; Preissner, R.; Kuster, B. Chemical Proteomics Reveals Ferrochelatase as a Common Off-Target of Kinase Inhibitors. *ACS Chem. Biol.* **2016**, *11* (5), 1245–1254.
- (41) Koenders, S. T. A.; Gagetein, B.; van der Stelt, M. Opportunities for Lipid-Based Probes in the Field of Immunology. In *Activity-Based Protein Profiling*; Cravatt, B. F., Hsu, K.-L., Weerapana, E., Eds.; Current Topics in Microbiology and Immunology; Springer International Publishing: Cham, 2019; pp 283–319.
- (42) Junker, M.; Rapoport, T. A. Involvement of VAT-1 in Phosphatidylserine Transfer from the Endoplasmic Reticulum to Mitochondria. *Traffic* **2015**, *16* (12), 1306–1317.
- (43) Faugaret, D.; Chouinard, F. C.; Harbour, D.; El azreq, M.-A.; Bourgoin, S. G. An Essential Role for Phospholipase D in the Recruitment of Vesicle Amine Transport Protein-1 to Membranes in Human Neutrophils. *Biochem. Pharmacol.* **2011**, *81* (1), 144–156.
- (44) Van Esbroeck, A. C. M.; Kantae, V.; Di, X.; van der Wel, T.; den Dulk, H.; Stevens, A. F.; Singh, S.; Bakker, A. T.; Florea, B. I.; Stella, N.; Overkleeft, H. S.; Hankemeier, T.; van der Stelt, M. Identification of  $\alpha,\beta$ -Hydrolase Domain Containing Protein 6 as a Diacylglycerol Lipase in Neuro-2a Cells. *Front. Mol. Neurosci.* **2019**, *12*, 286.
- (45) Soethoudt, M.; Stolze, S. C.; Westphal, M. V.; van Stralen, L.; Martella, A.; van Rooden, E. J.; Guba, W.; Varga, Z. V.; Deng, H.; van Kasteren, S. I.; Grether, U.; IJzerman, A. P.; Pacher, P.; Carreira, E. M.; Overkleeft, H. S.; Ioan-Facsinay, A.; Heitman, L. H.; van der Stelt, M. Selective Photoaffinity Probe That Enables Assessment of Cannabinoid CB2 Receptor Expression and Ligand Engagement in Human Cells. *J. Am. Chem. Soc.* **2018**, *140* (19), 6067–6075.
- (46) Rappaport, J.; Mann, M.; Ishihama, Y. Protocol for Micro-Purification, Enrichment, Pre-Fractionation and Storage of Peptides for Proteomics Using StageTips. *Nat. Protoc.* **2007**, *2* (8), 1896–1906.
- (47) Labun, K.; Montague, T. G.; Gagnon, J. A.; Thyme, S. B.; Valen, E. CHOPCHOP v2: A Web Tool for the next Generation of CRISPR Genome Engineering. *Nucleic Acids Res.* **2016**, *44*, 272–276.
- (48) Cong, L.; Ran, F. A.; Cox, D.; Lin, S.; Barretto, R.; Habib, N.; Hsu, P. D.; Wu, X.; Jiang, W.; Marraffini, L. A.; Zhang, F. Multiplex Genome Engineering Using CRISPR/Cas System. *Science* **2013**, *339* (February), 819–824.
- (49) Ran, F. A.; Hsu, P. D.; Wright, J.; Agarwala, V.; Scott, D. A.; Zhang, F. Genome Engineering Using the CRISPR-Cas9 System. *Nat. Protoc.* **2013**, *8* (11), 2281–2308.

Profiling the anandamide reuptake inhibitor WOBE437

- (50) Peppard, J. V.; Mehdi, S.; Li, Z.; Duguid, M. S. ASSAY METHODS FOR IDENTIFYING AGENTS THAT MODIFY THE ACTIVITY OF NAPE-PLD OR Abh4. US20100143937A1, June 10, 2010.
- (51) Mock, E. D.; Mustafa, M.; Gunduz-Cinar, O.; Cinar, R.; Petrie, G. N.; Kantae, V.; Di, X.; Ogasawara, D.; Varga, Z. V.; Paloczi, J.; Miliano, C.; Donvito, G.; van Esbroeck, A. C. M.; van der Gracht, A. M. F.; Kotsogianni, I.; Park, J. K.; Martella, A.; van der Wel, T.; Soethoudt, M.; Jiang, M.; Wendel, T. J.; Janssen, A. P. A.; Bakker, A. T.; Donovan, C. M.; Castillo, L. I.; Florea, B. I.; Wat, J.; van den Hurk, H.; Wittwer, M.; Grether, U.; Holmes, A.; van Boeckel, C. A. A.; Hankemeier, T.; Cravatt, B. F.; Buczynski, M. W.; Hill, M. N.; Pacher, P.; Lichtman, A. H.; van der Stelt, M. Discovery of a NAPE-PLD Inhibitor That Modulates Emotional Behavior in Mice. *Nat. Chem. Biol.* **2020**, 1–9.
- (52) Piomelli, D.; Magotti, P.; Bauer, I.; Igarashi, M.; Babagoli, M.; Marotta, R.; Garau, G. Structure of Human N -Acylphosphatidylethanolamine-Hydrolyzing Phospholipase D: Regulation of Fatty Acid Ethanolamide Biosynthesis by Bile Acids. *Structure* **2015**, 23 (3), 598–604.



# Chapter 7

## Cyclopropene probes for live-cell imaging of signaling lipids\*

### Introduction

Lipidomics is a relatively new discipline that studies cellular lipids on a large scale, which uses analytical chemistry principles and technological tools, particularly mass spectrometry.<sup>1</sup> Recent advances in mass spectrometry techniques have made it possible to detect and quantify many different lipid species in complex biological samples.<sup>1,2</sup> However, this approach generally requires sample homogenization followed by lipid extraction, and while bulk analysis gives valuable information on lipid biology, it does not allow for investigation of cellular localization. This spatial information is especially important in the case of lipid signaling molecules, which can be short-lived and have very localized functions.<sup>3</sup> Currently, detailed investigation of lipid signaling molecules is restricted by the availability of tools.

---

\*The data presented in this chapter was gathered in collaboration with Iakovia Ttofi, Dennis Strobbe, Alexi Sarris, Herman S. Overkleeft, Sander van Kasteren, Mario van der Stelt.

Some of the most well-studied lipid signaling molecules are the endocannabinoids anandamide (AEA) and 2-arachidonoyl glycerol (2-AG), which are derivatives of the polyunsaturated arachidonic acid (AA, 20:4 n-6, **1**) (Figure 1).<sup>4</sup> These endocannabinoids act as lipid messengers on the cannabinoid receptors to modulate various signal transduction pathways in the brain and immune system.<sup>5</sup> However, even for these well-investigated lipid signaling molecules, the mechanism of their biosynthesis, intercellular transport and cellular uptake is still unclear. The most widely accepted model states that AEA and 2-AG are not pre-synthesized and stored in vesicles, but produced “on demand” and excreted through an unknown mechanism.<sup>6</sup> The following step, cellular reuptake of endocannabinoids, is a highly debated topic,<sup>7–11</sup> and different models have been proposed.<sup>10</sup> Research on endocannabinoid signaling would benefit from tools to visualize localization and transport of these signaling lipids *in vivo* in real-time.

A common approach for the visualization of lipids is to append a fluorescent group like nitrobenzoxadiazole.<sup>12</sup> However, the fluorophore affects the properties of the lipid, which may alter its localization and signaling functions.<sup>13–15</sup> Therefore, recent efforts have focused on introduction of small bioorthogonal tags to allow the introduction of a visualization element when required. Azide and alkyne groups have been widely used for this purpose, as they can undergo copper(I)-catalyzed azide-alkyne cycloaddition (CuAAC),<sup>16</sup> strain-promoted azide-alkyne cycloaddition (SPAAC)<sup>17</sup> and Staudinger ligation<sup>18</sup> for functionalization. However, the copper catalyst required for CuAAC is incompatible with live cells,<sup>19</sup> SPAAC requires large strained alkynes and the Staudinger ligation has slow reaction kinetics.<sup>20</sup> Therefore, these approaches are less suitable to follow fast lipid signaling events in living cells.

There is an increased interest in the inverse electron-demand Diels-Alder (IEDDA) reaction, which uses electron-rich olefins like trans-cyclooctene (TCO) and tetrazine reagents, as an alternative bioorthogonal reaction to visualize rapid cellular processes.<sup>21,22</sup> IEDDA chemistry has fast reaction kinetics without the need for a catalyst, as well as the ability to use fluorogenic tetrazines. The fluorophore is unquenched upon conjugation of the tetrazine with a dienophile, which allows for real-time imaging of tagged molecules (Figure 1A).<sup>23</sup> To avoid using the moderately large TCO group as the dienophile, cyclopropenes have been investigated as an alternative olefin.<sup>24</sup> The reactive, strained nature of cyclopropenes provides the ability to participate in IEDDA reactions.<sup>25,26</sup> A number of differently substituted cyclopropenes, such as 1,3-substituted and 3,3-substituted variants, have been characterized for use in IEDDA chemistry, but not 1,2-substituted cyclopropenes.<sup>27,28</sup> In this chapter, the use of 1,2-substituted cyclopropene-tagged lipids for live-cell imaging is investigated, as well as the synthesis of a cyclopropene-tagged arachidonic acid for the investigation of AEA (Figure 1B).

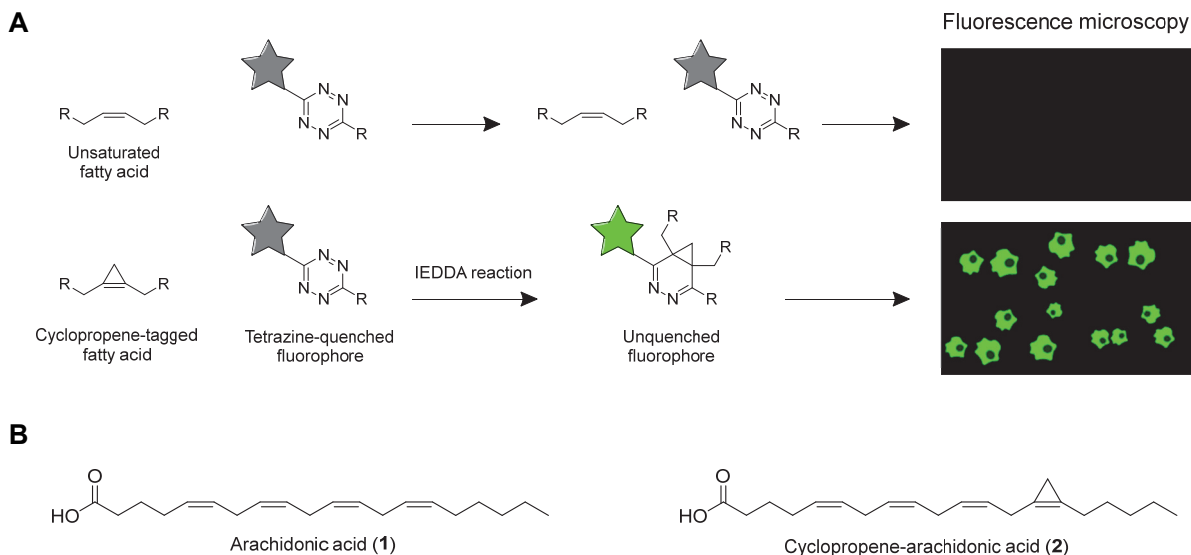


**Figure 1 | Cyclopropene lipids for live-cell imaging.** **(A)** Schematic representation of bioorthogonal labeling of cyclopropenes using tetrazine-quenched fluorophores. **(B)** Structure of arachidonic acid (**1**) and its cyclopropene analogue **2**.

## Results and discussion

To investigate 1,2-substituted cyclopropene lipids in live-cell imaging using IEDDA, commercially available sterculic acid (**3**) was used in tandem with oleic acid (**OA, 4**) as control (Figure 2). Sterculic acid is a cyclopropene lipid naturally found in plants such as *Sterculia foetida* and was first characterized in 1952<sup>29</sup> and synthesized in 1960.<sup>30</sup> Its suitability as dienophile in IEDDA reaction with tetrazine-quenched fluorophore **5** was tested in live cells.

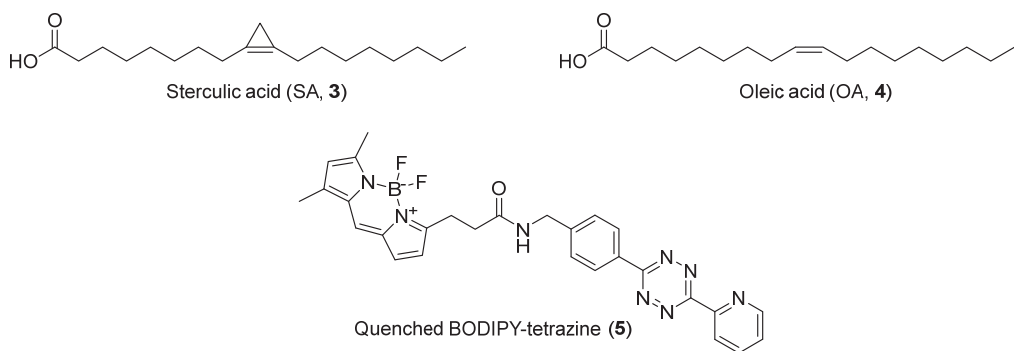


**Figure 2 |** Structures of oleic acid (**OA, 3**), sterculic acid (**SA, 4**) and BODIPY-tetrazine **5**.

U2OS cells were treated with OA (**4**) or SA (**3**) (50  $\mu$ M) for 1 h, washed and subsequently incubated with different concentrations of BODIPY-tetrazine **5** for 2 h. The cells were then washed extensively and analyzed by fluorescence microscopy (Figure 3). This resulted in dose-dependent labeling of sterculic acid with the BODIPY-tetrazine, indicating successful IEDDA reaction and unquenching. Little to no fluorescence was detected in oleic acid-treated cells. The fluorescent signal seemed to be focused on the endoplasmic reticulum (ER) as opposed to the cytoplasmic membrane, which can be explained by incorporation of the free fatty acids into phospholipids through Lands' cycle and the Kennedy pathway, which occurs mainly at the ER.<sup>31</sup>

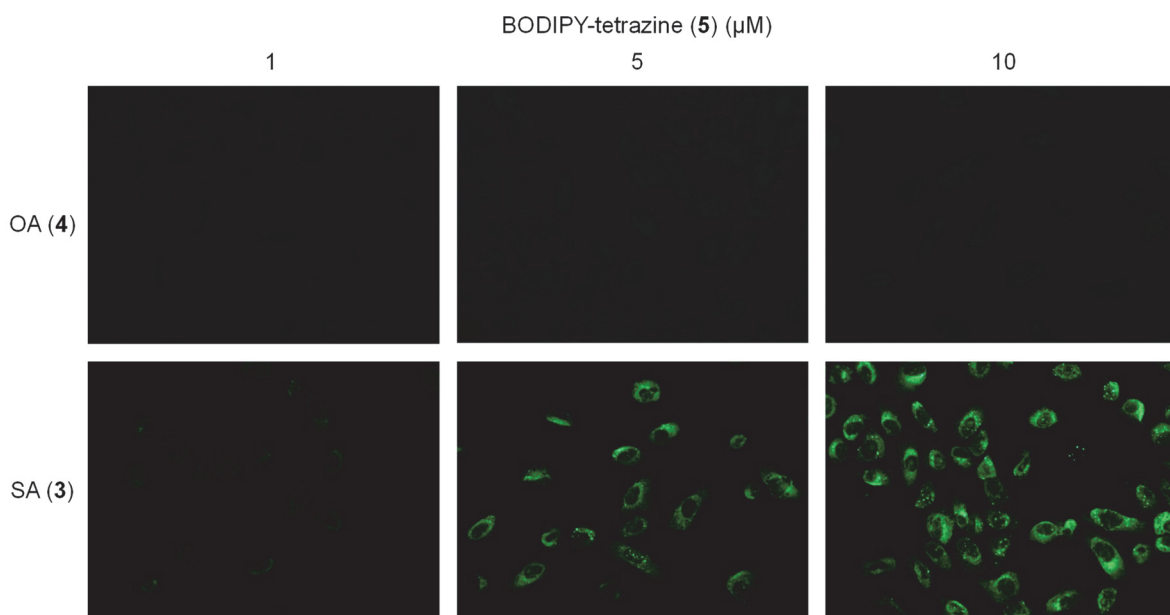


**Figure 3 | Sterculic acid is dose-dependently labeled by ligation to BODIPY-tetrazine **5** in live cells.** Live-cell image of U2OS cells incubated with indicated fatty acid (50  $\mu$ M) for 1 h, washed and incubated with indicated concentration of BODIPY-tetrazine for 2 h, then washed and imaged.

Next, the influence of incubation time with BODIPY-tetrazine **5** was investigated to survey the progression of the reaction. U2OS cells were treated with the lipids as before, incubated for indicated time with **5**, then washed and imaged (Figure 4). This revealed that after one hour, sufficient BODIPY-tetrazine had reacted to visualize sterculic acid in the cells. However, the reaction was not complete as indicated by increased fluorescence intensity after a longer incubation time. Whether the rate-limiting step in this process is the uptake of BODIPY-tetrazine **5** or the IEDDA reaction cannot be determined with this experiment, but the reaction between **3** and **5** seems to be facilitated by accumulation of both molecules in the membrane. These results indicated that 1,2-substituted cyclopropene lipids are suitable tools to visualize uptake and localization using IEDDA chemistry.

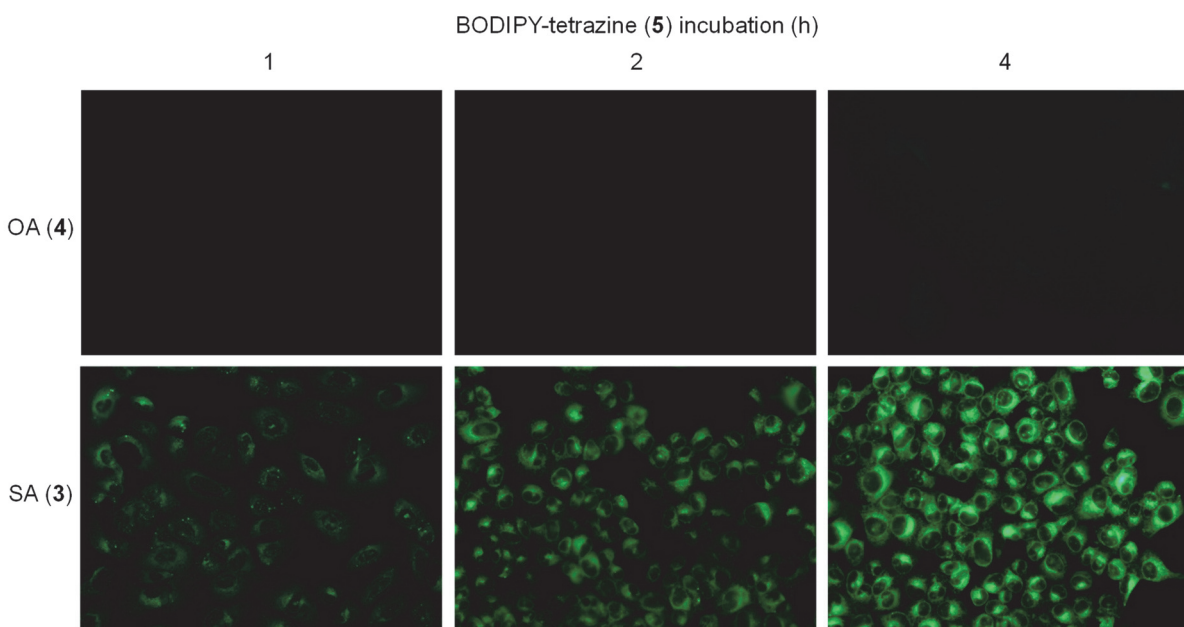
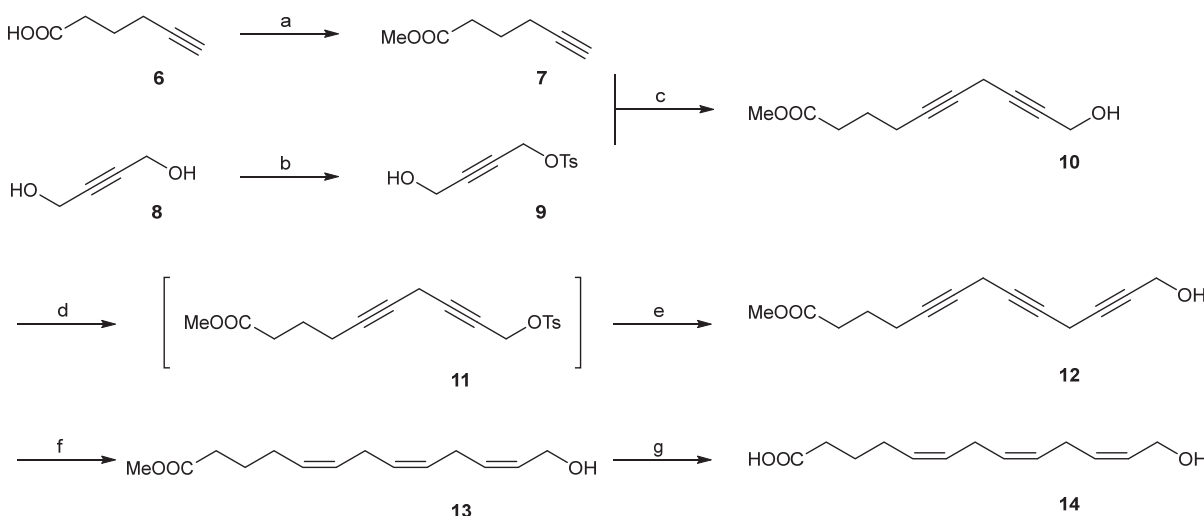


**Figure 4 | Sterculic acid reacts over time with BODIPY-tetrazine in live cells.** Live-cell image of U2OS cells incubated with indicated fatty acid ( $50 \mu\text{M}$ ) for 1 h, washed and incubated with of BODIPY-tetrazine ( $10 \mu\text{M}$ ) for indicated time, then washed and imaged.

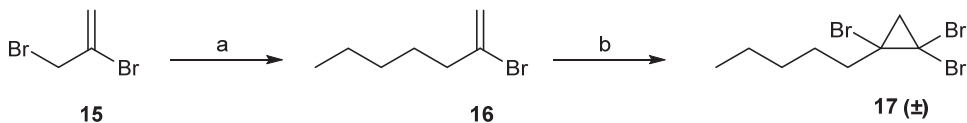
### Synthesis of cyclopropene-arachidonic acid **2**

In order to expand this approach to study the derivatives of arachidonic acid, cyclopropene-arachidonic acid was synthesized. To obtain the desired cyclopropene-arachidonic acid (**2**), two fragments were assembled and joined. For the first fragment, the three unmodified double bonds were generated by partial hydrogenation of skipped alkynes. The second fragment contained the cyclopropene which was introduced in the final step. The synthesis commenced with esterification of hex-5-ynoic acid (**6**) using acidic MeOH which afforded compound **7** in quantitative yield (Scheme 1). Then, but-2-yne-1,4-diol (**8**) was tosylated and purified by crystallization of disubstituted byproduct to obtain compound **9** in a yield of 56%. A copper-mediated cross-coupling between compounds **7** and **9** led to skipped alkyne **10** in a yield of 77%. Compound **10** was activated for further elongation via tosylation leading to unstable **11**. Subsequent cross-coupling of this sulfonate ester with prop-2-yn-1-ol afforded skipped alkyne **12** in a moderate yield of 32% over two steps. This was immediately partially hydrogenated using P-2 nickel boride catalyst<sup>32,33</sup> to obtain the more stable triene **13** in 46% yield, which was then saponified to obtain carboxylic acid **14** in 87% yield.



**Scheme 1 | Synthesis of (5Z,8Z,11Z)-13-hydroxytrideca-5,8,11-trienoic acid 14.** Reagents and conditions: (a)  $\text{SOCl}_2$ ,  $\text{MeOH}$ ,  $0^\circ\text{C}$  to rt, 16 h, quant.; (b) tosyl chloride, pyridine,  $\text{DCM}$ ,  $0^\circ\text{C}$  to  $10^\circ\text{C}$ , 2 h, 62%; (c)  $\text{CuI}$ ,  $\text{NaI}$ ,  $\text{K}_2\text{CO}_3$ ,  $\text{DMF}$ , rt, 16 h, 77%; (d) tosyl chloride, pyridine,  $\text{CHCl}_3$ ,  $0^\circ\text{C}$  to rt, 2 h; (e) prop-2-yn-1-ol,  $\text{CuI}$ ,  $\text{NaI}$ ,  $\text{K}_2\text{CO}_3$ ,  $\text{DMF}$ , rt, 16 h, 32% over two steps; (f)  $\text{H}_2$ ,  $\text{Ni}(\text{OAc})_2 \cdot 4\text{H}_2\text{O}$ ,  $\text{NaBH}_4$ , ethylenediamine,  $\text{EtOH}$ , rt, 4 h, 46%; (g) 1 M aq.  $\text{LiOH}$ ,  $\text{THF}$ , rt, 16 h, 87%.

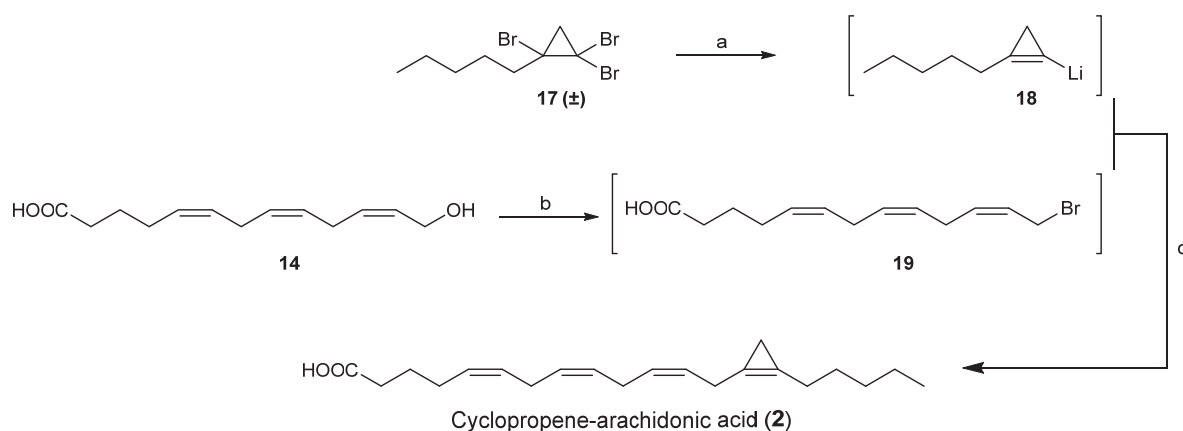
To obtain the cyclopropene fragment, 2,3-dibromopro-1-ene (**15**) was substituted by butylmagnesium bromide to obtain 2-bromohept-1-ene **16** in 69% yield after purification by distillation (Scheme 2). Cyclopropanation of **16** with dibromocarbene formed by deprotonation of bromoform was achieved under phase transfer conditions to afford the cyclopropane **17** in 36% yield.



**Scheme 2 | Synthesis of 1,1,2-tribromo-2-pentylcyclopropane 17.** Reagents and conditions: (a)  $\text{Mg}$ , 1,2-dibromoethane, 1-bromobutane,  $\text{Et}_2\text{O}$ , reflux, 15 min; then 2,3-dibromoprop-1-ene,  $\text{CuCl}$ ,  $\text{Et}_2\text{O}$ , reflux, 4 h, 79%; (b)  $\text{CHBr}_3$ , cetyltrimethylammonium bromide, aq.  $\text{NaOH}$  (50% w/v), rt, 16 h, 36%.

To complete the synthesis of the desired cyclopropene fatty acid **2**, two unstable intermediates were generated and conjoined (Scheme 3). Lithiocyclopropene **18** was formed by a 1,2-dihaloelimination followed by a metal-halogen exchange reaction using 2 equivalents of *n*-BuLi at  $-78^\circ\text{C}$  in dry  $\text{Et}_2\text{O}$ , leading to the intermediate nucleophile.<sup>34</sup> The electrophilic allyl bromide **19** was generated using *N*-bromosuccinimide (NBS) and dimethyl sulfide under mild conditions, but cyclized over time and had to be used immediately.

However, attempts to substitute allyl bromide **19** resulted mainly in intramolecular cyclization, due to high dilution of the reactants and poor nucleophilicity of lithiocyclopropene **18**.<sup>35</sup> As hexamethylphosphoramide (HMPA) is known to affect organolithium aggregates and increase their nucleophilicity when used as an additive,<sup>36</sup> the freshly formed solution of lithiocyclopropene **18** was concentrated to a reduced volume under a flow of nitrogen gas, and the electrophilic allyl bromide **19** was added as solution in HMPA. This resulted in conversion to the desired cyclopropene-arachidonic acid **2** which was obtained in a yield of 28% after purification as judged by mass. The purity was between 80-90% as estimated by <sup>1</sup>H NMR, but attempts at further purifications were unsuccessful and resulted in major loss of the product.



**Scheme 3 | Synthesis of cyclopropene-arachidonic acid (2).** Reagents and conditions: (a) *n*-BuLi, Et<sub>2</sub>O, -80 °C to rt, 25 min; (b) NBS, dimethyl sulfide, DCM, -25 °C to rt, 1 h; (c) HMPA, Et<sub>2</sub>O, 0 °C to rt, 15 min, 28%.

## Conclusion

In this chapter, the first use of 1,2-substituted cyclopropenes for live-cell imaging is reported. Plant-derived sterculic acid was compared to oleic acid and showed excellent fluorescent signal after reaction with tetrazine-quenched BODIPY **5**, whereas cells treated with oleic acid showed minimal background fluorescence. This demonstrates the possibility of substituting a fatty acid alkene for a cyclopropene to track lipid localization in live cells. Furthermore, the synthesis of a cyclopropene-tagged arachidonic acid is described which can be used to study arachidonic acid and its derivatives. However, the resulting cyclopropene proved to be unstable. Cyclopropenes are known to undergo ene reactions with alkenes, which could explain the tendency for degradation under solvent- and oxygen-free conditions observed for cyclopropene **2**.<sup>37,38</sup> It is recommended that further research on cyclopropene **2** minimizes the number of synthetic steps to obtain its derivatives. Nevertheless, as degradation products of the cyclopropene do not participate in the IEDDA reaction, cyclopropene-modified versions of arachidonic acid derivatives are in principle suitable for investigation of arachidonic acid and metabolites by microscopy.

## Experimental procedures

### General

Oleic acid (**3**, Cayman Chemicals) and steric acid (**4**, Matreya, SKU 1236) were stored as 10 mM DMSO solutions under nitrogen at -80 °C. BODIPY-tetrazine **5** was a kind gift from Alexi Sarris (Leiden University) and stored as 10 mM DMSO solution at -20 °C. All cell culture disposables were from Sarstedt.

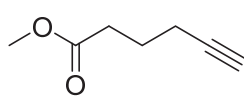
### Cell culture and imaging

U2OS cells were cultured at 37 °C under 7% CO<sub>2</sub> in DMEM (Sigma Aldrich, D1145) containing stable glutamine, 10% (v/v) New Born Calf Serum (Thermo Fisher) and penicillin and streptomycin (200 µg/mL each, Duchefa). Cells were passaged twice a week at 80-90% confluence by trypsinization and resuspension in fresh medium. Cell lines were purchased from ATCC and were tested regularly for mycoplasma contamination. Cultures were discarded after 2-3 months of use.

2.0x10<sup>4</sup> U2OS cells were plated in 12-well plates 24 h prior to microscopy experiments. Cells were treated with 600 µL of 50 µM oleic acid (**3**) or steric acid (**4**) in phenol red free DMEM with serum for 1 h at 37 °C under 7% CO<sub>2</sub>. The medium was aspirated, cells were washed twice with PBS and treated with tetrazine-BODIPY (**5**) in phenol red free DMEM with serum for the indicated incubation time at 37 °C under 7% CO<sub>2</sub>. Medium was aspirated, cells were washed three times with PBS and 600 µL of PBS was added for imaging, which was done using a EVOS M7000 Imaging System (Thermo Fisher).

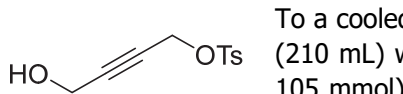
### Synthesis

Dry solvents were prepared by storage on activated 4 Å molecular sieves for at least 24 h. The reactions were performed under an inert atmosphere of nitrogen gas unless stated otherwise. All reagents were purchased from Alfa Aesar, Sigma Aldrich/Merck or Acros and used without further purification. Flash column chromatography was performed using SiliCycle silica gel type SiliaFlash P60 (230-400 mesh). TLC analysis was performed on Merck silica gel 60/Kieselguhr F254, 0.25 mm. Compounds were visualized using KMnO<sub>4</sub> stain (K<sub>2</sub>CO<sub>3</sub> (40g), KMnO<sub>4</sub> (6 g), and water (600 mL)). <sup>1</sup>H NMR and <sup>13</sup>C NMR spectra were recorded on a Bruker AV-400 (400 MHz) or AV-500 (500 MHz) spectrometer. Chemical shift values are reported in ppm relative to the tetramethylsilane signal for <sup>1</sup>H NMR ( $\delta$  = 0 ppm) and relative to the solvent signal of CDCl<sub>3</sub> for <sup>13</sup>C NMR ( $\delta$  = 77.16 ppm). Data are reported as follows: Chemical shifts ( $\delta$ ), multiplicity (s = singlet, d = doublet, dd = doublet of doublets, ddt = doublet of doublet of triplets, td = triplet of doublets, t = triplet, q = quartet, p = pentet, bs = broad singlet, m = multiplet), coupling constants *J* (Hz), and integration. High-resolution mass spectra (HRMS) were recorded on a Thermo Scientific Q Exactive HF Orbitrap Mass Spectrometer equipped with an electrospray ion source in positive mode (source voltage 3.5 kV, sheath gas low 10, capillary temperature 275 °C) with resolution R = 60,000 at m/z = 400 (mass range = 150-1,500).

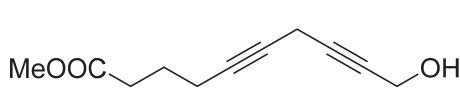
**Methyl hex-5-ynoate (7)**

To a cooled (0 °C) solution of hex-5-ynoic acid (5.19 g, 46.3 mmol) in dry MeOH (160 mL) was added thionyl chloride (3.70 mL, 50.9 mmol) dropwise over 10 min under vigorous stirring and the reaction was allowed to reach rt overnight.

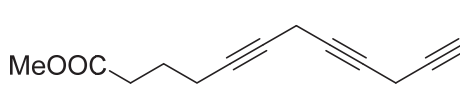
The reaction was diluted with DCM (250 mL) and quenched with sat. aq. NaHCO<sub>3</sub> (300 mL). The layers were separated and the aq. layer was extracted with DCM (2 x 250 mL). The combined organic layers were dried over MgSO<sub>4</sub>, filtered and concentrated under reduced pressure to afford the title compound as a pale yellow oil (5.82 g, 46.3 mmol, quant.). R<sub>f</sub> = 0.7 (Et<sub>2</sub>O/pentane = 1:3). <sup>1</sup>H NMR (400 MHz, CDCl<sub>3</sub>) δ 3.68 (s, 3H), 2.46 (t, J = 7.4 Hz, 2H), 2.26 (td, J = 6.9, 2.6 Hz, 2H), 1.97 (t, J = 2.6 Hz, 1H), 1.91 – 1.79 (m, 2H). <sup>13</sup>C NMR (101 MHz, CDCl<sub>3</sub>) δ 173.67, 83.38, 69.25, 51.74, 32.78, 23.72, 17.98. HRMS: Calculated for [C<sub>7</sub>H<sub>10</sub>O<sub>2</sub>+H]<sup>+</sup> 127.0754, found 127.0755.

**4-Hydroxybut-2-yn-1-yl 4-methylbenzenesulfonate (9)**

To a cooled (0 °C) solution of 2-butyne-1,4-diol (10.0 g, 116 mmol) in dry DCM (210 mL) was added pyridine (18.9 mL, 232 mmol) and tosyl chloride (20.0 g, 105 mmol) in small portions over a period of 10 min. The reaction was stirred for 1 h and then at 10 °C for 1 h. The mixture was diluted with H<sub>2</sub>O (100 mL) and 3 M aq. HCl was added until acidic (pH < 2). The layers were separated and the organic layer was washed with 1 M aq. HCl (120 mL) and brine (60 mL). The organic layer was dried over MgSO<sub>4</sub>, filtered and concentrated under reduced pressure. The mixture was dissolved in hot MeOH (50 mL) and cooled to -30 °C overnight. The mixture was filtered and rinsed with ice-cold MeOH (30 mL). The filtrate was concentrated under reduced pressure to afford the title compound as a yellow oil (15.7 g, 65.3 mmol 62%). R<sub>f</sub> = 0.6 (pentane/EtOAc = 1:1). <sup>1</sup>H NMR (400 MHz, CDCl<sub>3</sub>) δ 7.81 (d, J = 8.3 Hz, 2H), 7.39 – 7.32 (d, J = 7.8 Hz, 2H), 4.73 (t, J = 1.8 Hz, 2H), 4.16 (t, J = 1.9 Hz, 2H), 2.45 (s, 3H), 1.92 (bs, 1H). <sup>13</sup>C NMR (101 MHz, CDCl<sub>3</sub>) δ 129.98, 129.97, 128.30, 128.29, 57.99, 50.86, 21.81. HRMS: Calculated for [C<sub>11</sub>H<sub>12</sub>O<sub>4</sub>S+NH<sub>4</sub>]<sup>+</sup> 258.0795, found 258.0791.

**Methyl 10-hydroxydeca-5,8-dienoate (10)**

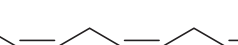
To a mixture of CuI (1.095 g, 10.00 mmol), NaI (1.499 g, 10.00 mmol) and K<sub>2</sub>CO<sub>3</sub> (1.383 g, 10.00 mmol) was added nitrogen-purged DMF (20 mL) and the mixture was stirred for 15 min. Then, methyl hex-5-ynoate **7** (1.262 g, 10 mmol) dissolved in nitrogen-purged DMF (5 mL) was added to the reaction mixture. Sulfonate ester **9** (2.64 g, 11.0 mmol) dissolved in nitrogen-purged DMF (5 mL) was added dropwise to the reaction over 10 min and the reaction was stirred overnight in the dark. The reaction was diluted in Et<sub>2</sub>O (50 mL), cooled to 0 °C and quenched with sat. aq. NH<sub>4</sub>Cl (2.0 mL). It was stirred at room temperature for 30 min, followed by gravity filtration over a celite/sand pad. The pad was rinsed with Et<sub>2</sub>O (1 L) and the filtrate was concentrated under reduced pressure to a reduced volume (100 mL). The organic layer was washed with sat. aq. NH<sub>4</sub>Cl (10 mL) and H<sub>2</sub>O (50 mL). The aqueous layer was extracted with Et<sub>2</sub>O (3 x 100 mL) and the combined organic layers were washed with brine (5 x 200 mL), dried over MgSO<sub>4</sub>, filtered and concentrated under reduced pressure. Purification of the residue by column chromatography (Et<sub>2</sub>O/pentane = 1:9 to Et<sub>2</sub>O) afforded the title compound as a yellow oil (1.50 g, 7.74 mmol, 77%). R<sub>f</sub> = 0.3 (Et<sub>2</sub>O/pentane = 1:1). <sup>1</sup>H NMR (400 MHz, CDCl<sub>3</sub>) δ 4.25 (t, J = 2.1 Hz, 2H), 3.67 (s, 3H), 3.22 – 3.13 (m, 2H), 2.43 (t, J = 7.5, 2H), 2.23 (tt, J = 6.9, 2.3 Hz, 2H), 1.90 – 1.74 (m, 2H). <sup>13</sup>C NMR (101 MHz, CDCl<sub>3</sub>) δ 173.84, 80.64, 79.89, 78.66, 74.57, 51.77, 51.34, 32.99, 23.90, 18.27, 9.95. HRMS: Calculated for [C<sub>11</sub>H<sub>14</sub>O<sub>3</sub>+H]<sup>+</sup> 195.1016, found 195.1019.

**Methyl 13-hydroxytrideca-5,8,11-triynoate (12)**

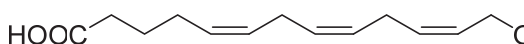
To a cooled (0 °C) solution of alcohol **10** (4.822 g, 24.83 mmol) in CHCl<sub>3</sub> (50 mL) was added pyridine (6.02 mL, 74.5 mmol) and subsequently tosyl chloride (9.47 g, 49.7 mmol) in portions over 15 min. The reaction was stirred at rt for 2 h. The reaction mixture was then cooled to 0 °C and diluted with Et<sub>2</sub>O (150 mL) and H<sub>2</sub>O (80 mL). The layers were separated

and the organic layer was washed with 1 M aq. HCl (80 mL), sat. aq. NaHCO<sub>3</sub> (80 mL) and brine (2 x 80 mL), dried over MgSO<sub>4</sub>, filtered and concentrated under reduced pressure. Column chromatography of the residue (Et<sub>2</sub>O/pentane = 1:9 to Et<sub>2</sub>O) afforded sulfonate ester **11**, which was used immediately due to its instability. To a mixture of CuI (4.73 g, 24.8 mmol), NaI (3.72 g, 24.8 mmol) and K<sub>2</sub>CO<sub>3</sub> (3.43 g, 24.8 mmol) was added nitrogen-purged DMF (25 mL) and the mixture was stirred for 15 min. Prop-2-yn-1-ol (1.67 g, 29.8 mmol) dissolved in nitrogen-purged DMF (20 mL) was added and the mixture was stirred for 30 min. A solution of sulfonate ester **11** in nitrogen-purged DMF (30 mL) was added to the reaction dropwise over 10 min and the reaction was stirred overnight in the dark. It was then diluted with Et<sub>2</sub>O (80 mL), quenched with sat. aq. NH<sub>4</sub>Cl (6 mL) and stirred for 30 min at rt. The mixture was filtered over celite and the filter was rinsed with Et<sub>2</sub>O (1 L). The filtrate was concentrated under reduced pressure to a reduced volume (100 mL). The organic layer was washed with sat. aq. NH<sub>4</sub>Cl (30 mL) and H<sub>2</sub>O (100 mL). The combined aqueous layers were extracted with Et<sub>2</sub>O (3 x 150 mL) and the combined organic layers were washed with brine (5 x 100 mL), dried over MgSO<sub>4</sub>, filtered and concentrated under reduced pressure. Purification of the residue by column chromatography (Et<sub>2</sub>O/pentane = 1:4 to 2:1) afforded the title compound as an orange oil (1.85 g, 7.97 mmol, 32%). R<sub>f</sub> = 0.5 (Et<sub>2</sub>O/pentane = 1:1). <sup>1</sup>H NMR (400 MHz, CDCl<sub>3</sub>) δ 4.26 (t, J = 2.1 Hz, 2H), 3.68 (s, 3H), 3.20 (p, J = 2.3 Hz, 2H), 3.12 (p, J = 2.4 Hz, 2H), 2.44 (t, J = 7.5 Hz, 2H), 2.23 (tt, J = 6.9, 2.4 Hz, 2H), 1.87 – 1.76 (p, J = 7.6 Hz, 2H), 1.68 (bs, 1H). <sup>13</sup>C NMR (101 MHz, CDCl<sub>3</sub>) δ 173.87, 79.73, 78.88, 75.78, 75.45, 74.81, 73.97, 51.76, 51.38, 33.01, 23.95, 18.31, 10.03, 9.88. HRMS: Calculated for [C<sub>14</sub>H<sub>16</sub>O<sub>3</sub>+H]<sup>+</sup> 233.1172, found 233.1176.

### Methyl (5Z,8Z,11Z)-13-hydroxytrideca-5,8,11-trienoate (13)

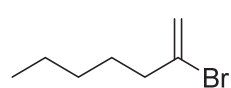
In a Schlenk flask, nickel acetate hydrate (0.214 g, MeOOCOH 0.861 mmol) and 96% EtOH (7 mL) were placed under H<sub>2</sub> atmosphere. Sodium borohydride (0.033 g, 0.861 mmol) in 96% EtOH (2 mL) was added over 40 s and stirred at room temperature for 20 min. Freshly distilled ethylenediamine (0.174 mL, 2.58 mmol) was added and the reaction was stirred for 10 min. Compound **12** (0.50 g, 2.15 mmol) in 96% EtOH (3 mL) was added and the reaction was stirred under H<sub>2</sub> atmosphere for 5 h. The reaction was then quenched with NH<sub>4</sub>Cl (2 g) and was stirred for 15 min under N<sub>2</sub> atmosphere. The mixture was filtered over celite and the pad was rinsed with EtOH (500 mL). The filtrate was concentrated under reduced pressure. The residue was dissolved in Et<sub>2</sub>O (100 mL) and washed with sat. aq. NH<sub>4</sub>Cl (100 mL). The aq. layer was extracted with Et<sub>2</sub>O (2 x 100 mL) and the combined organic layers were washed with brine (2 x 100 mL), dried over MgSO<sub>4</sub>, filtered and concentrated under reduced pressure. Purification of the residue by column chromatography (Et<sub>2</sub>O/pentane = 1:4 to 1:2) afforded the title compound as a colorless oil (0.234 g, 0.98 mmol, 46%). R<sub>f</sub> = 0.7 (Et<sub>2</sub>O/pentane = 3:1). <sup>1</sup>H NMR (500 MHz, CDCl<sub>3</sub>) δ 5.67 – 5.49 (m, 2H), 5.43 – 5.33 (m, 4H), 4.25 – 4.21 (m, 2H), 3.67 (s, 3H), 2.86 (t, J = 6.6 Hz, 2H), 2.79 (t, J = 6.0 Hz, 2H), 2.33 (td, J = 7.5, 1.2 Hz, 2H), 2.14 – 2.07 (m, 2H), 1.70 (m, 2H), 1.47 (bs, 1H). <sup>13</sup>C NMR (126 MHz, CDCl<sub>3</sub>) δ 130.98, 129.19, 128.97, 128.83, 128.80, 127.67, 58.70, 51.68, 33.57, 26.71, 25.97, 25.75, 24.88. HRMS: Calculated for [C<sub>14</sub>H<sub>22</sub>O<sub>3</sub>+Na]<sup>+</sup> 261.1461, found 261.1470.

### (5Z,8Z,11Z)-13-Hydroxytrideca-5,8,11-trienoic acid (14)

 To a solution of triene **13** (0.423 g, 1.776 mmol) in THF (16 mL) was added 1 M aq. LiOH (16 mL) and the reaction was stirred overnight. The reaction mixture was cooled to 0 °C and diluted with Et<sub>2</sub>O (50 mL). 1 M aq. HCl was added until acidic (pH <2) and NaCl was added to saturation. The aq. layer was extracted with Et<sub>2</sub>O (3 x 50 mL). The combined organic layers were dried over Na<sub>2</sub>SO<sub>4</sub>, filtered and concentrated under reduced pressure. Purification of the residue by column chromatography (MeOH/DCM = DCM to 1:49) afforded the title compound **7** (0.346 g, 1.54 mmol, 87%) as a colorless oil. R<sub>f</sub> = 0.2 (MeOH/DCM = 5:95). <sup>1</sup>H NMR (400 MHz, CDCl<sub>3</sub>) δ 6.67 (bs, 2H), 5.70 – 5.50 (m, 2H), 5.48 – 5.28 (m, 4H), 4.24 (d, J = 6.8 Hz, 2H), 2.87 (d, J = 6.9 Hz, 2H), 2.81 (t, J = 6.1 Hz, 2H), 2.36 (t, J = 7.0 Hz, 2H), 2.14 (q, J = 7.5 Hz, 2H), 1.70 (p, J = 7.0 Hz, 2H). <sup>13</sup>C NMR (101 MHz, CDCl<sub>3</sub>) δ 131.65,

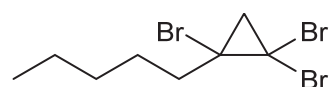
129.01, 129.00, 128.91, 128.26, 127.48, 58.49, 33.16, 26.52, 25.95, 25.80, 24.61. HRMS: Calculated for  $[C_{13}H_{20}O_3+Na]^+$  247.1305, found 247.1310.

### 2-Bromohex-1-ene (16)



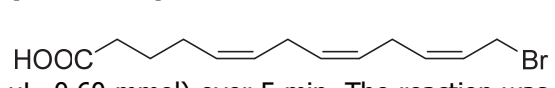
Magnesium (24.31 g, 1.00 mol) was placed in dry  $Et_2O$  (133 mL) and 1,2-dibromoethane (17  $\mu L$ , 0.20 mmol) was added. The mixture was heated to reflux and 1-bromobutane (27.4 g, 21.5 mL, 200 mmol) was added while maintaining a gentle reflux over 15 min to form butylmagnesium bromide, which was titrated.<sup>39</sup> In a different flask, CuCl (0.621 g, 6.28 mmol) was suspended in dry  $Et_2O$  (120 mL) and 2,3-dibromoprop-1-ene (25.1 g, 126 mmol) was added. Butylmagnesium bromide (83 mL, 109 mmol) was then added dropwise using a cannula to maintain a gentle reflux. The reaction was stirred for 4 h, cooled to 0 °C and quenched using sat. aq.  $NH_4Cl$  (100 mL). The aq. layer was extracted using  $Et_2O$  (2 x 200 mL) and the combined organic layers were dried over  $Na_2SO_4$ , filtered and concentrated under reduced pressure. Vacuum distillation (72-79 °C, 86 mmHg) afforded the title compound as an orange liquid (15.25 g, 86 mmol, 79%).  $^1H$  NMR (500 MHz,  $CDCl_3$ )  $\delta$  5.55 (d,  $J$  = 1.4 Hz, 1H), 5.38 (d,  $J$  = 1.6 Hz, 1H), 2.41 (d,  $J$  = 7.6 Hz, 2H), 1.55 (p,  $J$  = 7.4 Hz, 2H), 1.37 – 1.23 (m, 4H), 0.90 (t,  $J$  = 7.1 Hz, 3H).  $^{13}C$  NMR (126 MHz,  $CDCl_3$ )  $\delta$  135.10, 116.36, 41.52, 30.72, 27.71, 22.51, 14.13. The spectra were in full accordance with literature experimental data.<sup>40</sup>

### 1,1,2-Tribromo-2-pentylcyclopropane (17)

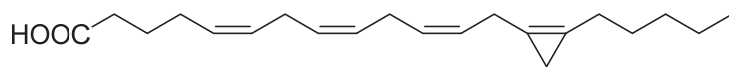


To a vigorously stirred mixture of compound **16** (3.238 g, 18.28 mmol), cetrimonium bromide (600 mg, 1.65 mmol) and bromoform (3.20 mL, 36.6 mmol) was added dropwise aq. NaOH (7.31 g, 50% (w/v)) over 10 min and the reaction was stirred overnight. The reaction was diluted with  $H_2O$  (100 mL) and extracted with DCM (3 x 150 mL). The combined organic layers were washed with brine (3 x 150 mL), dried over  $MgSO_4$ , filtered and concentrated under reduced pressure. Purification of the residue by column chromatography (pentane) and high vacuum afforded the title compound as a brown oil (2.30 g, 6.59 mmol, 36%).  $^1H$  NMR (400 MHz,  $CDCl_3$ )  $\delta$  2.11 – 1.95 (m, 2H), 1.95 (d,  $J$  = 9.2 Hz, 1H), 1.83 (d,  $J$  = 9.2 Hz, 1H), 1.80 – 1.61 (m, 2H), 1.42 – 1.27 (m, 4H), 0.92 (t,  $J$  = 6.9 Hz, 3H).  $^{13}C$  NMR (101 MHz,  $CDCl_3$ )  $\delta$  46.01, 41.85, 38.22, 33.34, 31.27, 27.53, 22.68, 14.15. The spectra were in full accordance with literature experimental data.<sup>40</sup>

### (5Z,8Z,11Z)-13-Bromotrideca-5,8,11-trienoic acid (19)



To a cooled (0 °C) mixture of NBS (0.089 g, 0.50 mmol) and dry DCM (2 mL) was added dimethyl sulfide (45  $\mu L$ , 0.60 mmol) over 5 min. The reaction was stirred for 15 min and then cooled to -25 °C. A solution of compound **14** (0.075 g, 0.33 mmol) in dry DCM (2 mL) was added dropwise to the mixture over 10 min. The reaction was allowed to reach rt and was stirred for an hour. It was then diluted with DCM (20 mL) and  $H_2O$  (10 mL). The aq. layer was separated and extracted with DCM (2 x 20 mL). The combined organic layers were washed with brine (2 x 20 mL), dried over  $MgSO_4$ , filtered and concentrated under reduced pressure at rt to afford title compound as a colorless oil, which was used immediately in the next reaction due to its instability. Purification of an aliquot by column chromatography ( $MeOH/DCM = DCM$  to 1:99) allowed characterization by NMR.  $R_f$  = 0.6 ( $EtOAc/pentane$  = 1:1).  $^1H$  NMR (500 MHz,  $CDCl_3$ )  $\delta$  5.81 – 5.70 (m, 1H), 5.64 – 5.52 (m, 1H), 5.48 – 5.30 (m, 4H), 4.02 (d,  $J$  = 8.4 Hz, 2H), 2.95 – 2.89 (m, 2H), 2.86 – 2.79 (m, 2H), 2.41 – 2.34 (m, 2H), 2.19 – 2.10 (m, 2H), 1.72 (p,  $J$  = 7.6 Hz, 2H).

**(5Z,8Z,11Z)-13-(2-pentylcycloprop-1-en-1-yl)trideca-5,8,11-trienoic acid (cyclopropene-arachidonic acid, 2)**

To a cooled (-80 °C) solution of 1,1,2-tribromo-2-pentylcyclopropane **17**

(233 mg, 0.668 mmol) in dry Et<sub>2</sub>O (1 mL) was added *n*-BuLi (1.6 M in hexanes, 836 µL, 1.34 mmol). The reaction was allowed to reach rt and stirred for 25 min, after which a stream of N<sub>2</sub> gas was passed over to reduce the volume of solvent by half. The mixture was cooled to 0 °C and a solution of bromide **19** (53.3 mg, 0.186 mmol) in dry HMPA (1 mL) was added, after which the reaction was stirred for 15 min. The reaction was quenched with aq. citric acid (10% (w/v), 2 mL) and diluted with Et<sub>2</sub>O (10 mL). The layers were separated and the aq. layer was extracted with Et<sub>2</sub>O (10 mL). The combined organic layers were washed with sat. aq. LiCl (10 mL), dried over MgSO<sub>4</sub>, filtered and concentrated under reduced pressure. Purification of the residue by column chromatography (Et<sub>2</sub>O/pentane = 1:39 + 0.1% AcOH to 1:11 + 0.1% AcOH) afforded the title compound with minor impurities as a clear oil (16.2 mg, 0.051 mmol, 28%). Attempts at further purification resulted in near complete degradation. R<sub>f</sub> = 0.5 (EtOAc/pentane = 1:3). <sup>1</sup>H NMR (400 MHz, CDCl<sub>3</sub>) δ 5.60 – 5.51 (m, 1H), 5.51 – 5.32 (m, 5H), 3.17 (d, J = 6.091 Hz, 2H), 2.85 (t, J = 6.553 Hz, 2H), 2.80 (t, J = 5.850 Hz, 2H), 2.42 – 2.33 (m, 5H), 2.18 – 2.09 (m, 2H), 1.77 – 1.67 (m, 2H), 1.59 – 1.50 (m, 2H), 1.34 – 1.29 (m, 3H), 0.89 (t, J = 6.726 Hz, 5H), 0.83 (s, 2H). <sup>13</sup>C NMR (101 MHz, CDCl<sub>3</sub>) δ 180.14, 129.16, 128.88, 128.35, 128.18, 125.82, 111.69, 107.83, 33.53, 31.74, 27.24, 26.58, 26.04, 25.80, 25.74, 24.79, 24.61, 22.61, 14.21, 7.84. LC-MS: Calculated for [C<sub>21</sub>H<sub>32</sub>O<sub>2</sub>+H]<sup>+</sup> 317.3, found 317.1.

## References

- (1) Rustam, Y. H.; Reid, G. E. Analytical Challenges and Recent Advances in Mass Spectrometry Based Lipidomics. *Anal. Chem.* **2018**, *90*(1), 374–397.
- (2) Porta Siegel, T.; Ekroos, K.; Ellis, S. R. Reshaping Lipid Biochemistry by Pushing Barriers in Structural Lipidomics. *Angew. Chem. Int. Ed.* **2019**, *58*(20), 6492–6501.
- (3) Hannun, Y. A.; Obeid, L. M. Principles of Bioactive Lipid Signalling: Lessons from Sphingolipids. *Nat. Rev. Mol. Cell Biol.* **2008**, *9*(2), 139–150.
- (4) Mechoulam, R.; Parker, L. A. The Endocannabinoid System and the Brain. *Annu. Rev. Psychol.* **2013**, *64*(1), 21–47.
- (5) Cravatt, B. F.; Lichtman, A. H. The Endogenous Cannabinoid System and Its Role in Nociceptive Behavior. *J. Neurobiol.* **2004**, *61*(1), 149–160.
- (6) Di Marzo, V.; Fontana, A.; Cadas, H.; Schinelli, S.; Cimino, G.; Schwartz, J. C.; Piomelli, D. Formation and Inactivation of Endogenous Cannabinoid Anandamide in Central Neurons. *Nature* **1994**, *372*(6507), 686–691.
- (7) Maccarrone, M. Metabolism of the Endocannabinoid Anandamide: Open Questions after 25 Years. *Front. Mol. Neurosci.* **2017**, *10*.
- (8) Deutsch, D. G. A Personal Retrospective: Elevating Anandamide (AEA) by Targeting Fatty Acid Amide Hydrolase (FAAH) and the Fatty Acid Binding Proteins (FABPs). *Front. Pharmacol.* **2016**, *7*.
- (9) Fowler, C. J. Anandamide Uptake Explained? *Trends Pharmacol. Sci.* **2012**, *33*(4), 181–185.
- (10) Nicolussi, S.; Gertsch, J. Chapter Fourteen - Endocannabinoid Transport Revisited. In *Vitamins & Hormones*; Litwack, G., Ed.; Hormones and Transport Systems; Academic Press, 2015; Vol. 98, pp 441–485.
- (11) Glaser, S. T.; Kaczocha, M.; Deutsch, D. G. Anandamide Transport: A Critical Review. *Life Sci.* **2005**, *77*(14), 1584–1604.
- (12) McIntosh, A. L.; Atshaves, B. P.; Huang, H.; Gallegos, A. M.; Kier, A. B.; Schroeder, F. Fluorescence Techniques Using Dehydroergosterol to Study Cholesterol Trafficking. *Lipids* **2008**, *43*(12), 1185–1208.
- (13) Andresen, M.; Schmitz-Salue, R.; Jakobs, S. Short Tetracysteine Tags to  $\beta$ -Tubulin Demonstrate the Significance of Small Labels for Live Cell Imaging. *Mol. Biol. Cell* **2004**, *15*(12), 5616–5622.
- (14) Sezgin, E.; Can, F. B.; Schneider, F.; Clausen, M. P.; Galiani, S.; Stanly, T. A.; Waithe, D.; Colaco, A.; Honigmann, A.; Wüstner, D.; Platt, F.; Eggeling, C. A Comparative Study on Fluorescent Cholesterol Analogs as Versatile Cellular Reporters. *J. Lipid Res.* **2016**, *57*(2), 299–309.
- (15) Adams, S. R.; Campbell, R. E.; Gross, L. A.; Martin, B. R.; Walkup, G. K.; Yao, Y.; Llopis, J.; Tsien, R. Y. New Biarsenical Ligands and Tetracysteine Motifs for Protein Labeling in Vitro and in Vivo: Synthesis and Biological Applications. *J. Am. Chem. Soc.* **2002**, *124*(21), 6063–6076.
- (16) Huisgen, R. 1,3-Dipolar Cycloadditions. *Proc Chem Soc* **1961**, No. October, 357–396.
- (17) Agard, N. J.; Prescher, J. A.; Bertozzi, C. R. A Strain-Promoted [3 + 2] Azide–Alkyne Cycloaddition for Covalent Modification of Biomolecules in Living Systems. *J. Am. Chem. Soc.* **2004**, *126*(46), 15046–15047.
- (18) Saxon, E.; Bertozzi, C. R. Cell Surface Engineering by a Modified Staudinger Reaction. *Science* **2000**, *287*(5460), 2007–2010.
- (19) Rostovtsev, V. V.; Green, L. G.; Fokin, V. V.; Sharpless, K. B. A Stepwise Huisgen Cycloaddition Process: Copper(I)-Catalyzed Regioselective “Ligation” of Azides and Terminal Alkynes. *Angew. Chem. Int. Ed.* **2002**, *41*(14), 2596–2599.
- (20) Prescher, J. A.; Bertozzi, C. R. Chemistry in Living Systems. *Nat. Chem. Biol.* **2005**, *1*(1), 13–21.
- (21) Blackman, M. L.; Royzen, M.; Fox, J. M. Tetrazine Ligation: Fast Bioconjugation Based on Inverse-Electron-Demand Diels–Alder Reactivity. *J. Am. Chem. Soc.* **2008**, *130*(41), 13518–13519.
- (22) Devaraj, N. K.; Weissleder, R.; Hilderbrand, S. A. Tetrazine-Based Cycloadditions: Application to Pretargeted Live Cell Imaging. *Bioconjug. Chem.* **2008**, *19*(12), 2297–2299.
- (23) Devaraj, N. K.; Hilderbrand, S.; Upadhyay, R.; Mazitschek, R.; Weissleder, R. Bioorthogonal Turn-On Probes for Imaging Small Molecules inside Living Cells. *Angew. Chem. Int. Ed.* **2010**, *49*(16), 2869–2872.
- (24) Liang, Y.; Mackey, J. L.; Lopez, S. A.; Liu, F.; Houk, K. N. Control and Design of Mutual Orthogonality in Bioorthogonal Cycloadditions. *J. Am. Chem. Soc.* **2012**, *134*(43), 17904–17907.
- (25) Yang, J.; Liang, Y.; Šečkuté, J.; Houk, K. N.; Devaraj, N. K. Synthesis and Reactivity Comparisons of 1-Methyl-3-Substituted Cyclopropene Mini-Tags for Tetrazine Bioorthogonal Reactions. *Chem. - Eur. J.* **2014**, *20*(12), 3365–3375.
- (26) Cole, C. M.; Yang, J.; Šečkuté, J.; Devaraj, N. K. Fluorescent Live-Cell Imaging of Metabolically Incorporated Unnatural Cyclopropene-Mannosamine Derivatives. *ChemBioChem* **2013**, *14*(2), 205–208.
- (27) Patterson, D. M.; Nazarova, L. A.; Xie, B.; Kamber, D. N.; Prescher, J. A. Functionalized Cyclopropenes as Bioorthogonal Chemical Reporters. *J. Am. Chem. Soc.* **2012**, *134*(45), 18638–18643.
- (28) Yang, J.; Šečkuté, J.; Cole, C. M.; Devaraj, N. K. Live-Cell Imaging of Cyclopropene Tags with Fluorogenic Tetrazine Cycloadditions. *Angew. Chem.* **2012**, *124*(30), 7594–7597.
- (29) Nunn, J. R. The Structure of Sterculic Acid. *J. Chem. Soc.* **1952**, 313–318.
- (30) Nicholas T. Castellucci; Claibourne E. Griffin. Synthesis of Sterculic Acid. *J. Am. Chem. Soc.* **1960**, *82*(15), 4107–4107.

## Cyclopropene probes for live-cell imaging of signaling lipids

- (31) Moessinger, C.; Klizaite, K.; Steinhagen, A.; Philippou-Massier, J.; Shevchenko, A.; Hoch, M.; Ejsing, C. S.; Thiele, C. Two Different Pathways of Phosphatidylcholine Synthesis, the Kennedy Pathway and the Lands Cycle, Differentially Regulate Cellular Triacylglycerol Storage. *BMC Cell Biol.* **2014**, *15*(1), 43.
- (32) Brown, C. A.; Ahuja, V. K. Catalytic Hydrogenation. VI. Reaction of Sodium Borohydride with Nickel Salts in Ethanol Solution. P-2 Nickel, a Highly Convenient, New, Selective Hydrogenation Catalyst with Great Sensitivity to Substrate Structure. *J. Org. Chem.* **1973**, *38*(12), 2226–2230.
- (33) Brown, C. A.; Ahuja, V. K. "P-2 Nickel" Catalyst with Ethylenediamine, a Novel System for Highly Stereospecific Reduction of Alkynes to Cis-Olefins. *J. Chem. Soc. Chem. Commun.* **1973**, No. 15, 553–554.
- (34) Baird, M. S.; Hussain, H. H.; Nethercott, W. The Preparation and Lithiation of 1-Halogenocyclopropenes. *J. Chem. Soc. Perkin Trans 1* **1986**, No. 0, 1845–1853.
- (35) Dulayymi, J. R. A.; Baird, M. S.; Simpson, M. J.; Nyman, S.; Port, G. R. Structure Based Interference with Insect Behaviour - Cyclopropene Analogues of Pheromones Containing Z-Alkenes. *Tetrahedron* **1996**, *52*(38), 12509–12520.
- (36) Reich, H. J.; Sanders, A. W.; Fiedler, A. T.; Bevan, M. J. The Effect of HMPA on the Reactivity of Epoxides, Aziridines, and Alkyl Halides with Organolithium Reagents. *J. Am. Chem. Soc.* **2002**, *124* (45), 13386–13387.
- (37) Yan, N.; Liu, X.; Pallerla, M. K.; Fox, J. M. Synthesis of Stable Derivatives of Cycloprop-2-Ene Carboxylic Acid. *J. Org. Chem.* **2008**, *73*(11), 4283–4286.
- (38) Dowd, P.; Gold, A. The Thermal Dimerization of Cyclopropene. *Tetrahedron Lett.* **1969**, *10*(2), 85–86.
- (39) Krasovskiy, A.; Knochel, P. Convenient Titration Method for Organometallic Zinc, Magnesium, and Lanthanide- Reagents. *Synthesis* **2006**, *2006* (5), 890–891.
- (40) Bigot, A.; Breuninger, D.; Breit, B. One-Pot Desymmetrizing Hydroformylation/Carbonyl Ene Cyclization Process: Straightforward Access to Highly Functionalized Cyclohexanols. *Org. Lett.* **2008**, *10* (23), 5321–5324.



# Chapter 8

## Summary and future prospects

*The overarching aim of the research presented in this thesis was to develop and apply chemical tools to study lipid metabolism, transport and signaling.*

**Chapter 1** provided an overview of the diversity of lipids and highlighted bioorthogonal chemistry as a method for their investigation. Lipids are structurally and functionally diverse biomolecules that are difficult to study, particularly their localization and protein interaction partners. This is due to their small size, lipophilicity, and high rate of metabolism. Most analytical methods for lipids rely on sample homogenization and lipid extraction, which allows for sensitive detection of lipids, but discards spatial information.

Bioorthogonal chemistry has enabled the investigation on lipids in a more versatile manner. A small bioorthogonal ligation handle, such as an alkyne, can be introduced and conjugated to a reporter group through 'click' chemistry such as the copper(I)-catalyzed azide-alkyne cycloaddition (CuAAC).<sup>1</sup> This has allowed the investigation of localization, metabolism, uptake and incorporation of the lipid as post-translational modification. Moreover, to capture noncovalent lipid-protein interactions, a photoactivatable group can be added. Photoactivatable groups can be irradiated to generate a reactive intermediate, which can form a covalent and irreversible bond with a lipid-interacting protein. The combination of a photoactivatable group and bioorthogonal ligation handles has propelled the investigation of

lipid-protein interactions. This approach holds promise for the investigation of polyunsaturated fatty acids (PUFAs) and their metabolites, which have become increasingly appreciated for their role as signaling molecules, especially in the immune system. However, the availability of chemical tools based on these lipids is limited, in part due to their synthetic difficulty.

**Chapter 2** provided an overview of lipid-based photoaffinity probes developed in the last decade and their main discoveries. The first implementations of photoactivatable lipid probes contained radioisotopes or bulky fluorophores and were only capable of investigating interactions with a predetermined protein. In recent years, lipid probes have shifted to diazirine- and alkyne-containing structures, partly due to increased synthetic methodologies and commercial availability of compatible click reagents. The scope of projects involving lipid probes has also moved towards large-scale profiling of lipid-interacting proteins and using probes to tackle challenging biological questions. However, challenges in using lipid probes remain their lipophilicity and fast cellular metabolism. Due to this lipophilicity, many probe targets can be non-specific binding partners, which makes it difficult to identify specific interacting proteins. As a resource for future research, a list of promiscuous lipid-binding proteins is compiled in Chapter 2. Looking forward, improved synthetic accessibility—usually followed by commercial availability—of probes and expanding on their functionality will lead to improved understanding of the complex and multifaceted roles of lipids.

**Chapter 3** described the synthesis and use of photoaffinity-click (pac)-probes based on the omega-3 fatty acid docosahexaenoic acid (DHA, 22:6 n-3, **1**) and its oxidized metabolite, 17-hydroxy-DHA (17-HDHA) in comparative photoaffinity-based protein profiling (AfBPP). DHA is oxidized through different pathways into biologically active metabolites that lower inflammatory response and signal for the resolution of inflammation.<sup>2</sup> 17-HDHA is an important intermediate in this process. Two photoaffinity probes, pac-DHA and pac-17-HDHA, were synthesized to investigate the specific interaction partners of 17-HDHA in human immune cells. Synthesis of pac-DHA was achieved by generation of the six cis double bonds inherent to DHA through a combination of partial hydrogenation of alkynes and Wittig reactions. To obtain pac-17-HDHA, the hydroxyl was introduced by enzymatic oxidation using soy bean lipoxygenase.

Using the two probes in comparative AfBPP in primary macrophages (Figure 1), prostaglandin reductase 1 (PTGR1) was identified and validated as a specific pac-17-HDHA binding target capable of converting 17-HDHA into 17-oxo-DHA. PTGR1 was shown to act as a metabolic hub in oxidative metabolism of PUFAs, simultaneously inactivating pro-inflammatory lipids and producing anti-inflammatory oxidative metabolites. Moreover, comparative AfBPP was shown to be an effective method to distinguish genuine probe targets.

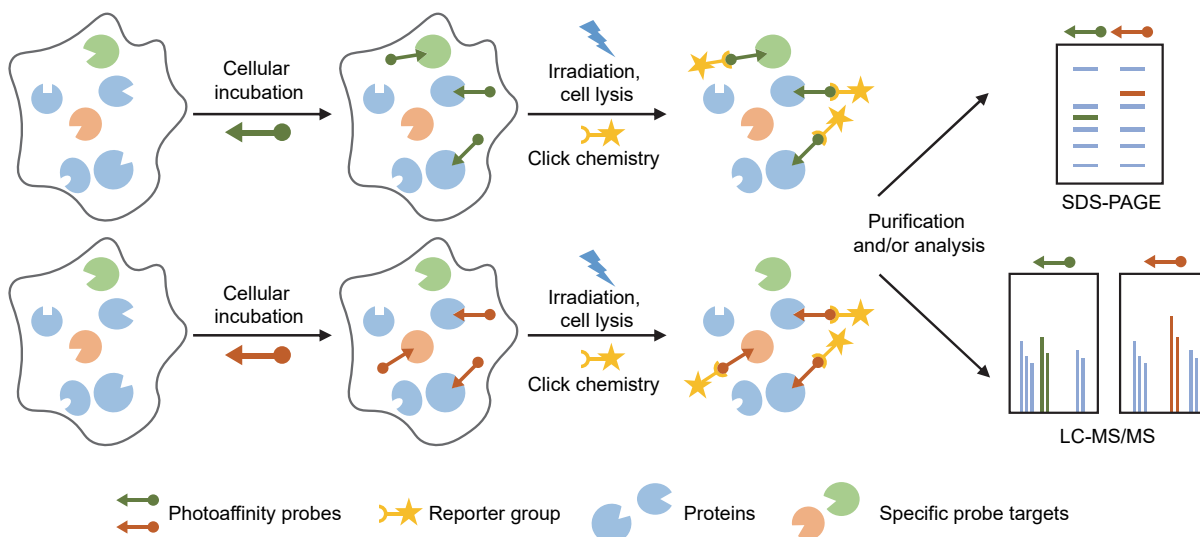


**Figure 1 | Schematic representation of comparative AfBPP for lipid photoaffinity probes.**

Neutrophils are key players in the acute inflammatory response and perpetuate the response via an autocrine loop that is regulated through the secretion of LTB4.<sup>3</sup> Murine neutrophils produce less 5-HETE and LTB4 after being exposed to 17-HDHA *in vivo*,<sup>4</sup> and previously similar results were found in isolated human neutrophils.<sup>5</sup> However, neutrophils have not been well-studied in the context of chronic inflammation despite their importance in the immune system.<sup>6</sup> The DHA- and 17-HDHA-based probes described in Chapter 3 were used to discover protein interaction partners in primary neutrophils in a similar approach to the M2 macrophages. Comparative AfBPP on neutrophils resulted in 29 UV-enriched targets of pac-17-HDHA (Figure 2, Table S1). The pac-17-HDHA probe was found to UV-enrich the LTB4 receptor and 5-lipoxygenase-activating protein (ALOX5AP), although ALOX5AP was equally enriched by both probes. These protein interaction partners are involved in the metabolism and function of LTB4, and constitute interesting targets for further investigation of the anti-inflammatory properties of DHA and 17-HDHA.

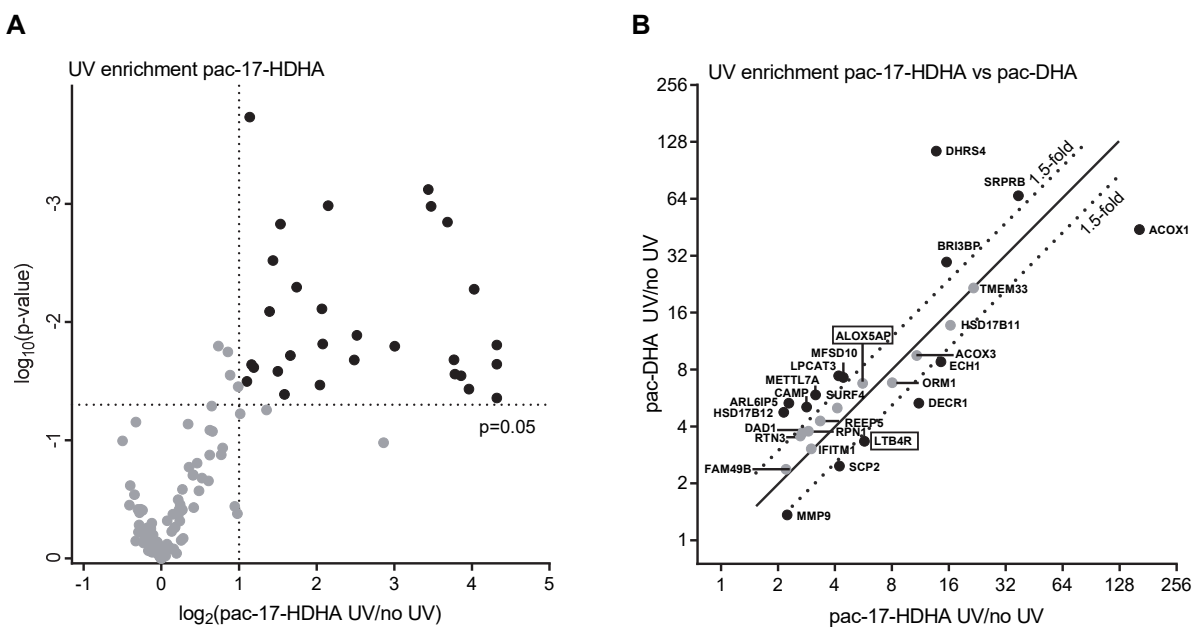


**Figure 2 | Comparative AfBPP using pac-DHA and pac-17-HDHA in human neutrophils.**

**Chapter 4** described the use of a photoaffinity-click probe based on the neuroprotective and anti-inflammatory *N*-docosahexaenoylethanolamine (DHEA). pac-DHEA was synthesized and used to identify its protein binding partners in a microglial cell line. Eleven specific binding partners were identified using the comparative AfBPP approach. Three targets were investigated in further detail. NENF, an excreted neurotrophic factor, reduced inflammatory response, although not in combination with DHEA. Stable overexpression of APMAP and GSTM1 in microglial cells exacerbated LPS-induced inflammation as measured by NO and IL-6 production. These effects were reversed by pretreatment of the cells with DHEA, while DHA was less effective. These results indicate that DHEA confers anti-inflammatory effects through binding to these proteins, although their exact function remains to be established.

Although DHEA has been shown to have direct signaling functions,<sup>7</sup> anti-inflammatory oxidative metabolites have also been reported.<sup>8,9</sup> Oxidative metabolites of PUFAs are mainly detected in cells with high oxidative activity, such as macrophages. Since the binding of pac-DHEA to GSTM1 in microglia could not be recapitulated in an overexpression system, this may suggest that an oxidative metabolite may be responsible for the anti-inflammatory effects of DHEA via GSTM1.

**Chapter 5** described an improved, facile method for synthesis of an alkyne-functionalized DHA analog, cDHA (**2**, Figure 3). Synthesis of PUFA derivatives by partial hydrogenation of skipped alkynes suffers from formation of undesired *E*-alkenes, poor reproducibility and overhydrogenated products.<sup>10</sup> In this chapter, an alternative synthetic route for cDHA (**2**) starting from DHA is developed. This clickable lipid was used to visualize DHA metabolism and cellular exchange using thin-layer chromatography and flow cytometry.

This synthetic methodology can be expanded to other PUFA derivatives. For example, conjugation of aldehydes **3** and **4** to isotopically labelled phosphonium salts would afford internal standards **5**, **6** and **7** for mass spectrometry analysis (Figure 3). Moreover, alkyne-functionalized derivatives of arachidonic (AA, 20:4 n-6, **8**) or eicosapentaenoic acid (EPA, 22:5 n-3) would be readily accessible using this synthetic approach, affording cAA (**9**) and cEPA (**10**) respectively.

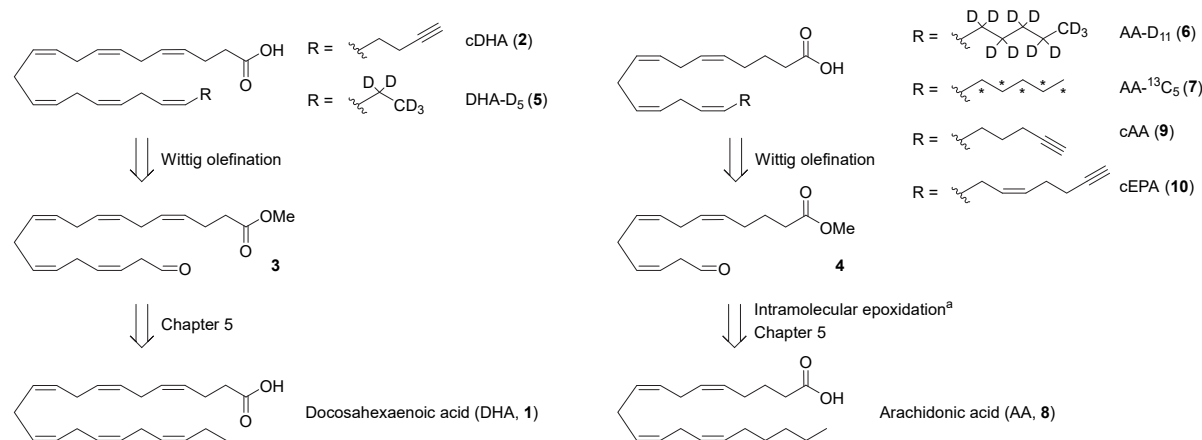


**Figure 3 | Synthetic routes towards alkyne- or isotope-modified PUFAs.** AA, arachidonic acid, DHA, docosahexaenoic acid; EPA, eicosapentaenoic acid; a<sup>11,12</sup>

Another application of cDHA (**2**) is the investigation of protein modification by electrophilic lipids.<sup>13</sup> PUFA oxidation results in the formation of many reactive products, such as aldehydes, α,β-unsaturated ketones and epoxides, which can react with nucleophilic residues of proteins, such as cysteines.<sup>13</sup> Reaction with a catalytic cysteine of an enzyme is often responsible for loss of activity, but a few proteins are actually activated by covalent modification, leading to downstream signaling.<sup>14</sup> Reactive lipids, such as epoxyeicosanoids or 17-oxo-DHA described in Chapter 3, have therapeutic potential in cardiovascular and inflammatory diseases.<sup>15,16</sup> Moreover, electrophilic lipids have a central role in a newly discovered form of cell death, ferroptosis.<sup>17–19</sup> Mapping of lipid electrophile-modified proteins has recently been demonstrated using alkyne-linoleic acid<sup>20</sup> and alkyne-arachidonic acid.<sup>21</sup> This can also be done using cDHA (**2**), which is demonstrated by the visualization of specific protein adducts in N9 microglia and RAW264.7 cells when compared to DHA (**1**) and click-palmitic acid (cPA, **11**) (Figure 4). The cDHA (**2**) reported in this thesis enables the investigation of the proteins modified by electrophilic DHA derivatives.

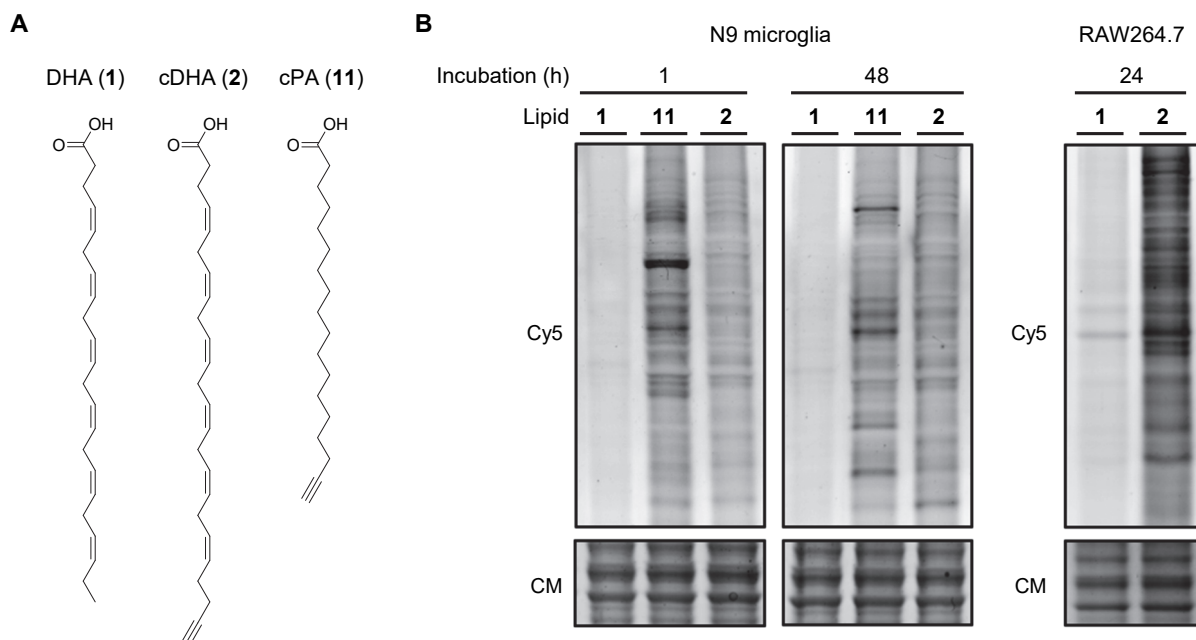


**Figure 4 | Mapping of lipid-modified proteins.** **(A)** Structures of DHA (**1**), cDHA (**2**) and cPA (**11**). **(B)** Labeling pattern of proteins derived from N9 microglia and RAW264.7 cells treated with 10  $\mu$ M indicated lipid for 1, 24 or 48 h. Cells were lysed, reversible conjugates were reduced using NaBH<sub>4</sub><sup>13,20</sup> and lipid-bound proteins were conjugated to Cy5-N<sub>3</sub> using CuAAC chemistry and analyzed by SDS-PAGE and in-gel fluorescence scanning. Coomassie served as a protein loading control.

Chapter 6 describes the characterization of an anandamide (AEA) reuptake inhibitor. Anandamide, or *N*-arachidonylethanolamine, is a lipid signaling molecule in the endocannabinoid system (ECS) and modulates neurotransmitter release via activation of the cannabinoid receptor type 1 (CB1R).<sup>22</sup> Although it is interesting to target the ECS for therapeutic purposes, an AEA transport protein has not been identified.<sup>23–27</sup> Recently, WOBE437 has been reported as a novel, natural product-based AEA reuptake inhibitor.<sup>28</sup> In this thesis, WOBE437 was found to surprisingly increase AEA uptake in Neuro-2a cells, which was accompanied by reduced cellular levels of AEA and related *N*-acylethanolamines (NAEs). A photoaffinity-click probe based on WOBE437 identified SCCPHD, VAT1 and FECH as WOBE437-interacting proteins. However, further genetic studies indicated that SCCPDH and VAT1 were not responsible for the WOBE437-induced reduction in NAE levels. Further exploration of the mechanism of action of WOBE437 should investigate the drop in cellular NAE levels found in this thesis. This observation conflicts with the hypothesis of inhibition of an endocannabinoid membrane transporter, and indicates more complicated processes could be involved.

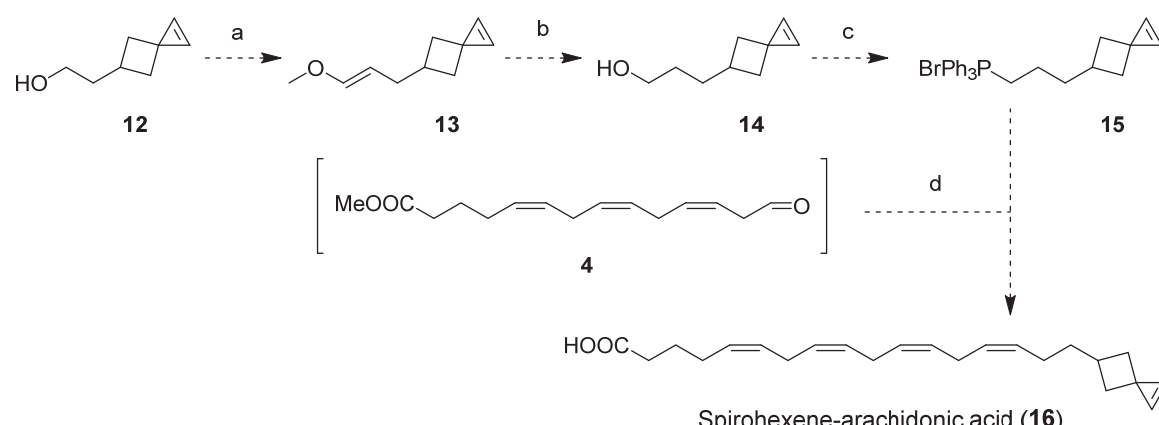
Another path to explore would be the use of chemical biology tools to gain more information on the process of AEA uptake. The current method to measure uptake, using radiolabeled AEA, does not take into account metabolism or excretion, measuring only a single endpoint. Moreover, the use of radiolabeled AEA is costly and requires special equipment. A more versatile tool would be alkyne-tagged AEA, which could be used to measure uptake and

exchange<sup>30</sup> as well as metabolism<sup>31,32</sup> and localization.<sup>33</sup> This approach would result in a better understanding of the process of AEA uptake. A facile synthetic route would be the selective epoxidation of the terminal alkene of arachidonic acid<sup>11,12</sup> followed by the steps outlined in Chapter 5 (Figure 3).

Notwithstanding the versatility of alkyne-tagged lipids, the required copper catalyst excludes their use in living cells. This problem is addressed in **Chapter 7**, which describes the synthesis of cyclopropene-modified arachidonic acid and use of 1,2-substituted cyclopropene lipids for live-cell imaging. Cyclopropenes act as dieneophiles in an inverse-electron demand Diels–Alder (IEDDA) reaction with tetrazine.<sup>34,35</sup> A cyclopropene lipid found in nature, sterculic acid, was tested in U2OS cells using a tetrazine-quenched BODIPY fluorophore. This resulted in successful IEDDA reaction in the cells as indicated by an intense fluorescent signal with a good signal-to-noise ratio, which was due to the fluorogenic property of the tetrazine-quenched BODIPY. Motivated by these results, cyclopropene-tagged arachidonic acid was synthesized through partial hydrogenation of three skipped alkynes and addition of the cyclopropene through nucleophilic substitution.

Although it was possible to synthesize and isolate cyclopropene-tagged arachidonic acid, it proved to be unstable. This instability is likely due to ene chemistry which would explain the observed tendency for degradation under solvent- and oxygen-free conditions.<sup>36,37</sup> Future use of cyclopropene-tagged arachidonic acid and its derivatives should take these properties in consideration and minimize handling steps.

Another possibility would be to use 3,3-substituted cyclopropenes, as they are more stable yet more reactive towards tetrazines in IEDDA reactions (Scheme 1).<sup>38</sup> Elongation<sup>39</sup> of reported spirohexene **12**<sup>38</sup> followed by Wittig reaction to aldehyde **4** would afford spirohexene-arachidonic acid **16** with all four alkenes intact, although it remains to be seen if this modification is tolerated for the investigation of arachidonic acid and derivatives in live cells.



**Scheme 1 | Synthetic route towards spirohexene-tagged arachidonic acid **16**.** Reagents and conditions: (a) DMP, DCM, then added to  $\text{MeOCH}_2\text{PPh}_3\text{Cl}$ ,  $\text{KO}^+\text{Bu}$ , THF; (b) aq. HCl, then  $\text{NaHCO}_3$ ,  $\text{NaBH}_4$ ; (c)  $\text{CBr}_4$ ,  $\text{PPh}_3$ , DCM, then  $\text{PPh}_3$ , ACN; (d)  $\text{KO}^+\text{Bu}$ , THF, then aq. LiOH.

## Challenges and opportunities for lipid probes

Lipids are a diverse class of biomolecules that serve a multitude of roles in the cell, from energy storage and membrane architecture to serving as signaling molecules in numerous cellular processes. The cellular distribution of lipids and their role in signaling events is regulated by a complex network of transport proteins and metabolic enzymes. Although technical advances in analytical chemistry have allowed for the detection and quantification of many lipid metabolites, unraveling the network of proteins and cellular processes involved is still a difficult task. This is especially true for polyunsaturated fatty acids and their metabolites, many of which have been found to have immunomodulatory signaling functions through unknown targets, while being processed through interweaving metabolic pathways. For concurrent investigation of localization, metabolism, intercellular exchange and signaling functions, innovative approaches are required.

Chemical biology offers a solution to this problem, as multiple aspects of lipid biology can be studied using the same chemical tool. Alkyne-modified lipids, for example, are versatile tools to study lipid localization and transport using fluorescence microscopy<sup>33</sup> and flow cytometry,<sup>30</sup> metabolism by LCMS<sup>40</sup> or thin-layer chromatography,<sup>40</sup> as well as incorporation as post-translational modification<sup>41</sup> and reaction with proteins by reactive oxidative metabolites.<sup>20,21</sup> Since protein modification by these reactive species is an important aspect in ferroptosis, chemical tools will be valuable to study this newly discovered form of cell death.<sup>14,18</sup> These tools would benefit from increased synthetic and commercial availability, along with approachable procedures to employ them. This will enable their use in labs with different areas of expertise—as has happened with tools to profile serine hydrolases—to tackle questions in lipid biology in a multidisciplinary fashion.<sup>42,43</sup>

Photoaffinity probes have proven to be powerful tools to study lipid-protein interactions, which is highlighted by the diversity of reported probes discussed in Chapter 2. However, lipid photoaffinity probes have a ‘blind spot’ for high-affinity interactions with low-abundant proteins, such as G-protein coupled receptors.<sup>44</sup> Although appropriate control experiments can distinguish specific interactions, abundant lipid-interacting proteins will quickly saturate the analytical capacity of gel- or mass spectrometry-based approaches. Technological advances in mass spectrometry analysis will mitigate this problem, as identification coverage of probe-bound proteins will increase. Moreover, optimization of experimental conditions can be guided by prior biological knowledge to improve analysis of relevant probe targets. For example, when investigating cytosolic, the proteome can be prefractionated by centrifugation and removal of membrane proteins.<sup>45</sup>

The next step for lipid probes is the study of signaling events in living cells, but more challenges need to be overcome. As the CuAAC reaction requires a cytotoxic metal catalyst, other bioorthogonal chemistry is required. However, selectivity and reaction speed are crucial in order to visualize dynamic processes.<sup>46</sup> Inverse-electron demand Diels-Alder (IEDDA) is a

bioorthogonal reaction that possesses sufficient selectivity and a high reaction speed, and is possible with strained cyclopropenes as the dienophile.<sup>47</sup> The use of cyclopropenes as a bioorthogonal handle shows potential for the investigation of signaling lipids, as it is a minimally intrusive modification. The use of IEDDA for real-time imaging of lipid metabolism has been demonstrated using a method developed by Dr. Baskin and coworkers, termed IMPACT.<sup>48,49</sup> This thesis provides evidence that 1,2-substituted cyclopropenes are capable of visualizing lipids in live cells and are deserving of further examination.

Another challenge is the metabolic fate of exogenous lipids, which may not mimic the subcellular distribution of lipids synthesized by the cellular machinery.<sup>50</sup> A promising approach is the addition of a caging group, which can be released upon irradiation.<sup>51–53</sup> This allows for unbiased distribution and spatiotemporally controlled release of a signaling lipid,<sup>52</sup> and this approach has been applied to photoactivatable lipids to afford trifunctional probes.<sup>54</sup> As these probes are extremely versatile tools, extension of this approach to other lipids will be of great value for the investigation of lipids as signaling molecules.

## Conclusion

In this thesis, a number of chemical tools are reported which enable the study of different aspects of lipid biology. The focus was the study of polyunsaturated fatty acids, which are underrepresented in the field of chemical biology due to the synthetic challenge posed by their derivatives. The photoaffinity probes reported in Chapters 3 and 4 as well as the comparative AfBPP approach were used to discover new lipid-protein interactions and to provide more background for the anti-inflammatory properties of DHA and its metabolites. The synthetic method developed in Chapter 5 allows for improved accessibility of DHA derivatives and demonstrated the versatility of clickable lipids. The photoaffinity probe reported in Chapter 6 allowed for target discovery of an inhibitor of anandamide reuptake, although outstanding questions remain about this process. The first use of 1,2-substituted cyclopropenes for live-cell imaging of lipids is reported in Chapter 7, as well as the synthesis of cyclopropene-tagged arachidonic acid for future investigation of anandamide in real-time.

*Overall, the use of chemical tools is a versatile approach for the investigation of lipid biology and the increasing repertoire of tools and techniques in chemical biology will lead to a greater understanding of lipids as signaling molecules.*

## Experimental procedures

### General

Lipids were purchased from Cayman Chemicals and stored as 10 mM ethanolic stocks under nitrogen at -80 °C. Cy5-N<sub>3</sub> and cPA (**11**) were prepared as previously reported in literature.<sup>55,56</sup> All cell culture disposables were from Sarstedt. All other reagents were purchased from Sigma Aldrich or Cayman Chemicals unless otherwise specified.

### Cell culture

RAW264.7 cells were cultured at 37 °C under 7% CO<sub>2</sub> in DMEM (Sigma Aldrich, D1145) containing phenol red, stable glutamine, 10% (v/v) New Born Calf Serum (Thermo Fisher) and penicillin and streptomycin (200 µg/mL each, Duchefa). Cells were passaged twice a week at 80-90% confluence by scraping and resuspension in fresh medium. N9 microglia were cultured at 37 °C under 5% CO<sub>2</sub> in RPMI 1640 (Sigma) containing phenol red, stable glutamine, 10% (v/v) sterile-filtered Fetal Calf Serum (Thermo Fisher) and penicillin and streptomycin (200 µg/mL each, Duchefa). Cells were passaged every two days by washing with PBS and trypsinization, subsequently quenching the trypsin with medium and removal of the trypsin by spinning down the cell suspension (200 g, 5 min). The resulting pellet was resuspended in culture medium by vortexing and subsequently seeded on new plates. Cells were tested regularly for mycoplasma contamination. Cultures were discarded after 2-3 months of use.

### SDS-PAGE analysis of protein lipidation

For gel-based profiling, cells were plated on 6-well plates and treated with 10 µM of indicated lipid for the indicated time. Then, cells were washed with PBS (1 mL) and harvested by pipetting and scraping into ice-cold PBS (1 mL), then pelleted by centrifugation (1,000 g, 10 min, 4 °C). The supernatant was removed and the cells were lysed by resuspension in lysis buffer (250 mM sucrose, 20 mM HEPES pH 7.5, 1 mM MgCl<sub>2</sub>) and sonication in a bath sonicator (10 s, 0 °C). Protein concentration was measured by Qubit™ assay (Invitrogen) and the samples were adjusted to 1.5 mg/mL and a volume of 100 µL, after which reversible adducts were reduced<sup>13,20</sup> using NaBH<sub>4</sub> (5 mM, 45 min, 4 °C) which was quenched with acetone (1 µL, 15 min, 4 °C). Then, the samples were treated with 10.95 µL click mix (5.5 µL aq. 25 mM CuSO<sub>4</sub>, 3.25 µL aq. 250 mM NaAsc, 1.1 µL 25 mM THPTA in DMSO, 1.1 µL 0.9 mM Cy5-N<sub>3</sub> in DMSO) at rt for 1 h. Then, samples were quenched with 4X Laemmli buffer, boiled (5 min, 95 °C) and resolved by SDS-PAGE (10% acrylamide gel, ±80 min, 180 V) along with protein marker (PageRuler™ Plus, Thermo Fisher). In-gel fluorescence was measured in the Cy3- and Cy5-channel (Chemidoc™ MP, Bio-Rad) and the gels were subsequently stained with Coomassie and imaged as a loading control.

### AfBPP analysis of neutrophils

Neutrophils, harvested as described in Chapter 3, were isolated in DPBS with MgCl<sub>2</sub> and CaCl<sub>2</sub> (D8662, Merck) and divided over two 50 mL falcon tubes, centrifuged (800 g, 5 min, no brakes) and resuspended in DPBS supplemented with 0.1% (w/v) delipidated BSA (15 mL) with pac-DHA or pac-17-HDHA (10 µM from 10 mM ethanolic stock) by careful vortexing. Next, neutrophils were incubated at 37 °C for 25 min. The cells were pelleted by centrifugation (800 g, 5 min, no brakes), the supernatant was aspirated and the cells were resuspended in ice-cold PBS (6.3 mL) by careful vortexing. The cells were distributed over 12-well plates (1 mL portions) and were irradiated at using a Caprobox™ (10 min, 4 °C, 350 nm, "UV") or exposed to ambient light (10 min, 4 °C, "No UV"). The cells were then transferred to 1.5 mL tubes, spun down (10 min, 1,000 g) and the supernatant was aspirated. The cells were then lysed with lysis buffer (250 µL, 250 mM sucrose, 2X protease inhibitor cocktail (Roche), 20 mM HEPES pH 7.5, 1 mM MgCl<sub>2</sub>). This was sonicated (Branson Sonifier probe sonicator, 10 x 1 s pulses, 10% amplitude). Protein concentration was measured by Qubit™ assay (Invitrogen) and the samples were adjusted to 0.6 mg/mL and a volume of 400 µL. This lysate is subjected to proteomic analysis as described in Chapter 3 under 'Mass spectrometric analysis of tryptic peptides, identification and quantification'.

## Supplementary data

**Table S1 | Proteins significantly UV-enriched by pac-17-HDHA in neutrophils.**

Gene name	Unique peptides	Description	UV/no UV pac-17-HDHA	p-value	UV/no UV pac-DHA	Enrichment pac-17-HDHA/pac-DHA
ACOX1	7	Peroxisomal acyl-coenzyme A oxidase 1	163.14	0.0437	43.95	3.71
SRPRB	7	Signal recognition particle receptor subunit beta	37.36	0.0156	66.43	0.56
TMEM33	4	Transmembrane protein 33	21.62	0.0227	21.60	1.00
HSD17B1 1	6	Estradiol 17-beta-dehydrogenase 11	16.32	0.0053	13.71	1.19
BRI3BP	2	BRI3-binding protein	15.57	0.0367	29.58	0.53
ECH1	5	Delta(3,5)-Delta(2,4)-dienoyl-CoA isomerase, mitochondrial	14.53	0.0283	8.79	1.65
DHRS4	2	Dehydrogenase/reductase SDR family member 4	13.75	0.0275	114.23	0.12
DECRL	2	2,4-dienoyl-CoA reductase, mitochondrial	11.12	0.0010	5.31	2.09
ACOX3	4	Peroxisomal acyl-coenzyme A oxidase 3	10.83	0.0008	9.48	1.14
ORM1	4	Alpha-1-acid glycoprotein 1	8.04	0.0160	6.82	1.18
LTB4R	4	Leukotriene B4 receptor 1	5.73	0.0129	3.33	1.72
ALOX5AP	6	Arachidonate 5-lipoxygenase-activating protein	5.60	0.0208	6.76	0.83
MFSD10	3	Major facilitator superfamily domain-containing protein 10	4.44	0.0010	7.27	0.61
SCP2	6	Non-specific lipid-transfer protein	4.23	0.0153	2.47	1.71
LPCAT3	2	Lysophospholipid acyltransferase 5	4.19	0.0077	7.40	0.57
SURF4	4	Surfeit locus protein 4	4.12	0.0340	5.00	0.82
REEP5	3	Receptor expression-enhancing protein 5	3.35	0.0051	4.28	0.78
METTL7A	2	Methyltransferase-like protein 7A	3.16	0.0191	5.87	0.54
IFITM1	2	Interferon-induced transmembrane protein 1	3.00	0.0408	3.04	0.99
RPN1	7	Dolichyl-diphosphooligosaccharide--protein glycosyltransferase subunit 1	2.90	0.0015	3.78	0.77
CAMP	7	Cathelicidin antimicrobial peptide	2.83	0.0260	5.06	0.56
DAD1	2	Dolichyl-diphosphooligosaccharide--protein glycosyltransferase subunit DAD1	2.71	0.0030	3.72	0.73
RTN3	3	Reticulon-3	2.63	0.0081	3.56	0.74
ARL6IP5	2	PRA1 family protein 3	2.28	0.0241	5.30	0.43
MMP9	9	Matrix metalloproteinase-9	2.24	0.0229	1.36	1.65
FAM49B	2	Protein FAM49B	2.20	0.0002	2.37	0.93
HSD17B1 2	5	Very-long-chain 3-oxoacyl-CoA reductase	2.15	0.0317	4.76	0.45

## References

- (1) Hein, J. E.; Fokin, V. V. Copper-Catalyzed Azide–Alkyne Cycloaddition (CuAAC) and beyond: New Reactivity of Copper(I) Acetylides. *Chem. Soc. Rev.* **2010**, *39* (4), 1302–1315.
- (2) Serhan, C. N. Pro-Resolving Lipid Mediators Are Leads for Resolution Physiology. *Nature* **2014**, *510* (7503), 92–101.
- (3) Nakanishi, Y.; Tan, M.; Ichiki, T.; Inoue, A.; Yoshihara, J.; Maekawa, N.; Takenoshita, I.; Yanagida, K.; Yamahira, S.; Yamaguchi, S.; Aoki, J.; Nagamune, T.; Yokomizo, T.; Shimizu, T.; Nakamura, M. Stepwise Phosphorylation of Leukotriene B4 Receptor 1 Defines Cellular Responses to Leukotriene B4. *Sci. Signal.* **2018**, *11* (544).
- (4) Robinson, B. S.; Rathjen, D. A.; Trout, N. A.; Easton, C. J.; Ferrante, A. Inhibition of Neutrophil Leukotriene B4 Production by a Novel Synthetic N-3 Polyunsaturated Fatty Acid Analogue,  $\beta$ -Oxa 21:3n-3. *J. Immunol.* **2003**, *171* (9), 4773–4779.
- (5) von Hegedus, J. H.; Kahnt, A. S.; Ebert, R.; Heijink, M.; Toes, R. E. M.; Giera, M.; Ioan-Facsinay, A. Toll-like Receptor Signaling Induces a Temporal Switch towards a Resolving Lipid Profile in Monocyte-Derived Macrophages. *Biochim. Biophys. Acta BBA - Mol. Cell Biol. Lipids* **2020**, *1865* (9), 158740.
- (6) Soehlein, O.; Steffens, S.; Hidalgo, A.; Weber, C. Neutrophils as Protagonists and Targets in Chronic Inflammation. *Nat. Rev. Immunol.* **2017**, *17* (4), 248–261.
- (7) Kim, H.-Y.; Spector, A. A. N-Docosahexaenoylethanolamine: A Neurotrophic and Neuroprotective Metabolite of Docosahexaenoic Acid. *Mol. Aspects Med.* **2018**, *64*, 34–44.
- (8) McDougle, D. R.; Watson, J. E.; Abdeen, A. A.; Adili, R.; Caputo, M. P.; Krapf, J. E.; Johnson, R. W.; Kilian, K. A.; Holinstat, M.; Das, A. Anti-Inflammatory  $\omega$ -3 Endocannabinoid Epoxides. *Proc. Natl. Acad. Sci.* **2017**, *114* (30), E6034–E6043.
- (9) Yang, R.; Fredman, G.; Krishnamoorthy, S.; Agrawal, N.; Irimia, D.; Piomelli, D.; Serhan, C. N. Decoding Functional Metabolomics with Docosahexaenoyl Ethanolamide (DHEA) Identifies Novel Bioactive Signals. *J. Biol. Chem.* **2011**, *286* (36), 31532–31541.
- (9½) Gagestein, B; Mock, E.D. Clickable lipids versus lickable clipids: Opportunities for a synergistic paradigm shift in cutting-edge profiling of global *in vivo* target engagement using A.I. *ChemBioChemBio*. **2020**, *11* (8), 420–422.
- (10) Vik, A.; Hansen, T. V. Synthetic Manipulations of Polyunsaturated Fatty Acids as a Convenient Strategy for the Synthesis of Bioactive Compounds. *Org. Biomol. Chem.* **2018**, *16* (48), 9319–9333.
- (11) Ryan, W. J.; Banner, W. K.; Wiley, J. L.; Martin, B. R.; Razdan, R. K. Potent Anandamide Analogs: The Effect of Changing the Length and Branching of the End Penty Chain. *J. Med. Chem.* **1997**, *40* (22), 3617–3625.
- (12) Corey, E. J.; Niwa, H.; Falck, J. R. Selective Epoxidation of Eicosa-Cis-5,8,11,14-Tetraenoic (Arachidonic) Acid and Eicosa-Cis-8,11,14-Trienoic Acid. *J. Am. Chem. Soc.* **1979**, *101* (6), 1586–1587.
- (13) Schopfer, F. J.; Cipollina, C.; Freeman, B. A. Formation and Signaling Actions of Electrophilic Lipids. *Chem. Rev.* **2011**, *111* (10), 5997–6021.
- (14) Spickett, C. M.; Pitt, A. R. Modification of Proteins by Reactive Lipid Oxidation Products and Biochemical Effects of Lipoxidation. *Essays Biochem.* **2020**, *64* (1), 19–31.
- (15) Shimanaka, Y.; Kono, N.; Taketomi, Y.; Arita, M.; Okayama, Y.; Tanaka, Y.; Nishito, Y.; Mochizuki, T.; Kusubara, H.; Adibekian, A.; Cravatt, B. F.; Murakami, M.; Arai, H. Omega-3 Fatty Acid Epoxides Are Autocrine Mediators That Control the Magnitude of IgE-Mediated Mast Cell Activation. *Nat. Med.* **2017**, *23* (11), 1287.
- (16) Schunck, W.-H.; Konkel, A.; Fischer, R.; Weylandt, K.-H. Therapeutic Potential of Omega-3 Fatty Acid-Derived Epoxyeicosanoids in Cardiovascular and Inflammatory Diseases. *Pharmacol. Ther.* **2018**, *183*, 177–204.
- (17) Kathman, S. G.; Boshart, J.; Jing, H.; Cravatt, B. F. Blockade of the Lysophosphatidylserine Lipase ABHD12 Potentiates Ferroptosis in Cancer Cells. *ACS Chem. Biol.* **2020**.
- (18) Yang, W. S.; Stockwell, B. R. Ferroptosis: Death by Lipid Peroxidation. *Trends Cell Biol.* **2016**, *26* (3), 165–176.
- (19) Shah, R.; Shchepinov, M. S.; Pratt, D. A. Resolving the Role of Lipoxygenases in the Initiation and Execution of Ferroptosis. *ACS Cent. Sci.* **2018**, *4* (3), 387–396.
- (20) Beavers, W. N.; Rose, K. L.; Galligan, J. J.; Mitchener, M. M.; Rouzer, C. A.; Tallman, K. A.; Lamberson, C. R.; Wang, X.; Hill, S.; Ivanova, P. T.; Brown, H. A.; Zhang, B.; Porter, N. A.; Marnett, L. J. Protein Modification by Endogenously Generated Lipid Electrophiles: Mitochondria as the Source and Target. *ACS Chem. Biol.* **2017**, *12* (8), 2062–2069.
- (21) Isobe, Y.; Kawashima, Y.; Ishihara, T.; Watanabe, K.; Ohara, O.; Arita, M. Identification of Protein Targets of 12/15-Lipoxygenase-Derived Lipid Electrophiles in Mouse Peritoneal Macrophages Using Omega-Alkynyl Fatty Acid. *ACS Chem. Biol.* **2018**, *13* (4), 887–893.
- (22) Pacher, P.; Bátikai, S.; Kunos, G. The Endocannabinoid System as an Emerging Target of Pharmacotherapy. *Pharmacol. Rev.* **2006**, *58* (3), 389–462.

- (23) Maccarrone, M. Metabolism of the Endocannabinoid Anandamide: Open Questions after 25 Years. *Front. Mol. Neurosci.* **2017**, *10*.
- (24) Deutsch, D. G. A Personal Retrospective: Elevating Anandamide (AEA) by Targeting Fatty Acid Amide Hydrolase (FAAH) and the Fatty Acid Binding Proteins (FABPs). *Front. Pharmacol.* **2016**, *7*.
- (25) Fowler, C. J. Anandamide Uptake Explained? *Trends Pharmacol. Sci.* **2012**, *33* (4), 181–185.
- (26) Nicolussi, S.; Gertsch, J. Chapter Fourteen - Endocannabinoid Transport Revisited. In *Vitamins & Hormones*; Litwack, G., Ed.; Hormones and Transport Systems; Academic Press, 2015; Vol. 98, pp 441–485.
- (27) Glaser, S. T.; Kaczocha, M.; Deutsch, D. G. Anandamide Transport: A Critical Review. *Life Sci.* **2005**, *77* (14), 1584–1604.
- (28) Chicca, A.; Nicolussi, S.; Bartholomäus, R.; Blunder, M.; Rey, A. A.; Petrucci, V.; Reynoso-Moreno, I. del C.; Viveros-Paredes, J. M.; Gens, M. D.; Lutz, B.; Schiöth, H. B.; Soeberdt, M.; Abels, C.; Charles, R.-P.; Altmann, K.-H.; Gertsch, J. Chemical Probes to Potently and Selectively Inhibit Endocannabinoid Cellular Reuptake. *Proc. Natl. Acad. Sci.* **2017**, *114* (25), E5006–E5015.
- (29) Reynoso-Moreno, I.; Chicca, A.; Flores-Soto, M. E.; Viveros-Paredes, J. M.; Gertsch, J. The Endocannabinoid Reuptake Inhibitor WOBE437 Is Orally Bioavailable and Exerts Indirect Polypharmacological Effects via Different Endocannabinoid Receptors. *Front. Mol. Neurosci.* **2018**, *11*.
- (30) Poulcharidis, D.; Belfor, K.; Kros, A.; Kasteren, S. I. van. A Flow Cytometry Assay to Quantify Intercellular Exchange of Membrane Components. *Chem. Sci.* **2017**, *8* (8), 5585–5590.
- (31) Thiele, C.; Papan, C.; Hoelper, D.; Kusserow, K.; Gaebler, A.; Schoene, M.; Piotrowitz, K.; Lohmann, D.; Spandl, J.; Stevanovic, A.; Shevchenko, A.; Kuerschner, L. Tracing Fatty Acid Metabolism by Click Chemistry. *ACS Chem. Biol.* **2012**, *7* (12), 2004–2011.
- (32) Robichaud, P. P.; Poirier, S. J.; Boudreau, L. H.; Doiron, J. A.; Barnett, D. A.; Boilard, E.; Surette, M. E. On the Cellular Metabolism of the Click Chemistry Probe 19-Alkyne Arachidonic Acid. *J. Lipid Res.* **2016**, *57* (10), 1821–1830.
- (33) Gaebler, A.; Penno, A.; Kuerschner, L.; Thiele, C. A Highly Sensitive Protocol for Microscopy of Alkyne Lipids and Fluorescently Tagged or Immunostained Proteins. *J. Lipid Res.* **2016**, *57* (10), 1934–1947.
- (34) Blackman, M. L.; Royzen, M.; Fox, J. M. Tetrazine Ligation: Fast Bioconjugation Based on Inverse-Electron-Demand Diels–Alder Reactivity. *J. Am. Chem. Soc.* **2008**, *130* (41), 13518–13519.
- (35) Devaraj, N. K.; Weissleder, R.; Hilderbrand, S. A. Tetrazine-Based Cycloadditions: Application to Pretargeted Live Cell Imaging. *Bioconjug. Chem.* **2008**, *19* (12), 2297–2299.
- (36) Yan, N.; Liu, X.; Pallerla, M. K.; Fox, J. M. Synthesis of Stable Derivatives of Cycloprop-2-Ene Carboxylic Acid. *J. Org. Chem.* **2008**, *73* (11), 4283–4286.
- (37) Dowd, P.; Gold, A. The Thermal Dimerization of Cyclopropene. *Tetrahedron Lett.* **1969**, *10* (2), 85–86.
- (38) Yu, Z.; Lin, Q. Design of Spiro[2.3]Hex-1-Ene, a Genetically Encodable Double-Strained Alkene for Superfast Photoclick Chemistry. *J. Am. Chem. Soc.* **2014**, *136* (11), 4153–4156.
- (39) Magauer, T.; Mulzer, J.; Tiefenbacher, K. Total Syntheses of (+)-Echinopine A and B: Determination of Absolute Stereochemistry. *Org. Lett.* **2009**, *11* (22), 5306–5309.
- (40) Thiele, C.; Wunderling, K.; Leyendecker, P. Multiplexed and Single Cell Tracing of Lipid Metabolism. *Nat. Methods* **2019**, *16* (11), 1123–1130.
- (41) Storck, E. M.; Morales-Sanfrutos, J.; Serwa, R. A.; Panyain, N.; Lanyon-Hogg, T.; Tolmachova, T.; Ventimiglia, L. N.; Martin-Serrano, J.; Seabra, M. C.; Wojciak-Stothard, B.; Tate, E. W. Dual Chemical Probes Enable Quantitative System-Wide Analysis of Protein Prenylation and Prenylation Dynamics. *Nat. Chem.* **2019**, *11* (6), 552–561.
- (42) Deng, H.; Lei, Q.; Wu, Y.; He, Y.; Li, W. Activity-Based Protein Profiling: Recent Advances in Medicinal Chemistry. *Eur. J. Med. Chem.* **2020**, *191*, 112151.
- (43) Simon, G. M.; Cravatt, B. F. Activity-Based Proteomics of Enzyme Superfamilies: Serine Hydrolases as a Case Study. *J. Biol. Chem.* **2010**, *285* (15), 11051–11055.
- (44) Niphakis, M. J.; Lum, K. M.; Cognetta III, A. B.; Correia, B. E.; Ichu, T.-A.; Olucha, J.; Brown, S. J.; Kundu, S.; Piscitelli, F.; Rosen, H.; Cravatt, B. F. A Global Map of Lipid-Binding Proteins and Their Ligandability in Cells. *Cell* **2015**, *161* (7), 1668–1680.
- (45) Gleissner, C. M.-L.; Pyka, C. L.; Heydenreuter, W.; Gronauer, T. F.; Atzberger, C.; Korotkov, V. S.; Cheng, W.; Hacker, S. M.; Vollmar, A. M.; Braig, S.; Sieber, S. A. Neocarzilin A Is a Potent Inhibitor of Cancer Cell Motility Targeting VAT-1 Controlled Pathways. *ACS Cent. Sci.* **2019**, *5* (7), 1170–1178.
- (46) Patterson, D. M.; Nazarova, L. A.; Prescher, J. A. Finding the Right (Bioorthogonal) Chemistry. *ACS Chem. Biol.* **2014**, *9* (3), 592–605.
- (47) Lang, K.; Chin, J. W. Bioorthogonal Reactions for Labeling Proteins. *ACS Chem. Biol.* **2014**, *9* (1), 16–20.
- (48) Liang, D.; Wu, K.; Tei, R.; Bumpus, T. W.; Ye, J.; Baskin, J. M. A Real-Time, Click Chemistry Imaging Approach Reveals Stimulus-Specific Subcellular Locations of Phospholipase D Activity. *Proc. Natl. Acad. Sci.* **2019**, *116* (31), 15453–15462.
- (49) Bumpus, T. W.; Baskin, J. M. Clickable Substrate Mimics Enable Imaging of Phospholipase D Activity. *ACS Cent. Sci.* **2017**, *3* (10), 1070–1077.
- (50) Wang, D.; Du, S.; Cazenave-Gassiot, A.; Ge, J.; Lee, J.-S.; Wenk, M. R.; Yao, S. Q. Global Mapping of Protein–Lipid Interactions by Using Modified Choline-Containing Phospholipids Metabolically Synthesized in Live Cells. *Angew. Chem.* **2017**, *129* (21), 5923–5927.

## Chapter 8

- (51) Laguerre, A.; Schultz, C. Novel Lipid Tools and Probes for Biological Investigations. *Curr. Opin. Cell Biol.* **2018**, *53*, 97–104.
- (52) Laguerre, A.; Hauke, S.; Qiu, J.; Kelly, M. J.; Schultz, C. Photorelease of 2-Arachidonoylglycerol in Live Cells. *J. Am. Chem. Soc.* **2019**, *141* (42), 16544–16547.
- (53) Schuhmacher, M.; Grasskamp, A. T.; Barahtjan, P.; Wagner, N.; Lombardot, B.; Schuhmacher, J. S.; Sala, P.; Lohmann, A.; Henry, I.; Shevchenko, A.; Coskun, Ü.; Walter, A. M.; Nadler, A. Live-Cell Lipid Biochemistry Reveals a Role of Diacylglycerol Side-Chain Composition for Cellular Lipid Dynamics and Protein Affinities. *Proc. Natl. Acad. Sci.* **2020**, *117* (14), 7729–7738.
- (54) Höglinder, D.; Nadler, A.; Haberkant, P.; Kirkpatrick, J.; Schifferer, M.; Stein, F.; Hauke, S.; Porter, F. D.; Schultz, C. Trifunctional Lipid Probes for Comprehensive Studies of Single Lipid Species in Living Cells. *Proc. Natl. Acad. Sci.* **2017**, *114* (7), 1566–1571.
- (55) Ogasawara, D.; Deng, H.; Viader, A.; Baggelaar, M. P.; Breman, A.; den Dulk, H.; van den Nieuwendijk, A. M. C. H.; Soethoudt, M.; van der Wel, T.; Zhou, J.; Overkleeft, H. S.; Sanchez-Alavez, M.; Mori, S.; Nguyen, W.; Conti, B.; Liu, X.; Chen, Y.; Liu, Q.-S.; Cravatt, B. F.; van der Stelt, M. Rapid and Profound Rewiring of Brain Lipid Signaling Networks by Acute Diacylglycerol Lipase Inhibition. *Proc. Natl. Acad. Sci.* **2016**, *113* (1), 26–33.
- (56) Menger, F. M.; Chen, X. Y.; Brocchini, S.; Hopkins, H. P.; Hamilton, D. Synthesis and Thermotropic Properties of Macroyclic Lipids Related to Archaeabacterial Membranes. *J. Am. Chem. Soc.* **1993**, *115* (15), 6600–6608.





# Nederlandse samenvatting

*Het doel van het in dit proefschrift beschreven onderzoek was het ontwikkelen en toepassen van chemisch gereedschap (tools) waarmee metabolisme, transport en signaleringsfuncties van lipiden onderzocht kunnen worden.*

**Hoofdstuk 1** besprak de diversiteit van lipiden en het gebruik van bioorthogonale chemie om ze te bestuderen. Lipiden zijn structureel en functioneel diverse biomoleculen die moeilijk te onderzoeken zijn, met name de lokalisatie en eiwitinteractiepartners. Dit komt door de geringe grootte, vettigheid en snelle metabolisme. De meeste methodes om lipiden te onderzoeken vereisen de extractie van de lipiden uit gehomogeniseerd biologisch materiaal, wat nauwkeurige detectie mogelijk maakt, maar waarbij alle ruimtelijke informatie verloren gaat.

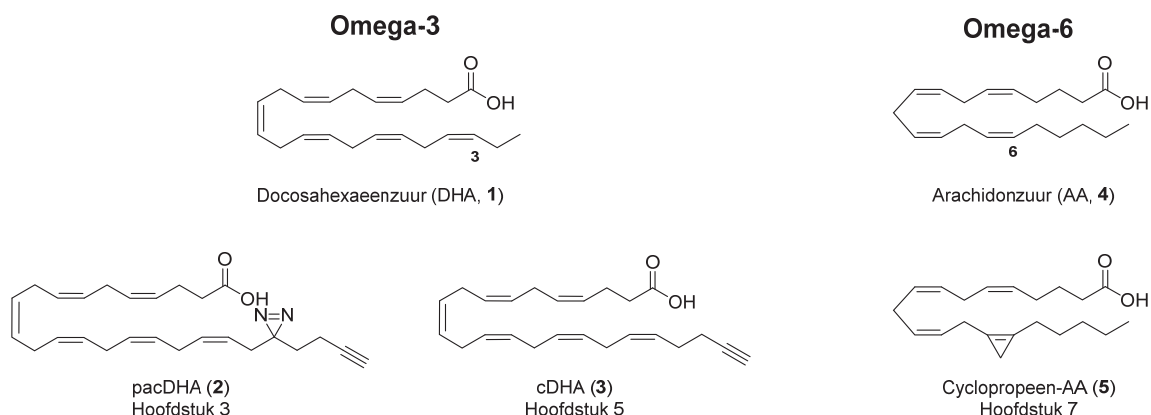
Bioorthogonale chemie heeft het mogelijk gemaakt om lipiden op een veelzijdigere manier te onderzoeken. Een klein bioorthogonaal handvat, zoals een alkyn, kan worden toegevoegd aan een lipide. Daarmee wordt het mogelijk om het te koppelen aan een detectiemolecuul via bioorthogonale chemie, zoals de koper(I)-gekatalyseerde azide-alkyn cycloadditie (CuAAC). Dit stelt de *tool* in staat om verschillende eigenschappen van het lipide te bestuderen, zoals de lokalisatie, het metabolisme, het transport en de incorporatie in eiwitten als posttranslationele modificatie. Daarbij kan een fotoreactieve groep worden toegevoegd aan de *tool* om niet-covalente interacties tussen lipiden en eiwitten te bestuderen. Het bestralen van een fotoreactieve groep resulteert in de vorming van een reactief intermediair, wat een covalente binding kan maken met een lipide-bindend eiwit. De

combinatie van een bioorthogonaal handvat en fotoreactieve groep resulteert in chemische sensoren (*probes*) die een grote bijdrage hebben geleverd aan onderzoek naar lipide-eiwit interacties. Voor het onderzoeken van meervoudig onverzadigde vetzuren is deze aanpak veelbelovend, aangezien deze lipiden in steeds grotere mate worden gewaardeerd als signaalmoleculen met belangrijke functies, met name in het immuunsysteem. De beschikbaarheid van chemische *tools* gebaseerd op dit soort vetzuren is echter ontoereikend, onder andere dankzij de synthetische uitdaging die deze moleculen vormen.

**Hoofdstuk 2** gaf een samenvatting van de op lipiden gebaseerde fotoreactieve *probes* van het afgelopen decennium. De eerste voorbeelden van fotoreactieve *probes* bevatten radioactieve isotopen of omvangrijke fluoroforen en waren vaak alleen in staat om interacties met vooraf bepaalde eiwitten te bestuderen. De laatste jaren hebben *probes* een verschuiving laten zien naar diazirine- en alkynengroepen, deels door verbeteringen in synthetische mogelijkheden en deels door de grotere beschikbaarheid van compatibele reagentia.

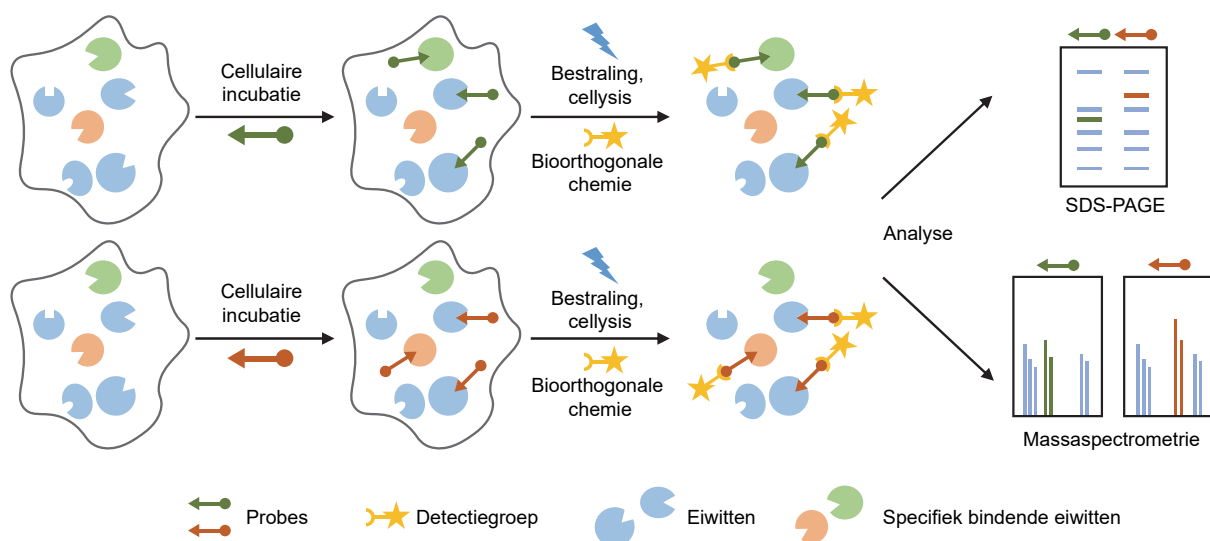
De ambitie van projecten met fotoreactieve *probes* is ook verschoven naar het grootschalig in kaart brengen van lipidebindende eiwitten en het aanpakken van uitdagende biologische kwesties. Er blijven echter grote uitdagingen bestaan in het gebruik van dit soort *probes*. Een grote aanwezigheid van aspecifiek bindende eiwitten maakt het bijvoorbeeld moeilijk om bonafide interactiepartners te onderscheiden. Een overzicht van promiscue eiwitten is beschikbaar in hoofdstuk 2 ter referentie. In de toekomst zal verbeterde synthetische beschikbaarheid–doorgaans gevolgd door commerciële beschikbaarheid–evenals uitgebreidere functionaliteit van chemische *tools* zorgen voor een completer begrip van de eigenschappen en functies van lipiden.

**Hoofdstuk 3** omschreef de synthese en het gebruik van chemische *tools* gebaseerd op een omega-3 vetzuur, docosahexaenzuur (DHA, **1**, Figuur 1) en een oxidatief metaboliet, 17-HDHA. DHA ondergaat verschillende oxidatieve transformaties die resulteren in signaalmoleculen met anti-inflammatoire en pro-resolutie eigenschappen. 17-HDHA is een belangrijk intermediair in dit proces. De rol van 17-HDHA in het immuunsysteem werd onderzocht door middel van comparatieve fotoaffinitéit–gebaseerde eiwitprofiling (*Affinity-based protein profiling*, AfBPP) (Figuur 2). Voor dit doeleinde werden twee *probes*, pac-DHA (**2**) en pac-17-HDHA, gesynthetiseerd om de eiwitinteractiepartners te onderzoeken in menselijke immuuncellen.



**Figuur 1 | Structuren van de vetzuren, chemische *tools* en *probes* centraal in deze thesis.**

Comparatieve AfBPP in menselijke macrofagen resulteerde in de identificatie van PTGR1 als pac-17-HDHA-specifiek bindend eiwit wat in staat is om 17-HDHA te converteren naar 17-oxo-DHA. Dit gaf aan dat PTGR1 een centrale rol heeft in oxidatief metabolisme van meervoudig onverzadigde vetzuren, aangezien het pro-inflammatoire signaallipiden kan inactiveren en anti-inflammatoire signaallipiden kan produceren. Dit liet ook zien dat comparatieve AfBPP een effectieve methode is om bona fide interactiepartners van *probes* te onderscheiden.



**Figuur 2 | Schematische weergave van comparatieve AfBPP met fotoreactieve *probes*.**

**Hoofdstuk 4** beschreef de synthese en de toepassing van een *probe* gebaseerd op een neurobeschermd en anti-inflammatoire derivaat van DHA, docosahexaenzuur ethanolamide (DHEA). De eiwitinteractiepartners van deze *probe* werd onderzocht in microglia, een neuronale immuuncel. Elf specifieke interactiepartners van de DHEA *probe* werden geïdentificeerd door middel van comparatieve AfBPP. Drie van deze eiwitten werden verder onderzocht. NENF, een neurotrofe factor, verlaagde de immuunrespons van microglia, zij het niet in combinatie met DHEA. Stabiele overexpressie van APMAP en GSTM1, de twee andere targets, versterkte de immuunrespons. Dit was meetbaar door een verhoogde NO en IL-6 productie. Dit effect kon deels worden teruggedraaid door behandeling met DHEA, wat aangeeft dat interacties met deze eiwitten deels verantwoordelijk zijn voor de anti-inflammatoire eigenschappen van DHEA in de hersenen. Omdat er weinig bekend is over GSTM1 en APMAP, is meer onderzoek nodig naar de functie van deze eiwitten en het effect hierop van DHEA.

**Hoofdstuk 5** beschreef de ontwikkeling van een vereenvoudigde en geoptimaliseerde methode voor de synthese van een alkyngelabeld derivaat van DHA, cDHA (**3**, Figuur 2). Synthese van derivaten van meervoudig onverzadigde vetzuren, zoals beschreven in Hoofdstuk 3, is een moeizaam proces dat wordt vergezeld door de vorming van verscheidene ongewenste bijproducten. Een alternatieve syntheseroute voor cDHA (**3**) werd ontwikkeld beginnende vanuit DHA zelf. Het gebruik van cDHA (**3**) voor onderzoek naar metabolisme en cellulaire uitwisseling werd gedemonstreerd. Deze betere synthetische strategie kan worden toegepast voor het maken van andere vetzuurderivaten die voorheen lastig te verkrijgen waren. Omdat alkyn- of isotoopgelabelde vetzuren breed inzetbaar zijn voor het onderzoeken van deze biomoleculen is deze synthetische route waardevol voor verder onderzoek.

**Hoofdstuk 6** richtte zich op een ander vetzuur dat een belangrijke rol speelt in de hersenen, anandamide (AEA). AEA is afgeleid uit arachidonzuur (**4**, Figuur 1) en is een signaalmolecuul in het endocannabinoïde systeem (ECS), waar het neurotransmissie reguleert. Farmacologische interventie in dit proces zou interessant zijn voor verschillende toepassingen, maar het transportproces van AEA en de identiteit van een eventueel transporteiwit is nog onduidelijk. Recentelijk werd een remmer van AEA transport gerapporteerd, WOBE437. Het is aangetoond dat dit molecuul concentratieafhankelijk de opname van AEA remt in de Neuro-2a cellijn en in primaire neuronen. In muizen was WOBE437 oraal beschikbaar en resulteerde in CB1R-afhankelijke anti-inflammatoire en verdovende effecten. Echter werd in dit proefschrift gevonden dat WOBE437 de opname van AEA verhoogt en een verlaging van cellulair AEA en gerelateerde  $\Delta$ -acylethanolamines veroorzaakt. Een *probe* gebaseerd op de structuur van WOBE437 resulteerde in de identificatie van drie WOBE437-interacterende eiwitten, SCCPDH, VAT1 en FECH. Manipulatie van SCCPDH en VAT1 op genetisch niveau toonde echter aan dat deze eiwitten niet verantwoordelijk zijn voor de cellulaire verlaging van AEA. Verder onderzoek is nodig naar de verlaging van  $\Delta$ -acylethanolamines, aangezien dit conflicteert met de theoretische inhibitie van een transporteiwit.

Om transport van AEA in levende cellen te kunnen bestuderen, werd in **Hoofdstuk 7** onderzocht of bioorthogonale handvaten beschikbaar zijn die dit mogelijk maken. De katalysator die nodig is in het gebruik van alkyngeabelde lipiden is toxicisch, wat onderzoek in levende cellen uitsluit. In plaats daarvan wordt het gebruik van een cyclopropeengroep onderzocht, die een *inverse electron demand Diels–Alder* (IEDDA) reactie kan ondergaan met gesubstitueerde tetrazines. Een plantaardig vetzuur met een 1,2-gesubstitueerde cyclopropeengroep werd onderzocht in U2OS cellen in combinatie met een tetrazinegebonden fluorofoor. Dit resulteerde in succesvolle cellulaire IEDDA reactie en uitstekend fluorescent signaal, wat aangeeft dat cyclopropeengroepen gebruikt kunnen worden om lipiden te visualiseren. Gedreven door deze resultaten werd arachidonzuur met een cyclopropeengroep (**5**, Figuur 1) succesvol gesynthetiseerd en geïsoleerd. Het gevormde molecuul bleek echter instabiel te zijn, zelfs in de afwezigheid van zuurstof en licht. Bij toekomstig gebruik van deze *tool* zullen deze eigenschappen in acht genomen moeten worden.

## Tot slot

Lipiden zijn een diverse klasse biomoleculen die verschillende rollen spelen in de cel, van energieopslag en membraanorganisatie tot signalering in verscheidene cellulaire processen. De distributie van lipiden en hun rol in signalering wordt gereguleerd door een complex netwerk van transporteiwitten en metabole enzymen. Alhoewel technologische vooruitgang er voor heeft gezorgd dat een steeds groter repertoire van lipiden kan worden gedetecteerd en gekwantificeerd, is het nog altijd lastig om de bijbehorende eiwitten in kaart te brengen. Dit aspect is juist interessant voor meervoudig onverzadigde vetzuren, waarvan vele een rol spelen in het immuunsysteem, maar waarvan het mechanisme onduidelijk is. Voor het gelijktijdig onderzoeken van lokalisatie, metabolisme, cellulaire uitwisseling en signaleringsfuncties is een innovatieve aanpak benodigd.

Chemische biologie is een aanpak die de benodigde flexibiliteit aanbiedt. Met dezelfde chemische *tool*/ kunnen verschillende aspecten worden onderzocht. Met bijvoorbeeld alkyn-gemodificeerde vetzuren kan lokalisatie worden onderzocht met fluorescentiemicroscopie of flowcytometrie, metabolisme door massaspectrometrie of dunnelaagchromatografie evenals binding van de *tool*/aan eiwitten als posttranslationele modificatie of als elektrofiel metaboliet. Deze *tools* zouden baat hebben bij verbeterde synthetische of commerciële beschikbaarheid en een breder scala aan procedures om ze toe te passen. Deze toegankelijkheid zal zorgen voor een bredere inzet in verschillende disciplines, wat essentieel is om lipiden beter te kunnen bestuderen.

In dit proefschrift wordt de synthese en toepassing van verschillende chemische tools gerapporteerd voor het onderzoeken van verschillende biologische aspecten van lipiden. De focus was meervoudig onverzadigde vetzuren, die ondervertegenwoordigd zijn in het veld van chemische biologie door hun synthetische uitdaging. De fotoactiveerbare probes en de comparatieve AfBPP aanpak in Hoofdstuk 3 en 4 werden gebruikt om nieuwe lipideiwitinteracties te ontdekken en uitleg te geven voor de anti-inflammatoire eigenschappen van DHA en metabolieten. De ontwikkelde synthetische methode gerapporteerd in Hoofdstuk 5 maakt synthetische derivaten van DHA toegankelijker en toonde de veelzijdigheid van alkyngelabelde lipiden aan. De fotoactiveerbare *probe* gerapporteerd in Hoofdstuk 6 maakte het mogelijk om doelwitten te ontdekken van een remmer van AEA transport, al blijft dit proces open ter discussie. Het gebruik van 1,2-gesubstitueerde cyclopropeenvetzuren voor het in beeld brengen van lipiden in levende cellen werd beschreven in Hoofdstuk 7, samen met de synthese van een cyclopropeengelabeld derivaat van arachidonzuur voor het onderzoeken van anandamide.



# List of Publications

## Opportunities for Lipid-Based Probes in the Field of Immunology

S. T. A. Koenders, B. Gagestein, M. van der Stelt. *Activity-Based Protein Profiling* **2018**, 420, 283-319.

## Comprehensive structure-activity-relationship of azaindoles as highly potent FLT3 inhibitors

S. H. Grimm, B. Gagestein, J. F. Keijzer, N. Liu, R. H. Wijdeven, E. B. Lenselink, A. W. Tuin, A. M. C. H. van den Nieuwendijk, G. J. P. van Westen, C. A. A. van Boeckel, H. S. Overkleef, J. Neefjes, M. van der Stelt. *Bioorganic & medicinal chemistry* **2019**, 27, 692-699.

## Olaparib based photo-affinity probes for PARP-1 detection in living cells

J. Voorneveld, B. I. Florea, R. J. Mendowicz, M. S. van der Veer, B. Gagestein, M. van der Stelt, H. S. Overkleef, D. Filippov. *ChemBioChem* **2020**, 21(17), 2431.

## Bioorthogonal photoaffinity probes of omega-3 signaling lipids reveal PTGR1 as a metabolic hub in human macrophages

B. Gagestein, J. H. von Hegedus, J. C. Kwekkeboom, M. Heijink, B. I. Florea, H. van den Elst, K. Wals, H. S. Overkleef, M. Giera, R. E. M. Toes, A. Ioan-Facsinay, M. van der Stelt. *Manuscript submitted*

## A method for expeditious synthesis of DHA derivatives

B. Gagestein, H. Minnee, J. H. von Hegedus, J. C. Kwekkeboom, H. van den Elst, K. R. Peter, Overkleef, M. Giera, R. E. M. Toes, A. Ioan-Facsinay, M. van der Stelt. *Manuscript in preparation*

## Profiling the anandamide reuptake inhibitor WOBE437

B. Gagestein, A.F. Stevens, D. Fazio, B.I. Florea, A. Bakker, H. den Dulk, K. Wals, A. Smids, H. S. Overkleef, M. Maccarrone, M. van der Stelt. *Manuscript in preparation*

## **Curriculum Vitae**

Berend Gagestein was born on September 26<sup>th</sup>, 1992 in Capelle aan den IJssel, the Netherlands. He obtained his high school diploma at the Augustinianum in Eindhoven in 2010. In the same year, he started the bachelor Molecular Science and Technology at Leiden University and Delft University of Technology, which he completed in 2013. He continued his academic education in September 2013 with a research master in Chemistry with a specialization in 'Design and Synthesis', which he completed in 2015 *cum laude*.

As a part of his master program, he performed a research internship in the Molecular Physiology group at Leiden University under the supervision of prof. dr. Mario van der Stelt titled 'Design and synthesis of FLT3 inhibitors and development of a proteomics-based kinase selectivity assay'. A second internship was performed at Mercachem, under the supervision of Dr. Ruben Leenders. Here, inhibitors were designed and synthesized in a medicinal chemistry project.

He started his doctoral studies in January 2016 in the Molecular Physiology group at Leiden university under the supervision of prof. dr. Mario van der Stelt.

The research described in Chapters 3 and 5 was performed in collaboration with prof. dr. René E.M. Toes and dr. Andreea Ioan-Facsinay at the Leiden University Medical Center and the work presented in Chapter 6 was performed in collaboration with prof. dr. Mauro Maccarrone at the Department of Medicine, Campus Bio-Medico of the University of Rome. The Institute for Chemical Immunology is kindly acknowledged for the funding of this PhD research.

The work described in this thesis was orally presented at the Activity-Based Protein Profiling (ABPP) meeting (BE, 2019) and CHAINS (NL, 2019). Posters were presented at CHAINS (NL, 2016-2018), the 28<sup>th</sup> International Cannabinoid Research Society conference (NL, 2018), the Activity-Based Protein Profiling (ABPP) meeting (UK, 2019) and the Institute of Chemical Immunology (ICI) conference (NL, 2017-2019) where a poster prize was awarded in 2019.

## Dankwoord

Het doen van een PhD is een tumultueus proces, wat niet gedaan had kunnen worden zonder de hulp van een aantal mensen. Deze wil ik dan ook graag op deze plek hartelijk danken.

Allereerst wil ik mijn promotoren Mario van der Stelt en Hermen Overkleeft bedanken. Mario, bedankt voor de jarenlange begeleiding in dit onderzoekstraject. Je gaf de vrijheid om nieuwe projecten in te duiken, maar ook zeer welkom was de nodige bijsturing wanneer de plannen uit de hand begonnen te lopen. Hermen, je hebt al vroeg gedemonstreerd in je colleges dat het aanpakken van moeilijke biologische vraagstukken net zo belangrijk is als het maken van mooie moleculen.

Graag wil ik ook mijn collega's van MolPhys hier bedanken. Alexander, Anthe, Bing, Daan, Floor, Hedwich, Jessica, Joel, Kim, Laura, Ming, Mirjam, Na, Noëlle, Rob, Timo, Tom, Verena and Wouter, I appreciate how close we have been as a group and how this created a great environment for (non)scientific discussion and support. I hope this environment can persist for many years to come.

I would also like to thank colleagues who have moved on to greener pastures. Andrea, Annelot, Elliot, Eva, Freek, Hui, Juan, Marc, Marjolein and Sebastia(a)n, thanks for forming an amazing group and sharing your experience when yet another chemist wandered into the biolab. Mijn bijzondere waardering gaat uit naar Anthe en Sebastian, die beiden onvermoeibaar de rol van mentor op zich hebben genomen en over de jaren veel hebben bijgedragen aan het onderzoek in deze thesis en het leven daarbuiten.

Mijn ICI-partner, Joost, ik ben dankbaar voor onze jarenlange samenwerking aan de omega-3 vetzuren. We hebben veel van elkaar opgestoken, over de wetenschap, maar ook alles wat daarbij komt kijken. Ook de andere collaborators op het LUMC wil ik bedanken. Andreea Ioan-Facsinay en René Toes, jullie kwamen met invalshoeken en experimenten waar wij niet snel op zouden zijn gekomen, maar die toch essentieel waren voor de totstandkoming van dit werk.

Voor hun bijdrage aan dit onderzoek wil ik ook enkele studenten bedanken. Hugo, Dennis and Iakovia, I appreciate you for joining me on this lipid probe journey and want to thank you for the unwavering enthusiasm in the face of probes with a shorter half-life than the average coffee break.

I would also like to thank our collaborators abroad, Mauro Maccarrone, Domenico Fazio and Ilaria Falanga, for their support in characterization of that anandamide 'reuptake inhibitor'. Bobby, Hans van den Elst, Hans den Dulk, Rian, Richard, Fons en Karthick, dank voor alle ondersteuning met zuiveringen en metingen.

Ook mijn ouders, familie en vrienden wil ik bedanken voor het (on)begrip dat weekenden de beste werkdagen waren. Nancy, bedankt voor alle support de afgelopen jaren. Wanneer de paniek insloeg was je de stem van de rede en door jou heb ik nooit het gevoel gehad dat ik er alleen voor stond. I love you!



